Long-range interacting quantum systems

Nicolò Defenu, Tobias Donner, Tommaso Macrì, Guido Pagano, Stefano Ruffo, and Andrea Trombettoni

Rev. Mod. Phys. **95**, 035002 — Published 29 August 2023

DOI: 10.1103/RevModPhys.95.035002

Long-range interacting quantum systems

Nicolò Defenu

Institute for Theoretical Physics, ETH Zürich,
Wolfgang-Pauli-Str. 27, 8093 Zürich,
*Switzerland**

Tobias Donner

Institute for Quantum Electronics, ETH Zürich,
Otto-Stern-Weg 1, 8093 Zürich,
Switzerland

Tommaso Macrì

Departamento de Física Téorica e Experimental,
Universidade Federal do Rio Grande do Norte, &
International Institute of Physics,
59072-970 Natal-RN,
Brazil

Guido Pagano

Department of Physics and Astronomy, Rice University,
6100 Main Street,
Houston, TX 77005,
USA

Stefano Ruffo

SISSA and INFN,
Sezione di Trieste,
Via Bonomea 265,
I-34136 Trieste, Italy &
CNR-ISC, Via Madonna del Piano 10,
I-50019 Sesto Fiorentino,
Italy

Andrea Trombettoni

Department of Physics,
University of Trieste,
Strada Costiera 11,
I-34151 Trieste, &
CNR-IOM DEMOCRITOS Simulation Centre and SISSA,
Via Bonomea 265, I-34136 Trieste,
Italy

In this review we summarise recent investigations of many-body quantum systems with long-range interactions, which are currently realized in Rydberg atom arrays, dipolar systems, trapped ion setups, and cold atoms in cavities. In these experimental platforms parameters, can be easily changed, and control of the range of the interaction has been achieved. Our main aim is to present and identify the common and (mostly) universal features induced by long-range interactions in the behavior of quantum many-body systems. We will discuss both the case of strong non-local couplings, i.e. the non-additive regime, and the one in which energy is extensive, but low-energy, long-wavelength properties are altered with respect to the short-range case. When possible, the comparison with the corresponding results for classical systems will be presented. Finally, cases of competition with local effects will be also reviewed.

CONTENTS

* Corresponding author: ndefenu@phys.ethz.ch

I. INTRODUCTION

The successful use of mathematical models in the theory of critical phenomena lies in the universal behavior of continuous phase transitions. Due to universality, it is possible to describe different physical situations within the same theoretical framework. The $O(\mathcal{N})$ symmetric models provided privileged tools to investigate the universal behavior occurring close to criticality in a large class of physical systems ranging from magnets and superconductors to biological systems and cold atom ensembles (P. M. Chaikin, 1995; Pelissetto and Vicari, 2002). Within the last century, intense investigations of the properties of $O(\mathcal{N})$ models, dating back to the original Ising's paper (Ising, 1925), have granted the physical community with a deep insight in the physics of phase transitions (Cardy, 1996; Mussardo, 2009; Nishimori and Ortiz, 2015).

For several decades such understanding has been mostly limited to the universal behavior of systems with local, short-range interactions, such as lattice systems with nearest neighbors couplings or local ϕ^4 field theories. Only in more recent times has the overall picture of the universal phenomena appearing in classical systems due to long-range interactions been delineated. The range of the effective interactions among the constituents of a system is in general one of its main properties, and it can affect in many ways the phase diagram, the critical properties, and the dynamical behavior of physical observables. Therefore, a very natural question to be asked both for classical and quantum systems is how the properties of the system are modified by increasing the range of the interactions V, or equivalently reducing the power exponent α, where $V(r) \sim 1/r^{\alpha}$ for large inter-constituents distances r.

For classical systems, the effect of long-range interactions has been systematically investigated both in the equilibrium and the out-of-equilibrium realms (Campa *et al.*, 2014). There, the range of interactions in most of the cases is given and one studies its consequences on – among others – ensemble equivalence, thermodynamic properties such as specific heat and the occurrence of quasi-stationary states, i.e. metastable configurations whose lifetime scales super-linearly with the system size. We refer to reviews (Campa *et al.*, 2014; Campa *et al.*, 2009; Dauxois *et al.*, 2002) for discussions and references on equilibrium and out-of-equilibrium properties of classical systems, including $O(\mathcal{N})$ models, with long-range interactions.

At the same time, the study of the influence of non-local couplings, and especially of the competition between local and long-range interactions, in *quantum* systems has seen an extraordinary surge in the wake of several experimental realizations in atomic, molecular, and optical (AMO) systems (see Fig. 1 for an artistic illustration). Of course, the same set of questions on how

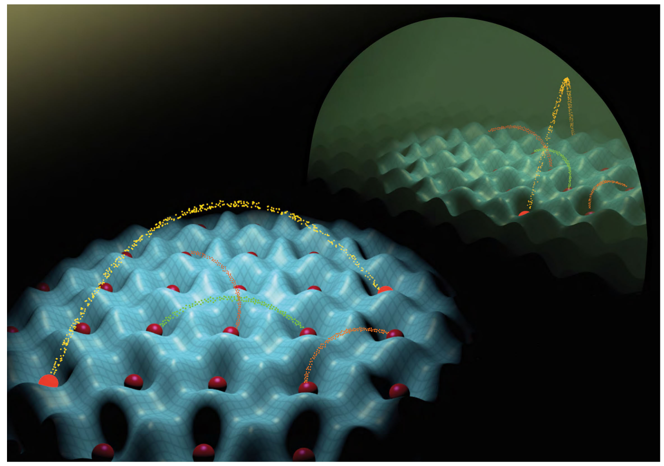

Figure 1 **Artistic illustration of long-range interactions in quantum many-body systems.** Atoms (red spheres), trapped in a potential landscape (blue) are coupled to the light field inside an optical cavity. Far distant atoms can interact with each other via the exchange of photons (yellow arc) confined in the cavity mode. Using diverse tools of AMO systems – provided e.g. by trapped ions, Rydberg atoms, or dipolar atoms – also other types of long-range interactions (colored arcs) can be induced.

long-range interactions modify the properties of models when the interactions are varied from the short-range limit to the strong long-range regime is present not only in classical systems but also in the quantum realm.

The recent interest in quantum long-range systems not only derives from the desire of understanding the fundamental physics of non-local systems and the interplay between local and long-distance properties in presence of very non-local interactions, and how it is changed with respect to the classical counterpart, but it is rooted as well in the role of long-range systems as powerful tools for efficient quantum computing and quantum simulation, as they allow to realise highly entangled or correlated dynamical states (Gyongyosi and Imre, 2019; Jozsa and Linden, 2003; Vidal, 2003). Long-range interactions promise to play a crucial role in quantum technology applications, since their prominent collective character promotes entanglement spreading and leads to novel forms of dynamical scaling, which cannot be observed in traditional systems with local interactions. As a major example, the physics of long-range interacting atomic assemblies provides a clear route to circumventing the constraints imposed by thermal equilibrium, linear entanglement spreading and fast decoherence.

Despite outnumbering investigations, the current literature still lacks a comprehensive perspective on long-range interacting quantum systems, making it difficult to place novel results in the existing framework. Indeed, most current publications present their findings in comparison with the traditional results on short-range systems, rather than with more recent, but established, results in the quantum long-range realm. While this has often helped to raise the interest of the broad physics community on these investigations, it is eventually hindering the drawing of a comprehensive picture on long-range interacting quantum systems as well as the admission of this knowledge in the domain of general-interest physics.

With the present review we aim at constructing an exhaustive account of the unique phenomena arising due to long-range couplings in quantum systems, with special focus on the universal common features that may be observed in AMO experiments. After having reminded basic notions of classical long-range models and discussed the phases of non-local systems, we will extend our understanding beyond the equilibrium properties and clarify paradigmatic questions regarding relaxation and thermalization dynamics. Long-range quantum systems, as they are typically experimentally realized, are mostly isolated and their dynamics is governed by unitary time evolution. In this context, several open questions derive from the comparison with the conventional local interacting case, as motivated by recent remarkable progress in the experimental simulation of quantum long-range systems with tunable range. At variance, the strong coupling to the environment is inevitable for cold atom ensembles in cavities and the discussion about their properties necessarily connects with non-additive classical systems.

The main motivation of this review, i.e. identifying the universal features induced by long-range interactions in quantum many-body systems, directly points to the overwhelming amount of novel research, appearing almost every day in the literature, featuring both theoretical results and state-of-the-art experimental measurements of the dynamical universal behavior of highly non-local interacting systems, such as trapped ions, cavity quantum electrodynamics (CQED), Rydberg atom arrays and cold atoms. All these experimental platforms present a high degree of complexity and the comprehensive picture, which we aim to draw, will serve as a chart to set in a context both novel experimental realizations and recent theoretical findings.

Our ambition is not only the derivation of an all-in-one picture to direct curious outsiders in the realm of long-range-induced physical effects, but also to pinpoint the most relevant and broad results in the field. This effort will hopefully provide a step towards the inclusion of the physics of long-range many-body systems into the inventory of university-taught physics. Given this purpose and the growing amount of publications in the field, we are necessarily forced to a selection of themes and the reader should not be surprised if not all the expected references are to be found. For each topic, we have tried to include only the references relevant for our main goal of the discussion of universal properties of quantum long-range systems or the ones that are better suited to summarise the previous literature on the issue. Whenever possible, we will point to the reader the references containing accounts of previous efforts on the different topics.

The review is organized as follows: in the remaining part of the present section, Sec. I, we will start with a definition of what we refer to as a long-range interaction and we present reminders on the behavior of classical long-range systems, that will be used in the subsequent presentation. We then move to the classification of quantum systems in different groups. A brief account of the most relevant properties of each group will be presented, with a special focus on the classical case. In Sec. II, we will discuss the most relevant experimental realizations of each of the aforementioned groups. Sec. III will be devoted to the definition and identification of critical and universal behavior in classical many-body long-range systems, both at equilibrium and in the dynamical regime. The content of Sec. IV will mainly concern the equilibrium critical properties of long-range interacting quantum many-body systems, evidencing the analogies and differences with respect to the classical case. Finally, Sec. V will focus on the rich mosaics of dynamical critical scalings observed in long-range systems, when driven out of their equilibrium state. The concluding remarks and outlook are reported in Sec. VI.

A. Classification of long-range systems

Since the concept of long-range interactions encompasses non-local terms, beyond on-site or nearest-neighbor couplings, it is rather natural to classify long-range systems based on the shape of the considered interactions. This arrangement does not only reflect differences in the interaction shapes, but indicates the radically different properties that appear in each class.

The word **long-range** conventionally, but not universally, refers to couplings that, as a function of the distance r between the microscopic components, decay as a power-law in the large r limit, $r \to \infty$, as

$$V(r) \sim \frac{1}{r^{\alpha}}. \tag{1}$$

The exponent α will be the one the main characters of this review, together with the related one

$$\sigma \equiv \alpha - d, \tag{2}$$

where d is the dimension of the system.

A preliminary disclaimer is due at this point. The word “long-range” is sometimes used to denote generic *non-local* couplings, where the latter are beyond on-site or nearest-neighbor couplings, so that within this convention an exponentially decaying coupling would be called "long-range". In this review, for the sake of clarity, we prefer to stick (and to a certain extent promote) the use of the word "**non-local**" for a generic coupling which is not local – exponential or finite-range or power-law *et* *cetera* – and "long-range" for interactions that at large distances decay as a power-law of the form (1), i.e. $1/r^{\alpha}$, with an exponent α "small enough", in a sense that will be defined below.

An important result on the critical properties of classical systems with power-law interactions (Defenu *et al.*, 2020; Sak, 1973) is that if α is larger than a critical value, α_*, then the critical behavior is indistinguishable from the short-range limit of the model, retrieved for $\alpha \to \infty$. So, for $\alpha > \alpha_*$, the behavior of the model is not "genuinely" long-range and its universal behavior is the same as in the short-range limit. The specific value of α_* depends on the system and on the transition under study.

Among the unique effects produced by long-range interactions, remarkable features appear in the case α smaller than the dimension of the system, d. There, the interaction energy of homogeneous systems becomes infinite, due to the diverging long-distance contribution of the integral $\int r^{-\alpha} d^d r$. Therefore, when $\alpha < d$ the energy is not extensive (Campa *et al.*, 2014).

Since α_* is larger than d, then there is an interval of values of α for which the energy is extensive, yet the long-distance properties of the system are altered by the long-range nature of the interactions.

Given this, for the sake of our presentation we will employ the following classification:

- **weak long-range interactions**: *infinite-range interactions* with power-law behaviour (1) for large r, and α such that $d < \alpha < \alpha_*$.

- **strong long-range interactions**: *infinite-range interactions* with power-law behaviour (1) for large r, and $\alpha < d$.

Therefore, with **"short-range interactions"** we will refer to the limit $\alpha \to \infty$ and by extension to α larger than α_*, bearing in mind that for $\alpha > \alpha_*$ it is the *critical* behavior to be of short-range type, but non-universal properties may of course be affected.

In both the above definitions for weak and strong long-range interactions, with "infinite-range interactions with power-law behavior" we mean that the power-law decay is present for large distances, i.e. for the tails of the potential, irrespectively of the short-range structure of the interactions (Mukamel, 2008). To appropriately cover the cases in which there is competition between excitations on different length-scales, e.g. between a certain long-range interaction and another one acting at short-range, we will use the following additional notation:

- **competing non-local interactions**: *finite- and/or infinite-range interactions* with different sign.

It is worth noting that this classification has been introduced to ease the discussion, but it does not pretend to be rigorous or perfect. Indeed, certain strong long-range systems may exhibit critical scaling analogous to the general weak long-range case, – or in an infinite-range interacting system the dominant effect could be the creation of non-homogeneous patterns, so that its physics is more similar to the case of finite-range sign changing interactions. Similarly, it could happen that in a system with finite-range interaction plus a power-law interaction with power decay α, the long-range tail does not affect ground-state properties so that according to the classification the interaction could be "long-range" and nevertheless, the system would behave as a non-long-range system. Given the variety of situations, when needed for the sake of the clarity of the presentation, we will regroup the material according to the phenomena exhibited by the different systems. Nevertheless, when not misleading, we will stick to the previous convention, which has the merit to classify different interactions independently of further considerations and of the knowledge of the actual behavior of the quantity of interest studied in the particular models at hand.

In Tab. I we schematically summarize physical systems governed by long-range interactions. Results for some of them in the classical limit are summarized in the remaining part of this section, and further discussed in the quantum case in the next sections.

B. Reminders on classical systems with long-range interactions

In the rest of the section, we will make a brief account of the most established phenomena occurring in each of the previously introduced classes in the classical limit to set the ground for the quantum case.

1. Strong long-range interactions

For $\alpha < d$, the common definitions for internal energy turn out to be non-extensive and traditional thermodynamics does not apply.

These properties are shared by a wide range of physical systems, ranging from gravity to plasma physics, see Tab. I. Apart from the cases summarised there, the general results of strong long-range systems often apply also to mesoscopic systems, far from the thermodynamic limit, whose interaction range, even if finite, is comparable with the size of the system. In the perspective of quantum systems, this situation is particularly relevant for Rydberg gases (Böttcher *et al.*, 2020).

Due to the lack of extensivity, theoretical investigations in the strong long-range regime need a suitable procedure to avoid encountering divergent quantities. This has been obtained in the literature scaling the long-range interaction term by a volume pre-factor $1/V^{\alpha-d}$, which

System	α	α/d	Comments
Gravitational systems	1	1/3	Attractive forces, possibly non homogenous states
Non-neutral plasmas	1	1/3	Some LR effects are also present in the neutral case
Dipolar magnets	3	1	Competition with local ferromagnetic effects
Dipolar Gases	3	1	Anisotropic interactions
Single-mode cavity QED systems	0	0	Interactions mediated by cavity photons
Trapped ions systems	$\sim$ 0-3	$\sim$ 0-3	Interactions mediated by crystal phonons

Table I Table listing different applications where systems are governed by long-range interactions (LR stands for long-range). These systems present interactions which remain long-range up to the thermodynamics limit. In the table, the ratio α/d, signaling how strong the long-range is, refers to $d = 3$ in the first four lines (see the text for a discussion of different d). Notice that for multi-mode cavity QED systems α is tunable.

is the so-called Kac's prescription (Kac *et al.*, 1963).

The salient feature of the Kac prescription is that it allows a proper thermodynamic description of strong long-range systems, without disrupting their key property, i.e. non-additivity. Indeed, other possible regularisations, where the long-range tails of the interactions are cutoff exponentially or at a finite-range tend to disrupt the peculiar physics of these systems. Similar cutoff regularisations are often employed in neutral Coulomb systems, where the $1/r$ potential tails are naturally screened by the presence of oppositely charged particles. However, even in the screened case, the long-range tails of the interaction potential may give rise to finite corrections to thermodynamic quantities from the boundary conditions, which also remain finite in the thermodynamic limit (Lewin and Lieb, 2015).

Similarly, the appearance of non-additivity in strong long-range systems is connected with a finite contribution of the system boundaries to the thermodynamic quantity, as in the prototypical case of fully connected systems where the boundary and bulk contributions are of the same order. It is in fully connected systems that most of the spectacular properties of strong long-range systems have been first identified, such as *ensemble in-equivalence* (Barré *et al.*, 2001). The latter is the property of non-additive systems to produce different results when described with different thermodynamical ensembles, leading to apparently paradoxical predictions such as negative specific heats or susceptibilities. These models also present the so-called *quasi-stationary states* (QSS) in the out-of-equilibrium dynamics, i.e. metastable configurations whose lifetime scales super-linearly with the system size. An extensive account of the peculiar properties of long-range systems in the classical case can be found in Refs. (Campa *et al.*, 2014; Dauxois *et al.*, 2002), while in the following we are going to explicitly focus only on the quantum case.

Based on the discussion above, one may be tempted to exclusively relate peculiar properties such as ensemble inequivalence, negative specific heat, and QSS to the non-extensive scaling of strong long-range systems in the thermodynamic limit. However, similar effects appear also in mesoscopic systems, where the interaction range is finite, but of the same order as the system size, or for attractive systems where most of the density is localized within a finite radius (Thirring, 1970).

To point out that effective strong long-range models with $\alpha = 0$ can emerge also when the couplings do not occur between components separated in space, but rather in another, "internal" space, we mention effective models of interacting neutrino models where the energy and the momentum dependence of the neutrinos enter an Heisenberg model in a magnetic field with $\alpha = 0$ (Pehlivan *et al.*, 2011).

2. Weak long-range interactions

The focus on short-range interactions in the theory of critical phenomena (Nishimori and Ortiz, 2015) is not only motivated by simplicity reasons, but rather by the resilience of the universal behavior upon the inclusion of non-local couplings, at least in homogeneous systems. Indeed, the common wisdom states that universal properties close to a critical point do not depend upon variations of the couplings between the microscopic components, but only on the symmetry of the order parameter and the dimension of the system under study. However, this statement is not generally true, when long-range interactions are introduced into the system.

Indeed, while universal properties are insensible to the intermediate range details of the interactions, for critical systems with homogeneous order parameters, they are sensitive to the power-law decaying tails of long-range couplings (and, to be explicit, not on the strength of the interaction itself). For $\alpha < d$, the interaction energy diverges and the universal behavior typically belongs to the mean-field universality class. On the contrary, as a function of the parameter $\sigma \equiv \alpha - d > 0$ three different regimes may be found (Defenu *et al.*, 2020):

- for $\sigma \leq \sigma_{\rm mf}$ the mean-field approximation correctly describes the universal behavior, where $\sigma_{\rm mf}$ can be calculated in the mean-field approximation.

- for $\sigma > \sigma_*$, the model has the same critical exponents of its short-range version, i.e. the $\sigma \to \infty$

limit;

- for $\sigma_{\rm mf} < \sigma \leq \sigma_*$ the system exhibits peculiar long-range critical exponents,

where the notation $\sigma_* \equiv \alpha_* - d$ has been used. Therefore, it exists a range of long-range decay exponents $0 < \sigma \leq \sigma_*$, where thermodynamics remains well defined and the critical behavior is qualitatively similar to the one appearing in the limit $\sigma \to \infty$. Nevertheless, the universal properties become σ-dependent and, loosely, mimic the dependence of the short-range universal properties as a function of the geometric dimension d (Fisher *et al.*, 1972). In other words, varying σ at fixed dimension is, approximately, equivalent to changing the geometric dimension in short-range systems. Notice that this equivalence is expected to be not exact in general, but it does at the gaussian level, as one can explicitly see for the spherical model (Joyce, 1966).

While the boundary $\sigma_{\rm mf}$ can be exactly calculated by appropriate mean-field arguments, the location of the σ_* is the result of a complex interplay between long-range and short-range contributions to critical fluctuations. This fascinating interplay is at the root of several interesting phenomena, which appear in a wide range of different critical systems upon the inclusion of long-range interactions in the weak long-range regime (Defenu *et al.*, 2020). The appearance of novel effects is not limited to the equilibrium universal properties, but also extends to the out-of-equilibrium realm, whose plethora of intriguing long-range phenomena has only been partially understood. Given these considerations, most of the focus of the forthcoming discussion on weak long-range interacting systems will concern universal properties both at and out of equilibrium.

3. Competing non-local interactions

Systems with non-local interactions whose tails are rapidly decaying, with $\sigma > \sigma_*$ or exponentially decaying, may still produce interesting universal features, due to the interplay with other local couplings or to the presence of frustration in the system. Indeed, when long-range repulsive interactions compete with short-range attractive ones the pertinent order parameter of the system may form spatial modulations in the form, e.g., of lamellae, cylinders, or spheres. These *modulated phases* are ubiquitous in nature and emerge in a large variety of physical systems ranging from binary polymer mixtures, cold atoms, and magnetic systems, to high-temperature superconductors (Seul and Andelman, 1995). Especially in two dimensions, modulated phases lead to rich phase diagrams with peculiar features, which are far from being fully understood. In particular, the appearance of modulated phases has been invoked to describe several interesting properties of strongly correlated electronic systems, including e.g. high temperature superconductors and manganites with colossal magnetoresistance (Bustingorry *et al.*, 2005; Ortix *et al.*, 2008).

At finite temperatures, another striking effect of modulated phase is the so-called inverse melting, which is a consequence of reentrant phases. Indeed, a modulated phase may be "too hot to melt" (Greer, 2000), when the system recovers the disordered state at very low temperature after being in a symmetry broken state in an intermediate temperature regime. The extension of this reentrance becomes appreciable for systems where the homogeneous and modulated phases present similar energy cost and the order parameter remains small, and it is thus strongly influenced by the form and intensity of non-local interactions (Mendoza-Coto *et al.*, 2019).

The study of the universal properties of modulated phases has been initiated long ago (Brazovskii, 1975), but a comprehensive picture of their critical properties is yet lacking, despite the large amount of investigations (Cross and Hohenberg, 1993), due to the difficulty to devise reliable approximation schemes. However, the increasing number of experimental realizations featuring striped phases could lead to a renovated interest in such problems within the framework of the physics of long-range interactions.

II. EXPERIMENTAL REALISATIONS

As mentioned above, the rising interest for long-range physics has been made pressing by the current developments of the experimental techniques for the control and manipulation of AMO systems. Indeed, long-range *quantum* systems are being currently realised in several experimental platforms such as Rydberg atoms (Saffman *et al.*, 2010), dipolar quantum gases (Lahaye *et al.*, 2009), polar molecules (Carr *et al.*, 2009), quantum gases coupled to optical cavities (Mivehvar *et al.*, 2021; Ritsch *et al.*, 2013) and trapped ions (Blatt and Roos, 2012; Monroe *et al.*, 2021; Schneider *et al.*, 2012). Long-range interactions with tunable exponent α can currently be realised using trapped ions off-resonantly coupled to motional degrees of freedom stored in a Paul trap (Islam *et al.*, 2013; Jurcevic *et al.*, 2014; Richerme *et al.*, 2014), in a Penning trap (Britton *et al.*, 2012; Dubin and O'Neil, 1999) or neutral atoms coupled to photonic modes of a cavity (Douglas *et al.*, 2015; Vaidya *et al.*, 2018). We also mention that the dependence of the decay at intermediate length scales can, in turn, be tuned, as e.g. in polar gases in one-dimensional lattices (Li *et al.*, 2020).

Based on the aforementioned classification, we are going to focus our attention on three different classes of experimental systems: *trapped ions*, *quantum gases in cavities* and *dipolar systems*, including, in particular, Rydberg states. All of these systems are quantum in nature and represent prototypical applications of recent investigations in long-range physics. Trapped ions present the almost unique possibility to experimentally realize long-range interactions with decay exponent which may be tuned in the range $\alpha \in 0 \sim 3$ exploring both the strong and weak long-range regimes. Conversely, cavity mediated interactions between atoms are typically flat ($\alpha = 0$) and constitute the experimental counterpart of the celebrated Dicke or Lipkin-Meshkov-Glick (LMG) models (Dicke, 1954; Hepp and Lieb, 1973; Lipkin *et al.*, 1965), two real workhorses of long-range interactions. Finally, Rydberg states and dipolar atoms in general present several common features with thin magnetic films, which have been the traditional experimental setup for the study of modulated critical phenomena at finite temperatures (Selke, 1988).

Thus, each of these experimental platforms represents a realization of the peculiar physics in each of the long-range regimes. However, this statement should not be considered strictly, but mostly a general guideline to ease our presentation. The reason for such a disclaimer is that in the following we will describe several examples violating such correspondence – such as the observation of QSS in the strong long-range regime of trapped ions (Neyenhuis *et al.*, 2017); the presence of pattern formation in cavity systems (Baumann *et al.*, 2010; Landini *et al.*, 2018); and the realisation of the LMG model in the fully-blockade limit of Rydberg atoms (Henkel *et al.*, 2010; Zeiher *et al.*, 2016).

A. Trapped ions

Laser cooled ions confined in radiofrequency traps are one of the most advanced platforms for both quantum computing (Ladd *et al.*, 2010) and quantum simulation (Monroe *et al.*, 2021). In these systems, time-dependent electric fields create an effective harmonic, eV-deep potential (Brown and Gabrielse, 1986; Dehmelt, 1967; Paul, 1990) allowing a long storage time of collections of charged particles in vacuum systems (Pagano *et al.*, 2018). When laser-cooled (Leibfried *et al.*, 2003a), the atomic ions form Wigner crystals whose equilibrium positions and vibrational collective modes are determined by the competition between the Coulomb interactions and the harmonic confinement induced by the trap. In the following sections, we will first review the experimental techniques used to realize spin models with tunable power-law interactions. We will then describe the experimental realizations of these models where the long-range character of the interaction allowed the observations of new physical phenomena in many-body quantum systems.

1. Phonon-mediated interactions

In trapped ions systems, the spin degree of freedom can be encoded in two long-lived atomic states, either in the hyperfine ground state manifold (Knight *et al.*, 2003) or using a metastable electronic state (Blatt and Wineland, 2008). Both approaches guarantee coherence time of the order of a few seconds, near-perfect initialization via optical pumping (Happer, 1972) and high-fidelity detection via state-dependent fluorescence (Christensen *et al.*, 2020; Myerson *et al.*, 2008; Noek *et al.*, 2013).

Without any spin-motion coupling, the ion crystal can be described as a set of normal modes of motion (phonons) and an independent set of internal (spin) degrees of freedom, with the Hamiltonian

$$H = \sum_m \hbar\omega_m a_m^\dagger a_m + \sum_i \vec{B}_i \cdot \vec{\sigma}_i, \tag{3}$$

where $a_m^\dagger(a_m)$ is the creation(annihilation) operator of the m-th phonon mode with $[a_m, a_n^\dagger] = \delta_{mn}$, and $\vec{\sigma}_i = \{\mathbb{1}_i, \sigma_i^x, \sigma_i^y, \sigma_i^z\}$ and $\vec{B}_i$ are the Pauli matrix vector and effective magnetic fields associated with the i-th ion, respectively. The effective magnetic fields are implemented experimentally with microwaves or one-photon and two-photon laser-induced processes.

Laser cooling and sub-Doppler techniques, e.g. resolved Raman sideband cooling (Monroe *et al.*, 1995) and Electromagnetic-Induced Transparency (EIT) cooling (Feng *et al.*, 2020; Jordan *et al.*, 2019; Lin *et al.*, 2013; Roos *et al.*, 2000), can prepare all motional states near their ground states, which is crucial for the simulation of the spin models described below.

Quantum operations can be carried out by exerting a spin-dependent optical force on the ion crystal, coherently coupling spin and motional degrees of freedom. High-fidelity coherent spin-motion coupling can be realized with one-photon optical transitions in the case of optical qubits (Blatt and Wineland, 2008), two-photon stimulated Raman transitions in the case of hyperfine qubits (Britton *et al.*, 2012; Harty *et al.*, 2014; Kim *et al.*, 2009) and near-field microwaves (Harty *et al.*, 2016; Ospelkaus *et al.*, 2011; Srinivas *et al.*, 2021).

Considering the momentum $\hbar\Delta k$ imparted by the laser on the ions confined in a harmonic potential well, the general light-atom Hamiltonian in the rotating frame of the qubit is:

$$H = \frac{\hbar\Omega}{2} \sum_i \left[(\vec{\theta} \cdot \vec{\sigma}_i)\, e^{i(\Delta k X_i - \mu t - \phi)} + \text{h.c.} \right], \tag{4}$$

where Ω, μ and ϕ are the Rabi frequency, the laser beatnote frequency and the laser phase, respectively. The spin Pauli operators $\vec{\sigma}_i = \{\mathbb{1}_i, \sigma_i^x, \sigma_i^y, \sigma_i^z\}$ are multiplied by the complex coefficients $\vec{\theta} = \{\theta_0, \theta_1, \theta_2, \theta_3\}$ depending on the specific experimental configuration. The position

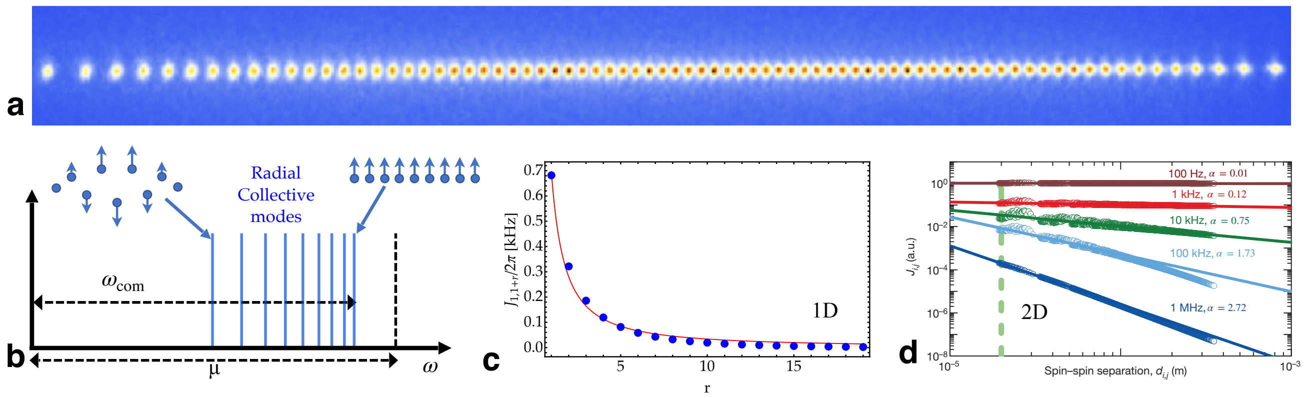

Figure 2 **Trapped ions systems.** **(a)** A 77 linear chain of ^{171}Yb$^+$ ions. The harmonic confinement and Coulomb interactions cause the spacing between ions to be inhomogenous, breaking translational invariance. **(b)** A laser drive at frequency μ is detuned from the radial center of mass mode frequency $\omega_{\rm com}$ to create phonon-mediated spin-spin interactions. **(c)** Calculated spin-spin interaction (blue circles) for a 1D chain of 20 ions versus distance from the edge ion. In this case $\delta = \mu - \omega_{\rm com} = 2\pi\cdot 100$ kHz and $J_{1,1+r} \sim 1/r^{1.3}$ (red solid line). **(d)** Calculated Ising couplings in a 2D crystal of 217 ions versus a sampling of the distance d_{ij} between ion pairs (empty circles). The solid lines are best-fit power law exponents ($\alpha = 0.01, 0.12, 0.75, 1.73, 2.72$ from top to bottom) for various detunings from the center-of-mass (COM) mode of 795 kHz. Adapted from Ref. (Britton *et al.*, 2012).

operator can be written in terms of collective phononic modes as

$$X_i = \sum_{m=1}^{N} \eta_{im}(a_m^\dagger e^{i\omega_m t} + a_m e^{-i\omega_m t}),$$

with $\eta_{im} = \eta_m b_{im}$ where b_{im}[1] is the normal mode transformation matrix and $\eta_m = \Delta k\sqrt{\hbar/2m\omega_m}$ is the Lamb-Dicke parameter associated to the m-th normal mode at frequency ω_m.

2. Mapping to spin models

In the Lamb-Dicke regime, $\Delta k\langle X_i\rangle \ll 1$, the first-order term of Hamiltonian (4) gives rise to spin-phonon couplings of the form $(\sigma_i^{\pm,z} a_m e^{i\omega_m t} + \text{h.c.})$, where the spin operator depends on the experimental configuration. These terms generate an evolution operator under a time-dependent Hamiltonian that can be written in terms of Magnus expansions (Zhu *et al.*, 2006). In the limit of $(\mu - \omega_m) \gg \eta_m\Omega$ for all m, the motional modes are only virtually excited, meaning that only the second-order term of the Magnus expansion is dominant and leads to the following pure spin-spin Hamiltonian:

$$H = \sum_{ij} J_{ij}\sigma_i^{\vec\theta}\sigma_j^{\vec\theta}, \tag{5}$$

where the choice of the Pauli spin operator $\sigma_i^{\vec\theta}$ is controlled by the laser configuration[2]. One common configuration $\{\theta_1 = 1/2, \theta_2 = i/2, \theta_0 = \theta_3 = 0\}$ leads to the so-called Mølmer-Sørensen gate (Sørensen and Mølmer, 1999), where two laser beat-notes are tuned close to the motional mode transitions with opposite detunings $\pm\mu$. In this configuration $\sigma_i^{\vec\theta} = \sigma_i^{\phi} = \sigma_i^x\cos(\phi) + \sigma_i^y\sin(\phi)$, where ϕ can be tuned by controlling the phases of the two laser beat-notes (Monroe *et al.*, 2021). Another widely used laser configuration is $\{\theta_1 = \theta_2 = \theta_0 = 0, \theta_3 = 1\}$ (Leibfried *et al.*, 2003b) where the ion motion is modulated by a spin-dependent light shift.

The spin-spin interaction matrix J_{ij} can be explicitly calculated given the frequencies of the normal modes ω_m and the detuning μ as follows:

$$J_{ij} = \Omega^2\omega_{\rm rec}\sum_{m=1}^{N}\frac{b_{im}b_{jm}}{\mu^2 - \omega_m^2} \tag{6}$$

where $\omega_{\rm rec} = \hbar(\Delta k)^2/2M$ is the recoil frequency associated with the transfer of momentum $\hbar(\Delta k)$ (see Fig. 2). The spin-spin interaction can be approximated with a tunable power law:

$$J_{ij} = \frac{J_0}{|i-j|^\alpha}. \tag{7}$$

The approximate power-law exponent can be adjusted in the $0 < \alpha < 3$ range by tuning the detuning μ and the trap frequencies ω_m. In the limit $\mu \gg \Delta\omega$, with $\Delta\omega$ being the typical mode separation, all modes contribute equally, and the spin-spin interaction decays with a dipolar power law, e.g. $J_{ij} \sim 1/|i-j|^3$. On the other hand, when μ is tuned close to $\omega_{\rm com}$ (see Fig. 2), the exponent α decreases.

It is worth noting that in the quantum simulation regime, large transverse fields ($\mu - \omega_{\rm com} \gg B_z \gg J_0$)

[1] $\sum_i b_{im}b_{in} = \delta_{nm}$ and $\sum_m b_{im}b_{jm} = \delta_{ij}$
[2] For a detailed derivation of Eq. (5) we refer to (Monroe *et al.*, 2021).

have been used in the Mølmer-Sørensen configuration to tune Hamiltonian (5) and experimentally realize a long-range XY model:

$$H = \sum_{ij} J_{ij}(\sigma_i^x\sigma_j^x + \sigma_i^y\sigma_j^y) = \sum_{ij} J_{ij}(\sigma_i^+\sigma_j^- + \sigma_i^-\sigma_j^+). \quad (8)$$

Qualitatively, the large field B_z transverse to the interaction direction suppresses energetically the processes involving two spin-flips ($\sim \sigma_i^+\sigma_j^+ + \sigma_i^-\sigma_j^-$) of the Ising Hamiltonian (5) and retains only the spin preserving part ($\sim \sigma_i^+\sigma_j^- + \sigma_i^-\sigma_j^+$). Note that some papers refer to Hamiltonian (8) as XX Hamiltonian instead of XY. In the following we will use these two as synonyms, depending on the specific reference that is being discussed.

B. Cold atomic gases in cavities

Also when microscopic interactions between particles are local, effective non-local models can be also realized by coupling the particles to the mode of microwave or optical resonators (Leroux *et al.*, 2010; Majer *et al.*, 2007). Photons delocalized over the volume of a resonator can then mediate interactions between the particles, leading to highly tunable long-range or global-range interactions. Since the photons constantly decay from the resonator, these systems have to be externally driven. Depending on parameters, the lossy character of the cavity can thus be made dominant, such that the physics has to be effectively described by non-equilibrium, driven-dissipative models. In the following, we discuss how this basic scheme has been applied to cold thermal ensembles of atoms to realize effective spin interactions, and to quantum degenerate ensembles of atoms to realize effective density interactions.

1. Thermal ensembles with cavity-mediated interactions

Thermal ensembles of cold atoms coupled to optical cavities have proven to be a versatile platform for engineering long-range spin interactions. Non-local, tunable Heisenberg models and spin-exchange dynamics have been implemented using photon-mediated interactions in atomic ensembles, where the coupling between atomic sublevels is controlled via magnetic and optical fields.

For example, by coupling the clock-transition of an ensemble of Strontium atoms to a detuned narrow-linewidth optical resonator, photons mediate an effective spin-exchange interaction which can be widely tuned, since it scales inversely with the detuning between drive and cavity resonance (Norcia *et al.*, 2018). The long-range interactions featured by this system have been exploited to explore the non-equilibrium phase diagram of the LMG model with transverse and longitudinal fields (Muniz *et al.*, 2020), see also Sec. V.D.

Photon-mediated spin-exchange interactions have also been realized in a spin-1 system of Rb atoms (Davis *et al.*, 2019, 2020). Here, a detuned four-photon Raman process is induced: A first atom absorbs a drive photon and emits it virtually into the cavity mode while changing its internal state. This virtual photon is absorbed by a second atom which then emits the photon back into the drive field, while also changing its internal state, thereby realizing a "flip-flop interaction". Since these processes depend via the Zeeman shift on the applied magnetic field, also spatially dependent interactions can be generated. Using multi-frequency drives in conjunction with a magnetic field gradient, highly tailorable interactions in arrays of atomic ensembles within an optical cavity have been recently realized (Periwal *et al.*, 2021), see also (Hung *et al.*, 2016) for a theoretical proposal in crystal waveguides. This approach allowed to generate a multitude of interesting structures such as Möbius strips with sign-changing interactions or treelike geometries. With these tools, models that exhibit fast scrambling connecting spins separated by distances that are powers of two were proposed in Ref. (Bentsen *et al.*, 2019b), which neatly connects to 2-adic models.

2. Quantum gases with cavity-mediated interactions

Dilute quantum gases of neutral atoms are a powerful platform to study many-body physics (Bloch *et al.*, 2008a). However, these gases typically only interact via collisional, short-range interactions. Non-local dipole-dipole interactions can nevertheless be implemented employing either particles with a large static dipole moment (such as heteronuclear molecules or atomic species with large magnetic dipole moments) or with an induced dipole moment, such as Rydberg atoms. These approaches will be discussed in section II.C. A complementary route to exploit induced dipolar interactions is to couple the quantum gas to one or multiple modes of an optical cavity (Mivehvar *et al.*, 2021; Ritsch *et al.*, 2013). In the following sections, we will first provide an introduction to the fundamental mechanism giving rise to cavity-mediated long-range interactions and then turn to experimental realizations of relevance for the current review.

The basic setting is shown in Fig. 3(a). A Bose-Einstein condensate (BEC) is trapped by an external confining potential at the position of the mode of an optical cavity. The quantum gas is exposed to a standing wave transverse pump laser field with wave vector $\mathbf{k}_p$, whose frequency ω_p is far detuned by $\Delta_a = \omega_p - \omega_a$ from the atomic resonance ω_a. In this dispersive limit, the atoms are not electronically excited, but form a dynamical dielectric medium, that scatters photons. At the same time, the resonance frequency ω_c of a cavity mode with wave vector $\mathbf{k}_c$ (where $|\mathbf{k}_c| \approx |\mathbf{k}_p| = k$) is tuned

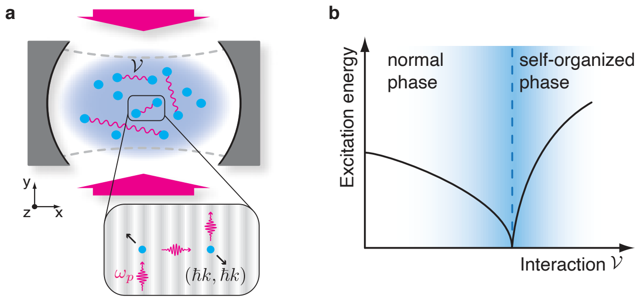

Figure 3 **Experimental scheme for realizing cavity-mediated interactions and mode softening at the superradiant phase transition. (a)** A BEC (shaded cloud) inside an optical cavity is transversally illuminated by a far-red–detuned standing-wave laser field. In a quantized picture, atoms off-resonantly scatter photons from the pump field into a close-detuned cavity mode and back, creating and annihilating pairs of atoms in the superposition of momenta $(p_x, p_y) = (\pm\hbar k, \pm\hbar k)$ (one of four possible processes is shown schematically). This results in global interactions between all atoms. The interaction strength $\mathcal{V}$ is controlled via the power of the transverse laser field and the detuning Δ_c. **(b)** The cavity-mediated atom-atom interaction causes a softening of a collective excitation mode with energy $\hbar\omega_s$ at the momenta $(\pm\hbar k, \pm\hbar k)$ and a diverging susceptibility (shaded area) at a critical interaction strength (dashed line). Adapted from Ref. (Mottl *et al.*, 2012).

close to the frequency of the transverse pump field, such that photons scattered off the atoms are preferentially scattered into the cavity mode. Compared to free space, such vacuum-stimulated scattering is greatly enhanced by a factor proportional to the finesse of the optical cavity.

The scattering of a photon from the pump off a first atom into the cavity and then back into the pump off a second atom is the microscopic process mediating the interaction between two atoms. Such a photon scattering process imparts each one recoil momentum along the cavity direction and the pump field direction onto the atoms, such that atoms initially in the zero-momentum BEC state $|\mathbf{p}_0\rangle = |p_x, p_y\rangle = |0,0\rangle$ are coupled to a state $|\mathbf{p}_1\rangle$, which is the symmetric superposition of the four momentum states $|\pm\hbar\mathbf{k}_c \pm \hbar\mathbf{k}_p\rangle$. Since the photon is delocalized over the cavity mode this interaction is of global range. The strength of the interaction can be increased by either reducing the absolute value of the detuning $\Delta_c = \omega_p - \omega_c$ between pump frequency and cavity resonance, or by increasing the power of the transverse pump field. The interaction inherits its shape from the interference of the involved mode structures of the transverse pump and cavity.

More formally, after adiabatically eliminating the electronically excited atomic states, a quantum gas driven by a standing wave transverse pump field with mode function $\chi(\mathbf{r})$ and coupled to a linear cavity with mode function $\xi(\mathbf{r})$ can be described by the second-quantized many-body Hamiltonian (Maschler *et al.*, 2008) $H = H_c + H_a + H_{ac}$ with

$$\begin{aligned} H_c &= -\hbar\Delta_c a^\dagger a \\ H_a &= \int \mathrm{d}^3\mathbf{r}\Psi^\dagger(\mathbf{r})\left[\frac{\mathbf{p}^2}{2m} + V_p\chi^2(\mathbf{r}) + \frac{g}{2}\Psi^\dagger(\mathbf{r})\Psi(\mathbf{r})\right]\Psi(\mathbf{r}) \\ H_{ac} &= \int \mathrm{d}^3\mathbf{r}\Psi^\dagger(\mathbf{r})\hbar\left[\eta\chi(\mathbf{r})\xi(\mathbf{r})(a+a^\dagger) + U_0\xi^2(\mathbf{r})a^\dagger a\right]\Psi(\mathbf{r}), \end{aligned} \tag{9}$$

where H_c describes the dynamics of a single cavity mode with photon creation (annihilation) operator $a^\dagger(a)$. The atomic evolution in the potential provided by the pump field with depth V_p is captured by the term H_a, where $\mathbf{p}$ is atomic momentum, m is atomic mass, g describes the atomic contact interactions, and $\Psi(\mathbf{r})$ is the bosonic atomic field operator. The term H_{ac} finally describes the interaction between atoms and light fields. Its first term captures the photon scattering between cavity and pump fields at a rate given by the two-photon Rabi frequency $\eta = \frac{g_0\Omega_p}{\Delta_a}$, where g_0 is the maximum atom-cavity vacuum-Rabi coupling rate and Ω_p is the maximum pump Rabi rate. The second term describes the dynamic dispersive shift of the cavity resonance with $U_0 = \frac{g_0^2}{\Delta_a}$ being the light-shift of a single maximally coupled atom.

The atomic system evolves on a time scale given by the energy $\sim \hbar\omega_r$ of the excited momentum state, where $\omega_r = \hbar k^2/(2m)$ is the recoil frequency of the photon scattering and k the cavity wave-vector. If the cavity evolution is fast compared to this time scale, i.e. if the cavity decay rate $\kappa \gg \omega_r$, the cavity field can be adiabatically eliminated which yields

$$a = \frac{\eta\Theta}{\tilde{\Delta}_c + i\kappa}, \tag{10}$$

where $\tilde{\Delta}_c = \Delta_c - U_0 \int \mathrm{d}^3\mathbf{r}\Psi^\dagger(\mathbf{r})\xi^2(\mathbf{r})\Psi(\mathbf{r})$ is the dispersively shifted cavity detuning. Eq. (10) shows that the cavity field is proportional to the order parameter operator $\Theta = \int \mathrm{d}^3\mathbf{r}\Psi^\dagger(\mathbf{r})\chi(\mathbf{r})\xi(\mathbf{r})\Psi(\mathbf{r})$ which measures the overlap between atomic density modulation and the mode structure of the interfering light fields. This relation is essential for the real-time observation of the atomic system via the light field leaking from the cavity.

Eliminating the steady-state cavity field in Eqs. (9) using Eq. (10), an effective Hamiltonian is obtained (Mottl *et al.*, 2012),

$$H_{\text{eff}} = H_a + \int \mathrm{d}^3\mathbf{r}\mathrm{d}^3\mathbf{r}'\Psi^\dagger(\mathbf{r})\Psi^\dagger(\mathbf{r}')\mathcal{V}_{lr}(\mathbf{r},\mathbf{r}')\Psi(\mathbf{r})\Psi(\mathbf{r}'), \tag{11}$$

with the long-range interaction potential

$$\mathcal{V}_{lr}(\mathbf{r},\mathbf{r}') = \mathcal{V}\chi(\mathbf{r})\xi(\mathbf{r})\chi(\mathbf{r}')\xi(\mathbf{r}'). \tag{12}$$

This periodic interaction potential with strength $\mathcal{V} = \hbar\frac{\eta^2\tilde{\Delta}_c}{\tilde{\Delta}_c^2+\kappa^2}$ is of global range and favors a density modulation of the atomic system with a structure given by the interference of pump and cavity fields. For a standing wave transverse pump field impinging on the BEC perpendicular to the cavity mode, this interference has a checkerboard shape of the form $\cos(kx)\cos(ky)$.

While integrating out the light field provides access to a simple description in terms of a long-range interacting quantum gas, it is important to keep in mind that the system is of driven-dissipative nature. The excitations of the system are polaritons that share the character of both the atomic and the photonic fields. Furthermore, as we detail below, in the sideband resolved regime $\kappa \lesssim \omega_r$ the cavity field cannot be integrated out anymore and the interaction becomes retarded (Klinder *et al.*, 2015b).

The sign of the interaction $\mathcal{V}$ can be chosen by an according change in the detuning $\tilde{\Delta}_c$. For $\mathcal{V} < 0$, this interaction leads to density correlations in the atomic cloud favoring a λ-periodic density structure, where $\lambda = 2\pi/k$ is the wavelength of the pump laser field. This can also be understood by inspecting the first term in H_{ac} from Eqs. (9). A λ-periodic density structure would act as a Bragg lattice, enhancing the coherent scattering of photons between pump and cavity. The emerging intra-cavity light field interferes with the pump lattice and builds an optical potential in which the atoms can lower their energy. However, the long-range interaction favoring the density modulation competes with the kinetic energy term. Only above a critical interaction strength, the system undergoes a quantum phase transition to a self-ordered state characterized by a density modulated cloud and a coherent field in the cavity mode, see Section IV.G.2.

Also, tunable-range interactions can be engineered by extending the scheme described above to multi-mode cavities (Gopalakrishnan *et al.*, 2010, 2009, 2011). In such cavities, a very large number of modes with orthogonal mode functions (in theory an infinite number, in practice several thousands) are energetically quasi-degenerate. An atom within the quantum gas will thus scatter the pump field into a superposition of modes, with the weights set by the position of the atom and a residual detuning between the modes. These modes interfere at large distances destructively, such that only a wave packet localized around the scattering atom remains where constructive interference dominates. Accordingly, the effective atomic interaction acquires a finite-range set by the number of contributing modes.

Full degeneracy can only be reached in a multi-mode cavity that is either planar or concentric, both of which are marginally stable cavity configurations (Siegman, 1986). However, also the - experimentally stable - confocal cavity configuration supports a high degree of degeneracy, where either all even or all odd modes are degenerate. The resultant effective atomic interaction also features a tunable short-ranged peak, see Fig. 4. This interaction has been experimentally realized (Kollár *et al.*, 2017; Vaidya *et al.*, 2018), and can be further employed to realize sign-changing effective atomic interactions (Guo

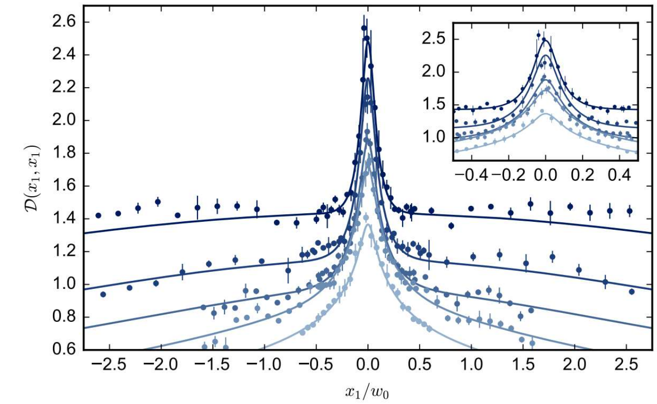

Figure 4 **Tunable-range cavity-mediated interaction in a multi-mode cavity.** Dimensionless interaction strength $\mathcal{D}(x_1, x_1)$ as a function of BEC position in a mode with waist w_0 for five different cavities, indicated by the saturation of the color. The darkest data corresponds to a confocal cavity at high degeneracy of modes, while the brighter shades correspond to fewer interacting modes. The inset shows a close-up near the cavity center, illustrating how a larger number of interacting modes allows to engineer a more localized effective atomic interaction. Reproduced from (Vaidya *et al.*, 2018).

et al., 2020, 2019). Changing the range of the mediated interaction is expected to impact also the universality class of the self-ordering phase transition we describe in Section IV.G.2. With an increasing number of modes, the initially second-order phase transition is expected to develop into a weakly first-order phase transition (Gopalakrishnan *et al.*, 2010, 2009; Vaidya *et al.*, 2018).

3. Mapping to spin models

One of the most fundamental models in quantum optics is the Dicke model, which describes the collective interaction between N two-level atoms (captured as collective spin $\mathbf{S}$) with resonance frequency ω_0 and a single electromagnetic field mode at frequency ω (Dicke, 1954; Kirton *et al.*, 2019). The Dicke model exhibits for sufficiently strong coupling Λ between matter and light, $\Lambda > \Lambda_c \equiv \sqrt{\omega\omega_0}/2$, a quantum phase transition to a superradiant ground state (Hepp and Lieb, 1973; Wang and Hioe, 1973), with a macroscopically populated field mode $\langle a \rangle$ and a macroscopic polarization $\langle S_x \rangle$ of the atoms. The observation of the Dicke phase transition employing a direct dipole transition was hindered due to the limited realizable dipole coupling strengths. However, it was theoretically proposed to make use of Raman transitions between different electronic ground states, allowing to reach the critical coupling in a rotating frame of the driven-dissipative Dicke model (Dimer *et al.*, 2007).

Neglecting atomic collisional interactions and the dis-

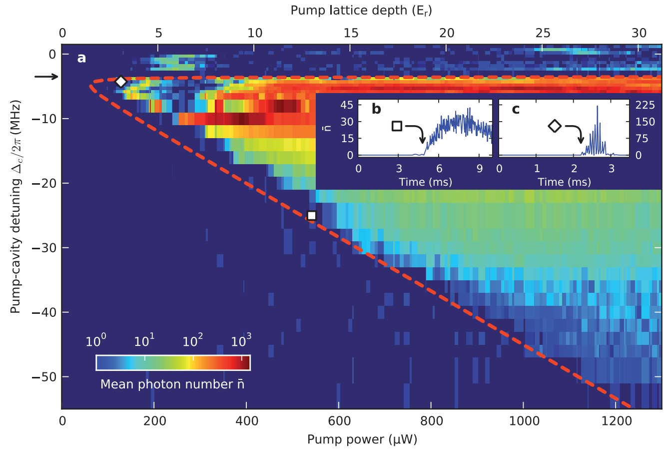

Figure 5 **Dicke model phase diagram.** **(a)** The power of the transverse pump is increased over 10 ms for different values of the pump-cavity detuning Δ_c. The recorded mean intracavity photon number is displayed (intensity scale) as a function of pump power (and corresponding pump lattice depth) and pump–cavity detuning, Δ_c. A sharp phase boundary is observed over a wide range of values; this boundary is in good agreement with a theoretical mean-field model (dashed curve). The dispersively shifted cavity resonance for the non-organized atom cloud is marked by the arrow on the vertical axis. **(b, c)** Typical traces showing the intracavity photon number for different pump–cavity detunings as indicated by the symbols. Reproduced from (Baumann *et al.*, 2010).

persive shift of the cavity, also the self-organization phase transition (see Section IV.G.2) can be mapped to the superradiant quantum phase transition of the Dicke model (Baumann *et al.*, 2010; Nagy *et al.*, 2010). Exploiting the quantized atomic motion, the two-mode ansatz $\Psi = \psi_0 c_0 + \psi_1 c_1$ for the atomic wave-function can be inserted into the Hamiltonian (9). Here c_0 and c_1 are bosonic mode operators annihilating a particle in the flat BEC mode ψ_0, respectively in the excited motional mode $\psi_1 \propto \psi_0 \cos(kx)\cos(ky)$. Introducing the collective spin operators $S_+ = S_-^\dagger = c_1^\dagger c_0$ and $S_z = (c_1^\dagger c_1 - c_0^\dagger c_0)/2$, one arrives at the Dicke Hamiltonian

$$H/\hbar = -\Delta_c a^\dagger a + \omega_0 S_z + \frac{\Lambda}{\sqrt{N}}(a^\dagger + a)(S_+ + S_-), \quad (13)$$

with bare energy of the motional excited state $\hbar\omega_0$ and coupling strength $\Lambda = \eta\sqrt{N}/2$. Compared to the original Dicke model, the mode frequency ω has been mapped to $-\Delta_c$ in the rotating frame of the pump field. The observation of the onset of self-organization in the transversally pumped BEC constitutes the first realization of the Dicke phase transition (Baumann *et al.*, 2010). The phase diagram of the self-ordering phase transition is shown in Fig. 5 together with the well-matching theoretical prediction for the open Dicke model phase transition.

It is instructive to rewrite the long-range interaction Eq. 12 in terms of center-of-mass and relative coordinates. Focusing for simplicity on the 1D case, this results in

$$\begin{aligned}\mathcal{V}_{lr}(x,x') =& \mathcal{V}\cos(kx)\cos(kx') \\ =& \frac{\mathcal{V}}{2}\left[\cos(2kx_{\mathrm{com}}) + \cos(kx_{\mathrm{rel}}))\right]\end{aligned} \quad (14)$$

with $x_{\mathrm{com}} = (x + x')/2$ and $x_{\mathrm{rel}} = x - x'$. The term $\cos[2kx_{\mathrm{com}}]$ originates from the cavity standing-wave mode structure and breaks continuous translational invariance, pinning the center of mass of the system at the phase transition onto the underlying mode structure with periodicity $\lambda/2$. More interesting is the term $\cos[kx_{\mathrm{rel}}]$, which leads to the tendency of atoms to separate by a multiple of the wavelength λ. Due to the different periodicity of the two terms, a parity symmetry is broken at the self-ordering phase transition. The interaction term capturing the relative coordinate allows mapping this system to the Hamiltonian-Mean-Field model (Antoni and Ruffo, 1995; Campa *et al.*, 2014; Dauxois *et al.*, 2002; Ruffo, 1994; Schütz and Morigi, 2014). This model is a paradigmatic model of the statistical mechanics of non-additive long-range systems. Employing this mapping it was possible to show that the transition to spatial self-organization is a second-order phase transition of the same universality class as ferromagnetism, whose salient properties can be revealed by detecting the photons emitted by the cavity (Keller *et al.*, 2017).

4. Lattice models with cavity-mediated long-range interactions

Ultracold atoms loaded into optical lattices are an unprecedented resource for the quantum simulation of condensed matter systems such as the Hubbard model (Bloch *et al.*, 2008b; Lewenstein *et al.*, 2007). A prominent example is the experimental realization of the superfluid-to-Mott insulator quantum phase transition (Greiner *et al.*, 2002), caused by the competition of kinetic and interaction energy. However, since the dominant interaction in quantum gases is the collisional interaction, simulating models with long-range interactions poses a challenge. Adding cavity-mediated long-range interactions to this setting thus opens the path to access long-range interacting, extended Hubbard models. If this additional energy scale competes with the other two, the phase diagram will feature besides the superfluid and the Mott insulating phases also a density modulated superfluid phase – the lattice supersolid – and a density modulated insulating phase – the charge density wave. Theoretical predictions discussed the resulting phases and phase diagrams in the case of commensurate and incommensurate lattices (Bakhtiari *et al.*, 2015; Caballero-Benitez and Mekhov, 2015; Chen *et al.*, 2016; Dogra *et al.*, 2016; Fernández-Vidal *et al.*, 2010; Habibian *et al.*, 2013; Himbert *et al.*, 2019; Larson *et al.*, 2008; Li *et al.*, 2013; Lin *et al.*, 2019).

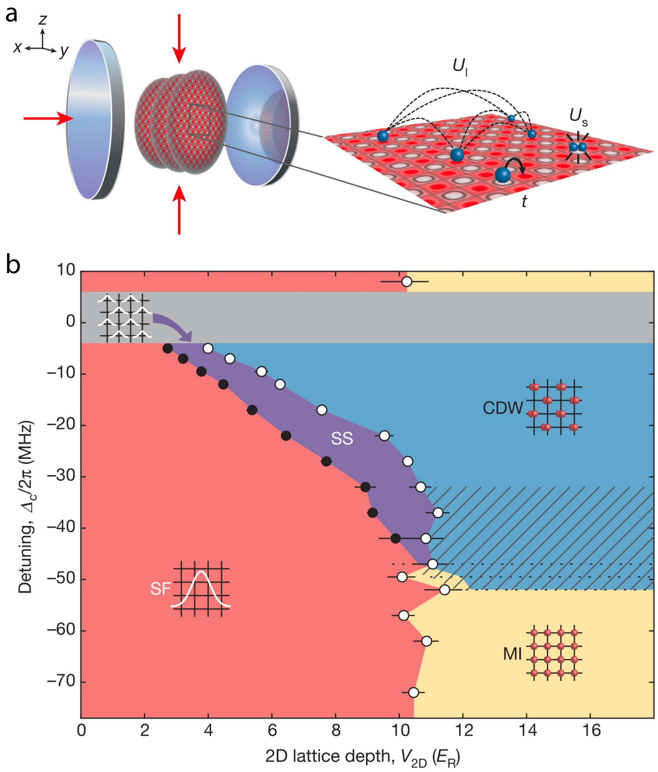

Figure 6 **Lattice models with cavity-mediated long-range interactions.** (**a**) Left, Experimental scheme. A stack of 2D systems along the y axis is exposed to a 2D optical lattice in the $x - z$ plane (red arrows). Right, illustration of the three competing energy scales: tunneling t, short-range collisional interactions U_s and global-range, cavity mediated interactions U_l. (**b**) Measured phase diagram as a function of detuning Δ_c between pump field and cavity, and 2D lattice depth V_{2D}, featuring superfluid (SF), lattice supersolid (SS), charge-density wave (CDW) and Mott insulating (MI) phases. Figure reproduced from (Landig *et al.*, 2016).

The system is captured in a wide parameter range by the following extended Bose-Hubbard model:

$$\begin{aligned} H = &-t \sum_{\langle e,o\rangle} (b_e^\dagger b_o + \text{h.c.}) + \frac{U_s}{2} \sum_{i\in e,o} n_i(n_i - 1) \\ &- \frac{U_l}{V} \left(\sum_e n_e - \sum_o n_o \right)^2 - \sum_{i\in e,o} \mu_i n_i . \end{aligned} \tag{15}$$

Here e and o refer to the even or odd lattice sites, b_i is the bosonic annihilation operator at site i, $n_i = b_i^\dagger b_i$ counts the number of atoms on site i, V is the total number of lattice sites, and μ_i is the local chemical potential which depends on the external trapping potential. The first term captures the tunneling between neighboring sites at rate t. It supports superfluidity in the system since it favors delocalization of the atoms within each 2D layer. In contrast, the second term represents the on-site interaction with strength U_s, and leads to a minimzation of the energy if the atoms are localized on the individual lattice sites, favoring a balanced population of even and odd sites. The third term describes the effective global-range interactions of strength U_l, mediated by the cavity, and favors an imbalance between even and odd sites. The last term leads to an inhomogeneous distribution due to the trapping potential.

Self-organization in a cavity typically results in a 2D structuring of the atomic medium. If the cloud is additionally confined in a lattice along the third direction, it can be brought into an insulating, density modulated regime (Klinder *et al.*, 2015a). An experimental scheme to implement a setting that in addition also features the above-mentioned superfluid to Mott insulator phase transition, and thus also a transition between non-modulated and modulated insulating phases, is shown in Fig. 6(a) (Landig *et al.*, 2016). A BEC is sliced into 2D systems which are subsequently exposed to a 2D optical lattice formed from one on-axis beam pumping the cavity and a standing wave lattice perpendicular to the cavity. The latter simultaneously acts as a transverse pump field inducing cavity-mediated global range interactions in the atomic system. The combined control over the lattice depth V_{2D} and the detuning Δ_c allows to independently tune the ratios of collisional short-range interaction U_s, tunneling t, and global-range interaction U_l. The observables of this experiment are absorption images of the atomic cloud after ballistic expansion, indicating if the atomic system is insulating or superfluid, and the field leaking from the cavity, indicating a homogeneous or a density modulated system. Their combination allows to determine the phase diagram, as shown in Fig. 6(b), featuring the above-mentioned phases.

Of special interest in the context of global-range interaction is the first-order phase transition between the non-modulated Mott insulating and the density modulated charge density wave phase. A system with only short-range interactions supports the formation of domain walls due to additivity. The reduction in energy scales with the volume of the domain, while the energy cost for the domain wall scales with its surface area. Fluctuations creating a domain will thus grow and lead to a decay of the metastable state (Dauxois *et al.*, 2002). This is different in a global-range interacting system, where non-additivity makes domain formation energetically costly: the energy of a domain wall here is proportional to the system size and not to the surface area. Accordingly, long-range interactions can stabilize metastable phases, whose lifetime then scales with system size and diverges in the thermodynamic limit (Antoni and Ruffo, 1995; Campa *et al.*, 2009; Levin *et al.*, 2014; Mukamel *et al.*, 2005).

Quenching the system between these two insulating phases by changing the strength U_l of the global-range interaction leads to hysteresis and metastability, which has been observed in the cavity field measuring the imbalance between even and odd sites (Hruby *et al.*, 2018). The quench eventually triggers a switching process that results in a rearranged atomic distribution and self-consistent potential. The time scale during which this process takes place is intrinsically determined by the many-body dynamics of the gas and is continuously monitored in the experiment. The Mott insulator, in which the system is initially prepared, forms a wedding-cake structure consisting of an insulating bulk surrounded by superfluid shells at the surface. Such an inhomogeneous finite-size system can exhibit a first-order phase transition of the bulk material (the Mott insulator), which is triggered by a second-order phase transition that took place previously on the system's surface (Lipowsky, 1987; Lipowsky and Speth, 1983), where the superfluid atoms possess higher mobility than in the insulating bulk (Hung *et al.*, 2010). Ground state phases and quantum relaxation have been calculated exactly for a 1D lattice in the thermodynamic limit (Blaß *et al.*, 2018).

C. Dipolar and Rydberg systems

The study of modulated and incommensurate phases arising from the competition between short-range attractive interactions and long-range repulsive ones has been a long-standing topic in condensed matter physics (Blinc and Levanyuk, 1986; Fisher *et al.*, 1984). Traditionally, several theoretical investigations have focused on simplified models, where the competition was limited to finite-range interaction terms (Brazovskii, 1975; Fisher and Selke, 1980; Swift and Hohenberg, 1977). However, the natural occurrence of modulated phases is mostly due to repulsive interaction decaying as a power law of the usual form $1/r^{\alpha}$. The most relevant examples include dipolar ($\alpha = 3$) and Coulomb ($\alpha = 1$) interactions.

In the framework of condensed matter experiments, dipolar interactions are known to produce modulated structures in monolayer of polar molecules (Andelman *et al.*, 1987), block co-polymers (Bates and Fredrickson, 1990), ferrofluids (Cowley and Rosensweig, 1967; Dickstein *et al.*, 1993), superconducting plates (Faber, 1958) and thin ferromagnetic films (Saratz *et al.*, 2010). On the other hand, long-range Coulomb interactions are typical of low-dimensional electron systems, but experimental results are limited in this case. Evidences of stripe order have been found in 2D electron liquids (Borzi *et al.*, 2007), quantum Hall states (Lilly *et al.*, 1999; Pan *et al.*, 1999) and doped Mott insulators (Kivelson *et al.*, 1998). In this perspective, the appearance of stripe order is believed to be an ingredient in high-temperature superconductivity (Parker *et al.*, 2010; Tranquada *et al.*, 1997).

The strong relation between traditional investigations in solid-state systems and cold atomic platforms has emerged since the long-range nature of the forces between the atoms has begun to be exploited in experiments. Rydberg gases have been used to observe and study spatially ordered structures (Schauß *et al.*, 2012, 2015) and correlated transport (Schempp *et al.*, 2015). Dipolar spin-exchange interactions with lattice-confined polar molecules were as well observed (Yan *et al.*, 2013). Furthermore dipolar atoms (Lu *et al.*, 2012; Park *et al.*, 2015) can open a new window in the physics of competing long-range and short-range interactions (Natale *et al.*, 2019), clearing the path for the comprehension of modulated phases in strongly interacting quantum systems, as well as to higher-spin physics dynamics (Gabardos *et al.*, 2020; Lepoutre *et al.*, 2019; Patscheider *et al.*, 2020; de Paz *et al.*, 2013).

In the following we provide a brief reminder of basic notions on dipole-dipole interaction and dipolar gases, as needed for the following presentation. Then, we move to Rydberg atoms, focusing on their interactions and the mapping of their effective Hamiltonian on spin systems.

1. Dipolar interactions and dipolar gases

In the context of ultracold atoms, several platforms have been used to study the effect of electric and magnetic dipole-dipole interactions. A typical example is provided by electric dipole moments using heteronuclear molecules (Carr *et al.*, 2009; Moses *et al.*, 2017) or Rydberg atoms in an electric field (Saffman *et al.*, 2010). We remind that, due to rotational symmetry, there is no permanent electric dipole moment in an atom or in a molecule in its non-degenerate rotational ground state. However, when an external electric field couples to the electric dipole moment operator, an electric dipole moment may be induced. A permanent electric dipole moment in homonuclear molecules can be obtained with a ground-state atom bound to a second atom electronically excited to a high-lying Rydberg state (Li *et al.*, 2011). Another very active area of research is provided by the manipulation of heteronuclear molecules, where an electric field mixes two rotational states within the electronic molecular ground state. In this way, one can generate ultracold molecular systems with a large electric dipole moment. Very recent progress in this direction include the creation of an ultracold gas of triatomic Na-K molecules from an atom–diatomic molecule mixture (Yang *et al.*, 2022) and the magneto-optical trapping of calcium monohydroxide polyatomic molecule (Vilas *et al.*, 2022). At variance, neutral atoms can have permanent magnetic dipole moments even at zero fields and the effect of magnetic dipolar interactions can be studied under full rotational symmetry at arbitrarily small magnetic fields.

In general, for two particles, denoted by 1 and 2, with dipole moments along the unit vectors $\mathbf{e}_1$ and $\mathbf{e}_2$, and whose relative position is $\mathbf{r}$, the energy due to their dipole-dipole interaction reads

$$U_{dd} = \frac{C_{dd}}{4\pi} \frac{(\mathbf{e}_1 \cdot \mathbf{e}_2)R^2 - (\mathbf{e}_1 \cdot \mathbf{R})(\mathbf{e}_2 \cdot \mathbf{r})}{R^5}. \tag{16}$$

The coupling constant C_{dd} is $\mu_0\mu^2$ for particles having a permanent magnetic dipole moment μ (μ_0 is the permeability of vacuum) and d^2/ϵ_0 for particles having a permanent electric dipole moment d (ϵ_0 is the permittivity of vacuum) (Weber *et al.*, 2017). A relevant character of the dipolar interaction is its anisotropy. In fact, the dipole-dipole interaction has the angular symmetry of the Legendre polynomial of second order $P_2(\cos\theta)$, i.e. d-wave.

Dipolar gases, and dipolar Bose-Einstein condensates in particular, have been intensively studied (Baranov *et al.*, 2012; Lahaye *et al.*, 2009; Trefzger *et al.*, 2011). The presence on the non-local interaction $\propto r^3$ and its anisotropy give rise to a series of very interesting properties which have been theoretically and experimentally studied. At the mean-field level, a non-local Gross-Pitaevskii equation describes the static ground-state properties, as well as the dynamical effects, such as the excitation spectrum, and the hydrodynamic behavior. Solitons, vortices, and the formation of patterns have intensively been studied, see the review (Lahaye *et al.*, 2009), and as well the role of dipolar interactions in spinor Bose-Einstein condensates (Kawaguchi and Ueda, 2012; Ueda, 2017). The energy scale associated with dipolar interactions in alkali atoms is relatively small, in the Hz range. On the contrary, highly magnetic atoms, such as Cr, Er, and Dy, display dipole moments of 6, 7 and 10 Bohr magnetons respectively (Chomaz *et al.*, 2022). It is customary to define the length

$$a_{dd} \equiv \frac{C_{dd}m}{12\pi\hbar^2}. \tag{17}$$

This parameter plays the role of a dipolar length, giving a measure of the absolute strength of the dipole-dipole interaction. The ratio $\varepsilon_{dd} \equiv a_{dd}/a$ of the dipolar length over the s-wave scattering length a may be also introduced in order to compare the relative strength of the dipolar and contact interactions. Thus, ε_{dd} often determines the physical properties of the system. It is clear that the possibility to have a large dipole moment allows the exploration of regimes induced by the $1/r^3$ tail of the interaction (Chomaz *et al.*, 2022).

We refer to the reviews (Baranov *et al.*, 2012; Böttcher *et al.*, 2020; Chomaz *et al.*, 2022; Lahaye *et al.*, 2009; Trefzger *et al.*, 2011) for further details and references on dipolar gases, and to Refs. (Bause *et al.*, 2021; Bohn *et al.*, 2017; Carr *et al.*, 2009; Gadway and Yan, 2016; Matsuda *et al.*, 2020; Moses *et al.*, 2017; Valtolina *et al.*, 2020) for polar molecules. We will comment about dipolar gases and polar molecules later in the text discussing phenomena where the non-local, possibly long-range (depending on the dimension d), tail of the interactions $1/r^3$ plays a crucial role.

In the remaining part of the present section, the focus is centered on Rydberg atoms due to their recent applications for the simulation of spin systems with long-range and non-local interactions, which are the target of the present review.

2. Interactions between Rydberg atoms

For the present discussion, we briefly review the main mechanisms leading to the simulation of paradigmatic long-range spin Hamiltonians with Rydberg atoms in the frozen motion limit.

Restricting to alkali atoms and denoting by $\mathbf{d}_i$, $i = 1, 2$, the electric dipole moments, the dominant interaction term in the large r limit is the dipole-dipole interaction (16)

$$U_{dd} = \frac{1}{4\pi\epsilon_0}\frac{\mathbf{d_1}\cdot\mathbf{d_2} - 3(\mathbf{d_1}\cdot\mathbf{n})(\mathbf{d_2}\cdot\mathbf{n})}{R^3}, \tag{18}$$

with $\mathbf{n} = \mathbf{r}/r$. Representing with $|\alpha\rangle$ and E_α the single eigenstates and eigenergies of each atom, one can compute in perturbation theory the effect of the perturbation given by Eq. (18). The unperturbed eigenenergies of the two-atom states are given by $E_{\alpha,\beta} = E_\alpha + E_\beta$, where for simplicity the Greek letters α describes the set of quantum numbers (n, l, j, m_j). Depending on the states involved, the relative energies and the dipole-dipole interaction strength, one identifies two main regimes: the van der Waals regime and the resonant dipole-dipole regime. To illustrate the main difference between the two, we assume that two atoms that are in the state $|\alpha\beta\rangle$ are coupled to a single two-atom state $|\gamma\delta\rangle$, see Fig. 7(a). Then the reduced Hamiltonian in this two-state basis takes the form

$$H_{\rm red} = \begin{pmatrix} 0 & \tilde{C}_3/R^3 \\ \tilde{C}_3/R^3 & -\Delta_F \end{pmatrix}, \tag{19}$$

where $\Delta_F = E_\gamma + E_\delta - E_\alpha - E_\beta$ is the Förster defect, $\tilde{C}_3$ is an effective strength of the dipole-dipole interaction, and R is the distance of the two atoms. The eigenvalues of $H_{\rm red}$ are then $\Delta E = -\Delta_F/2 \pm \sqrt{\Delta_F^2 + 4\left(\tilde{C}_3/R^3\right)^2}$. The van der Waals regime is recovered if $\tilde{C}_3/R^3 \ll \Delta_F$, then the state $|\alpha\beta\rangle$ is only weakly admixed to $|\gamma\delta\rangle$. Its energy is perturbed to $\Delta E \approx \frac{1}{\Delta_F}\left(\frac{\tilde{C}_3}{R^3}\right)^2 \equiv \frac{\tilde{C}_6}{R^6}$. One obtains the scaling of the van der Waals coefficient with the principal quantum number n as $\tilde{C}_6 \propto n^{11}$, as verified experimentally in several cases (Béguin *et al.*, 2013; Weber *et al.*, 2017). More generally, to properly estimate the van der Waals coefficient, one has to formally include the contribution of all non-resonant states employing second-order perturbation theory to compute the two-atom energy shift

$$\Delta E_{\alpha\alpha} = \sum_{\beta,\gamma}\frac{|\langle\alpha\alpha|\, U_{dd}\, |\beta\gamma\rangle|^2}{E_{\alpha\alpha} - E_{\beta\gamma}}, \tag{20}$$

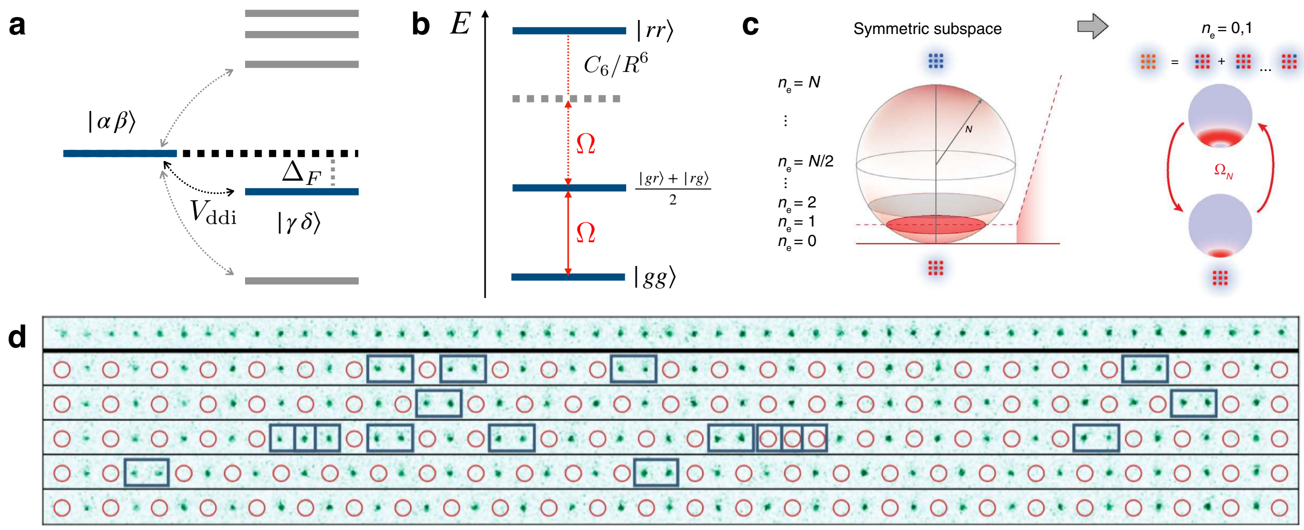

Figure 7 **Long-range interactions in systems of Rydberg atoms for many-body dynamics.** **(a)** Illustration of the interaction between pairs of atoms excited to Rydberg states. Shown are the relevant dipole-coupled pair states labeled by quantum numbers $\alpha, \beta, \ldots$ with the Förster defect Δ_F relative to the pair states $|\alpha\beta\rangle$ and $|\gamma\delta\rangle$. **(b)** Principle of the Rydberg blockade. For two nearby atoms, the van der Waals interaction $\propto C_6/R^6$ (R is the interatomic distance) shifts the doubly-excited state $|rr\rangle$ preventing the double excitation of the atomic pair when $R < R_b = (C_6/\hbar\Omega)^{1/6}$. **(c)** Illustration of a superatom from the collective blockaded lattice of N atoms. Bloch sphere with its basis states (labeled by excitation numbers n_e) and coupled states highlighted [south pole ($n_e = 0$) and singly excited state ($n_e = 1$), represented by the shaded (red) plane]. The small pictograms above and below the sphere depict the lattice system with atoms in the ground (below, in red) and Rydberg (above, in blue) states. The dashed (red) line indicates a zoom into the subspace spanned by the lowest two states. The Husimi distribution of these states and their enhanced coupling Ω_N is shown in the center. Adapted from Ref. (Zeiher *et al.*, 2015). **(d)** The first row displays the experimental image of the initial state of a Rydberg atom array. The following rows represent the atom array after a slow sweep across the phase transition, showing larger average sizes of correlated domains for the slower sweep. Green spots (open circles) represent atoms in the ground (Rydberg) state. Blue rectangles mark the position of domain walls [courtesy of A. Omran].

where the sum extends to all the states that are dipole-coupled to $|\alpha\rangle$.

In the case where the $|\alpha\beta\rangle$ is resonant with $|\gamma\delta\rangle$, i.e. $E_{\alpha\beta} \approx E_{\gamma\delta}$, or equivalently $\Delta_F \ll \tilde{C}_3/R^3$, then the two eigenvalues of $H_{\rm red}$ become $E_\pm \approx \pm\frac{C_3}{R^3}$ and the corresponding eigenstates are $|\pm\rangle = \frac{|\alpha\beta\rangle \pm |\beta\alpha\rangle}{\sqrt{2}}$. This is equivalent to a resonant flip-flop interaction $|\alpha\beta\rangle\langle\gamma\delta| +$ h.c. In this case the interaction energy scales as $1/R^3$ whatever the distance between the two atoms (Förster resonance). In the case of Rb it is easy to achieve resonance with very weak electric fields (Ravets *et al.*, 2014). The resonant dipole-dipole interaction is also naturally realised for two atoms in two dipole-coupled Rydberg states. Moreover, this interaction is anisotropic, varying as $V(\theta) = 1 - 3\cos^2(\theta)$, with θ the angle between the internuclear axis and the quantization axis.

A central concept, essential for both many-body physics and quantum technology, is the Rydberg blockade (Gaetan *et al.*, 2009; Isenhower *et al.*, 2010; Jaksch *et al.*, 2000; Lukin *et al.*, 2001; Urban *et al.*, 2009; Wilk *et al.*, 2010), where the excitation of two or more atoms to a Rydberg state is prevented due to the interaction (Browaeys and Lahaye, 2020; Morgado and Whitlock, 2020). The blockade concept is illustrated in Fig. 7(b). The strong interactions between atoms excited to a Rydberg state can be exploited to suppress the simultaneous excitation of two atoms and to generate entangled states. Consider a resonant laser field coherently coupling the ground state $|g\rangle$ and a given Rydberg state $|r\rangle$, with a Rabi frequency Ω. In the case of two atoms separated by a distance R, the doubly excited state $|rr\rangle$ is shifted in energy by the quantity C_6/R^6 due to the van der Waals interaction with C_6 being the interaction coefficient (all the other pair states have energy nearly independent of R). Assuming that the condition $\hbar\Omega \ll C_6/R^6$ is fulfilled, that is, $R \ll R_b = (C_6/\hbar\Omega)^{1/6}$ (blockade radius), then, starting from the ground state $|gg\rangle$, the system performs collective Rabi oscillations with the state $|\psi\rangle = \frac{|rg\rangle+|gr\rangle}{\sqrt{2}}$. The above considerations can be extended to an ensemble of N atoms all included within a blockade volume. In this case, at most one Rydberg excitation is possible, inducing collective Rabi oscillations with an enhanced frequency $\Omega_{\rm coll} = \sqrt{N}\Omega$, leading to the so-called superatom picture illustrated in Fig. 7(c). The system dynamics is confined to the symmetric subspace of zero ($n_r = 0$) and one ($n_r = 1$) excitations, whose basis are the Fock states $|0\rangle = |g_1, \ldots, g_N\rangle$ and the entangled W-state $|1\rangle = \frac{1}{\sqrt{N}}\sum_{i=1}^{N} |g_1, \ldots, r_i, \ldots, g_N\rangle$, where g_i and

r_i label the i-th atom in the ground or Rydberg state (Zeiher *et al.*, 2015).

An important objective is to implement interacting many-body systems combining atomic motion with tunable long-range interaction via Rydberg atoms. The main experimental challenge is to bridge the mismatch in energy and timescales between the Rydberg excitation and the dynamics of the ground state atoms. A possible solution is the so-called Rydberg dressing where ground state atoms are coupled off-resonantly to Rydberg states leading to effectively weaker interaction with lower decay rates (Balewski *et al.*, 2014; Henkel *et al.*, 2010; Jau *et al.*, 2016; Johnson and Rolston, 2010; Macrì and Pohl, 2014; Pupillo *et al.*, 2010). The main difficulty in this approach is that decay and loss processes of Rydberg atoms have to be controlled on timescales that are much longer than for near-resonant experiments and more exotic loss processes become relevant (Guardado-Sanchez *et al.*, 2021; Zeiher *et al.*, 2016, 2017). Rydberg dressing also allows imposing local constraints which are at the heart of the implementation of models related to gauge theories, like the quantum spin ice (Glaetzle *et al.*, 2014). Other predictions include cluster Luttinger liquids in 1D, supersolid and glassy phases, see Sec. IV.E for more details. It might be even possible to implement a universal quantum simulator or quantum annealer based on Rydberg dressing (Glaetzle *et al.*, 2017; Lechner *et al.*, 2015).

3. Mapping to spin models

The two-atom picture described in the previous section can be extended to the many-body case. Including the coupling of single-atom states to an external coherent laser drive, one obtains in the rotating frame of the laser the Ising Hamiltonian (Labuhn *et al.*, 2016; Schauß *et al.*, 2012, 2015)

$$H_{\text{Ising}} = \frac{\hbar\Omega}{2}\sum_i \sigma_x^i - \sum_i \hbar\Delta n_i + \sum_{i<j}\frac{C_6}{R_{ij}^6} n_i n_j, \tag{21}$$

where $n_i = |r\rangle_i \langle r| = (1+\sigma_z^i)/2$ is the projector to the excited state $|r\rangle$, and Δ is the single-atom detuning from the Rydberg state $|r\rangle$. A discussion with references on the simulation of quantum Ising models in a transverse field can be found in Refs. (Morgado and Whitlock, 2020; Schauss, 2018). We refer to (Lewenstein *et al.*, 2007; Trefzger *et al.*, 2011) for references on effective interacting lattice models obtained for dipolar gases in optical lattices at low energy.

The realization of the Ising Hamiltonian in Rydberg atoms quantum simulators led to the observation of many interesting effects, from the Kibble-Zurek mechanism and its related critical dynamics (Keesling *et al.*, 2019) [see Fig. 7(d)], to antiferromagnetic phases (Ebadi *et al.*,

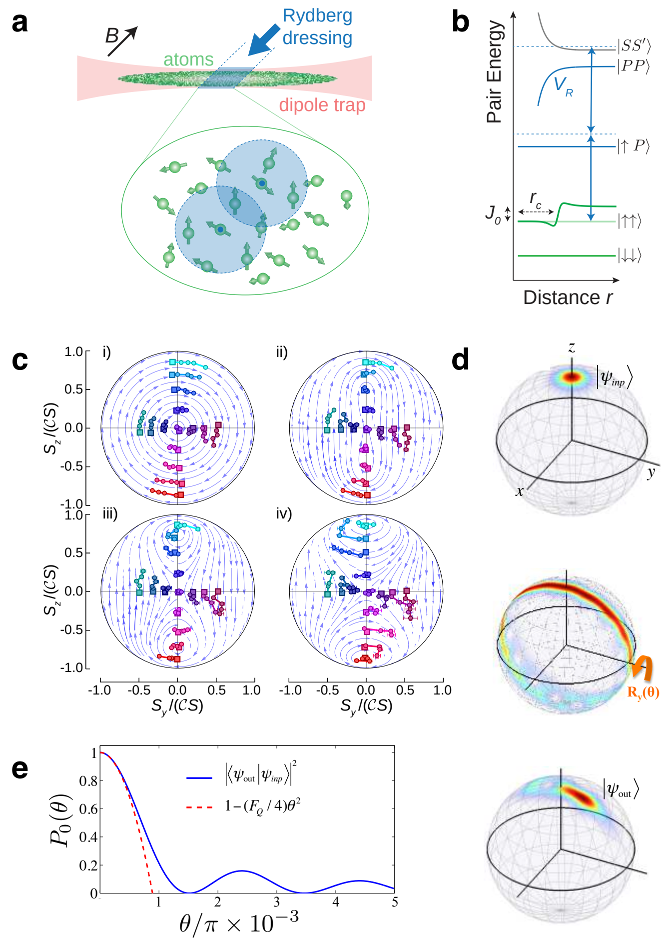

Figure 8 **Finite-range interactions in spin systems: dynamics and applications.** **(a)** Experimental setup and Rydberg dressing scheme for a cloud of Cs atoms is held in an optical dipole trap and locally illuminated with 319 nm light to generate Ising interactions of characteristic range r_c and strength J_0. The quantization axis is set by a 1 G magnetic field B. **(b)** Energy level diagrams for a pair of atoms. **(c)** Transverse-field Ising dynamics. Trajectories $S(k)$ for initial states $|\theta,\phi\rangle$ (square data points) and up to $k=4$ Floquet cycles, obtained with dressing parameters $(\Omega,\Delta)=2\pi\times(2.8,25)$ MHz. Plots (i-iv) are for $\Lambda_{\text{eff}}=0, 1.2(2), 1.8(3), 2.7(4)$. Blue flow lines show mean-field theory for best fit $\Lambda=0, 1.1, 1.5, 2.2$ (see main text). Figures (a)-(c) adapted from Ref. (Borish *et al.*, 2020). **(d)** Loschmidt echo protocol applied to the LMG (one-axis twisting) model. Snapshot of the Husimi distribution. (Top panel) A spin-polarized state is prepared at north pole of the Bloch sphere. (Central panel) Interaction is switched on for a time t_1 [transformation U_1]. The state is then rotated of an angle θ [$R_y(\theta)$]. (Bottom panel) Interaction is switched on again for a time t_2 [transformation U_2] such that $U_1U_2=1$. In these plots $\theta/\pi=0.01$ and $\tau/\pi=0.05$. **(e)** Probability $P_0(\theta)$ (solid line) as a function of phase shift. as a function of θ for $\tau/\pi=0.05$. The dashed line is the second-order expansion involving the quantum Fisher information F_Q. Here $N=101$. Figures (d) and (e) adapted from Ref. (Macrì *et al.*, 2016).

2021; Guardado-Sanchez *et al.*, 2018; Lienhard *et al.*, 2018; Scholl *et al.*, 2020), quantum spin liquids (Samajdar *et al.*, 2021; Semeghini *et al.*, 2021; Verresen *et al.*, 2021), and the quantum critical dynamics of a 2D Ising quantum phase transition (Ebadi *et al.*, 2021). The trapping and manipulation of Rydberg atoms in optical tweezers with defect-free configurations has also played a major role in this perspective (Anderegg *et al.*, 2019; Barredo *et al.*, 2016; Bohrdt *et al.*, 2020; Covey *et al.*, 2019; Endres *et al.*, 2016; Festa *et al.*, 2021; Ohl de Mello *et al.*, 2019; Schymik *et al.*, 2021; Wang *et al.*, 2020).

Rydberg dressing also provides an alternative way to implement quantum Ising models with important implications beyond quantum simulation. Two internal ground states are used to encode spin-up and spin-down states in the dressing protocol. Coherent many-body dynamics of Ising quantum magnets built up by Rydberg dressing are experimentally studied both in an optical lattice and in an atomic ensemble. An illustration of the Ising dynamics in a finite-range model is presented in Fig. 8, where we show the trajectories of the collective spin $S(k)$ from (Borish *et al.*, 2020). An important application of this Hamiltonian is for the study of Loschmidt echo protocol applied to the LMG (one-axis twisting) model for quantum metrology purposes (Gil *et al.*, 2014), e.g. for the preparation of non-gaussian states that can be detected via the quantum Fisher information (Borish *et al.*, 2020; Macrì *et al.*, 2016). Rydberg dressing of atoms in optical tweezers can also be employed for the realization of programmable quantum sensors based on variational quantum algorithms, capable of producing entangled states on demand for precision metrology(Kaubruegger *et al.*, 2019). This investigation is not limited to Rydberg atoms, but extends naturally also to ion platforms (Davis *et al.*, 2016; Morong *et al.*, 2021).

A special case of the quantum Ising model arises when $a_{\rm latt} < R_c < 2a_{\rm latt}$ with $a_{\rm latt}$ the lattice spacing (nearest-neighbor blockade) and $V_{ij} \approx 0$ for everything beyond nearest neighbors. Such a situation was experimentally realized in a 1D chain of Rydberg atoms in (Bernien *et al.*, 2017; Bluvstein *et al.*, 2021). In this case one can derive an effective Hamiltonian for the low-energy subspace which amounts to neglecting configurations with two adjacent excitations. In 1D the resulting Hamiltonian takes the form of a PXP model

$$H = \sum_i \frac{\Omega_i}{2} P_{i-1}\sigma_x^i P_i, \tag{22}$$

where $P_i = |g\rangle\langle g|$ is the projector onto the ground state.

Resonant dipole-dipole interactions between Rydberg atoms are at the basis of several proposals to simulate the quantum dynamics of many-body spin systems. As a major example, it is possible to see that a system containing two dipole-coupled Rydberg states can be mapped to a spin-1/2 XY model, see the review (Wu *et al.*, 2021) and references therein. Coherent excitation transfer between two types of Rydberg states of different atoms has been observed in a three-atom system (Barredo *et al.*, 2015). The resulting long-range XY interactions give rise to many-body relaxation (Orioli *et al.*, 2018).

Given the well-known mapping between the XY model and hard-core bosons (Friedberg *et al.*, 1993), it is possible to provide an experimental realization of the bosonic Su-Schrieffer-Heeger model (Su *et al.*, 1979) and its symmetry protected topological order with a single-particle edge state (de Léséleuc *et al.*, 2019; Lienhard *et al.*, 2020), see also (Kanungo *et al.*, 2021). Proposals to observe topological bands (Peter *et al.*, 2015) and topologically protected edge states (Weber *et al.*, 2018) were presented. Moreover, a realization of a density-dependent Peierls phase in a spin-orbit coupled Rydberg system has been recently demostrated (Lienhard *et al.*, 2020).

We finally mention that with Rydberg systems one could implement digital simulation techniques (Georgescu *et al.*, 2014). The total unitary evolution operator $U(t)$ is decomposed in discrete unitary gates (Weimer *et al.*, 2011, 2010) and one can study a broad class of dynamical regimes of spin systems, such as nonequilibrium phase transitions and non-unitary conditional interactions in quantum cellular automata (Gillman *et al.*, 2020; Lesanovsky *et al.*, 2019; Wintermantel *et al.*, 2020). Kinetically constrained Rydberg spin systems, in which a chain of several traps each loaded with a single Rydberg atom and coupled with the bosonic operators expressing the deviation from the trap centers, also referred to as facilitated Ryberg lattices, were as well studied (Mazza *et al.*, 2020).

A further promising line of research is provided by Rydberg ions both for quantum simulation purposes (Gambetta *et al.*, 2020; Müller *et al.*, 2008) as well as for the realization of fast quantum gates for quantum information processing (Mokhberi *et al.*, 2020; Müller *et al.*, 2008). 2D ion crystals for quantum simulation of spin-spin interactions using interactions of Rydberg excited ions have been proposed in (Nath *et al.*, 2015) to emulate topological quantum spin liquids using the spin-spin interactions between ions in hexagonal plaquettes in a 2D ion crystal. The role of a Rydberg ion is to modify the phonon mode spectrum in order to realize the constrained dynamics of the Balents-Fisher-Girvin model on the Kagome lattice. There, the effective spin-spin interaction for the hexagonal plaquette can be written as an extended XXZ model

$$H_{SS} = \sum_{i<j} J_{ij}^z S_i^z S_j^z + \sum_{i<j} J_{ij}^{\perp}(S_i^x S_j^x + S_i^y S_j^y). \tag{23}$$

Long-range XXZ Hamiltonians with tunable anisotropies can be Floquet-engineered using resonant dipole-dipole interaction between Rydberg atoms and a periodic external microwave field coupling the internal spin states (Geier *et al.*, 2021; Scholl *et al.*, 2021).

It is worth noting that in a realistic Rydberg atom system, coherent driving offered by external fields often competes with dissipation induced by coupling with the environment. Such a controllable driven-dissipative system with strong and nonlocal Rydberg-Rydberg interactions can be used to simulate many-body phenomena distinct from their fully coherent counterparts. Evolution of such an open many-body system is often governed by the master equation $\partial_t \rho = -i[H, \rho] + L\rho$, where ρ is the state of the system, H the system Hamiltonian and L is the Liouvillian superoperator (Benatti and Floreanini, 2005; Gardiner and Zoller, 2004; Manzano, 2020). Correspondingy, several aspects of driven-dissipative dynamics in Rydberg systems and dissipative Rydberg media were addressed (Bienias *et al.*, 2020; Goldschmidt *et al.*, 2016; Lee *et al.*, 2015, 2019; Lesanovsky and Garrahan, 2013; Letscher *et al.*, 2017; Levi *et al.*, 2016; Lourenço *et al.*, 2021; Pistorius *et al.*, 2020; Torlai *et al.*, 2019).

III. THERMAL CRITICAL BEHAVIOUR

Phase transitions are among the most remarkable phenomena occurring in many-body systems. Among various kinds of phase transitions, continuous phase transitions are particularly fascinating since they are tightly bound with the concept of universality. Thanks to the universality phenomenon the same formalism can be applied both to phase transitions occurring at a finite temperature and at $T = 0$. The latter are usually denoted as quantum phase transitions (Sachdev, 1999). Nowadays the intense efforts of the scientific community have paid their rewards and the critical properties of several physical systems have been characterized (Pelissetto and Vicari, 2002).

Usually, universality is defined as the insensitivity of the critical scaling behavior of thermodynamic functions with respect to variations of certain microscopic details of the system under study, such as the lattice configurations or the precise shape of the couplings. This definition alone cannot be considered rigorous unless one specifies all the possible adjustments of the microscopic features, which preserve universality. In the following, we will reserve the adjective "universal" to all those phenomena which may be quantitatively described by a suitable continuous formulation. Therefore, in our language, the concept of universality is strictly tied to the existence of a continuous field theory formulation, which, albeit ignoring the microscopic details of the lattice description, is able to produce an exact estimate for the universal quantities.

The quantum critical behavior of local models in dimension d at $T = 0$ can be ofter related with their critical scaling at finite temperature T, but in a dimension $d + 1$ (Sachdev, 1999; Sondhi *et al.*, 1997), a typical example being the nearest-neighbour quantum Ising model in a transverse field (at $T = 0$) and the short-range classical Ising model at finite temperature (Mussardo, 2009). The situation changes for long-range models and for this reason we are going to review in this section the basics properties of equilibrium critical long-range systems at finite temperature, and compare them in Sec. IV with the corresponding properties at zero temperature.

The prototypical playground for the study of universal properties at finite temperature are the classical $O(\mathcal{N})$ spin systems, whose Hamiltonian reads

$$H = -\frac{1}{2} \sum_{i \neq j} J_{ij} \mathbf{S}_i \cdot \mathbf{S}_j \,. \tag{24}$$

where $\mathbf{S}_i$ is a $\mathcal{N}$-component spin vector with unit modulus, $J_{ij} > 0$ are ferromagnetic translational invariant couplings and the indices i, j run over all sites on any d-dimensional regular lattice of V sites. The usual terminology is that $\mathcal{N} = 1$ is the Ising model, $\mathcal{N} = 2$ the XY model, $\mathcal{N} = 3$ the Heisenberg model and $\mathcal{N} \to \infty$ is the spherical model (Stanley, 1968). It is well known (Mussardo, 2009; Nishimori and Ortiz, 2015) that for $\mathcal{N} \geq 1$ and $d > 2$ the Hamiltonian in Eq. (24) and fast enough decaying couplings (i.e., in the short-range limit) presents a finite temperature phase transition between a low temperature state $T < T_c$ with finite magnetisation $m = |\langle \sum_i \mathbf{S}_i \rangle|/N \neq 0$ and an high temperature phase with $m = 0$. For $\mathcal{N} = 1$, the phase transition occurs of course also for $d = 2$ (Mussardo, 2009; Nishimori and Ortiz, 2015).

Close to the critical point the thermodynamic quantities display power law behaviour as a function of the reduced temperature $\tau \equiv (T - T_c)/T_c$, with universal critical exponents which only depend on the symmetry index $\mathcal{N}$ and the dimension d of the system. These critical exponents coincide with the ones of the $O(\mathcal{N})$-symmetric field theory with action

$$S[\varphi] = \int d^d x \left\{ \partial_\nu \varphi_i \partial_\nu \varphi_i + \mu |\boldsymbol{\varphi}|^2 + g |\boldsymbol{\varphi}|^4 \right\} \tag{25}$$

where $\boldsymbol{\varphi}$ is an $\mathcal{N}$-component vector with unconstrained modulus, the lattice summation has been replaced by a real space integration, $\nu = 1, \cdots, d$ runs over the spatial dimensions, $i = 1, \cdots, \mathcal{N}$ refers to the different components, the quadratic coupling controls the distance from the critical point ($\mu \propto \tau$), the value of the constant coupling is $g > 0$ and the summation over repeated indices is intended.

An extensive amount of theoretical investigations has been performed on the critical properties of $O(\mathcal{N})$ symmetric models, both in their continuous and lattice formulation, reaching an unmatched accuracy in the determination of universal properties with a fair degree of consistency in the whole dimension range $2 \leq d \leq 4$ (Cappelli *et al.*, 2019; Codello *et al.*, 2015; Holovatch and Shpot, 1992; Kleinert, 2001; Pelissetto and Vicari, 2002). Numerical simulations, which are limited to integer dimensional cases $d \in \mathbb{N}$, are mostly consistent with theoretical investigations (Pelissetto and Vicari, 2002), while the recently emerged conformal bootstrap results confirmed and extended the existing picture (Poland *et al.*, 2019).

A. The weak long-range regime

Having introduced the formalism and notation for universality problems, we can start with the case of interest of long-range $O(\mathcal{N})$ spin systems, i.e. the Hamiltonian in Eq. (24) with $J_{ij} = J/r_{ij}^{d+\sigma}$, where r_{ij} is the distance between sites i and j, a coupling constant $J > 0$, and a positive decay exponent $d+\sigma \geq 0$. The Fourier transform of the matrix J_{ij} produces a long-wavelength mean-field propagator of the form $G_{\rm mf} \sim J_\sigma q^\sigma + J_2 q^2$, setting the mean-field threshold for the relevance of long-range interactions to $\sigma_*^{\rm mf} = 2$ (Fisher *et al.*, 1972).

The renormalisation group (RG) approach (Polchinski, 1984; Wegner and Houghton, 1973) can provide a comprehensive picture for the universal properties of long-range $O(\mathcal{N})$ models. In the so-called functional RG (FRG) one writes an – in principle – exact equation for the flow of the effective average action, Γ_k, of the model and then resort to various approximation schemes (Berges *et al.*, 2002; Delamotte, 2011; Wetterich, 1993). The Γ_k is obtained by the introduction of a momentum space regulator $R_k(q)$, which cutoffs the infra-red divergences caused by slow modes $q \ll k$, while leaving the high momentum model $q \gg k$ almost untouched. The problem of weak long-range interactions in the continuous space could be then represented by the scale-dependent action

$$\Gamma_k[\varphi] = \int d^d x \left\{ Z_k \partial_\nu^{\frac{\sigma}{2}} \varphi_i \partial_\nu^{\frac{\sigma}{2}} \varphi_i + U_k(\rho) \right\}, \tag{26}$$

where $\rho = \frac{1}{2}\varphi_i\varphi_i$ and the index $i = 1, \cdots, \mathcal{N}$ being summed over as in the previous section.

The ansatz in Eq. (26) is already sufficient to qualitatively clarify the influence of long-range interactions on the universal properties. Indeed, the difference between the bare action (25) and the effective action (26) is limited to the presence of the fractional derivative $\partial_\mu^{\frac{\sigma}{2}}$ into the kinetic term instead of the traditional ∇^2 term. The definition of the fractional derivative in the infinite volume limit (Kwaśnicki, 2017; Pozrikidis, 2016) leads to the straightforward result that its Fourier transform yields a fractional momentum term q^σ. The renormalization of such anomalous kinetic term q^σ is parametrised in Eq. (26) by a running wave-function renormalization Z_k as it is customary done in the short-range case (Dupuis *et al.*, 2020).

The actual subtlety of the weak long-range universality resides in the competition between the analytic momentum term q^2 and the anomalous one q^σ arising due to long-range interaction. Such effect cannot be properly reproduced by the ansatz in Eq. (26), which only includes the most relevant momentum term at the canonical level in the low energy behavior of long-range $O(\mathcal{N})$ models. Yet, Eq. (26) reveals to be a useful approximation to recover and extend the mean-field description of the problem at least in the limit $\sigma \ll 2$, where the non-analytic momentum term is certainly the leading one.

Close to the transition, the correlation length of the system, which controls the spatial extent of the correlations, $\langle\varphi(x)\varphi(0)\rangle \approx \exp(|x|/\xi)/x^{d-2}$, diverges as $\xi \propto \tau^{-\nu}$. Thus, the diverging critical fluctuations produce an anomalous scaling of the correlation functions via the presence of a finite anomalous dimension η. The standard definition used for short-range models (Nishimori and Ortiz, 2015) is

$$\langle\varphi(x)\varphi(0)\rangle \approx \frac{1}{|x|^{d-2+\eta}}. \tag{27}$$

Conventionally, we refer to a correlated universality when $\eta \neq 0$ and anomalous scaling appears. If one refers to the definition (27) of the decay of correlation functions in short-range systems, then the anomalous dimension of long-range model is already finite at mean-field level giving $\eta_{\rm lr} = 2 - \sigma$, due to the contributions of the power-law couplings to the scaling of the correlations (here and in the following the indices $_{\rm lr}$ and $_{\rm sr}$ stand for long- and short-range, respectively) . However, to have a proper account of correlation effects, it is convenient to re-define the anomalous dimension $\eta_{\rm lr}$ of the long-range $O(\mathcal{N})$ models as follows

$$\eta_{\rm lr}(d,\sigma) \equiv 2 - \sigma + \delta\eta\,, \tag{28}$$

with respect to the canonical dimension of the long-range terms, in agreement with the definition in the classic paper (Fisher *et al.*, 1972).

Therefore the low-momentum scaling of the critical propagator shall become $G(q)^{-1} \approx q^{\sigma-\delta\eta}$. Within the RG formalism such correction $\delta\eta$ is expected to appear as a divergence of the wave-function renormalization, which signals the rise of a modified scaling. Yet, the β-function of the wave-function renormalization for the fractional momentum term identically vanishes ($k\,\partial_k Z_k = 0$) for any d and σ, at least in the approximation parameterized by Eq. (26). Therefore, the correlated correction for long-range interactions vanishes

$$\delta\eta = 0,$$

a result first obtained by J. Sak in 1973 (Sak, 1973). The flow of the effective potential remains the only non-trivial RG evolution for the ansatz in Eq. (26).

Similarly to the wave-function flow, the RG evolution of the effective potential $U_k(\rho)$ has been obtained following the traditional derivative expansion approach of the

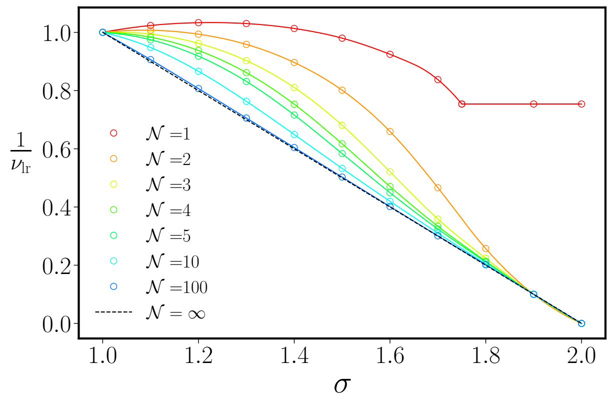

Figure 9 **Classical correlation length exponent**. Correlation length exponent $1/\nu_{\rm lr}$ as a function of σ in $d = 2$ for several values of $\mathcal{N}$ (from top: $\mathcal{N} = 1, 2, 3, 4, 5, 10, 100$). The discrepancy between the $\mathcal{N} = 1$ and the $\mathcal{N} \geq 2$ cases is in agreement with the expectations of the Mermin-Wagner theorem. The black dashed line is the analytical result obtained for the spherical model $\mathcal{N} = \infty$ (Joyce, 1966). Adapted from Ref. (Defenu *et al.*, 2015).

FRG (Delamotte, 2011) by introducing a suitable regulator function $R_k(q) = Z_k(k^\sigma - q^\sigma)\theta(k^\sigma - q^\sigma)$. The resulting β-function for the effective potential reads

$$\partial_t \bar{U}_k = -d\bar{U}_k(\bar{\rho}) + (d-\sigma)\bar{\rho}\,\bar{U}_k'(\bar{\rho}) + \frac{\sigma}{2}c_d(N-1)\frac{1}{1+\bar{U}_k'(\bar{\rho})} + \frac{\sigma}{2}c_d\frac{1}{1+\bar{U}_k'(\bar{\rho})+2\bar{\rho}\,\bar{U}_k''(\bar{\rho})}\,, \tag{29}$$

with $c_d^{-1} = (4\pi)^{d/2}\Gamma\left(d/2+1\right)$ and as usual in RG calculations we set $t = \log(k/\Lambda_{uv})$ as the RG time, with Λ_{uv} the ultra-violet scale, typically $\sim 1/a_{\rm latt}$. In Eq. (29) rescaled units are as well used: $\bar{\rho} = Z_k k^{\sigma-d}\rho$ and $U_k(\bar{\rho}) = k^{-d}U_k(\rho)$.

1. Competing momentum contributions

The determination of the threshold decay exponent σ_* represents one of the most fascinating questions in the study of weak long-range universality. Its value is the result of a subtle interplay between different momentum terms in the critical propagator and of their contribution to the universal behavior. In particular, the question concerns the renormalization of the long-range (p^σ) term and its effect on the (p^2) one.

The first answer to this question was given in Ref. (Fisher *et al.*, 1972) by a second-order ε-expansion approach. This analysis suggested that the mean-field result $\eta = 2 - \sigma$ holds at all orders in perturbation theory with respect to the parameter $\varepsilon = 2\sigma - d$, a result later extended by Ref. (Honkonen, 1990). The conclusion of this study implied a discontinuity of the anomalous dimension η as a function of the parameter σ, when σ reaches $\sigma_* = 2$, the mean-field prediction for σ_* (Fisher *et al.*, 1972). The discontinuity issue was later solved by the inclusion of both non-analytic p^σ and analytic p^2 terms in the propagator, see Ref. (Sak, 1973), which confirmed the result $\eta = 2 - \sigma$, but found a different threshold value

$$\sigma_* = 2 - \eta_{\rm sr}.$$

Most Monte Carlo (MC) investigations, featuring specific algorithms for long-range interactions (Fukui and Todo, 2009; Gori *et al.*, 2017; Luijten and Blöte, 1997), appear to be in agreement with the Sak's scenario ($\sigma_* = 2 - \eta$) (Angelini *et al.*, 2014; Gori *et al.*, 2017; Horita *et al.*, 2017; Luijten and Blöte, 2002). Nevertheless, up to very recent times, several different theoretical pictures have been compatible with the $\sigma_* = 2$ result (Blanchard *et al.*, 2013; van Enter, 1982; Grassberger, 2013; Picco, 2012; Suzuki, 1973; Yamazaki, 1977). Recently, conformal bootstrap results (Behan *et al.*, 2017) confirmed Sak's scenario and, albeit not giving numerical estimates for the long-range critical exponents, furnished a rigorous framework for its understanding. A detailed study of RG fixed points in a model of symplectic fermions with a nonlocal long-range kinetic term is reported in (Giuliani *et al.*, 2021).

In the framework of the FRG approach, the absence of the analytic term in Eq. (26) makes the aforementioned approximation not suitable to properly investigate the $\sigma \simeq \sigma_*$ regime, where the momentum terms interplay is crucial. A more complete parametrization, which accounts for the leading and first sub-leading term in the expansion of the mean-field propagator, has been introduced in (Defenu *et al.*, 2015).

The flow equations obtained in Ref. (Defenu *et al.*, 2015) yield the following picture: when a fixed point can emerge for non-vanishing long-range coupling $J_\sigma \neq 0$ this implies $\eta = 2 - \sigma$. Therefore, the fixed point value for the long-range coupling J_σ^* has to be such that the short-range momentum term in the propagator is renormalized with $\eta = 2 - \sigma$. Such solution is only possible for $d/2 < \sigma < 2 - \eta_{\rm sr}$, consistently with Sak's scenario, where $\eta = 2 - \sigma$. Therefore, while at the short-range fixed point the long-range coupling vanishes $J_\sigma = 0$, at the long-range one the short-range momentum term does not vanish, but its scaling dimension is increased to match the one of the long-range terms. This complex structure demonstrates that the effective dimension approach described for the long-range spherical model in Ref. (Joyce, 1966) – i.e. that the critical properties of a long-range system are the same of the corresponding short-range model, but in a higer dimension – apparently does not hold in the interacting case, as the critical propagator of the long-range universality class features a multiple power-law structure, already noticed in MC simulations (Angelini *et al.*, 2014), which is absent in the short-range case, see also the discussion in Refs. (Defenu *et al.*, 2015, 2016, 2017b).

The final summary for the universality picture for weak long-range ferromagnetic interactions is the following:

- for $\sigma \leq d/2$ the mean-field approximation correctly describes the universal behavior;
- for σ greater than a threshold value, $\sigma_* = 2 - \eta_{\rm sr}$, the model has the same critical exponents as the short-range model (the local, short-range model is strictly defined as the limit $\sigma \to \infty$);
- for $d/2 < \sigma \leq \sigma_*$ the system exhibits peculiar long-range critical exponents, which may be approximated by the ones of the short-range model in the effective fractional dimension $d_{\rm eff} = (2 - \eta_{\rm sr})d/\sigma$.

These results, albeit obtained in the approximated framework of the derivative expansion, see Ref. (Defenu *et al.*, 2015), appear to hold also for the full theory and the result $\eta = 2 - \sigma$ has now been established with multiple techniques (Behan *et al.*, 2017; Defenu *et al.*, 2015; Gori *et al.*, 2017; Horita *et al.*, 2017). In the FRG context, the validity of the Sak's scenario has been confirmed also for long-range disordered systems (Balog *et al.*, 2014).

The approximate nature of the effective dimension approach described in Ref. (Defenu *et al.*, 2015) shall not hinder its adoption to compute numerical estimates for the critical exponents. Indeed, the actual correction, rising from analytical contributions to the critical propagator, appears to be rather small and the application of the effective dimension approach produced rather accurate theoretical benchmarks for MC data, both in the long-range Ising and percolation models, see Fig. 10.

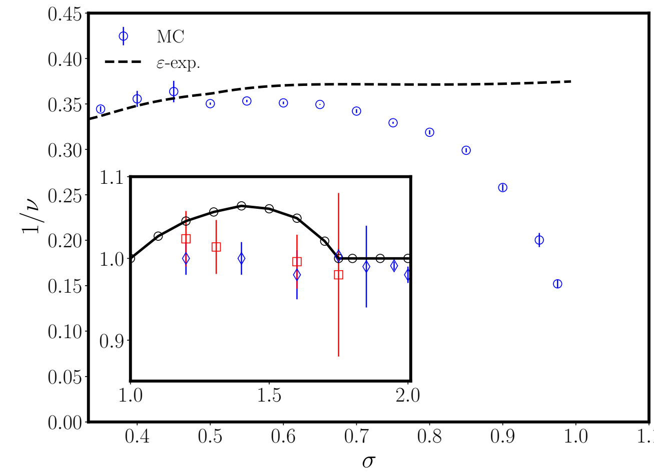

Figure 10 **Inverse correlation length exponent of long-range interactions.** Reults obtained from MC simulations for 1D long-range percolation are compared with the results of the effective dimension approach. The MC data of Ref. (Gori *et al.*, 2017) (empty blue circles) are compared with the results obtained using an effective dimension and the ε-expansion result (black dashed line) for the short-range model (Gracey, 2015). The low accuracy of the analytical result in the $\sigma \to 1$ limit is due to the appearance of BKT scaling (Cardy, 1999), which cannot be captured by the ε-expansion. **(Inset)** MC simulations for the long-range Ising model in $d = 2$ in Refs. (Angelini *et al.*, 2014; Luijten and Blöte, 1997) (blue diamonds and red squares respectively). The black circles have been obtained by mapping the conformal bootstrap results for the short-range critical exponents (El-Showk *et al.*, 2014) via the effective dimension approach described in Ref. (Defenu *et al.*, 2015). The axis labels of the inset coincide with main axis labels.

2. Berezinskii-Kosterlitz-Thouless scaling

For short-range interacting models with continuous symmetry, the occurrence of spontaneous symmetry breaking (SSB) in $d = 2$ is forbidden by the Mermin-Wagner theorem (Hohenberg, 1967; Mermin and Wagner, 1966). Yet, the inclusion of long-range interactions with $0 < \sigma < \sigma_*$ modifies the scaling dimension of operators, allowing SSB also in low dimensions. The effect of such altered scaling is conveniently summarised by the effective dimension approach, which consists in the possibility for a long-range interacting system in d dimensions to reproduce, at least approximately, the scaling of any $d_{\rm eff}$-dimensional short-range system with $d_{\rm eff} \in [d, \infty]$.

Given these considerations, it is not difficult to generalise the results of the Mermin-Wagner theorem to long-range interactions (Bruno, 2001), leading to the vanishing of the inverse correlation length exponent in the $\sigma \to 2$ limit for $\mathcal{N} \geq 2$, see Fig. 9. Then, for $d = \mathcal{N} = \sigma = 2$ the traditional picture for short-range models is recovered and the Berezinsky-Kosterlitz-Thouless (BKT) scenario shall occur (José, 2013; Kosterlitz, 1974; Kosterlitz and Thouless, 1973).

BKT scaling is a characteristic of two-dimensional systems, ranging from condensed matter (Nelson and Kosterlitz, 1977; Yong *et al.*, 2013) and cold atoms (Hadzibabic *et al.*, 2006; Murthy *et al.*, 2015) to network theory (Dorogovtsev *et al.*, 2008) and biology (Nisoli and Bishop, 2014). Its most renown realization is certainly the XY model, where its properties have been very well characterised (Gupta and Baillie, 1992; Gupta *et al.*, 1988; Hasenbusch *et al.*, 1992) and its relation with topological excitations first discovered (Kosterlitz, 2017).

Yet, first theoretical indications of this topological phase transition have occurred in long-range interacting classical systems (Thouless, 1969). In particular, the Coulomb gas problem and the Ising model with $d = \sigma = 1$ have been known to display such infinite order transition, well before its traditional formulation (Anderson and Yuval, 1969; Anderson *et al.*, 1970). This fact shall not surprise, since for $d = \sigma = 1$ the scaling dimension of the operators is consistent with the one of short-range interactions in $d = 2$. Understanding in detail the difference between the number of degrees of freedom in the traditional short-range BKT scaling with $d = \mathcal{N} = 2$ and the long-range one occurring for $d = \mathcal{N} = \sigma = 1$ is a more complicated and possibly open task, but it is probably related to the irrelevance of amplitude fluctuations in $d = 2$ (Defenu *et al.*, 2017a; Jakubczyk and Metzner, 2017; Krieg and Kopietz, 2017). It is worth noting that long-range BKT scaling occurring in $d = \sigma = 1$ does not only occur in the Ising model, but also for long-range percolation and Potts models (Cardy, 1999; Gori *et al.*, 2017).

Despite this long-lasting relation between BKT scaling and long-range interactions, the influence of power-law couplings on topological scaling has been the subject of a very limited amount of research so far. Indeed, the applicability of the aforementioned threshold value $\sigma_* = 2 - \eta_{\rm sr}$ to BKT scaling seems questionable, since the anomalous dimension of two-point correlations in $d = \mathcal{N} = 2$ does not originate from critical fluctuations, but from long wave-length phase fluctuations, which disrupt the zero-temperature magnetization. Interestingly, long-range interactions with $\sigma < 2$ can be mathematically proven to stabilise spontaneous magnetization in the 2D XY model (Kunz and Pfister, 1976), implicitly suggesting that $\sigma_* = 2$. On the other hand, early results concerning the XY model on diluted Lévy graphs (Berganza and Leuzzi, 2013), which has been conjectured to lie in the same universality class of the long-range XY model, appeared to be consistent with $\sigma_* = 2 - \eta_{\rm sr}$. However, these results, have been recently challenged (Cescatti *et al.*, 2019). Moreover, self-consistent harmonic approximation results give an upper bound for σ_* equal to 2 (Giachetti *et al.*, 2021b). No MC results for the 2D XY with (non-disordered) power-law long-range couplings around $\sigma = 2$ are available, to the best of our knowledge.

Extending the RG approach first employed by Kosterlitz (Kosterlitz, 1974), in a recent paper (Giachetti *et al.*, 2021a), it has been possible to propose a scenario of the complex phase diagram of the $d = 2$ long-range XY model, which features a novel transition between a low-temperature magnetized state ($T < T_*$) and an intermediate temperature state with topological scaling ($T_* < T < T_c$), which disappears at higher temperatures ($T > T_c$). Interestingly, this unexpected transition only occurs for $2 - 1/4 = 7/4 < \sigma < 2$, while for $\sigma \geq 2$ one has only two phases separated by a BKT transition, as in the short-range 2D XY model.

Thus, the introduction of long-range interaction patterns in systems with $U(1)$ symmetry in $d = 2$ generates exotic critical features, which have no counterpart in the traditional universality classification (Raju *et al.*, 2019). This is not surprising since the interplay between $U(1)$ systems and complex interaction patterns is known to generate peculiar critical behaviour as in the anisotropic 3D XY model (Shenoy and Chattopadhyay, 1995), coupled XY planes (Bighin *et al.*, 2019), 2D systems with anisotropic dipolar interactions (Maier and Schwabl, 2004; Vasiliev *et al.*, 2014) or four-body interactions (Antenucci *et al.*, 2015), and high-dimensional systems with Lifshitz criticality (Defenu *et al.*, 2021; Jacobs and Savit, 1983).

B. Strong long-range regime

1. Ensemble in-equivalence

The traditional universality problem concerns the numerical characterization of universal quantities, in the strongly correlated regime, where long-range collective correlations are relevant and mean-field, as well as other perturbative techniques, cannot be applied. Such questions have no actual application to the case of long-range interactions with $\sigma < 0$, i.e. $\alpha < d$, since the divergent interaction strength stabilizes the mean-field solution of the problem and the Gaussian theory reproduces the universal features also at the critical point.

Nevertheless, several interesting effects arise due to strong long-range interactions, in the thermodynamic behavior of statistical mechanics models. These effects may be loosely regarded as universal since they appear irrespectively of the particular model considered, as well as irrespectively of the introduction of any finite-range couplings, and they may be often characterized starting from a continuous description (Antoniazzi *et al.*, 2007; Bachelard *et al.*, 2011).

At equilibrium, the most striking feature of systems in the strong long-range regime is probably ensemble in-equivalence, i.e. the appearance of substantial differences in the phase diagram of strong long-range systems depending on the application of the micro-canonical or the canonical thermodynamic descriptions (Barré *et al.*, 2001). This property has been extensively revised in several review articles and books on the physics of classical long-range systems (Campa *et al.*, 2014; Campa *et al.*, 2009; Dauxois *et al.*, 2002) and there is no need to discuss it here, in detail. For the sake of the following discussion, we are only going to briefly mention the existence of two diverse issues of ensemble in-equivalence.

The first example of ensemble in-equivalence is found in systems with long-range attractive or antiferromagnetic interactions, which feature a two-phase coexistence state. Such coexistence states are usually connected with a ‘dip’ or a ‘convex intruder’ in an otherwise concave entropy, possibly leading to a negative specific heat. The phase boundary associated with such coexistence states carries an infinite entropy cost, which makes them unstable in the canonical ensemble. On the other hand, in the micro-canonical description, such entropy cost is not relevant and such equilibrium states may be realized by tuning the energy (Dauxois *et al.*, 2002; Ispolatov and Cohen, 2001; Lynden-Bell, 1999). Interestingly, the same phenomenon is observed on sparse random graphs, where the condition of a negligible surface in the thermodynamic limit is violated (Barré and Gonçalves, 2007).

The second example of ensemble in-equivalence is conventionally found in long-range systems with a two parameter-dependent free-energy $S(\varepsilon, \lambda)$, which present a line of second-order critical points along a line $\varepsilon_c(\lambda)$, terminating at a tricritical point at λ_c. The location of such tricritical point, as well as the structure of the first-order lines beyond it, strongly depend on the thermodynamic ensemble considered. In particular, the microcanonical description as a function of the temperature $1/T = \partial S/\partial\varepsilon$ does not match the standard canonical description as it should be for short-range interacting systems (Barré *et al.*, 2001).

It is worth noting that the "convex intruder" causing the first case of ensemble inequivalence is not exclusive of long-range interacting systems, but it is also present on short-range systems with finite sizes, where the boundary contribution is comparable to the one from the finite bulk (Ispolatov and Cohen, 2001). This feature is then washed away in the thermodynamic limit for short-range systems, while it remains for strong long-range ones.

2. Violation of hyperscaling

Apart from ensemble in-equivalence, the relevance of boundaries in the scaling theory of strong long-range systems produces several anomalies, which influence the understanding of their critical behavior. In particular, let us comment on the usual finite-size scaling theory, which relates the thermodynamic critical exponent of any quantity, e.g. the susceptibility

$$\chi \propto |T - T_c|^{-\gamma} \tag{30}$$

with its finite-size correction (Cardy, 1996)

$$\chi_N \propto N^{\gamma/\nu}, \tag{31}$$

where the subscript N indicates the corresponding quantity in a system of size N. In long-range systems, the correspondence between thermodynamic exponents and finite-size scaling ones is not obtained via the correlation length exponent ν, but via an exponent $\nu_* = \nu_{\rm mf} d_{\rm uc}$, where $\nu_{\rm mf}$ and $d_{\rm uc}$ are respectively the mean-field correlation length exponent and the upper critical dimension of the corresponding short-range system (Botet *et al.*, 1982).

Such modification of finite size scaling theory has been related to the violation of hyperscaling and, more in general, to a non-trivial power-law scaling of the correlation length ξ with the system size N (Flores-Sola *et al.*, 2015), leading to several anomalous differences between the actual finite-size scaling of strong long-range systems and the mean-field solution (Colonna-Romano *et al.*, 2014). These observations are not peculiar of strong long-range systems, but have been also found in the study of critical phenomena in short-range systems above the upper critical dimension (Binder, 1985; Flores-Sola *et al.*, 2016a; Luijten and Blöte, 1996).

C. Competing non-local systems

Modulated phases, resulting from the competition of interactions at different length scales, are ubiquitous in nature (Seul and Andelman, 1995) and also display universal scaling close to their critical points. Despite this ubiquity, a comprehensive description of their universal behavior has not emerged yet and their understanding is apparently behind the one of homogeneous phase transition. A convenient effective action for modulated phases has been firstly introduced by Brazovskii (Brazovskii, 1975) and it reads

$$S[\varphi] = \frac{1}{2}\int \frac{d^d q}{(2\pi)^d}\vec{\varphi}(q)\left(\lambda + \frac{(q-q_0)^2}{m}\right)\vec{\varphi}(q) + u\int d^d x \frac{|\vec{\varphi}(x)|^4}{4!} \tag{32}$$

where $\varphi(q)$ is the Fourier transform of $\varphi(x)$, which is a $\mathcal{N}$-components vector field, $q = |\vec{q}|$ is the momentum amplitude and q_0 a constant given by the nature of competing interactions. In writing Eq. (32) we assumed that the long-range tails of the interactions are not relevant ($\alpha > \alpha_*$).

The system described by the Hamiltonian in Eq. (32) represents a different paradigm with respect to the ordinary $\mathcal{N}$-vector models. Indeed, the Hamiltonian in Eq. (32) for $\lambda < 0$ supports a condensate with any of the finite wave-vectors occurring on the $d-1$-dimensional sphere $|\vec{q}| = q_0$. Therefore, the condensed phase of the model is somehow "doubly" symmetry-broken, since the model does not only choose the $i = 1$ component of the field in which it condenses, but must also make a single choice for the wave-vector $\vec{q} = \vec{q}_0$, out of the infinite set of equivalent order parameters with $|\vec{q}| = q_0$. The diversity in the symmetry breaking procedure also reflects in different phase space for fluctuations, since the d-dimensional phase space around the $|\vec{q}| = q_0$ surface is anisotropic, with fluctuations parallel to the surface, which are exactly degenerate, and fluctuations away from it, which are only nearly degenerate. This discussion should have clarified that the Brazovskii model in Eq. (32) does not belong to any of the usual universality classes of isotropic models and presents its own set of universal properties as a function of the parameters $\mathcal{N}$ and d.

Interesting applications of the physics described by the Brazovskii model occur in two dimensional or highly anisotropic systems, such as quantum Hall platforms (Fradkin and Kivelson, 1999), high T_c superconductors (Kivelson *et al.*, 2003, 1998) and ultra-thin magnetic films (Kashuba and Pokrovsky, 1993; Saratz *et al.*, 2010; Vaterlaus *et al.*, 2000). Nevertheless, the first efforts to apply the momentum shell renormalization group theory (Wilson and Kogut, 1974) to the Hamiltonian in Eq. (32) with $d = 2$ resulted in the impossibility to construct a reliable perturbative picture (Hohenberg and Swift, 1995). Applying the RG approach described by Shankar for fermionic systems (Shankar, 1994), Hohenberg and Swift (Hohenberg and Swift, 1995) found out that momentum dependent corrections to the interacting coupling u are relevant and no weak coupling expansion is possible in the treatment of modulated phases. Nevertheless, a symmetry analysis of these relevant corrections suggests the appearance of a second-order nematic-isotropic transition (Barci and Stariolo, 2007). Similar difficulties have been encountered by more modern treatments (Shiwa, 2006) and the description of systems belonging to the Brazovskii universality has remained confined to mean-field theory (Barci *et al.*, 2013; Barci and Stariolo, 2007; Capati *et al.*, 2015), scaling arguments (Barci and Stariolo, 2009, 2011; Mendoza-Coto and Stariolo, 2012; Portmann *et al.*, 2010) and numerical simulations (Cannas *et al.*, 2006; Poderoso *et al.*, 2011).

Recently, the study of the nematic-isotropic transitions in the Brazovskii model has been extended beyond the analytic momentum paradigm in Eq. (32) to include long-range repulsive interactions of the form $1/r^{\alpha'}$, with particular focus on the Coulomb ($\alpha' = 1$) and dipolar ($\alpha' = 3$) cases (Mendoza-Coto *et al.*, 2015b). It is particularly interesting to note that, within the effective field theory approach of Ref. (Mendoza-Coto *et al.*, 2015b), it is possible to show the exact correspondence between the universality of the nematic-isotropic transition and the one of homogeneous rotor models at finite temperature with decay exponent $\alpha = \alpha' + 2$ (Mendoza-Coto *et al.*, 2017). Therefore, for modulated phases in $d = 2$, the relevant regime for long-range interactions is rigidly shifted in such a way that any power-law decay $\alpha' > 2$ is always irrelevant, while for $\alpha' < 2$ the interaction energy remains finite also in absence of any rescaling, due to the modulation pattern of the order parameter.

Within this framework, the scalar φ^4-theory with competing long-range and short-range interactions lies in the same universality class of the long-range ferromagnetic $O(2)$ model with $\sigma = \alpha'$ (Mendoza-Coto *et al.*, 2015b), described in Sec. III.A. Therefore, for $\alpha' > 2$ the isotropic nematic transition displays in d=2 BKT scaling as in the short-range XY model, while for $\alpha' < 2$ actual orientational order shall occur. Given this relation, one expects that for $\alpha' \in [1.75, 2]$ the same phenomenology described in Sec. III.A.2 shall occur.

IV. QUANTUM CRITICAL BEHAVIOUR

Our discussion of zero-temperature criticality starts by observing that field theory approaches allow to relate the universal behavior at a $T = 0$ quantum critical point with the one of the corresponding $T \neq 0$ classical phase transition in dimension $d + z$, where z is the dynamical critical exponent (Sachdev, 1999). This correspondence is exact for local, continuous $O(\mathcal{N})$ field theories with $z = 1$ and it can also be proven for the one-dimensional lattice Ising model in a transverse field (Dutta *et al.*, 2015; Mussardo, 2009). Thus, it will be rather natural to connect, whenever possible, the universal behavior in the quantum regime with the one of finite-temperature phase transitions also for long-range models.

In the following, we are going to divide our presentation according to the nature of the variables at hand.

A. Quantum rotor models

Given the correspondence between quantum and classical universalities, $O(\mathcal{N})$ field theories constitute a paradigmatic model also for quantum critical behavior. However, differently from the classical case, they do not describe in general the universality of ferromagnetic quantum spin systems, since quantum spins possess $SU(\mathcal{N})$ rather than $O(\mathcal{N})$ symmetry. Nevertheless, the low energy behavior of quantum $O(\mathcal{N})$ models describes the physics of several quantum models, such as the quantum Ising model, $\mathcal{N} = 1$; superfluid systems, $\mathcal{N} = 2$; and antiferromagnetic quantum Heisenberg spin systems, which correspond to $\mathcal{N} = 3$ (Sachdev, 1999).

In this context, a convenient lattice representation of quantum $O(\mathcal{N})$ field theories is provided by quantum rotor models, whose Hamiltonian reads

$$H_{\mathrm{R}} = -\sum_{ij} \frac{J_{ij}}{2} \hat{\boldsymbol{n}}_i \cdot \hat{\boldsymbol{n}}_j + \frac{\lambda}{2} \sum_i \hat{\mathcal{L}}_i^2, \tag{33}$$

where the $\hat{\boldsymbol{n}}_i$ are n components unit length vector operators ($\hat{\boldsymbol{n}}_i^2 = 1$), λ is a real constant and $\mathcal{L}$ is the invariant operator formed from the asymmetric rotor space angular momentum tensor (Sachdev, 1999). As above, we are going to focus on power-law decaying ferromagnetic couplings $J_{ij} = \frac{J}{r_{ij}^{d+\sigma}}$ with $J > 0$.

In the short-range limit ($\sigma \to \infty$) the continuum formulation of quantum $O(\mathcal{N})$ rotor models would exactly correspond to a $d+1$-dimensional $O(\mathcal{N})$ field theory, with the extra dimension representing the temporal propagation of quantum fluctuations. However, in the long-range regime the field theory action is anisotropic as the spatial coordinates feature a leading non-analytic momentum term, at least for $\sigma < \sigma_*$. Following the same FRG approach as in Sec. III.A, one can introduce the following ansatz for the effective action of an $O(\mathcal{N})$ quantum rotor model

$$\Gamma_k = \int d\tau \int d^d x \{K_k \partial_\tau \varphi_i \partial_\tau \varphi_i - Z_k \varphi_i \Delta^{\frac{\sigma}{2}} \varphi - Z_{2,k} \varphi_i \Delta \varphi + U_k(\rho)\} \quad (34)$$

where Δ is the spatial Laplacian in d dimensions, τ is the "Trotter"/imaginary time direction, $\varphi_i(x)$ is the i-th component ($i \in \{1, \cdots, n\}$) of the system and $\rho \equiv \sum \frac{\varphi_i^2}{2}$ is the system order parameter. In Eq. (34) the summation over repeated indices is again intended.

It is worth reminding that the ansatz in Eq. (34) for the effective action, albeit sufficient to characterize the physics of long-range rotor models, it only approximately represents the exact critical action of correlated models. Indeed, it only contains two kinetic terms in the d spatial directions, as necessary to represent the competition between long-range and short-range contributions to the critical propagator, but it does not contain momentum-dependent corrections to the theory vertices (Dupuis *et al.*, 2020). As expected, the time direction τ does not contain any fractional derivative so that one may obtain a non-unity value for the dynamical critical exponent z, defined by the relation $\omega \propto q^z$.

1. Effective dimension approach

The characterisation of the critical properties of the action in Eq. (34) proceeds in full analogy with the case of classical anisotropic systems (Defenu *et al.*, 2016), but it leads to a far more interesting picture. Scaling analysis allows to approximately relate the universal properties of long-range quantum rotor models in d dimensions with the ones of their short-range correspondents in an effective dimension

$$d_{\text{eff}} = \frac{2(d+z)}{\sigma}, \quad (35)$$

where d and z are respectively the dimension and the dynamical critical exponent of the long-range model under study. Interestingly, the anisotropy between the time and spatial direction in the long-range model is already apparent in the mean-field estimations for the critical exponents (Dutta and Bhattacharjee, 2001a; Monthus, 2015)

$$\eta = 2 - \sigma, \quad (36)$$

$$z = \frac{\sigma}{2}, \quad (37)$$

$$\nu = 1/\sigma. \quad (38)$$

Upon inserting the result in Eq. (37) into the effective dimension relation in Eq. (35) one obtains the mean-field expression $d_{\text{eff}} = \frac{2d}{\sigma} + 1$, which proves that the effective dimension of quantum rotor models is increased by 1 with respect to the classical case, as it occurs for traditional short-range systems.

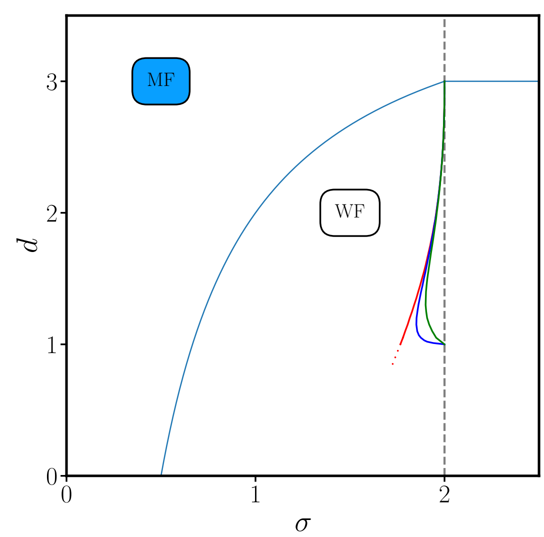

Figure 11 **Phase diagram of long-range quantum rotors models in the plane d, σ.** The universal behaviour features the mean-field critical exponents in Eqs. (36), (37) and (38) in the cyan shaded region (upper left corner), while the universal properties are associated to an interacting Wilson-Fisher (WF) point in the white region. The color lines (red, blue, green) represent the boundary between long-range and short-range universality ($\mathcal{N} = 1, 2, 3$ from left to right respectively). Finally, the gray shaded region (lower right corner) displays no phase transition at all.

The correspondence between quantum and classical $O(\mathcal{N})$ models based on the effective dimension approach in Eq. (35) exactly applies to quadratic models in general (Vojta, 1996) and it is expected to be very good close to the upper critical dimension. Then, we can employ the effective dimension approach to construct the phase diagram displayed in Fig. 11. Indeed, the upper critical dimension result d_{uc} can be derived by the condition $d \geq 4$, so that

$$d_{\text{uc}} = \frac{3}{2}\sigma, \quad (39)$$

as it follows also by standard scaling arguments (Dutta and Bhattacharjee, 2001b). Correspondingly, the lower critical dimension d_{lc} for continuous symmetries $\mathcal{N} \geq 2$ follows from the condition $d_{\text{eff}} \leq 2$, which yields

$$d_{\text{lc}} = \frac{\sigma}{2}. \quad (40)$$

It is worth stressing once again that relation (40) is only valid for continuous symmetries $\mathcal{N} \geq 2$. As a result, correlated universality shall be observed in the region $2 \leq d_{\text{eff}} < 4$, i.e. the cyan shaded region in Fig. 11. Therefore, the critical exponents do not coincide with the mean-field result and we need to take into account the effective potential in Eq. (34).

2. Beyond mean-field critical exponents

The study of the action in Eq. (34) closely follows the classical case, as the same mechanism is found for the transition between the long-range and the short-range universality which occurs at $\sigma_* = 2-\eta_{\rm sr}$ as in the classical case. For $\sigma > \sigma_*$ the effective action of quantum rotors models is isotropic and analytic in the momentum sector, then its flow equations are identical to the ones in the classical $d+1$ case (Codello *et al.*, 2015). For $\sigma < \sigma_*$ however the anisotropy between spatial and imaginary time dimensions produces novel flow equations for the effective potential and the wave-function renormalization K_k:

$$\partial_t \bar{U}_k = (d+z)\bar{U}_k(\bar{\rho}) - (d+z-\sigma)\bar{\rho}\,\bar{U}'_k(\bar{\rho}) - \frac{\sigma}{2}(N-1)\frac{1-\frac{\eta_\tau z}{3\sigma+2d}}{1+\bar{U}'_k(\bar{\rho})} - \frac{\sigma}{2}\frac{1-\frac{\eta_\tau z}{3\sigma+2d}}{1+\bar{U}'_k(\bar{\rho})+2\bar{\rho}\,\bar{U}''_k(\bar{\rho})}, \tag{41}$$

$$-\frac{\partial_t K_k}{K_k} = \eta_\tau = \frac{f(\tilde{\rho}_0, \tilde{U}^{(2)}(\tilde{\rho}_0))(3\sigma+2d)}{d+(3\sigma+d)(1+f(\tilde{\rho}_0,\tilde{U}^{(2)}(\tilde{\rho}_0)))}. \tag{42}$$

In the derivation of Eqs. (41) and (42), analytic terms in the spatial direction are discarded (Defenu *et al.*, 2017b), setting $Z_{2,k} = 0$ in Eq. (34), as their contributions to the RG running of other quantities remain very small up to $\sigma \simeq \sigma_*$, see the discussion in Sec. III.A.1.

Interestingly, the numerical study of quantum long-range $O(\mathcal{N})$ models appears to be more extended in literature than the classical case. Numerical simulations both for the quantum long-range Ising and $O(2)$ rotor models have been performed, yielding numerical curves for both the critical exponents z and ν, while confirming the mean-field result $\eta = 2-\sigma$ also in the correlated regime (Sperstad *et al.*, 2012). Fig. 12 compares the numerical estimates obtained by the flow Eqs. (41) and (42) using the solution approach described in Refs. (Codello *et al.*, 2015; Defenu *et al.*, 2015) with the results from MC simulations of Ref. (Sperstad *et al.*, 2012).

In Fig. 12 (upper panel) the dynamical critical exponent z is reported as a function of σ in $d = 1$. These numerical results have been obtained solving Eqs. (41), (42) at the fixed points and studying their stability matrix accordingly, as described in Refs. (Codello *et al.*, 2015; Defenu *et al.*, 2015). The mean-field region $\sigma < \frac{2}{3}$ is not shown as it is exactly described by the analytical estimates in Eqs. (36), (37) and (38). Numerical results for $\sigma < 1/2$ deviating from the mean-field expectation have not been reported (Fey and Schmidt, 2016). The dynamical critical exponents of the transverse-field Ising model with long-range power-law interaction in the weak long-range regime have been derived in (Maghrebi *et al.*, 2017) up to the two-loop order within the renormalization group theory. Recent QMC simulation have shown substantial agreement with the behaviours displayed in Fig. 12 (Koziol *et al.*, 2021). It is worth noting that recent

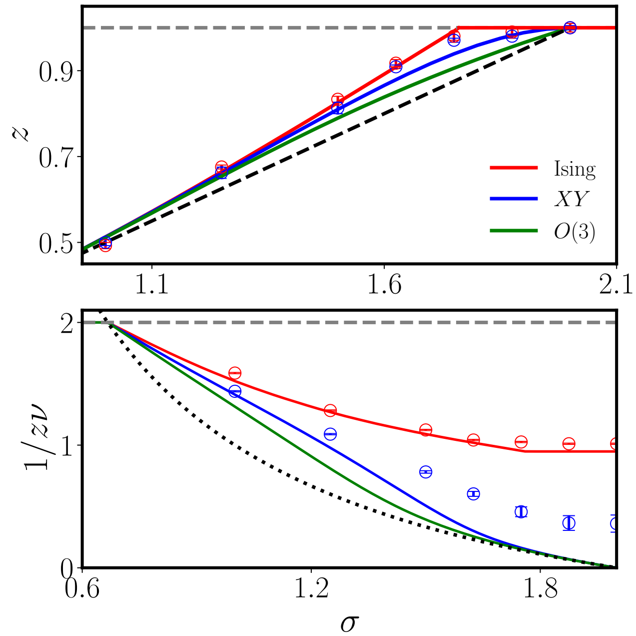

Figure 12 **Universal properties long-range quantum rotor models. (upper panel)** reports the estimates for the dynamical critical exponent $z = \sigma/(2-\eta_\tau)$ obtained by the fixed point solution of the evolution Eqs. (41) and (42) in the cases $\mathcal{N} = 1,2,3$ in red, blue and green (from top to bottom) respectively. **(lower panel)** reports the inverse correlation length exponent $\mathcal{N} = 1,2,3$ from top to bottom. The MC simulations in Ref. (Sperstad *et al.*, 2012) are shown as empty circles in the $\mathcal{N} = 1,2$ cases top (red) and bottom (blue) respectively. In both panels the upper grey dashed lines represent the mean-field results, while dashed lower black lines represent the spherical model ($\mathcal{N} = \infty$) results.

simulation have also targeted the finite temperature transition at $\alpha < d$ (Gonzalez-Lazo *et al.*, 2021), and the two-dimensional case (Fey *et al.*, 2019; Koziol *et al.*, 2019). Interestingly, non-local dissipation can act on Ising lattices molding the universality class of their critical points (Marino, 2021) and potentially realized and characterized in cavity experiments (Seetharam *et al.*, 2021).

Out of the mean-field region, correlation effects tend to increase the value of the dynamical critical exponent, increasing the gap with the analytic prediction in Eq. (37). This effect is mitigated for continuous symmetries $\mathcal{N} \geq 2$ due to the vanishing of the anomalous dimension at the short-range threshold $\sigma_* = 2$. Accordingly, the agreement between the FRG curves and the numerical MC results (red solid line and circles in Fig. 12) remains consistent in the whole σ range. On the other hand, the $\mathcal{N} = 2$ case displays overall poorer consistency, mostly due to the inaccuracy of MC estimates. Indeed, while the effective action parametrization in Eq. (34) proved unable to properly describe the continuous BKT line (Gräter and Wetterich, 1995), it consistently reproduces the scaling of critical exponents in the BKT limit (Codello *et al.*, 2015)[3].

The lower accuracy found for the $\mathcal{N}=2$ case is confirmed by the comparison of MC simulation for the correlation length estimates with the FRG curve (blue circles and line in Fig. 12). Indeed, the MC data provide a finite correlation length exponent in the limit $\sigma \to 2$ for the $O(2)$ model, in contradiction with rigorous analytical predictions from $d_{\rm eff}-2$ expansion (Brézin and Zinn-Justin, 1976). On the contrary, the FRG curve correctly reproduces the expected feature as it did in the classical case, see Fig. 9. Therefore, the flow Eqs. (41) and (42) yield all the qualitative features and reach quantitative accuracy for all values d, σ and N in the phase diagram of quantum long-range $O(\mathcal{N})$ models, producing nice accuracy with exact numerical simulations. The difficulties in the FRG characterization of the BKT transition (Gräter and Wetterich, 1995; Jakubczyk *et al.*, 2014; Jakubczyk and Metzner, 2017) appear not to be problematic in this case, as MC simulations are as well plagued by severe finite-size effects. Recent numerical results on the long-range XY model have been reported in (Adelhardt *et al.*, 2020).

An interesting fact is that the MC points in Fig. 12 appear to provide $\sigma_* = 2-\eta_{\rm sr}$ with $\eta = \frac{1}{4}$ also for $\mathcal{N}=2$, without any apparent distinction between the $\mathcal{N}=1$ and 2 cases. As already mentioned, this is in stark contradiction with the picture furnished by FRG, which suggests $\sigma_* = 2$ identically for all continuous symmetries. The correct picture is most likely in between, as suggested by the analysis pursued in Sec. III.A.2.

B. Kitaev chain

The introduction of long-range couplings in Fermi systems produces radically different results with respect to the bosonic case. The Kitaev chain (Kitaev, 2001) emerged as one of the most studied playgrounds in which effects of long-range terms have been investigated. In the fermionic context we will first consider the generalized Kac-normalized (Kac *et al.*, 1963) long-range Kitaev chain (Maity *et al.*, 2019). Its Hamiltonian reads

$$H = -\sum_{j=1}^{N}\sum_{r=1}^{R}\left(J_r c_j^\dagger c_{j+r} + \Delta_r c_j^\dagger c_{j+r}^\dagger + \text{H.c.}\right) \tag{43}$$

$$-h\sum_{j=1}^{N}\left(1-2c_j^\dagger c_j\right), \tag{44}$$

where

$$J_r = t\frac{d_r^{-\alpha}}{\mathcal{N}_\alpha}, \quad \Delta_r = g\frac{d_r^{-\beta}}{\mathcal{N}_\beta}, \tag{45}$$

are the hopping and pairing profiles, respectively, with hopping $t>0$ and normalization satisfying one of the two relations

$$\mathcal{N}_x = \begin{cases} \sum_{r=1}^{R} d_r^{-x}, & \text{Kac rescaling} \\ 1 & \text{otherwise,} \end{cases} \tag{46}$$

where R denotes the range of the interactions, d_r is the distance between the sites i and $i+r$, $x \equiv \alpha, \beta$ refer to the power-law exponents, h the chemical-potential strength, and $c_j, c_j^\dagger$ the fermionic annihilation and creation operators, which obey the canonical anti-commutation relations $\{c_l, c_j^\dagger\} = \delta_{l,j}$ and $\{c_l, c_j\} = 0$. In Eq. (46) we allowed both the possibility to implement Kac rescaling or to leave the couplings unscaled as in the literature both conventions are employed.

The definition of distance depends on the choice of the boundary conditions. So, a ring structure, i.e. closed boundary conditions, leads to the definition $d_r = \min(r, L-r)$, while open boundary conditions simply produce $d_r = r$. Conventionally, (anti)periodic boundary conditions allow the straightforward analytical solution of the problem in the short-range limit. Yet, long-range couplings extending over the whole chain length will lead to the cancellation of the hopping (pairing) operators for anti-periodic (periodic) boundary conditions, due to the anti-commutation relations (Alecce and Dell'Anna, 2017). This issue justifies the introduction of a finite interaction range R into the Hamiltonian in Eq. (43).

In the following we are going to mainly discuss the ring convention with $d_r = \min(r, L-r)$ and fix $R = L/2-1$, where L is the number of sites in the ring chain. This choice allows us to adequately deal with ring boundary conditions, but still obtain a non-trivial thermodynamic limit $L\to\infty$, where the couplings display infinite-range tails. One can thus introduce the Fourier transform

$$c_j = \frac{1}{\sqrt{L}}\sum_{k}^{\text{B.z.}} c_k e^{ikj}, \tag{47}$$

where the sum is over the first Brillouin zone. On a finite ring the values of the momenta have to be chosen in order to comply with periodic ($k = \frac{2\pi n}{L}$) or anti-periodic ($k = \frac{2\pi(n+1/2)}{L}$) boundary conditions. The Hamiltonian in momentum space reads

$$H = \sum_{k}^{\text{B.z.}}\left[(c_k^\dagger c_k - c_{-k}c_{-k}^\dagger)(h-J_k) + (c_k^\dagger c_{-k}^\dagger - c_k c_{-k})\Delta_k\right], \tag{48}$$

[3] It is worth noting that the power-law scaling of BKT correlations originates from phase correlations and does not contradict the vanishing of the anomalous dimension defined according to Eq. (42) (Defenu *et al.*, 2017a).

where the momentum space couplings have been obtained by Fourier transforming J_r and Δ_r:

$$J_k = \frac{t}{\mathcal{N}_\alpha} \sum_{r=1}^{R} \frac{\cos(kr)}{r^\alpha}, \tag{49}$$

$$\Delta_k = \frac{g}{\mathcal{N}_\beta} \sum_{r=1}^{R} \frac{\sin(kr)}{r^\beta}. \tag{50}$$

The Hamiltonian in Eq. (48) is quadratic and it can be explicitly diagonalised via a Bogoliubov transformation

$$c_k = \mathrm{i} \sin \frac{\theta_k}{2} \gamma_k + \cos \frac{\theta_k}{2} \gamma_{-k}^\dagger, \tag{51}$$

where $\gamma_k, \gamma_k^\dagger$ are fermionic operators, which, respectively, annihilate and create Bogoliubov quasi-particles. They obey the conventional anti-commutation relations $\{\gamma_k, \gamma_p^\dagger\} = \delta_{k,p}$ and $\{\gamma_k, \gamma_p\} = 0$. The proper choice for the momentum dependent angle θ_k in order to diagonalise the Hamiltonian in Eq. (48) reads

$$\theta_k = \arctan \frac{\Delta_k}{h - J_k}. \tag{52}$$

which leads to the diagonal Hamiltonian

$$H = \sum_k^{\text{B.z.}} \omega_k (\gamma_k^\dagger \gamma_k - \gamma_{-k} \gamma_{-k}^\dagger), \tag{53}$$

with the quasi-particle spectrum

$$\omega_k = \sqrt{(h - J_k)^2 + \Delta_k^2}. \tag{54}$$

In the thermodynamic limit $L \to \infty$, the short-range model ($\alpha, \beta \to \infty$) features the familiar relations $J_k = t \cos(k)$ and $\Delta_k = g \sin(k)$. Accordingly, the minimal gap occurs at $k = 0, \pi$, depending on the sign of h, and vanishes as the chemical potential approaches the critical values $h \to \pm t$. Interestingly, the two short-range critical points $h = \pm t$ feature a soft mode at respectively $k = 0, \pi$, in correspondence with the appearance of ferromagnetic or antiferromagnetic order in the short-range Ising chain obtained by the Jordan-Wigner transformation (Fradkin, 2013). Yet, in terms of the fermionic operators of the Kitaev chain no local order is found, but the quantum critical points divide different topological phases, where only non-local string orders are found (Chitov, 2018).

Without loss of generality, we can then impose $t = g = 1$ from now on, fixing the location of the short-range critical point. Upon crossing the critical point the system undergoes a quantum phase transition between a topologically trivial phase at $|h| > 1$ and one featuring a finite winding number

$$w = \frac{1}{2\pi} \oint d\theta_k, \tag{55}$$

where the integral has to be taken along the periodic Brillouin zone.

In terms of topological properties, the quantum phase transition occurs between the trivial phase $w = 0$ at $|h| > 1$ and the topologically nontrivial phase at $|h| < 1$. The existence of a non-trivial topological order in the bulk of the system is connected with the occurrence of zero-energy Majorana modes at the boundaries with the normal phase. In particular, such zero-energy Majorana modes are found at the edges of the finite chain with open boundaries (Kitaev, 2001). The inclusion of interactions beyond the nearest-neighbors case radically modifies and extends this traditional picture.

Before continuing the discussion, we observe that the use of open boundary conditions allows to predict that the edge modes are exponentially localized at the chain edges in the isotropic case when pairing and tunneling rates are equal, i.e. $\alpha = \beta$ (Jäger *et al.*, 2020). Algebraic decay of the edge modes is found in the anisotropic case, when either the exponent and/or the rates of tunneling and pairing is different. In this latter case, the smallest exponent causes the algebraic scaling of the tails, while at short distances the decay is exponential.

For power-law decaying superconducting pairings, the massless Majorana modes at the edges pair into a massive non-local Dirac fermion localized at both edges of the chain dubbed topological massive Dirac fermion. with fractional topological numbers (Viyuela *et al.*, 2016).

It is worth noting that signatures of Majorana edge modes have been studied in ferromagnetic atomic chains on top of superconducting leads (Nadj-Perge *et al.*, 2014). In this context, the realization of power-law decaying couplings via Ruderman-Kittel-Kasuya-Yosida interactions has been proposed (Klinovaja *et al.*, 2013). A weakening of bulk-boundary correspondence in the presence of long-range pairing with Aubry-André-Harper on-site modulation has been observed (Fraxanet *et al.*, 2021). For this model, a 2D Chern invariant can still be defined. However, in contrast to the short-range model, this topological invariant does not correspond to the number of edge mode crossings.

1. Finite-range couplings

As usual, finite-range interactions with $R < \infty$ in the thermodynamic limit cannot alter the universal critical scaling close to the quantum phase transition, but they may alter the topological phase diagram, leading to modifications in the number and properties of the edge modes. However, this is not the case if finite-range interactions only appear in the hopping or the pairing sector separately, i.e. $\beta \to \infty$ or $\alpha \to \infty$ respectively. There the phase diagram remains almost unaltered with respect to the short-range case, apart from a modification of the critical boundaries, which become anisotropic, with the

$k = 0, \pi$ instabilities occurring at different values of $|h|$.

For generic values of α and β, the topological phase diagram also contains regions with $|w| > 1$, with a maximum value equal to the range of the interactions $|w|_{\max} = R$. The range of parameters in which w is maximum decreases with α and the phase diagram of the standard Kitaev chain model is recovered in the $\alpha \to \infty$ limit, independently of β. Interestingly, the winding number may also assume intermediate values between 1 and R with steps of 2. Therefore, for $R \in 2\mathbb{N}(2\mathbb{N}+1)$, the phase can be trivial, $w = 0$, it can feature a pair of Majorana edge modes, $w = 1$, or any even(odd) number of Majorana pairs smaller than the interaction range, $r \in 2\mathbb{N}(2\mathbb{N}+1) < R$.

The separation into even and odd numbers of Majorana modes depending on the range R is justified by the possibility for Majorana modes on the same edge to annihilate each other one by one per edge, according to the mechanism described in Ref. (Alecce and Dell'Anna, 2017). The topological phase with $|w| = 1$, instead, persists for each interaction range $R \geq 1$, because the annihilation of a single Majorana pair requires overlap between the two wave-functions peaked at the opposite edges of the chain.

In general, the influence of long-range interactions on topology has also been investigated for infinite-range couplings (see Sec. IV.B.2) in antiferromagnetic spin-1 chains where the α_* for the survival of the topological phase strongly depends on the frustrated or unfrustrated nature of the long-range terms, i.e. $\alpha \simeq 0$ or 3 (Gong *et al.*, 2016a,b). Moreover, the interplay between topology and long-range connectivity generates a wide range of peculiar phenomena, including novel quantum phases (Gong *et al.*, 2016a), modifications of the area law (Gong *et al.*, 2017), and breaking of the Lieb-Robinson theorem (Maghrebi *et al.*, 2016).

2. Infinite-range pairing

First studies (Vodola *et al.*, 2014) on the long-range Kitaev chain have been focusing on the case of infinite-range long-range coupings $R \propto L$ only in the paring sector, leading to the thermodynamic limit expressions

$$J_k = \cos(kr), \tag{56}$$

$$\Delta_k = \frac{1}{\mathcal{N}_\beta} \sum_{r=1}^{\infty} \frac{\sin(kr)}{r^\beta} = \frac{\mathrm{Im}[\,\mathrm{Li}_\beta\left(e^{ik}\right)]}{2\zeta(\beta)}, \tag{57}$$

where the case $\mathcal{N}_\beta = 1$ is discussed first. In absence of Kac rescaling, the critical line at $h = -1$ appearing in the short-range models persists independently of β, while the one at $h = 1$ disappears as soon as $\beta < 1$. Notably, some references discuss the persistence of the $h = -1$ critical line below $\alpha = 1$ to prove that the long-range Kitaev chain does not require Kac rescaling (Lepori and Dell'Anna, 2017; Lepori *et al.*, 2016). Subsequent work clarified that the ground state energy of the system

$$e_{\infty,\beta} = \int_{-\pi}^{\pi} \omega_k \, dk \tag{58}$$

remains finite for all β and h, due to the fermionic nature of the model and at variance with the classical case. Yet, the zero momentum spectrum diverges $\lim_{k\to 0} \omega_k \to \infty$ for $\beta < 1$ leading to the disappearance of the quantum critical point at $h = 1$, which could be made stable by the introduction of Kac rescaling as in the classical case, see Eq. (46). This whole picture is in loose agreement with the discussion in Sec. III.C, where we have shown that for modulated phases, characterized with instability at finite momentum, no internal energy divergence is detected for decay exponent $\alpha < d$, while ferromagnetic models with homogeneous order need Kac rescaling.

Then, the divergence in $k = 0$ is the cause for the disappearance of the $h = 1$ quantum critical point for $\alpha < 1$. At the same time, at every finite α divergences in some k-derivatives for ω_k occur both at $k = 0$ and at $k = \pi$ (Lepori *et al.*, 2016; Vodola *et al.*, 2014), giving rise to interesting effects both in the correlations decay and the dynamics (Lepori *et al.*, 2017). In particular, these divergencies generate several novel features in the equilibrium behavior of the Kitaev chain, which may be summarised in the following main effects:

- Hybrid decay of the static correlations with intermediate range exponential part and power law tails (Lepori *et al.*, 2017), which can be connected to the existence of a Lieb-Robinson bound peculiar to long-range systems (Foss-Feig *et al.*, 2015a; Hernández-Santana *et al.*, 2017; Van Regemortel *et al.*, 2016).

- Breakdown of conformal invariance for $\beta < 2$ has been found (Lepori *et al.*, 2016). Nevertheless, the scaling of the von-Neumann entropy fulfils the area law up to $\alpha = 1$, as in the short-range limit ($\beta \to \infty$) (Eisert *et al.*, 2010). At the critical point, also the central charge defined by the logarithmic correction to the von-Neumann entropy remains $c = 1/2$ as in the short-range limit as well (Lepori *et al.*, 2016).

- Below the threshold $\beta = 1$ logarithmic corrections to the area-law have been found out of criticality, modelled by the formula

  $$S(\ell) = \frac{c_{\mathrm{eff}}}{6} \log(\ell), \tag{59}$$

  where ℓ is the size of the bipartition (Vodola *et al.*, 2014, 2016). Notably, this correction, which is identical to the one of short-range systems at criticality (Calabrese and Cardy, 2004; Holzhey *et al.*, 1994), has been also found in the Ising model (Koffel *et al.*, 2012).

- Again below $\beta = 1$, the topological phase at $\mu < 1$ the Majorana edge modes, which remained well separated in the short-range limit, shall hybridize and produce a massive Dirac mode, effectively lifting the ground state degeneracy present for $\beta > 1$. This mechanism is analogous to the one occurring in the short-range limit at finite size (Kitaev, 2001). An explicit proof of this fact has been given in Ref. (Patrick *et al.*, 2017) for $\alpha = \beta = 0$.

All these striking features are also found in the general case $\alpha, \beta < \infty$, almost independently from the value of α (Alecce and Dell'Anna, 2017; Lepori and Dell'Anna, 2017; Vodola *et al.*, 2016) and they can be straightforwardly reproduced by an continuous effective field theory description (Lepori *et al.*, 2016). Therefore, all the aforementioned properties can be classified as universal according to our definition. It is worth noting that the peculiar nature of the long-range Kitaev chain at $\beta < 1$ is signaled by a non-integer value of the winding number defined in Eq. (55), which in principle is not admissible. This effect points towards a general breakdown of the traditional theory for topological phases in short-range systems (Kitaev *et al.*, 2009; Schnyder *et al.*, 2008), leading to modifications in the bulk-edge correspondance (Lepori and Dell'Anna, 2017).

3. The $\alpha = \beta$ case and the relation with the long-range Ising model

The topological features of the $\alpha < \infty$ case are not substantially different from the $\alpha \to \infty$ case, as it is the paring term in Eq. (43) that induces the topological behavior. Yet, the presence of long-range hopping substantially alters both the critical and the dynamical properties of the long-range Kitaev chain. Before, discussing such properties, it is convenient to briefly discuss the case $\alpha = \beta$, which is strongly tied with the case of 1/2-spins. In this perspective, it is convenient to first introduce the long-range Ising model Hamiltonian

$$H = -\sum_{l<j} J_{lj}\sigma_l^x\sigma_j^x - h\sum_j \sigma_j^z, \tag{60}$$

where $\sigma_j^{\{x,y,z\}}$ are the Pauli matrices on-site j, h is the transverse-field strength, and J_r, with $r = |l-j|$, is the spin coupling profile with power-law scaling ($\propto 1/r^\alpha$, $\alpha \geq 0$). As usual, in the limit $\alpha \to \infty$ one recovers the short-range Ising model, which is integrable and can be exactly solved with a Jordan-Wigner transformation (Fradkin, 2013). Another interesting limit is reached for $\alpha \to 0$, where the Hamiltonian in Eq. (60) represents the celebrated LMG model (Glick *et al.*, 1965; Lipkin *et al.*, 1965; Meshkov *et al.*, 1965). In this limit, the flat infinite-range interactions leads to permutation symmetry and allows to employ the Dicke basis (Nussenzveig, 1973), which scales linearly with the system size and yields a tractable description of the system amenable via exact diagonalization.

The equilibrium phase diagram of the Hamiltonian in Eq. (60) as well as its universal properties have been depicted in Sec. IV.A in the case $\mathcal{N} = d = 1$. In summary, the system displays a finite temperature phase transition for $\alpha < 2$ (Dutta and Bhattacharjee, 2001a; Dyson, 1969; Thouless, 1969) within the same universality class of the classical long-range Ising model (Defenu *et al.*, 2015). In the limit $T \to 0$, the system displays a quantum critical point at finite h, whose universal properties depend on the value of σ according to Fig. 11 (Defenu *et al.*, 2017b). In the nearest-neighbor limit $\alpha \to \infty$ the universal behaviour exactly corresponds with the ones of the Kitaev chain with $\alpha = \beta > 2$, as a consequence of the Jordan-Wigner mapping.

Therefore, one may expect that a qualitative understanding of the Hamiltonian in Eq. (60) shall result from the mapping of the spin operators $\sigma_j^{\{x,y,z\}}$ onto fermions (Jaschke *et al.*, 2017; Vanderstraeten *et al.*, 2018)

$$\sigma_j^z = 1 - 2c_j^\dagger c_j, \tag{61}$$

$$\sigma_j^y = -\mathrm{i}\Big[\prod_{m=1}^{j-1}\left(1 - 2c_m^\dagger c_m\right)\Big]\left(c_j - c_j^\dagger\right), \tag{62}$$

$$\sigma_j^x = -\Big[\prod_{m=1}^{j-1}\left(1 - 2c_m^\dagger c_m\right)\Big]\left(c_j + c_j^\dagger\right), \tag{63}$$

where the fermionic annihilation and creation operators are represented, respectively, by $c_j, c_j^\dagger$ and, according to the canonical anticommutation relations, one has $\{c_l, c_j\} = 0$ and $\{c_l, c_j^\dagger\} = \delta_{l,j}$. It is worth noting that the Jordan-Wigner transformation is highly non-local and, despite preserving the excitations spectrum of the system, yields radically different eigenstates and topological properties (Greiter *et al.*, 2014).

The fermionic Hamiltonian for the long-range Ising model reads

$$H = -\sum_{l<j} J_{|l-j|}\left(c_l^\dagger - c_l\right)\Big[\prod_{n=l+1}^{j-1}\left(1 - 2c_n^\dagger c_n\right)\Big]\left(c_j^\dagger + c_j\right) - h\sum_j\left(1 - 2c_j^\dagger c_j\right). \tag{64}$$

An exact solution of the Hamiltonian in Eq. (64) is not possible due to the inclusion of increasingly longer fermionic strings. In order to introduce a treatable model, valid close to the fully paramagnetic limit, one can employ the approximation (Jaschke *et al.*, 2017)

$$\prod_{n=l+1}^{j-1}\left(1 - 2c_n^\dagger c_n\right) = 1, \tag{65}$$

for every $j \geq l+2$ and neglect all the non-quadratic string operators in the first line of Eq. (64). The resulting Hamiltonian reads

$$H = -\sum_{l<j} J_{|l-j|}\left(c_l^\dagger c_j + c_l^\dagger c_j^\dagger - c_l c_j - c_l c_j^\dagger\right) - h\sum_j \left(1 - 2c_j^\dagger c_j\right), \tag{66}$$

which corresponds to the Hamiltonian in Eq. (43) in the infinite-range limit $R \to \infty$ with identical hopping and pairing functions, i.e. $g = t$ and $\alpha = \beta$.

In the nearest neighbor limit, the fermions in the Hamiltonian (66) can be interpreted as domain-walls in the spin language. Consistently, long-range interactions introduce an effective nonquadratic coupling between such domain walls, which we have discarded via the introduction of the approximation in Eq. (65)(Fradkin, 2013). Since the relevance of the quartic terms of the Hamiltonian in Eq. (64) crucially depends on the interaction range, it is not surprising that the approximation in Eq. (65) alters the universal properties of the model and, then, the Hamiltonian in Eq. (66) does not lie in the same universality class as the long-range Ising model for $\sigma = \alpha - 1 < 2$. The difficulty to reproduce the universal properties of the long-range Ising model at small α with the purely fermionic Hamiltonian can be also understood via an effective dimension argument.

According to Eq. (35), the long-range Ising model displays the effective dimension $d_{\mathrm{eff}} = 1$ for $\alpha > 3$ and, therefore, it is not surprising that the universal properties of the fermionic theory in Eq. (66) correspond to the ones of the effective bosonic theory described by Eq. (34). Conversely, for $\alpha < 5/3$ the effective dimension becomes large, $d_{\mathrm{eff}} > 4$, and the universal features of the effective action in Eq. (34) are exactly captured by the mean-field approximation, which features bosonic excitations and cannot be reduced to the purely fermionic theory in Eq. (66). In the intermediate range $5/3 < \alpha < 3$ the low-energy excitations shall possess hybrid fermionic-bosonic character, which cannot be captured by the purely fermionic Hamiltonian in Eq. (66).

4. The general $\alpha \neq \beta$ case

In Sec. IV.B.3, we have discussed the relation between the universal properties of the Ising model and the ones of the Kitaev chain with $\alpha = \beta$ and $t = g$. Now, we will explicitly derive the critical exponents of the Kitaev chain in the general case with $R \propto L$ and

$$J_k = \frac{1}{\zeta(\alpha)}\sum_{r=1}^{\infty}\frac{\cos(kr)}{r^\alpha} = \frac{\mathrm{Re}[\,\mathrm{Li}_\alpha\left(e^{ik}\right)]}{2\zeta(\alpha)}, \tag{67}$$

$$\Delta_k = \frac{1}{\zeta(\beta)}\sum_{r=1}^{\infty}\frac{\sin(kr)}{r^\beta} = \frac{\mathrm{Im}[\,\mathrm{Li}_\beta\left(e^{ik}\right)]}{2\zeta(\beta)}, \tag{68}$$

which are the momentum range couplings determining the single particle spectrum in Eq. (54). In analogy with the nearest-neighbour case the long-range Kitaev chain features two quantum critical points, corresponding to the softening of the $k = 0$ or $k = \pi$ modes. Employing the Kac normalised expressions in Eqs. (67) and (68), the location of the "homogeneous" critical point is fixed at $h_c^h = 1$ independently of the choice of α or β. Conversely, the $k = \pi$ instability occurs at the α dependent critical point $h_c^a = 1 - 2^\alpha$. The definition of critical exponents is given by the scaling of the excitation spectrum close to each of these quantum critical points

$$\lim_{h \to h_c^{h,a}} \omega_k \approx |h - h_c|^{z\nu} \quad k = 0, \pi \tag{69}$$

$$\lim_{k \to 0,\pi} \omega_k \approx k^z \quad h = h_c^{h,c}. \tag{70}$$

As in the case of rotor models, see Sec. IV.A, the two exponents z and ν are sufficient to characterize the entire critical scaling.

Following the definitions in Eqs. (69) , it is straightforward to check that $\lim_{k\to 0}\Delta_k = 0$ and that the critical exponents combination is $z\nu = 1$ for each of the two quantum critical points irrespectively of the values of α, β. The determination of the dynamical scaling exponent z close to the h_c^h quantum critical point requires the expansions of the Fourier couplings close to $k = 0$

$$J_k = 1 + \sin(\alpha\pi/2)\frac{\Gamma(1-\alpha)}{\zeta(\alpha)}k^{\alpha-1} - \frac{\zeta(\alpha-2)}{2\zeta(\alpha)}k^2 + O(k^3) \quad \text{if } \alpha < 3, \tag{71}$$

$$J_k = 1 + \frac{2\log(k) - 3}{4\zeta(3)}k^2 + O(k^3) \quad \text{if } \alpha = 3, \tag{72}$$

$$J_k = 1 - \frac{\zeta(\alpha-2)}{2\zeta(\alpha)}k^2 + O(k^{\alpha-1}) \quad \text{if } \alpha > 3, \tag{73}$$

and

$$\Delta_k = \cos(\beta\pi/2)\frac{\Gamma(1-\beta)}{\zeta(\beta)}k^{\beta-1} + \frac{\zeta(\beta-1)}{\zeta(\beta)}k + O(k^3) \quad \text{if } \beta < 2, \tag{74}$$

$$\Delta_k = \frac{6(1-\log(k))}{\pi^2}k + O(k^3) \quad \text{if } \beta = 2, \tag{75}$$

$$\Delta_k = \frac{\zeta(\beta-1)}{\zeta(\beta)}k + O(k^{\beta-1}) \quad \text{if } \beta > 2. \tag{76}$$

Apart from their relevance to the present case, the expansions above display the typical example of anomalous terms in the excitation spectrum generated by long-range interactions. A close inspection of the expressions above leads to the following result for the equilibrium dynamical critical exponent:

$$z = \begin{cases} \phi - 1 & \text{if } \phi < 2, \\ 1 & \text{if } \phi > 2, \end{cases} \tag{77}$$

where $\phi = \min(\alpha, \beta)$. According to the result in Eq. (77) the relevant region for long-range couplings in the long-range Kitaev chain radically differs from the case of $O(\mathcal{N})$ rotors model described in Sec. IV.A. Indeed, long-range interactions in the Kitaev chain remain irrelevant also in the range $2 < \alpha, \beta < 3$, while long-range couplings in rotor models would be relevant in the whole $\alpha < 3$ region. Yet, it is worth noting that even if long-range hopping couplings with $2 < \alpha < 3$ do not alter the critical behaviour, they still introduce relevant momentum terms in the hopping sector. Such discrepancy yields further evidence that the approximation in Eq. (65) crucially alters the universal behaviour at small α, β.

For the sake of the forthcoming discussion, it is crucial to notice that long-range interactions with different power-law exponents $\alpha \neq \beta$ modify the influence of the hopping and pairing term on the critical scaling. Indeed, while for short-range interactions the dynamical critical scaling exponents are determined by the low-momentum terms in the pairing coupling, for relevant long-range interactions with $\alpha < \beta$ it is the scaling of the hopping coupling which determines z. A similar scenario may also occur for finite-range competing interactions and it is known to cause peculiar dynamical features (Defenu *et al.*, 2019b; Deng *et al.*, 2009; Divakaran *et al.*, 2009), which will be discussed in the following sections.

In summary, this section has delineated the equilibrium critical properties of quadratic fermionic systems, with a power-law decaying coupling of different decay rates. Yet, the same characterization cannot be provided in the case of fermionic systems with long-range non-quadratic interactions, such as

$$H = \sum_{\langle ij\rangle, s} \left(c^{\dagger}_{i,s} c_{j,s} + \text{h.c.} \right) + \sum_{i\neq j} V_{ij} n_i n_j \tag{78}$$

where the $c^{\dagger}_{i,s}$ operator and its conjugate create and annihilate a fermion with spin s on the $i-th$ site of the lattice, while n_i represents the total density operator on the same site. The understanding of the influence of long-range density-density interactions on the critical behaviour of Fermi systems is still relatively incomplete. One notable counterexample is the 1D case, where mapping of fermionic systems into bosonic or spin degrees of freedom is possible.

In particular, the ground state of continuous 1D fermions interacting via unscreened Coulomb repulsion was characterized by bosonization techniques, finding metallic features and a classical Wigner crystal phase with slow-decaying charge correlations (Schulz, 1993; Wang *et al.*, 2001). Numerical confirmation of such a theoretical picture has been provided by density matrix renormalization group (DMRG) (Fano *et al.*, 1999) and variational MC methods (Astrakharchik and Girardeau, 2011; Casula *et al.*, 2006; Lee and Drummond, 2011). The corresponding lattice systems with commensurate filling have been numerically shown to display an insulating ground-state, still with Wigner crystal character, in contradiction with the bosonization picture in the continuum (Capponi *et al.*, 2000; Poilblanc *et al.*, 1997).

C. XXZ models

The Hamiltonian of the long-range XXZ spin chain reads

$$H = \sum_{i>j} J_{ij} \left(-\sigma_i^x \sigma_j^x - \sigma_i^y \sigma_j^y + \sigma_i^z \sigma_j^z \right), \tag{79}$$

where $J_{ij} \approx r_{ij}^{-\alpha}$ refers to the usual long-range couplings. Notice that in Eq. (79) all the couplings $x-x$, $y-y$ and $z-z$ are long-ranged. Putting the long-range couplings only in the $z-z$ directions corresponds actually to have hard-core bosons with long-range density-density interactions, see the next section for more details.

Conventionally, the solution in the $\alpha \to \infty$ limit is obtained through bosonization, showing that the universal properties of the spin Hamiltonian in Eq. (79) are exactly described by the effective action of the quantum sine-Gordon model, which also describes the universality of $O(2)$ quantum rotors (Fradkin, 2013; Giamarchi, 2004; Sachdev, 1999).

However, such mapping is not possible in presence of long-range couplings. Nevertheless, one can split the Hamiltonian into long-range and short-range contributions and consider the long-range couplings only as a perturbation of the short-range action (Maghrebi *et al.*, 2017), see also (Bermudez *et al.*, 2017). As a result one can consider the low energy action

$$\begin{aligned} S[\theta] = \frac{K}{2\pi u} \int d\tau\, dx \left\{ (\partial_\tau \theta)^2 + u^2 (\partial_x \theta)^2 \right\} \\ - g \int d\tau \int dx\, dy \frac{\cos(\theta(\tau,x) - \theta(\tau,y))}{|x-y|^{\alpha}} \end{aligned} \tag{80}$$

where K is the so-called Luttinger parameter, u is a velocity scale, and g is proportional to the strength of long-range interactions.

The final picture obtained for the critical behaviour of the action in Eq. (80) is analogous to the one discussed for the 2D XY classical case at finite temperature. In fact, one can define the shifted decay exponent $\sigma = \alpha - d = \alpha - 1$ and derive the flow equations

$$\begin{aligned} \frac{dy_k}{dt} &= -(2-4K) y_k \\ \frac{d\tilde{g}_k}{dt} &= -\left(2 - \sigma - \frac{1}{2K} \right) \tilde{g}_k, \end{aligned} \tag{81}$$

where y_k is the fugacity of topological excitations and $\tilde{g}_k$ the dimensionless long-range coupling, see the discussion in Sec. III.A.2. The phase diagram resulting from

Eqs. (81) follows in close analogy the one obtained in the classical case, see Sec. III.A.2.

As long as $\sigma > 2$ long-range interactions are irrelevant and the system displays universal BKT scaling. Conversely, for $\sigma < 2$ a new phase emerges at large enough K, where the long-range RG coupling $\tilde{g}$ grows indefinitely. As a consequence, a finite order parameter appears in the x-y plane $\langle \sigma^+ \rangle \neq 0$ and the system undergoes spontaneous symmetry breaking. Evidences of this *quasi- to true-* order transition have been found in a numerical density matrix renormalization group (DMRG) calculation. Indeed, computing the effective central charge of the model, Ref. (Maghrebi *et al.*, 2017) was able to show that this quantity changes from $c_{\rm eff} = c = 1$, typical of the isotropic short-range sine-Gordon model (Mussardo, 2009), to $c_{\rm eff} > 1$ at $\sigma < 2$. Such change in the effective central charge is compatible with the appearance of a new phase with broken Lorentzian symmetry (Maghrebi *et al.*, 2017). Correspondingly, also the dynamical critical exponents deviate from unity and acquire the expected value for anisotropic long-range field theories $z = \sigma/2$. Including the renormalization of the Luttinger parameter does not alter the aforementioned picture. Interestingly, the half-chain entanglement entropy scaling features an anomalous $\propto \log(L)$ contribution in the ordered phase caused by the Goldstone mode (Frérot *et al.*, 2017).

By a thoughtful characterization of the long-distance correlation functions, Ref. (Maghrebi *et al.*, 2017) showed that the ordered phase displays a finite correlation length ξ that diverges exponentially as the critical point with the quasi-ordered phase is reached. Such exponential divergence is reminiscent of the behavior of the correlation length at the BKT transition (Fradkin, 2013).

D. Hardcore bosons in 1d

In the section on the Kitaev chain, we already discussed the possibility to recover the homogeneous critical point of the Kitaev chain also for $\alpha, \beta < 1$ by explicitly introducing Kac rescaling, at variance with existing studies (Vodola *et al.*, 2014). In the present section, we are going to review results on this matter by explicitly showing that implementing (or not implementing) the Kac rescaling may significantly alter the equilibrium phase diagram of a long-range interacting quantum model.

Restricting our analysis to the one-dimensional case, we can relate the findings discussed in Sec. IV.C with the study of hardcore bosons with arbitrary power-law interactions. The Hamiltonian under consideration reads

$$H = -t \sum_{i=1}^{L} \left(c_i^\dagger c_{i+1} + \text{h.c.} \right) + \sum_{i>j} V_{ij}^{(\alpha)} n_i n_j, \qquad (82)$$

with the power-law decaying potential

$$V_{|i-j|}^{(\alpha)} = \frac{1}{N_\alpha} \frac{V}{d_{i-j}^{\alpha}} \quad V > 0. \qquad (83)$$

As in the Kitaev chain study presented in the above section, due to the quantum nature of the system, one can choose to implement or not Kac rescaling according to the physical situation, see Eq. (46). DRMG simulations

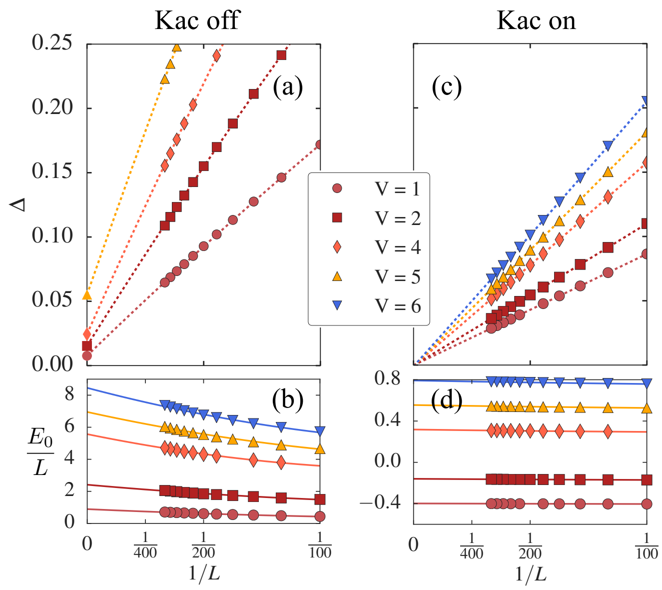

Figure 13 **Comparison between Kac-on and Kac-off finite-size scalings for hard-core bosons.** The scaling of the bosons single-particle energy, as defined in Eq. (84), as a function of the system size. The results have been obtained via a DRMG computation at half-filling $\langle n_i \rangle = 0.5$, for $\alpha = 1$ and different interaction strengths V (in units of the hopping energy t). The difference between the Kac scaled or unscaled scenario is rather evident, as in the first case the single-particle energy always vanishes in the thermodynamic limit, while in the second case the system remains gapped up to the thermodynamic limit.

have been performed on the Hamiltonian in Eq. (82) to characterize the phase of the system. In particular, from the energy of the N particles ground state $E_0(n)$ one can define the single particle gap

$$\Delta(n) = E_0(n+1) + E_0(n-1) - 2E_0(n) \qquad (84)$$

which displays radically different behaviours, depending on the implementation (or non-implementation) of the Kac rescaling, as it appears from the numerical results reported in Fig. 13.

In particular, the numerical simulations in absence of Kac rescaling predict a finite single-particle gap in the thermodynamic limit, which is consistent with an insulating phase for all values of the interaction coupling V of the potential in Eq. (83). This scenario has been first evidenced in Ref. (Capponi *et al.*, 2000) for $\alpha = 1$ and then confirmed, in the general α case, by the simulations discussed in Ref. (Botzung *et al.*, 2021). Conversely, the implementation of Kac rescaling induces metallic behavior in the entire range $0 \leq \alpha \leq 1$ independently on the interaction coupling $V > 0$. This proves that the restoration of extensive interaction energy significantly alters the phase diagram of Hamiltonian (82).

Theoretical understanding of the discrepancy between the scaled and unscaled theory can be obtained via the Luttinger liquid theory (Giamarchi, 2004), which reduces the universal behavior of the Hamiltonian in Eq. (82) to the one of the continuous action

$$H_{\rm LL} = \frac{u}{2\pi}\int dx \left\{K(\pi\Pi)^2 + \frac{(\partial_x\varphi)^2}{K} - \frac{g}{\pi}\cos(4\varphi)\right\}, \tag{85}$$

where the parameters u and K depend on the Fermi velocity $v_{\rm F}$ and wave-vector $k_{\rm F}$ according to the relations

$$uK = v_{\rm F}, \tag{86}$$

$$\frac{u}{K} = v_{\rm F} + \frac{1}{\pi}\sum_{r=1}^{L} V_r^{(\alpha)}(1-\cos(k_{\rm F}r)). \tag{87}$$

It is straightforward to show that the universal physics of the Luttinger Liquid Hamiltonian in Eq. (85) is the same as in the sine-Gordon model (Malard, 2013) featuring an infinite-order transition between a line of free fixed points with power-law bosonic correlations $\langle a_i^\dagger a_j\rangle = |i-j|^{-1/2K}$ and a massive phase with exponential correlations. Therefore, the free field theory phase corresponds with the metallic phase of the Hamiltonian in Eq. (82). One can show that g is given by

$$g = \sum_{r=1}^{L} V_r^{(\alpha)}\cos(2k_{\rm F}r) \tag{88}$$

and that the metallic phase breaks down beyond the critical coupling strength K_c, which at half-filling corresponds to $K_c = 1/2$, neglecting multiple um-klapp processes. In the nearest-neighbour limit $\alpha \to \infty$ this scenario describes the metal-insulator transition appearing at $V_c = 2t$. Such transition lies in the BKT universality and, indeed, the breakdown of the metallic phase is akin to vortex proliferation in the physics of the 2D XY model.

For $\alpha > 1$ the introduction of Kac rescaling does not influence the physics and the picture does not change, apart from obvious changes in the value of the critical interaction strength. On the other hand, the aforementioned universal picture is broken as soon as $\alpha = 1$, since, in absence of Kac rescaling, the first term in the summation of Eq. (87) diverges in the thermodynamic limit, $\sum_r V_r^1 \sim \log(L)$, leading to a vanishing K coupling. At the same time, the interaction coupling remains finite due to the alternating sign in Eq. (88) and, therefore, the system lingers in the insulating phase, as verified by numerical computations (Botzung *et al.*, 2021; Capponi *et al.*, 2000).

The situation is reversed by the introduction of Kac rescaling, which imposes convergence on the first summation of Eq. (87) irrespectively from the α value, while it makes the interaction coupling vanish identically. It, then, does not come as a surprise that the Kac scaled systems always lie in the metallic phase. While the Luttinger-Liquid theory can reproduce the metallic (insulator) character in the presence (absence) of Kac's rescaling, the actual features of the phase in both cases are not completely consistent with the continuous theory prediction. Indeed, the comparison between the numerical values for the K coupling obtained by the single-particle correlation functions (K_{1p}), the structure factor (K_{2p}) and the finite-size scaling of the gap ($K_\Delta = \partial\Delta/\partial L^{-1}$) (Kohn, 1964) do not match each other and especially do not match the prediction of Luttinger Liquid theory in the Kac rescaled case, see Fig. 14. Therefore, both the metallic and insulating phases at $\alpha < 1$ do not obey Luttinger liquid theory (Botzung *et al.*, 2021). It is worth noting that this picture does not apply to the flat interactions case $\alpha = 0$, which is analytically solvable and may be treated separately (Botzung *et al.*, 2021).

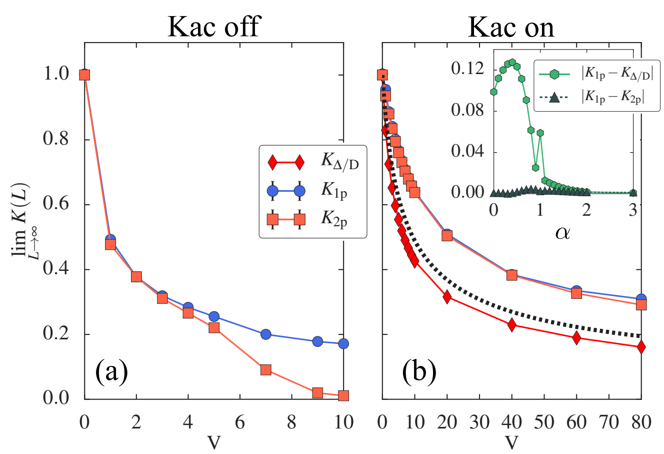

Figure 14 **Luttinger parameter.** Thermodynamic limit extrapolation of the Luttinger parameter K as a function of the long-range interaction strength V at half-filling, in the case $\alpha = 0.5$ (the same scenario has been obtained for several α values in the range $0 < \alpha < 1$). The three different definitions for the Luttinger parameter have been compared both in Kac unscaled, panel (a), and scaled, panel (b), cases (Botzung *et al.*, 2021). As a function of α, given a fixed value of the interaction ($V = 1.5$ in the inset of panel (b)), there is no discrepancy between the Luttinger parameter obtained by correlation function $K_{1p} = K_{2p}$, confirming the metallic character of the system. Still the conventional Luttinger Liquid theory is not obeyed since the Luttinger parameter does not fit the gap scaling K_Δ. As it is seen from the inset of panel (b), the traditional Luttinger Liquid picture is recovered for $\alpha > 1$.

E. Soft-core interactions

In this section, we are going to discuss the case of non-local interactions, addressing also cases of competing interactions relevant for some of the physical systems introduced in the previous sections. Given the rich variety of physical behaviors in these systems, we will not attempt to cover all the phenomena. Rather, after a brief introduction, we focus on two main classes of applications: the clustering phenomena induced by typical non-local interactions, and the structural phase transitions occurring in mesoscopic long-range interactions.

The phase structure of ensembles of particles interacting via non-local potentials diverging at the origin has been extensively studied in the last few decades both in the classical and more recently in the quantum regime (Likos, 2001). A major problem concerns the study of freezing transitions and the respective crystal structure, which depends on the steepness of the potential, the dimensionality, and the details of the external trapping. At the classical level, power-law diverging potentials of the form $V(r) = \varepsilon(\sigma/r)^{\alpha}$, where $\varepsilon > 0$ is an arbitrary energy scale, σ has the dimension of a length, and r is the interparticle distance, result into the formation of a crystalline state at arbitrarily high temperatures. Moreover, one can show that to ensure the stability against *explosion* (infinite thermodynamic observables, such as the energy per particle or pressure) one has to impose $\alpha > d$ (Weeks, 1981), with d the system dimensionality, i.e. to be in the weak long-range or short-range regimes. If this condition is violated, i.e. $\alpha \leq d$ a neutralizing background could be introduced to stabilize one-component systems, as e.g. the one-component plasma (Baus and Hansen, 1980). Notice that both Kac rescaling and the introduction of neutralizing background can be used to perform calculations and regularize physical quantities, but the reader should be alerted that while Kac rescaling preserves the functional power-law form of the interactions, a neutralizing background may introduce screening effects for charged systems. The study of quantum systems with density-density power-law interactions without any intrinsic length scale provides a quantum counterpart of these results holding for classical systems and it has been subsequently investigated (Büchler *et al.*, 2007; Dalmonte *et al.*, 2010; Pupillo *et al.*, 2010).

Another interesting class of interactions is the one in which does not diverge at the origin, i.e., it bounded. In soft-matter physics, such *soft-core* potentials arise as effective interactions between the centers of mass of soft, flexible macromolecules such as polymer chains, dendrimers, polyelectrolytes, etc. Indeed, the centers of mass of two macromolecules can coincide without violation of the excluded volume conditions, hence bringing about a bounded interaction (Likos *et al.*, 2007). A relevant consequence of the removal of the on-site divergence is the possibility of overlapping particles, which under certain conditions can lead to clustering. A rigorous criterion holding for a fluid at sufficiently high densities states that a non-attractive and bounded pair potential should satisfy the following requirements: *i)* it is bounded, *ii)* it is positive definite, *iii)* it decays fast enough to zero at large separations, so that it is integrable and its Fourier transform exists, and *iv)* it is free of attractive parts, i.e. it does not display clustering. Otherwise, if the Fourier transform of the pair potential has a negative value for a finite momentum k_m, then the system can freeze into clustered crystals with multiple occupied sites with an intercluster distance $\propto 1/k_m$ (Likos *et al.*, 2001). An intuitive way to understand such a criterion is via the high-density limit of the structure factor $S(k)$ of a fluid, which is a measure of the susceptibility of the system to a spontaneous spatial modulation having wavenumber k. Within the framework of the fluctuation-dissipation theorem, $S(k)$ appears as a proportionality factor between a weak external potential of wavenumber k and the associated linear density response. Employing the Ornstein-Zernike relation (McDonald, 2013; P. M. Chaikin, 1995) one finds that in the high-density limit, the structure factor can be well approximated by

$$S(\mathbf{k}) = \frac{1}{1 + \rho\,\beta\,V(\mathbf{k})}, \tag{89}$$

where $V(\mathbf{k})$ is the Fourier transform of the potential and ρ the system density. Hence, a structure factor with a high peak at some wavenumber k_m is a signal of an incipient transition of the fluid to a spatially modulated system, i.e., a crystal. Recently, Ref. (Mendoza-Coto *et al.*, 2021a) presented a sufficient criterion for the emergence of cluster phases with low filling (up to two particles per cluster) in an ensemble of interacting classical particles with generic (also diverging at the origin) repulsive two-body interactions in the *classical* zero-temperature limit valid at intermediate densities. The basis of the criterion is a zero-temperature comparison of the energy imbalance between the single-particle lattice and the first cluster-crystal configuration at small density obtained by the use of the Fourier transform of a regularized version of the potential. It determines the relevant characteristics of the interaction potential that make the energy of a two-particle cluster-crystal becomes smaller than that of a simple triangular lattice in two dimensions. See also (Díaz-Méndez *et al.*, 2017) for an application to the formation of a vortex glass in clean systems of thin films of "type-1.5" superconductors.

In the quantum regime, it is possible to provide a connection between the emergence of a structural transition to the structure factor $S(k)$ via the analysis of the spectrum of elementary excitation through the Feynman-Bijl relation (Feynman, 1954): $S(\mathbf{k}) = \hbar^2 k^2/2m\,\varepsilon(\mathbf{k})$, where $\varepsilon(\mathbf{k})$ is the energy of excitations at momentum $\mathbf{k}$. A peak at finite momentum $\mathbf{k}$ of $S(\mathbf{k})$ is associated to the presence of a roton minimum in the spectrum $\varepsilon(\mathbf{k})$. Eventually, upon softening of the roton minimum the system enters the roton instability. This connection has recently been realized in experiments, see e.g. (Chomaz *et al.*, 2018; Hertkorn *et al.*, 2021; Mottl *et al.*, 2012; O'Dell *et al.*, 2000, 2003; Santos *et al.*, 2003).

Dilute quantum gases can feature long-range interactions if the constituent particles have (*i*) a strong magnetic dipole moment, or (*ii*) a strong permanent electric dipole moment as in polar molecules, or (*iii*) an induced electric dipole moment as in Rydberg atoms or in cavity-mediated systems. Specifically, quantum gases of atoms with strong magnetic dipole moments have been extensively employed as an experimental platform to detect the relation between the microscopic long-range interactions and the low-energy excitation spectra (Bismut *et al.*, 2012) and to study crystallization in a quantum many-body setting (Baranov *et al.*, 2012; Böttcher *et al.*, 2020; Lahaye *et al.*, 2009; Trefzger *et al.*, 2011). The interplay between the collisional contact interactions, the magnetic dipolar interaction, and repulsive quantum fluctuations (Lima and Pelster, 2011) can give rise to the stabilization of droplets (Chomaz *et al.*, 2016) or to the formation of a supersolid phase if the droplets share phase coherence in the ground state (Böttcher *et al.*, 2021; Norcia *et al.*, 2021; Sohmen *et al.*, 2021; Tanzi *et al.*, 2019a, 2021), or to a rich set of patterns out of equilibrium (Parker *et al.*, 2009). An interesting case is provided by doubly dipolar systems, magnetic *and* electric, which may display dimensional crossover in the droplet phase, in the absence of an external confinement potential (Mishra *et al.*, 2020). For sufficiently strong interactions dipolar systems display a roton instability which triggers the phase transition to a dipolar supersolid and arrays of isolated quantum droplets (Baillie and Blakie, 2018; Baillie *et al.*, 2016), or filaments in three dimensions (Cinti *et al.*, 2017). A similar phenomenology of self-organized ground-state density modulations was predicted for a BEC illuminated by a single, circularly polarized laser beam in the weak saturation limit in (Giovanazzi *et al.*, 2002). The appearance of a structural transition via the softening of roton minimum has been extensively studied also in the context of Rydberg-dressed systems where an intrinsic soft-core potential can be engineered via laser coupling to highly excited electronic states. In the following we focus on results both in the continuum and on a lattice, leading to pattern formation in the presence of soft-core pairwise interactions.

1. Quantum phases

We start by considering a system of N bosons interacting via two-body soft-core potentials of the type

$$V(r) = \frac{V_0}{r^\alpha + R_c^\alpha}, \tag{90}$$

where R_c is a characteristic length of the pair potential. While the considered interactions do not straightforwardly occur in natural crystals, they can be designed in ultracold atom experiments. As we commented in Sec.II.C soft-core interactions of the type described by eq.(90) can be realized with Rydberg-dressed atoms where $\alpha = 6$, for which the Hamiltonian provides a prototype system for addressing the general physical picture. In general, this interaction approaches a constant value V_0/R^α as the inter-particle distance, r, decreases below the soft-core distance R_c, and drops to zero for $r \gg R_c$. The limiting case $\alpha \to \infty$ yields the soft-disc model (Pomeau and Rica, 1994), while $\alpha = 3$ and $\alpha = 6$ correspond to soft-core dipole-dipole (Cinti *et al.*, 2010) and van der Waals (Henkel *et al.*, 2012, 2010) interactions that can be realized with ultracold atoms (Maucher *et al.*, 2011) or polar molecules (Büchler *et al.*, 2007; Micheli *et al.*, 2007).

The mean-field analysis of the structure factor $S(k)$ suggests the occurrence of spontaneous symmetry breaking at zero temperature, in the form of a cluster crystal phase which occurs at sufficiently high densities. According to dimensional analysis, this phase should remain stable in dimensions $d > 1$. Moreover, due to the bosonic symmetry of this single-component system, in a certain parameter interval of the phase diagram, one might expect the system to display both crystalline and superfluid properties, i.e. the simultaneous breaking of continuous translational and global gauge symmetry, a supersolid state. The first mentioning of such a state goes back to Gross, who presented a theory for a density-modulated superfluid emerging from a mean-field model for solid Helium (Gross, 1957). A microscopic picture of supersolidity was proposed by Andreev, Lifshitz, and Chester (ALC) (Andreev and Lifshitz, 1969) and is based on two key assumptions that: *(i)* the ground state of a bosonic crystal contains defects such as vacancies and interstitials; and *(ii)* these defects can delocalize, thereby giving rise to superfluidity. For a review on the subject and the debate on the observation of such phase in solid Helium see (Boninsegni and Prokof'ev, 2012). For a more recent discussion of the observation of supersolid phases in dipolar systems both in quasi one- and two-dimensional setups see the review (Böttcher *et al.*, 2021).

Soft-core potentials for hard-core bosons or spinless fermions on 1D lattice systems described by the Hamiltonian

$$H = -t \sum_{\langle i,j \rangle} b_i^\dagger b_j + V \sum_{i<j; r_{ij} < r_c} n_i n_j, \tag{91}$$

where b_i, $(b_i^\dagger)$ are hard-core bosonic annihilation (creation) operators localized on site i, and $n_i = b_i^\dagger b_i$ is the density in i, lead to correlated quantum liquid phases that do not fall into the conventional Luttinger Liquid paradigm. Characteristic features of these anomalous

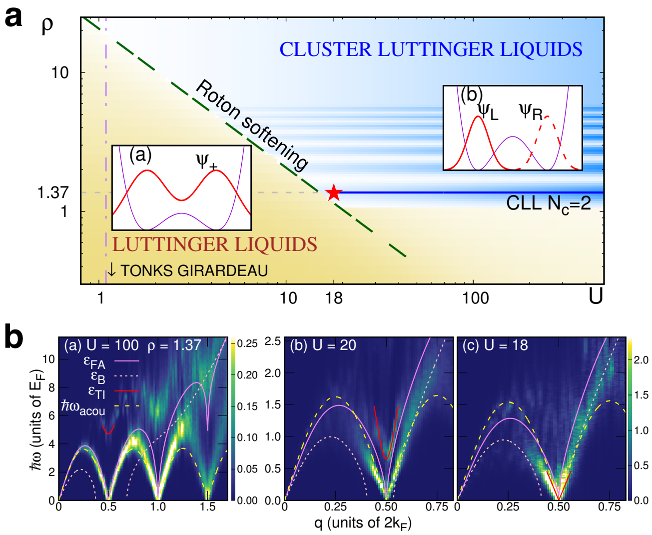

Figure 15 **Zero-temperature phase diagram of one-dimensional soft-core bosons in the continuum and their excitation spectrum.** (a) Phase diagram of one-dimensional soft-core bosons (log-log scale). A star marks the critical point between the Luttinger Liquid and CLL phases for densities commensurate to 2-particle clusters. The long-dashed line corresponds to the softening of the Bogoliubov roton. (b) Spectra at $\rho = 1.37$ with decreasing U, compared to Feynman ε_{FA} (thin solid) and Bogoliubov ε_B (dotted) approximations, and the harmonic chain acoustic mode $\omega_{\rm acou}$ (dashed). At $q \approx q_c$, the secondary mode is fitted by the transverse Ising spectrum ε_{TI} (thick solid). Figures (a) and (b) are adapted from Ref. (Rossotti *et al.*, 2017).

cluster Luttinger Liquids (CLL) include a deformation of the critical surface in momentum space and are evident in correlation functions such as momentum distributions and structure factors (Dalmonte *et al.*, 2015; Mattioli *et al.*, 2013) using DMRG and bosonization techniques. Recently, the spinful Fermi-Hubbard model with both on-site interactions and soft-core (density-density) interactions has been investigated (Botzung *et al.*, 2019), generalazing the extended Fermi-Hubbard model with a soft-core radius equal to one lattice site studied in Ref. (Nakamura, 2000). It displays different types of CLL and a nontrivial supersymmetric critical line. The continuum version of this model has been studied in Ref. (Rossotti *et al.*, 2017), which showed evidence of the CLL via exact quantum Monte Carlo simulations. The phase diagram of the system is shown in Fig. 15(a), together with the excitation spectrum in Fig.15(b). The acoustic mode of the CLL phase (panels a-b) is gapless at $q = q_c$, corresponding to k_F, at this density. Above the transition line, located at $U = U_c = 18$ (panel c), this lowest excitation turns into the rotonic mode (panels d-e). A weaker secondary mode appears also in the strongly correlated liquid phase, in the form of a secondary roton. This secondary excitation in the Luttinger Liquid phase can be linked to incipient cluster formation, due to particles being preferentially localized close to either the left or the right neighbor. The gap of both such Luttinger Liquid excitations, and the anharmonic optical modes of the CLL phase vanishes at the transition.

In the higher dimensional case in the continuum a good description is provided by a mean-field treatment (Henkel *et al.*, 2010; Macrì *et al.*, 2013; Pomeau and Rica, 1994), justified by the application of the first Born approximation to the two-body scattering problem, and the phases emerging from Eq.(90) at zero temperature (Cinti *et al.*, 2014). In mean-field theory the system dynamics is described by a non-local Gross-Pitaevskii equation (GPE), which reads

$$i\partial_t \psi(\mathbf{r},t) = \left(-\frac{\nabla^2}{2} + \gamma \int \mathrm{d}\mathbf{r}' U(\mathbf{r}-\mathbf{r}')|\psi(\mathbf{r}',t)|^2\right)\psi(\mathbf{r},t)\,, \tag{92}$$

where $\mathbf{r} \to \mathbf{r}/R_c$, $U(\mathbf{r}) = \frac{U_0}{1+r^6}$, and $\gamma = m\,n\,U_0/\left(\hbar^2 R_c^2\right)$ is a dimensionless interaction strength that determines the ground state properties and the excitation dynamics. Eq. (92) has been reported in reduced density units, which will be employed from now on. The energy can be derived from the GPE energy functional:

$$H = \int \mathrm{d}\mathbf{r}\, \frac{1}{2}\left|\nabla\psi_0\right|^2 + \frac{\gamma}{2}\int \mathrm{d}\mathbf{r}\,\mathrm{d}\mathbf{r}'\; |\psi_0(\mathbf{r})|^2 U(\mathbf{r}-\mathbf{r}')|\psi_0(\mathbf{r}')|^2. \tag{93}$$

In order to numerically determine the location of the transition from a uniform to a modulated ground state, once can first expand the wavefunction $\psi_0(\mathbf{r})$ in Fourier series:

$$\psi_0(\mathbf{r}) = \sum_{\mathbf{Q}} C_{\mathbf{Q}}\, e^{i\,\mathbf{Q}\cdot\mathbf{r}}, \tag{94}$$

where $\mathbf{Q} = n\,\mathbf{b}_1 + m\,\mathbf{b}_2$ with n, m integers and $\mathbf{b}_1 = \frac{2\pi}{a}\left(1, -\frac{1}{\sqrt{3}}\right)$, $\mathbf{b}_2 = \frac{2\pi}{a}\left(0, \frac{2}{\sqrt{3}}\right)$ are the reciprocal lattice basis vectors of a triangular lattice in two dimensions. One can then substitute Eq. (94) into Eq.(92) and iteratively solve the non-linear equations for $C_{\mathbf{Q}}$ until convergence is reached (Kunimi and Kato, 2012). This procedure allows determining the optimal lattice spacing, the chemical potential, and the coefficients $C_{\mathbf{Q}}$. One finds that for low interaction strengths ($\gamma < 28$) the ground state of the system is in a uniform superfluid phase. Upon increasing the interaction at $\gamma \approx 28$ one crosses a first-order phase transition to a cluster supersolid phase characterized by a finite superfluid fraction and broken translational invariance where particles arrange in clusters (each cluster contains an average number of particles according to the density) in a triangular geometry. For even larger interactions $\gamma > 38$ the ground state preserves triangular symmetry but superfluidity vanishes resulting into an uncorrelated cluster crystal.

The validity of the above mean-field theory is limited to the regime of high densities, where the depletion of the condensate remains small in a wide range of interaction strengths. At lower densities, one has to resort to *ab*

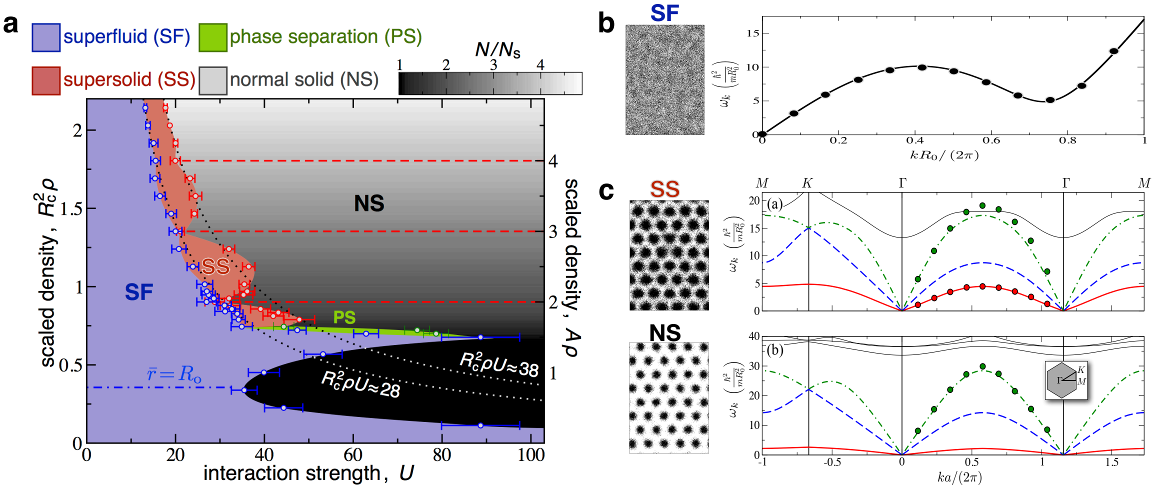

Figure 16 **Two-dimensional soft-core bosons in the continuum and their excitation spectrum.** (a) The phase diagram displays the emergence of superfluid (SF) and different solid (NS) and supersolid (SS) phases for varying interaction strength U and density ρ. The density on the left y-axis has been scaled by the soft-core radius R_c. The right axis gives the density in units of the inverse area, $A = \sqrt{3}(1.6R_c)^2/2$, of the unit cell of the high-density solid phase, corresponding to the lattice site occupation N/N_s for a given number of particles and lattice sites, N and N_s, respectively. For $A\rho \gtrsim 1.5$, the grey region labeled as NS corresponds to a cluster crystal with $N/N_s > 1$, as indicated by the greyscale. Horizontal dashed lines refer to integer filling. Supersolid phases with different occupation numbers are found between two hyperbolas, defined by $R_c^2\,\rho U = \text{const.}$ (dotted lines). At high densities ($A\rho \gtrsim 3.5$) they can be understood in terms of density modulated superfluids. In contrast, superfluidity within the low-density supersolid lobes emerges from delocalized zero-point defects according to the ALC scenario. Adapted from Ref. (Cinti *et al.*, 2014). (b) (left) PIMC snapshot illustrating the particle density profile in the SF phase. (right) Excitation spectrum in the superfluid phase at $\gamma = 11.86$ compared to the PIMC data (circles) of (Saccani *et al.*, 2012). (c) (left) PIMC snapshot illustrating the particle density profile in the SS and NS phases. (right) Mean-field spectra (solid, dashed, and dashed-dotted lines) at $\gamma = 16.93$ (top) and $\gamma = 30.62$ (bottom) numerically computed along the three symmetry directions of the Brillouin zone [see inset of bottom panel]. The symbols represent the PIMC data of (Saccani *et al.*, 2012) for longitudinal excitations computed along the direction $\Gamma - M - \Gamma$ in the first two Brillouin zones. Panels (b) and (c) adapted from Ref. (Macrì *et al.*, 2013).

initio methods to deal with the development of nontrivial correlations. Numerical results were obtained from Path-Integral Monte Carlo (PIMC) simulations (Ceperley, 1995) based on the continuous-space worm algorithm (Boninsegni *et al.*, 2006) to determine the equilibrium properties of the system in the canonical ensemble, that is, at a fixed temperature T and a fixed particle number (of the order of a few hundred). The properties of the system ground state are obtained by extrapolating observables, such as the total energy, superfluid fraction and pair-correlations to the zero temperature limit.

In Fig. 16(a) the zero-temperature phase diagram of one- and two-dimensional soft-core bosons in continuum space is presented. At small densities $R_c^2\rho \leq 0.5$ one finds two phases: a superfluid and an insulating triangular crystal composed of singly occupied sites, that is, where the number of lattice sites, N_s, equals the particle number N. A distinctive consequence of the soft-core interaction is that the energy cost for forming close particle pairs is bound by V_0. This fact potentially enables the formation of crystalline phases with $N > N_s$ above a critical density where doubly occupied lattice sites become energetically favorable on increasing the lattice constant.

The most interesting behavior takes place around the superfluid-solid quantum phase transition at $N/N_s = 2$. Starting from the insulating solid with doubly occupied lattice sites, removing a small number of particles does not cause structural changes of the ground state, but rather creates a small fraction $f_{\rm def} = (2N_s - N)/N_s > 0$ of zero-point crystal defects in the form of singly occupied sites. Such defects delocalize and give rise to a finite superfluid fraction, in agreement with the ALC scenario. It is worth noting that the coexistence of a cluster crystalline structure, breaking translational symmetry in equilibrium, and of particle diffusion is explained here by a thermally activated hopping mechanism, where particles delocalize without altering the underlying cluster crystalline matrix (Díaz-Méndez *et al.*, 2015).

The extension of this picture to the lattice case is readily obtained considering the 2D extended Bose-Hubbard model in presence of both finite-range soft-core interactions and an hard-core constraint. Already on the square lattice, this model displays an intriguing behavior (Masella *et al.*, 2019; Pupillo *et al.*, 2008) For intermediate interaction strengths $4 \leq V/t \leq 4.45$ the stripes can turn superfluid, thus leading to a self-assembled array of quasi-one-dimensional superfluids. These bosonic superstripes turn into an isotropic supersolid with decreasing interaction strength. It is relevant to notice that the mechanism for stripe formation is based on cluster self-assembling different from recently proposed mechanisms for dipolar magnetic atoms (Böttcher *et al.*, 2021), spin-orbit coupled BECs (Li *et al.*, 2017), or BECs with cavity-mediated interactions (Léonard *et al.*, 2017b). A two-component version of this model in the square lattice has also been recently proposed in (Li *et al.*, 2018), where, among the several phases of the model, one can observe that the components that interact via a soft-core potential can induce a supersolid phase in the other component. The out-of-equilibrium dynamics following a temperature quench to values well below the hopping amplitude $T/t \ll 1$ shows that together with classical solid phases and supersolids (for $3.8 \leq V/t \leq 4.2$) also a normal glass is observed (for $V/t > 5.5$) without any remnant superfluidity (Angelone *et al.*, 2020). It is interesting to observe that in a triangular lattice, the same system after a temperature quench displays a superglass and a normal glass phase (Angelone *et al.*, 2016). For high enough temperature, the glass and superglass turn into a floating stripe solid and a supersolid, respectively. Similar models of systems with nonlocal interactions diverging at the origin leading to glassy phases have been also recently investigated in the context of type-1.5 superconductors (Wang *et al.*, 2020) where the *particles* are point-like vortices in the presence of external disorder.

The three-dimensional soft-core model was investigated originally by (Ancilotto *et al.*, 2013; Henkel *et al.*, 2010) for the repulsive case and by (Maucher *et al.*, 2011) for the attractive one within a mean-field approach based on the solution of the 3D GPE of Eq. (92). In the repulsive isotropic case, the ground-state phase diagram displays a transition from a superfluid phase at low density and interactions to an fcc supersolid at intermediate densities, induced by a roton instability similar to the 2D case. For attractive interactions, one can prove the existence of (bright soliton) self-bound macroscopic states, stabilized purely by the competition of kinetic and negative mean-field energies.

2. Elementary excitations

The elementary excitations in the mean-field approximation are found by expanding the GPE energy functional around the solution $\psi_0(\mathbf{r})$, obtaining the so called Bogoliubov-de Gennes equations (Macrì *et al.*, 2013; Macrì *et al.*, 2014). Denoting the change in $\psi(\mathbf{r},t)$ by $\delta\psi(\mathbf{r},t) = e^{-i\mu t}\left[u(\mathbf{r})e^{-i\omega t} - v^*(\mathbf{r})e^{i\omega t}\right]$ and substituting this expression into the GPE Eq. (92) one finds a set of two coupled linear differential equations: for the Bogoliubov amplitudes $u(\mathbf{r})$ and $v(\mathbf{r})$. The solution of the Bogoliubov-de Gennes equations in the uniform superfluid phase is analytical

$$\epsilon_q = \sqrt{\frac{q^2}{2}\left(\frac{q^2}{2} + 2\gamma\, U_q\right)}, \tag{95}$$

and depends only on the modulus of the excitation vector $\mathbf{q}$. Here U_q is the Fourier transform of the potential. Eq.(95) can be extended to the case of multibody interactions (Laghi *et al.*, 2017). The spectrum is linear for small momenta and the slope defines the sound velocity of the system; for sufficiently large γ (the specific value depends on the shape of the interaction) one recovers the usual roton-maxon spectrum that is common to other physical systems with non-local interactions as ultracold dipolar systems or superfluid ^{4}He. In nonuniform phases, one has to rely on a numerical solution of the Bogoliubov equations. One can use a Fourier expansion of the Bogoliubov amplitudes followed by diagonalization of the corresponding equations. The results presented in Fig.16(b,c) are obtained using a grid-based solution in real space for the lowest excitation bands and for $\mathbf{q}$ vectors lying in the first Brillouin zone (FBZ) (Macrì *et al.*, 2013) for a soft-shoulder potential. The figure shows the excitation energies along the three symmetry axes of the Brillouin zone corresponding to the underlying triangular lattice. We find three gapless bands, i.e. three Goldstone modes reflecting the symmetries that are broken in the supersolid phase (Watanabe and Murayama, 2012, 2013). In addition to the superfluid band due to the breaking of global gauge symmetry, two bands correspond to longitudinal and transverse phonon excitations of the two-dimensional lattice. Even in the insulating phase, Bogoliubov-de Gennes equations yield excellent agreement for the longitudinal phonon mode with quantum Monte Carlo calculations based on the method of Genetic Inversion via falsification of the theories, which allows the calculation of the Laplace transform $F(k,\tau) = \int d\omega e^{-\tau\omega} S(k,\omega)$ of the dynamic structure factor (Saccani *et al.*, 2012). However, this technique is unable to describe the breakdown of global superfluidity. This indicates that each droplet maintains a high condensate fraction despite the apparent lack of global phase coherence between the crystalline ordered droplets. Proper identification of each band can be done by computing local fluctuations on top of the mean-field solution $\psi_0(r)$. One clearly distinguishes the transverse band from the direction of the fluctuations, orthogonal to the perturbing vector k. The contribution of this band to phase fluctuations is strongly suppressed. The first and third bands both contribute to density and phase fluctuations with different weights. The first band is mostly responsible for phase whereas the third for density fluctuations. Therefore the lower band can be associated with the superfluid response of the system, whereas the other two to the classical collective excitations of the crystal. The results for a Rydberg-dressed potential of Eq. (90)) are reported in (Macrì *et al.*, 2014). There the modes obtained by the solution of the Bogoliubov-de Gennes equations have been compared to quantum Monte Carlo calculations with the inclusion of the transverse excitation band. A good agreement between the two techniques has been obtained for all three excitation bands. We briefly comment that the calculation and the measurement of the excitation spectra received much attention also in the context of dipolar systems, both in trapped superfluid or droplet phases (Baillie *et al.*, 2017; Petter *et al.*, 2019), in supersolids (Petter *et al.*, 2020; Tanzi *et al.*, 2019b) both in the ground states and in excited states, e.g. in vortices (Cidrim *et al.*, 2018; Lee *et al.*, 2018; Roccuzzo *et al.*, 2020).

F. Structural transitions in mesoscopic long-range systems

The physics of structural transitions in power-law potentials has been deeply studied in prototypical mesoscopic systems of ions and dipolar systems thanks to the close connection to experimental realizations. The simplest one-dimensional case of a chain of singly-charged particles, confined by a harmonic potential, exhibits a sudden transition to a zigzag configuration when the radial potential reaches a critical value, depending on the particle number (Birkl *et al.*, 1992; Bluemel *et al.*, 1988). For charged particle interacting via the Coulomb potential ($\alpha = 1$) this structural change is a phase transition of second-order, whose order parameter is the crystal displacement from the chain axis (Fishman *et al.*, 2008; Morigi and Fishman, 2004; Piacente *et al.*, 2004; Schiffer, 1993) as was also experimentally observed (Enzer *et al.*, 2000; Kaufmann *et al.*, 2012). In the quantum limit the universality of the transition lies in the same class as the ferromagnetic Ising chain in a transverse field (Friedenauer *et al.*, 2008; Porras and Cirac, 2004; Shimshoni *et al.*, 2011). The zig-zag transition also appears in strongly interacting one-dimensional electrons systems, i.e. quantum wires, whose Wigner-crystal phase corresponds to a splitting of the Fermi gas into two chains (Meyer *et al.*, 2007). Interestingly, the zig-zag transition has been also related to the Peierls instability which occurs in antiferromagnetic spin chains coupled to phonon modes (Bermudez and Plenio, 2012).

As the range of the interactions decreases to $\alpha > 2$ the nature of the transition is radically modified due to the coupling between transverse and axial vibrations (Cartarius *et al.*, 2014), which leads to a weakly first-order transition in analogy with the case of ferromagnetic transitions in presence of phonon excitations (Imry, 1974; Larkin and Pikin, 1969). This is particularly relevant to the study of self-organized phases in polar systems (Astrakharchik *et al.*, 2007; Büchler *et al.*, 2007; Góral *et al.*, 2002). For the case of purely dipolar interactions, detailed QMC calculations at zero temperature investigated the fluid-solid transition (Moroni and Boninsegni, 2014), ruling out the microemulsion scenario for any physical realization of this system, given the exceedingly large predicted size of the bubbles. In higher dimensions crystals of repulsively interacting ions in planar traps form hexagonal lattices and undergo an instability towards a multilayer structure as the transverse trap frequency is reduced. The new structure is composed of three planes, with separation increasing continuously from zero. Mapping to the six-state clock model can be performed, implying that fluctuations split the buckling instability into two thermal transitions, accompanied by the appearance of an intermediate critical phase. A BKT phase is predicted interfacing the disordered and the ordered phase (Podolsky, 2016).

Another important case is the generalization to the case of multi-scale potentials which has been recently studied in the quantum regimes in Refs. (Abreu *et al.*, 2020; Cinti and Macrì, 2019; Pupillo *et al.*, 2020) which, for specific configurations of the pairwise potential, can support quasicrystalline phases or stripe phases. The corresponding criteria to realize structural phases in these more complex potentials have been investigated (Mendoza-Coto *et al.*, 2017, 2019; Mendoza-Coto and Stariolo, 2012; Mendoza-Coto *et al.*, 2015a,b, 2021b).

Finally, we comment on the presence of smectic, nematic, and hexatic phases in quantum systems with competing non-local interactions, which presents several analogies to the case of classical liquid-crystal systems(Abanov *et al.*, 1995). This parallel, which derives from the similarity between the anisotropic nature of the stripe order and the elongated shape of liquid-crystal molecules, allows the application of traditional results from liquid-crystal systems (P. G. de Gennes, 1993; P. M. Chaikin, 1995) to predict the qualitative, and to some extent also quantitative phase behavior of many systems with modulated order parameters.

In the context of dipolar Fermi gases theory has been, until now, ahead of experiments, with several preliminary theoretical calculations predicting exotic scenarios, such as p-wave superfluid (Bruun and Taylor, 2008), supersolid (Lu *et al.*, 2015), hexatic (Bruun and Nelson, 2014; Lechner *et al.*, 2014), and Wigner crystal phases (Matveeva and Giorgini, 2014). In these systems stripe formation (in the form of charge density waves) and nematic phases should also occur with features analogous to the ones present in low temperature long-range solid-state systems.

G. Flat interactions

Systems with flat interactions ($\alpha = 0$) constitute a unique setup in the realm of long-range interactions, since they often allow exact analytical solutions of their thermodynamic and critical properties, at least at large scales. Yet, several of their qualitative features exactly reproduce the more complex physics of general strong long-range systems with $0 < \alpha < d$. This special role makes such systems worthy of a special focus and in this section, we are going to consider examples of fully connected quantum systems.

1. The Lipkin-Meshkov-Glick model

The LMG, one the most famous example of strong long-range interacting model in the quantum realm, has been first introduced as a simple test for the validity of perturbative techniques in many-body theories (Glick *et al.*, 1965; Lipkin *et al.*, 1965; Meshkov *et al.*, 1965). Subsequently, the model has been applied to investigate many-body systems that allowed for a sensible descriptions in terms of mean-field interactions, such as coupled BECs (Cirac *et al.*, 1998) or BCS systems (Dusuel and Vidal, 2005b). The LMG Hamiltonian describes N 1/2-spins coupled by flat ferromagnetic interactions of strength J/N

$$H_{\mathrm{LMG}} = -\frac{J}{N}\sum_{i<j}(\sigma_i^x\sigma_j^x + \gamma\sigma_i^y\sigma_j^y) - h\sum_{j=1}^{N}\sigma_j^z. \quad (96)$$

where γ is the anisotropy parameter. At $\gamma = 0$, the former Hamiltonian corresponds to the fully connected quantum Ising model in a transverse field.

The key property of any flat interaction problem is the possibility to rephrase it in terms of the collective variable, which is the linear combination of all the microscopic variables. Indeed, in our case one can introduce the collective spin $S_\mu = \sum_{i=1}^{N}\sigma_i^\mu/2$, where $\mu \in \{x, y, z\}$. In terms of the new variables Eq. (96) reads

$$H_{\mathrm{LMG}} = -\frac{2J}{N}(S_x^2 + \gamma S_y^2) - 2hS_z + \frac{J}{2}(1+\gamma). \quad (97)$$

which describes a single self-coupled N-component spin immersed into a magnetic field. The Hamiltonian H_{LMG} preserves both the total spin and the total magnetization values

$$[H_{\mathrm{LMG}}, \boldsymbol{S}^2] = 0 \quad [H_{\mathrm{LMG}}, S_z] = 0, \quad (98)$$

where $\boldsymbol{S}^2 = S_x^2 + S_y^2 + S_z^2$. The highly symmetric nature of this model makes it particularly amenable also to numerical techniques, making it a prominent test-bed for novel algorithms (Albash and Lidar, 2018; Bapst and Semerjian, 2012). Moreover, it has been used to demonstrate several generic properties of quantum critical points, such as finite size (Botet *et al.*, 1982) and entanglement scaling (Amico *et al.*, 2008; Wichterich *et al.*, 2010).

Nowadays, the LMG model is subject to renewed interest also due to its relation with the celebrated Dicke model, which is often used to describe driven-dissipative experimental setups, such as the cavity QED experiments outlined in Sec. II.B. Its Hamiltonian contains spin-1/2 operators coupled to the cavity electromagnetic field. In analogy with the long-range Ising model, the Dicke model displays a phase transition between a disordered ground state with $\langle\sigma_x\rangle = \langle a^\dagger a\rangle = 0$ and a super-radiant one with polarised spins and finite photon density inside the cavity $\langle a^\dagger a\rangle \neq 0$ (Dicke, 1954). At equilibrium, it can be rigorously proven that the Hamiltonian of the Dicke and LMG models are equivalent in the thermodynamic limit and, then, produce the same critical behavior (Brankov *et al.*, 1975; Gibberd, 1974).

The contribution of quantum fluctuations to the thermodynamic observables is washed away in the large size limit $N \to \infty$ and the total spin $\boldsymbol{S}$ effectively becomes classical (Bapst and Semerjian, 2012; Chayes *et al.*, 2008). Therefore, the control parameter for quantum fluctuations in the LMG model is $1/N$, which plays the same role of $\hbar$ in more traditional single-body problems. In the following, we are going to restrict to $h > 1$, as the spectrum of the model is symmetric under inversion $h \to -h$, and to ferromagnetic interactions $J > 0$. A discussion on the physics of the antiferromagnetic problem $J < 0$ and its relation to the super-symmetric formalism can be found in (Vidal *et al.*, 2004). For ferromagnetic interactions $J > 0$, the ground state always belongs to the maximum spin $S = N/2$ sub-sector of the Hilbert space.

Apart from the fully isotropic limit $\gamma = 1$, the LMG Hamiltonian cannot be analytically solved (Botet and Jullien, 1983). Nevertheless, the LMG Hamiltonian is integrable and can be solved via algebraic Bethe ansatz (Pan and Draayer, 1999) or by mapping it to the Richardson-Gaudin Hamiltonian (Dukelsky *et al.*, 2004). Here, we are going to follow a simpler route and employ the $1/N$ expansion. First of all, we characterise the critical behaviour employing the mean-field approximation by using the non-interacting variational ansatz obtained via the external product of the single spin states

$$|\psi_l\rangle = \cos\left(\frac{\theta_l}{2}\right)e^{-i\frac{\varphi_l}{2}}|\uparrow\rangle + \sin\left(\frac{\theta_l}{2}\right)e^{i\frac{\varphi_l}{2}}|\downarrow\rangle. \quad (99)$$

Since the system is translationally invariant, we can assume $(\theta_l, \varphi_l) = (\theta, \varphi)\ \forall l$, corresponding to the spin expectation values

$$\boldsymbol{S} = \frac{N}{2}(\sin\theta\cos\varphi, \sin\theta\sin\varphi, \cos\theta), \quad (100)$$

which coincides with the classical spin value. Due to the inversion symmetry of the model $S_x \to -S_x$ one can select $\varphi = 0$ and $J = 1$, without loss of generality. From the energy minimization within the mean-field ansatz, one obtains the explicit expression

$$\theta = \begin{cases} 0 \text{ if } h \geq 1 \\ \arccos(h) \text{ if } 0 \leq h \leq 1 \end{cases} \quad (101)$$

for the angle θ. The semiclassical equations of motion for the total spin operators yield the system gap in the thermodynamic limit (Botet and Jullien, 1983)

$$\Delta = \begin{cases} 2\sqrt{(h-1)(h-\gamma)} \text{ if } h \geq 1 \\ 0 \text{ if } 0 \leq h \leq 1 \end{cases} \tag{102}$$

A close inspection of the formulas above is all one needs to comprehend the quantum phase transition in the LMG problem. At $h \geq 1$ only the solution $\varphi = \theta = 0$ exists and the system is fully magnetised along the magnetic field direction, $\langle S_z \rangle = 1$. As h decreases below $h_c = 1$ two-state appears with $\theta \neq 0$ and $\varphi = \pm\pi$ and the in-plane magnetisation continuously increases in the interval $[0, 1]$, while the transverse magnetisation only vanishes at $h = 0$. Accordingly, the gap Δ between the ground and the first excited state, which is finite at $h > 1$, smoothly vanishes as $h \to 1^+$ with scaling behavior characterized by the critical exponent $z\nu = 1/2$. It is worth noting that the mean-field scenario can be only faithfully applied to the thermodynamic limit, while it cannot capture finite-size fluctuations. Indeed, in the ordered phase $h < 1$ the system gap Δ cannot vanish at a finite size, since quantum fluctuations will lift the degeneracy and produce an exponentially vanishing gap $\Delta_N \propto \exp(-N)$ (Newman and Schulman, 1977).

In order to partially capture finite size fluctuations, it is convenient to perform the Holstein-Primakoff expansion (Holstein and Primakoff, 1940) for the N-spin variable $\boldsymbol{S}$ around the mean-field expectation value (Botet and Jullien, 1983; Dusuel and Vidal, 2005a). First, one shall rotate the total spin in order to align it with the meand field magentization introducting the new variable $\bar{S} = R(\theta)S$, with the rotation matrix

$$R(\theta) = \begin{pmatrix} \cos\theta & 0 & \sin\theta \\ 0 & 1 & 0 \\ -\sin\theta & 0 & \cos\theta \end{pmatrix} \tag{103}$$

where θ is given by Eq. (101). The re-aligned spin variables may be then expanded using the equivalence

$$\bar{S}_z = \frac{N}{2} - a^\dagger a \tag{104}$$

$$\bar{S}_+ = \bar{S}_x + i\bar{S}_y = \sqrt{N}\left(1 - \frac{a^\dagger a}{N}\right)^{1/2} a \tag{105}$$

$$\bar{S}_- = \bar{S}_x - i\bar{S}_y = \sqrt{N} a^\dagger \left(1 - \frac{a^\dagger a}{N}\right)^{1/2} \tag{106}$$

where the boson operators $[a, a^\dagger] = 1$ have been introduced. This excitation characterises a small depletion of the mean-field spin expectation due to finite size quantum fluctuations. At leading order in $1/N$ only quantum corrections up to order $1/N$ have to be retained, yielding a quadratic bosonic Hamiltonian which can be subsequently diagonalised by a Bogoliubov transformation $a \to b$ (Dusuel and Vidal, 2005a). The net result is

$$H_{\text{LMG}} = NE_0 + e_0 + \omega b^\dagger b + O\left(\frac{1}{N}\right) \tag{107}$$

such that we have reduced the many-body problem in Eq. (96) to an effective 0-dimensional one, described by a single harmonic oscillator mode. This is the peculiarity of several fully connected systems, the actual spectrum in the thermodynamic limit is not constituted by a continuum dispersion relation, but rather by a single quantum mode, whose contribution to the thermodynamic quantities is increasingly washed out approaching the thermodynamic limit.

The quantities appearing in Eq. (107) can be easily written in terms of the internal parameter and the average magnetization $m = 2\langle S_z \rangle/N$. The internal mean-field energy maintains the same form both in the symmetric and broken phases $E_0 = (-1 - 2hm + m^2)/2$, while the next-to-leading energy correction reads

$$e_0 = \begin{cases} -h + \frac{1+\gamma}{2} + \sqrt{(h-1)(h-\gamma)} & \text{for } h > 1, \\ -\frac{1-\gamma}{2} + \sqrt{(1-h^2)(1-\gamma)} & \text{for } h < 1, \end{cases} \tag{108}$$

and the dynamical gap

$$\omega = \begin{cases} 2\sqrt{(h-1)(h-\gamma)} \text{ for } h > 1, \\ \sqrt{(1-h^2)(1-\gamma)} \text{ for } h < 1. \end{cases} \tag{109}$$

Notice that ω is not the actual gap Δ of the system, at least not in the ordered phase, where the minimal gap occurs between the two classical ground-states with different symmetry, but it rather represents the minimal gap between two states connected by the Hamiltonian dynamics.

As expected, the dynamical gap in Eq. (109) vanishes approaching the transition with a dynamical critical exponent $z\nu = 1/2$ in agreement with the semiclassical prediction for the disordered phase, see Eq. (102). The exponent is symmetric on both sides of the transition and independent on the value of $\gamma \neq 1$ proving that the anisotropy plays no role in the universal behavior. The only exception is $\gamma = 1$ where the system acquires continuous rotation symmetry, giving rise to a gapless ordered phase and a critical exponent $z\nu = 1$; an analytical solution of the problem is available in this particular case (Dusuel and Vidal, 2005a).

The in-plane magnetisation $\langle S_x \rangle/N \propto \sqrt{1-h^2}$ is consistent with a critical exponent $\beta = 1/2$. Similar arguments can be used to show that all the *thermodynamic* critical exponents, i.e. the ones associated with global thermodynamic quantities, are in agreement with mean-field theory. The question becomes, however, more complex if we consider the scaling of spatial dependent quantities such as the correlation length. Conventionally, the critical exponent ν is associated with the scaling of the correlation length ξ at a (quantum) critical point $\xi \propto \lambda^{-\nu}$, where λ is the control parameter. Such critical exponent is particularly important since it relates the thermodynamic singularities of any critical quantity, with its finite-size scaling close to the transition (Fisher, 2002; Fisher and Barber, 1972). However, in a strong long-range system, and in particular in a fully connected one, no concept of length and, especially, of correlation length exists.

However, even in absence of any definition of length, it is possible to define a correlation number, which diverges close to the critical point $N_c \propto |h-1|^{\nu_*}$. In general such correlation number will be proportional to the correlation volume $N_c \propto \xi^d$ and, assuming that such scaling has to remain the same for all systems in the mean-field regime, one obtains the estimate

$$\nu_* = d_{\mathrm{uc}}\nu. \tag{110}$$

The quantity d_{uc} represents the upper critical dimension of the corresponding nearest neighbour model (Botet *et al.*, 1982). Since the LMG Hamiltonian in Eq. (96) corresponds to the one of the quantum Ising model in a transverse field with $d_{\mathrm{uc}} = 3$, the correlation number exponents shall read $\nu_* = 3/2$.

Interestingly, this scaling theory, first introduced in Ref. (Botet *et al.*, 1982), provides the exact value for the finite-size scaling of the dynamical gap ω_N which can be obtained by incorporating higher-order $1/N$ corrections into Eq. (109) via the continuous unitary transformation approach, yielding $\omega_N \approx N^{-1/3}$ (Dusuel and Vidal, 2004, 2005a) in perfect agreement with the generalised finite-size scaling theory $\omega_N \approx N^{-\frac{z\nu}{\nu_*}}$. Despite this apparent simplicity, it has been shown that for large enough anisotropy parameters the spectrum of the LMG model may not converge to the prediction of Eq. (107), due to the influence of two competing semiclassical trajectories (Ribeiro *et al.*, 2007).

More in general, the convergence to the "simple" thermodynamic limit solution in fully connected models has been shown to present several anomalous features (Colonna-Romano *et al.*, 2014). In particular, it has been shown that the actual picture for the finite-size scaling of many-body systems above the upper critical dimension d_{uc} is actually more complicated than the one depicted in Ref. (Botet *et al.*, 1982), since the zero and the fluctuations modes present different scaling behaviors and, therefore, different quantities may display different finite-size corrections depending on the dominating contribution to that quantity (Flores-Sola *et al.*, 2016b).

2. Self-organization phase transition in cavity QED

The LMG model can effectively be realized using cavity QED platforms, whose self-organization transition can be described by a pure fully-connected spin Hamiltonian upon elimination of the cavity field in Eq. (13). There, the cavity-mediated long-range interaction, Eq. (12), favors for $\mathcal{V} < 0$ a density modulation of the quantum gas and induces density correlations with spatial periodicity λ along pump and cavity directions. These density correlations are the collective elementary excitations of the system with energy $\hbar\omega_s$ and correspond to the creation and annihilation of correlated pairs of atoms in the momentum mode $|\mathbf{p}_1\rangle$. However, the kinetic energy term in Eqs. (9) stabilizes the gas against this modulation.

Only if the long-range interaction becomes sufficiently strong, the gain in potential energy will overcome the cost in kinetic energy, and the system undergoes a quantum phase transition to a self-ordered state (Nagy *et al.*, 2008; Piazza *et al.*, 2013). At this point, the energy $\hbar\omega_s$ of the collective excitation has softened such that the mode $|\mathbf{p}_1\rangle$ can be macroscopically populated without energetic cost. The atomic density acquires a checkerboard modulation that efficiently scatters photons into the resonator, and the atoms can further lower their energy in the emerging optical interference lattice potential.

A few years after self-organization of a thermal gas coupled to an optical cavity had been observed (Black *et al.*, 2003), the phase transition to a self-ordered state of a bosonic quantum gas coupled to a cavity was realized (Baumann *et al.*, 2010). While for a thermal gas the threshold is set by thermal density fluctuations, for a quantum gas the critical point scales with the recoil energy. A BEC of 10^5 ^{87}Rb atoms is harmonically trapped at the location of a single mode of a high-finesse optical cavity. The transverse pump power is linearly increased over tens of milliseconds. The experimental signature for self-ordering of a BEC, where the motion is quantized, is two-fold as shown in Fig. 17: The cavity photon occupation rises abruptly when the critical interaction is reached, as can be observed via the light field leaking from the cavity. In addition, the momentum state distribution, as observed from absorption images after ballistic expansion, changes from occupying only the zero-momentum state $|\mathbf{p}_0\rangle$ below the critical point to a superposition of the momentum states $|\mathbf{p}_0\rangle$ and $|\mathbf{p}_1\rangle$ above the critical point. In real space, this momentum state occupation corresponds to a chequerboard order of the atomic density. Ramping the transverse pump power down again, the normal phase with an empty cavity and macroscopic occupation of only the single momentum state $|\mathbf{p}_0\rangle$ is recovered. As discussed in Section II.B.3, the self-organization phase transition can be mapped to the Dicke phase transition.

The mode softening preceding the phase transition (Horak and Ritsch, 2001; Nagy *et al.*, 2008; Öztop *et al.*, 2013) has been studied using a variant of Bragg spectroscopy (Mottl *et al.*, 2012). The cavity is seeded with a weak coherent field at a variable detuning with respect to the transverse pump frequency. If the detuning matches the soft mode frequency ω_s, energy and momen-

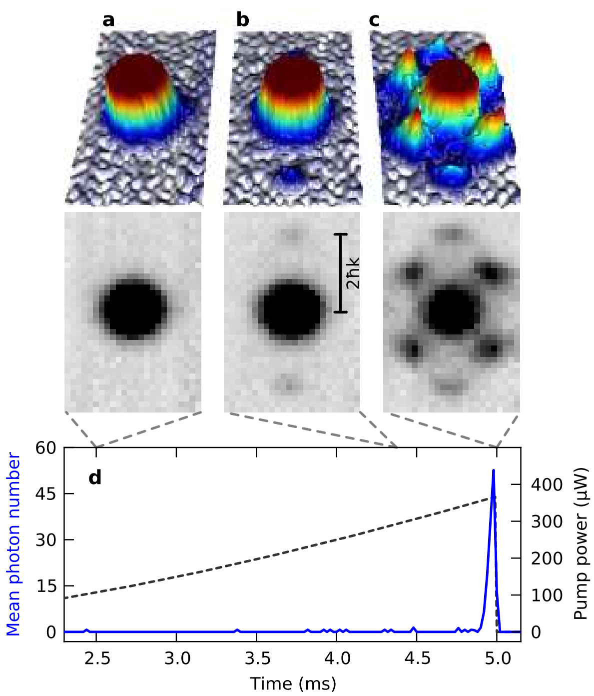

Figure 17 **Signatures of atomic self-organization in an optical cavity. (a)** The transverse pump power (dashed) is gradually increased while the mean intracavity photon number (solid) is monitored. After the sudden release of the atomic cloud and its subsequent ballistic expansion, absorption images are made for pump powers corresponding to transverse pump lattice depths of 2.6 E_r (b), 7.0 E_r (c) and 8.8 E_r (d). Self-organization is manifested by an abrupt build-up of the cavity field accompanied by the formation of momentum components at $(p_x, p_y) = (\pm\hbar k, \pm\hbar k)$ (d). The weak momentum components at $(0, \pm 2\hbar k)$ result from loading the atoms into the one-dimensional standing-wave potential of the transverse pump laser. Reproduced from (Baumann *et al.*, 2010).

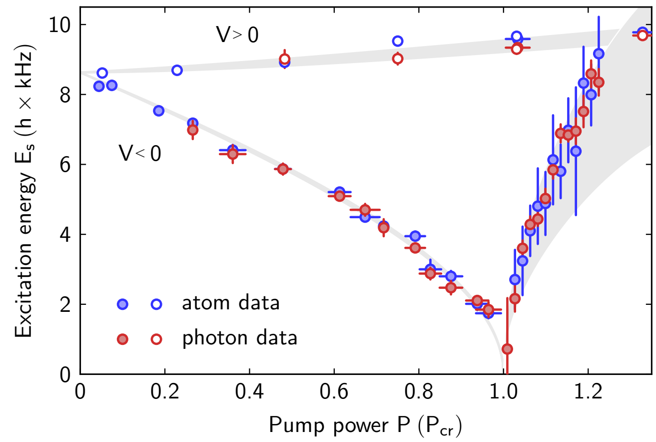

Figure 18 **Excitation spectrum across the self-organization phase transition.** Measured resonance frequencies $E_s = \hbar\omega_s$, obtained from atomic and photonic signals, are shown in blue and red, respectively, for positive (open circles) and negative (solid circles) interaction strength $\mathcal{V}$. Gray shading shows the theoretical prediction including experimental uncertainties. Reproduced from (Mottl *et al.*, 2012).

tum conservation are fulfilled, and the momentum mode $|\mathbf{p}_1\rangle$ becomes macroscopically occupied by the probing process. At the same time, photons from the transverse pump are scattered into the cavity. The measured mode frequency ω_s as a function of transverse pump power is displayed in Fig. 18. For the case of negative long-range interaction $\mathcal{V} < 0$, a clear mode softening towards the critical point of the self-organization phase transition is observed. In contrast, a positive long-range interaction $\mathcal{V} > 0$ is leading to a mode hardening without any phase transition.

Also in the case of a sideband-resolving cavity, $\kappa < \omega_s$, a self-organization phase transition takes place. However, due to the increased photon lifetime, the intra-cavity field acquires a retardation with respect to the atomic evolution, and the effective cavity-mediated atom-atom interaction can not be captured anymore in the simple form of Equation (12) (Klinder *et al.*, 2015a). In this case, it is more appropriate to stay with the coupled equation of motion. As we discuss below in Section V.C.4, the sideband resolved regime allows to study quench experiments that can be interpreted with a Kibble-Zurek model.

The long-range interaction can not only be engineered to act on the atomic density. Instead, exploiting the atomic vector polarizability or Raman schemes coupling different atomic ground states, an effective long-range interaction acting on the pseudospin can be realized (Camacho-Guardian *et al.*, 2017; Kroeze *et al.*, 2018; Landini *et al.*, 2018).

3. Discrete and continuous symmetry breaking

The Dicke Hamiltonian (13) is invariant under the parity transformation $(a, S_\pm) \to (-a, -S_\pm)$. Accordingly, at the phase transition to the self-organized phase a discrete $\mathbf{Z}_2$-symmetry is broken, where the atomic density localizes either on the even or odd sites of the emergent checkerboard lattice and the cavity light field phase locks to either 0 or π with respect to the pump field phase. Site-resolving real-space imaging of the atomic system has not been achieved yet. However, this discrete symmetry breaking has been observed in the phase of the light field leaking from the cavity using a phase-sensitive heterodyne detection system (Baumann *et al.*, 2011).

The discrete nature of this symmetry breaking is dictated by the boundary conditions of the single cavity mode. The symmetry can however be enhanced to a continuous $U(1)$-symmetry, as had been originally discussed for highly degenerate multimode cavities (Gopalakrishnan *et al.*, 2009). Also, the self-organization of a transversely driven BEC in the combined fields of two degenerate single-mode cavities crossing under an angle of

60° allows engineering an approximate continuous $U(1)$-symmetry, as was demonstrated experimentally (Léonard *et al.*, 2017b). Photons from the pump field were scattered into both cavities, and the atoms self-organized in the resulting interference potential. This system is invariant with respect to redistributing photons between the two modes, where the interference lattice potential breaks a continuous spatial symmetry depending on the relative photon occupation of the two cavities. The unique real-time access to the light field leaking from the optical cavities allowed one to identify the fundamental collective excitations of the underlying $U(1)$-symmetry as a phase and an amplitude mode (Léonard *et al.*, 2017a). The continuous symmetry can be reduced to a $\mathbf{Z}_2 \otimes \mathbf{Z}_2$ symmetry if atom-mediated scattering between the two cavities is present (Lang *et al.*, 2017; Morales *et al.*, 2018). Extending the scheme to multiple crossing cavities, also higher symmetries such as a continuous $SO(3)$ rotational symmetry might be realizable (Chiacchio and Nunnenkamp, 2018). A continuous symmetry can furthermore be broken if instead of two counterpropagating modes of a ring cavity are employed, as was proposed for a transversally driven BEC (Mivehvar *et al.*, 2018), and realized for a BEC coupled to a ring cavity where two longitudinal modes were simultaneously driven. This configuration can be regarded as the minimal model of a supersolid state of matter (Schuster *et al.*, 2020), which has been extensively discussed in Sec. IV.E.

4. Criticality of the self-ordering phase transition

The critical behavior of the single-mode self-organization phase transition corresponds to that of the open Dicke model, falling into the universality class of the mean-field classical Ising model (Emary and Brandes, 2003; Kirton *et al.*, 2019; Nagy *et al.*, 2010). The constant flow of energy from the pump laser to the cavity leakage causes additional fluctuations of the cavity field and accordingly larger density fluctuations. The cavity dissipation thus makes the system leave its ground state and irreversibly evolve into a non-equilibrium steady state. The global range interaction turns the phase transition rather into a quantum bifurcation in a zero-dimensional system, such that there is no notion of a divergent correlation length. However, one can investigate the critical exponent of the fluctuations of the order parameter. While a mean-field exponent of 1/2 is expected for the closed system, see the discussion in Sec. IV.G.1, the prediction for the open system is 1, given by the vanishing of the imaginary part of the spectrum at the critical point (Nagy *et al.*, 2011; Öztop *et al.*, 2012). The open system thus effectively behaves thermally. It is important to note that the actual steady state of the system might not be reached in experiments, since close to the critical point the quasinormal modes vanish, leading to a critical slowdown. An analysis going beyond the mapping to the open Dicke model and considering also a finite temperature of the quantum gas produces an interesting picture of the interplay between the self-organization phase transition and Bose-Einstein condensation (Piazza and Strack, 2014; Piazza *et al.*, 2013).

Monitoring the light field leaking from the cavity during self-organization gives real-time access to the order parameter of the phase transition, see Eq. (10). This allows not only to measure the mean density modulation of the atomic cloud but also to detect the fluctuations of the system (Brennecke *et al.*, 2013). Heterodyne detection of the light field provides the low-energy spectrum of the system which can be directly converted into the dynamical structure factor of the gas at the wave vector of self organization (Landig *et al.*, 2015), see Fig. 19 (a-d). The observed spectrum features a carrier at zero frequency with respect to the pump laser frequency and sidebands at positive and negative frequencies. The sidebands are signatures of density fluctuations, indicating either the creation or annihilation of quasi-particles. Approaching the critical pump power P_{cr}, the mode softening is visible in the vanishing sideband frequency. At the critical point, a strong coherent field emerges at the carrier frequency, indicating the buildup of a static coherent density modulation. The amplitude of the carrier and the integrated sidebands converted into density modulation and density fluctuations, respectively, is displayed in Fig. 19(f). While the density modulation changes by more than four orders of magnitude, the density fluctuations diverge towards the critical point. From this data, critical exponents of 0.7(1) and 1.1(1) for the fluctuations of the order parameter can be extracted on the normal and self-organized sides, respectively. The sideband asymmetry visible in Fig. 19(b-d) can be used to determine the occupation of the quasi-particle mode, but also to extract the irreversible entropy production rate (Brunelli *et al.*, 2018) while the system crosses the phase transition.

V. DYNAMICAL CRITICAL BEHAVIOUR

In this section, we review the multifaceted aspects of dynamical regimes in quantum long-range aspects, emphasizing as much as possible universal behaviors. Given the vast amount of literature on the subject, we decided to arrange the material presenting first a discussion of metastability, a hallmark of long-range systems, followed by a presentation of results on Lieb-Robinson bound, Kibble-Zurek mechanism, dynamical phase transitions, and confinement in quantum long-range systems. Miscellaneous material is presented in the last section.

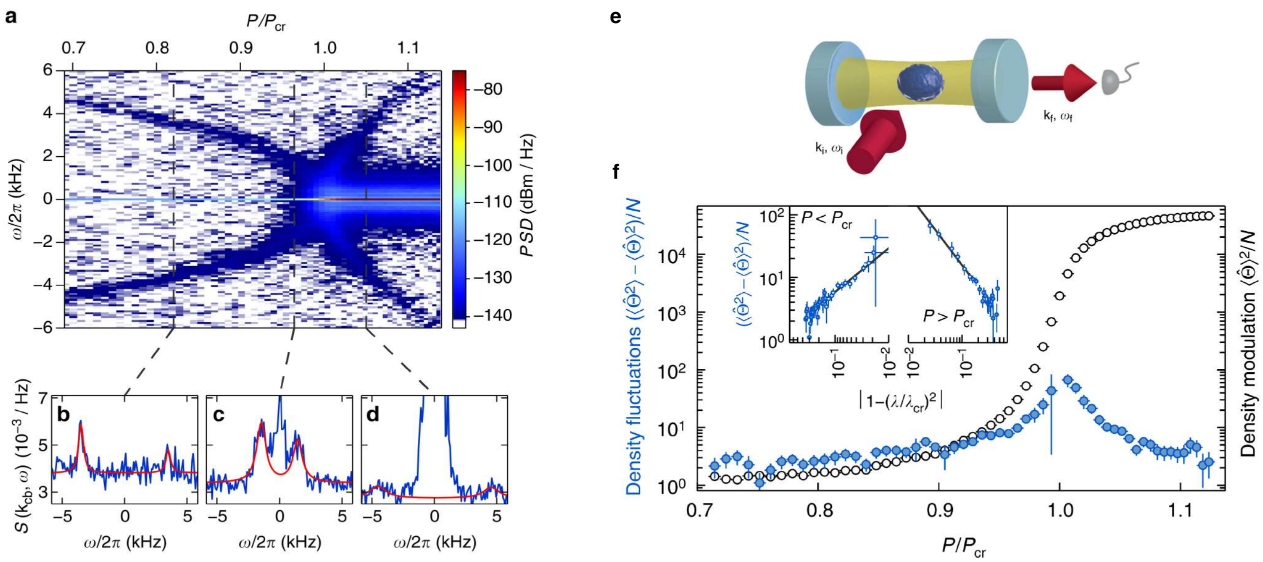

Figure 19 **Critical behavior of the self-organization phase transition.** (**a**) The power spectral density PSD of the light field leaking out of the cavity is shown as a function of frequency shift ω with respect to the pump laser frequency and relative transverse pump power $P/P_{\rm cr}$. Two sidebands are visible, corresponding to the incoherent creation ($\omega < 0$) and annihilation ($\omega > 0$) of quasi-particles. The energy of these quasi-particles vanishes towards the critical point. At the phase transition, a strong coherent field at the pump frequency appears ($\omega = 0$). The panels (**b–d**) show the normalized dynamic structure factor for three different values of $P/P_{\rm cr}$ (see dashed lines in upper panel). While the position and width of the sidebands give direct access to the energy and lifetime of the quasi-particles, the sideband asymmetry can be used to determine the occupation of the quasi-particle mode. Panel (**e**) is a sketch of the measurement setup: the atoms coupled to the cavity mode are illuminated by the transverse pump field at frequency ω_i, while the frequency emitted from the cavity is ω_f. A heterodyne detection system gives access to the PSD shown as a function of $\omega = \omega_i - \omega_f$ in (**a**). The data can be used to extract the divergent density fluctuations and the emerging density modulation, shown in (**f**). The inset shows the density fluctuations on a double logarithmic scale, allowing to determine critical exponents of 0.7(1) and 1.1(1) on the normal and self-organized sides, respectively. Figure reproduced from (Landig *et al.*, 2015).

A. Metastability and diverging equilibration times

Diverging equilibration times in the thermodynamic limit are a notorious characteristic of long-range interacting systems. Recently, the absence of equilibration of strong long-range quantum systems has been directly linked to their peculiar single-particle spectrum, which leads to a violation of Boltzmann's H-theorem and the appearance of finite Poincaré recurrence times in the thermodynamic limit (Defenu, 2021). These observations are in agreement with the aforementioned properties, see Sec. I.B, which are common to thermodynamically large long-range systems and finite local ones, such as the impossibility to fully disregard boundary over bulk phenomena (Barré and Gonçalves, 2007; Latella *et al.*, 2015), the existence of concave entropy regions (Ispolatov and Cohen, 2001) or the presence of a macroscopic energy gap between the ground state and the first excited state (Gupta *et al.*, 2012a,b).

The key point is that the spin-wave spectrum of the systems does not become continuous in the thermodynamic limit, as the eigenvalues of a long-range coupling matrix can be shown to remain discrete even in the infinite components limit, forming a pure point spectrum (Last, 1996) similar to the one appearing in strongly disordered systems (Fröhlich and Spencer, 1983; Scardicchio and Thiery, 2017; Simon *et al.*, 1985; Thouless, 1972). A discussion of the spectral discreteness of long-range couplings in the thermodynamic limit has been presented in Ref. (Defenu, 2021) in multiple linear approximations and employed to justify the observation of diverging equilibration times in a long-range Ising model, quenched across its quantum critical point (Kastner, 2011).

The first evidence of QSS in quantum systems has been described in the prototypical example of the long-range Ising chain, see (60). The QSS have been shown to appear for quenches starting well inside the paramagnetic phase in the $h \to +\infty$ limit and terminating in deep in the ferromagnetic phase at $h = 0$. Then, the system is prepared in the transversally polarised ground state and evolved according to the classical ferromagnetic Hamiltonian in absence of the transverse field. It follows that the expectation of the global operator $m_z = \langle \sum_i \sigma_i^z \rangle / N$ with the Hamiltonian in Eq. (60) evolves from the initial value $\lim_{t\to 0} m_z = 1$ to the equilibrium expectation $\lim_{t\to\infty} m_z = 0$, if the system actually equilibrates, see Fig. 20(a). These observations may be extended to any choice of the initial and final magnetic fields h_i, h_f using the Kitaev chain representation of the Ising model given in Eq. (65), see the discussion in Sec. IV.B.3.

It is worth recalling that for $1 < \alpha < 3$ the correspondence between the fermion and spin Hamiltonians in respectively Eqs. (60) and (65) is not exact. Yet, the existence of the quantum critical points is preserved and the equilibration scenario for the two systems is analogous (Essler *et al.*, 2012; Van Regemortel *et al.*, 2016). The analogy between the transition of the Ising and Kitaev chain has been discussed in Sec. IV.B.3 and in the Refs. (Defenu *et al.*, 2019a; Jaschke *et al.*, 2017). Within the Kitaev chain perspective, the critical point at $h = h_c = 1$ is signalled by the property $\lim_{k\to 0^\pm} \theta_k = \pm\frac{\pi}{2}$, where the critical Bogoliubov quasi-particles are constituted by an equal superposition of electrons and holes ($|u_{k=0}| = |v_{k=0}| = 1/\sqrt{2}$). This phenomenon is often interpreted as a Dirac mode resulting from the superposition of two Majorana edge states (Fradkin, 2013).

In the strong long-range regime ($0 < \alpha < 1$) and in presence of the Kac rescaling a full characterization of the quantum phase transition in the Kitaev chain has not been attempted yet. Indeed, no clear continuum limit can emerge for this regime in thermodynamic limit due to the spectral discreteness evidenced in Ref. (Defenu, 2021). Nevertheless, the existence of the quantum critical point can be also inferred in the strong long-range regime, analyzing the $k \to 0$ limit of the Bogoliubov angles.

The equilibration of a weak long-range Kitaev chain after a sudden quench of the chemical potential h is summarised in the upper sub-panel of Fig. 20(b). The initial state of the system is the ground state at $h = h_i \gg 1$, deep in the normal phase, where $m_z \approx 1$. Then, this initial state is evolved according to the ferromagnetic Hamiltonian with $h = h_f < 1$. The explicit description of the quench dynamics solution can be found in Ref. (Defenu *et al.*, 2019a). To compare with the aforementioned investigations regarding QSS in the long-range Ising model the pictures displays the evolution of the observable

$$m_z = 1 - \frac{2}{N}\sum_i \langle c_i^\dagger c_i\rangle, \tag{111}$$

which represents the transverse magnetization in terms of the Fermi quasi-particles.

From the long-time dynamics of the observable in Eq. (111) it is rather evident that the equilibration in the weak long-range Kitaev chain, see the upper panel Fig. 20(b), mimics the case of the long-range Ising model with $\alpha = 2$, see the upper panel Fig. 20(b). The initial value of the observable rapidly equilibrates to a long-time expectation which becomes time independent in the long time limit. In other words, any observable $A(t)$ relaxes to equilibrium if it approaches its Cesaro's average

$$\bar{A} = \lim_{T\to\infty} \langle A\rangle_T \quad \text{with} \quad \langle \cdots \rangle_T = \frac{1}{T}\int_0^T \cdots dt. \tag{112}$$

Moreover, the dynamical fluctuations, which are quantified by the parameter

$$Q_A(T) = \langle \left|A(t) - \bar{A}\right|^2 \rangle_T \tag{113}$$

must disappear in the long-time limit

$$\lim_{T\to\infty} Q_A(T) \approx 0. \tag{114}$$

Eq. (114) is the conventional way to define equilibration in closed quantum systems (de Oliveira *et al.*, 2018; Linden *et al.*, 2009; Reimann, 2008; Short, 2011).

In the weak long-range regime ($\alpha > d$) the result $\lim_{T\to\infty} Q_{m_z}(T) = 0$ can be exactly proven for most quadratic models as well as for the Ising model for sudden quenches from $h_i = +\infty$ to $h_f = 0$ thanks to the Riemann–Lebesgue lemma (Hughes-Hallett *et al.*, 2008). In other words, equilibration occurs in these systems as the Poincaré recurrence times diverge for $N \to \infty$. This phenomenon is evident in the numerical computation of the m_z expectation value both for the Ising and the Kitaev chain with $\alpha > 1$, see the upper panels of Fig. 20(a) and 20(b).

This picture is radically altered in the $\alpha < 1$ case, see the bottom panels in Fig. 20(b). Indeed, the dynamical evolution of the observable m_z persists in the vicinity of its initial value for longer times as the system size is increased, in agreement with the $\tau_{\text{eq}} \propto N^\beta$ expectation coming from classical systems (Campa *et al.*, 2009). Interestingly, the $\beta = 1/2$ scaling observed in the long-range Ising model appears to be related with the scaling of Poincaré recurrence time due to the discrete spectrum of long-range systems (Defenu, 2021; Kastner, 2011). It is also worth noting that the scaling of time scales in long-range systems is crucially influenced by the Kac rescaling and, then, these observations may be altered modifying the regularization procedures (Bachelard and Kastner, 2013).

While the phenomenology of the Kitaev and Ising models are analogous, the quantitative features of the dynamical evolution display some peculiar differences. In particular, in the long-range Ising model, no oscillatory fluctuations are present, while they occur in the Kitaev chain. These differences are probably due to the different quench boundaries between the two models. Despite these details, it is evident that the curves in the lower panels of Fig. 20(a) and 20(b) will both yield $\lim_{T,N\to\infty} Q_{m_z}(T) \neq 0$.

The appearance of the QSS has been often connected to the scaling of equilibration times of critical observables such as the magnetization (Antoni and Ruffo, 1995; Campa *et al.*, 2009; Mukamel *et al.*, 2005). However,

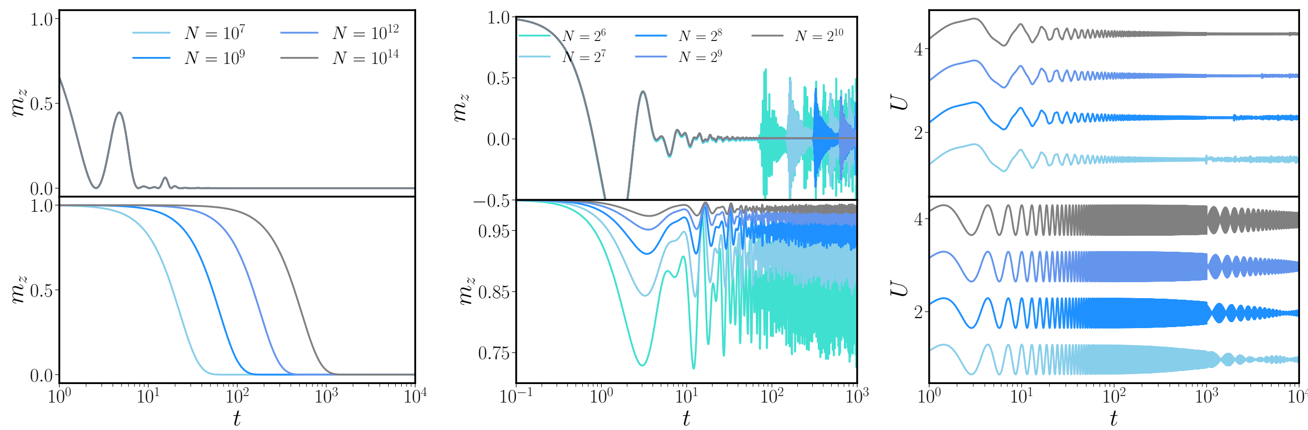

(a) Ising model (b) Kitaev chain (c) Spherical model

Figure 20 **Evidences of QSS in the long-range Ising chain, the Kitaev chain and the one dimensional spherical model, from left to right respectively.** In all panels the top sub-panel displays the case of weak long-range interactions $\alpha > 1$, where roughly the same equilibration properties of the nearest neighbour case are found. Conversely, the bottom sub-panel shows the case of strong long-range interactions $\alpha < d$, where dynamical fluctuations survive in the $t \to \infty$ limit. The leftmost panel displays the transverse magnetisation of the long-range Ising model, see the Hamiltonian in Eq. (60), after a quench from the fully paramagnetic state at $h \to \infty$ deep into the ordered phase at $h \to 0$. While the observable expectation equilibrates at long times for $\alpha = 2.0$ (top sub-panel), it persists in its initial value for increasingly longer times as the system size increases for $\alpha = 0.5$ (bottom sub-panel). See the discussion in Ref. (Kastner, 2011). A similar signature is noticed in the case of the Hamiltonian in Eq. (66), i.e. the Kitaev chain representation of the Ising model, where the dynamics can be exactly solved for any global quench across the phase boundary. The central panel shows the evolution of the spatial and quantum average of the σ_z in Eq. (61) for a long-range Kitaev chain with $\alpha \gtrsim 12$ (top sub-panel) and $\alpha = 0.4$ bottom sub-panel for $h_i \gg 1$ to $h_f = 0.4$. Lack of equilibration also appears for non-critical quenches, as it shown in the rightmost panel for the potential energy U of a quantum spherical model with long-range interactions. Dynamical fluctuations reduce as size increases for decay rates $\alpha > 1$, see the upper sub-panel where the $\alpha \gtrsim 12$ case is shown for increasing system sizes $N \in [2^9, 2^{10}, 2^{11}, 2^{12}]$ from bottom to top. Conversely dynamical fluctuations tend to increase for $\alpha < 1$, as shown in the lower sub-panel for $\alpha = 0.2$, again from bottom to top, see Ref. (Defenu, 2021).

signatures of persistent time fluctuations in classical systems have been also found in generic thermodynamic observables, as for the evolution of internal energy in systems of particles with attractive power-law pair interactions (Gabrielli *et al.*, 2010). The same picture can be also found in many-body quantum systems. Indeed, persistent dynamical fluctuations are also observed for non-critical quantities or quenches, as occurs for the internal energy of the spherical model, see Fig. 20(c).

B. Lieb-Robinson bound

Understanding the maximum speed at which information propagates in many-body systems allows to put tight bounds on fundamental questions, such as how fast a quantum system can thermalize (Calabrese and Cardy, 2006) or the amount of quantum information that can be transmitted through a quantum channel (Bose, 2007). In short-range interacting systems the Lieb-Robinson bound predicts a constant maximal velocity that confines the information to a linear effective light-cone (Lieb and Robinson, 1972a). Long-range interactions substantially alter this picture, since the traditional definition of group velocity does not apply to their case. Accordingly, the spreading of correlations, information, or entanglement speeds up dramatically, leading to a wide range of exotic dynamical properties, which may be exploited for fast information transmission, improved quantum state preparation, and similar applications. Then, it is not surprising that a large body of theory work has emerged in recent years in order to find tighter propagation bounds for different values of the power-law exponent α (Chen and Lucas, 2019; Eisert *et al.*, 2013; Else *et al.*, 2020; Foss-Feig *et al.*, 2015b; Gong *et al.*, 2014; Guo *et al.*, 2020; Hastings and Koma, 2006; Hauke and Tagliacozzo, 2013; Hazzard *et al.*, 2013, 2014; Hermes *et al.*, 2020; Kuwahara and Saito, 2020; Lashkari *et al.*, 2013; Matsuta *et al.*, 2017; Rajabpour and Sotiriadis, 2015; Schachenmayer *et al.*, 2013; Storch *et al.*, 2015; Sweke *et al.*, 2019; Tran *et al.*, 2020, 2019a,b)

Most of the current understanding of correlations and entanglement spreading in presence of long-range interactions has been based on prototypical systems. There, the synergy between analytical and numerical investigations has been particularly fruitful (Hauke and Tagliacozzo, 2013; Hazzard *et al.*, 2014; Nezhadhaghighi and Rajabpour, 2014; Rajabpour and Sotiriadis, 2015; Schachenmayer *et al.*, 2013, 2015a,b). The general understanding of propagation in long-range systems is summarised in Fig. 21. This qualitative picture applies almost independently to the particular model, the quantity or the decay range α.

In analogy with other universal results in the short-range regime, entanglement scaling in long-range models with $\alpha \gg 3$ reproduces the well-known light cone shape observed for local systems (Lieb and Robinson, 1972b) (See Fig. 21 on the right). For intermediate values of α (see the central panel in Fig. 21) cone-light propagation is observed at short distances, while correlations between distant sites are heavily influenced by the presence of the long-range terms. Multi-speed prethermalization for lattice spin models with long-range interactions in the regime $d < \alpha < d + 2$ was studied in (Frérot *et al.*, 2018). The behavior of correlations at intermediate decay is akin to the one found in the critical behavior of the long-range Kitaev chain in Sec. IV.B.4, where long-range hopping amplitudes with $2 < \alpha < 3$ do not modify the universal scaling behavior, but they alter the overall shape of excitations. However, in the Kitaev chain long-range hopping only influences the subcritical behavior for $\alpha < 3$, while the light-cone bending is observed also for $\alpha = 4$ (Rajabpour and Sotiriadis, 2015).

Finally at smaller α (left panel in Fig. 21) the universal scaling is altered by long-range interactions and, accordingly, the correlations propagate faster than any possible group velocity, disrupting the linear light-cone shape.

Analytical insight into information propagation in long-range system may be also achieved by general Lieb-Robinson-type bounds. A first contribution in this direction has been given in Ref. (Hastings and Koma, 2006), yielding for $\alpha > d$

$$||[O_A(t), O_B(0)]|| \leq C\, ||O_A||\, ||O_B||\, \frac{|A|\,|B|\,(e^{v|t|} - 1)}{[d_{A,B} + 1]^\alpha}. \tag{115}$$

The regions A, B are a disjunct subset of the d dimensional lattice. The generic operator expectations O_A and O_B only receive contributions from Hilbert-space states whose support lies in the spatial regions A and B, respectively. In Eq. (115) the symbol $||\cdot||$ denotes the operator norm, and $d_{A,B}$ is the distance between the regions A and B. The importance of the expression in Eq. (115) derives from its generality, since it applies to a wide range of observables, while it is straightforwardly extended also to other non-local quantities, such as the equal time correlators (Bravyi *et al.*, 2006; Nachtergaele *et al.*, 2006). In its regime of validity $\alpha > d$, the bound in Eq. (115) qualitatively reproduces the shape in the left panel of Fig. 21. However, the wave-front propagation obtained by Eq. (115) is logarithmic rather than power-law and, then, does not faithfully describe larger α values. Further insight into this problem was obtained in Ref. (Gong *et al.*, 2014), where a more general bound was derived, capable to reproduce both the Lieb-Robinson result in the local limit ($\alpha \to \infty$) and the expression in Eq. (115). Even this general bound does not appear to be tight on the entire α range, but rather to be more accurate at large α.

The extension of the previous picture to the strong long-range regime needs to account for the influence of diverging long-range interactions with $\alpha < d$ on the systems time scales. In analogy with the equilibration rate of QSS, see Sec. V.A, also the fastest propagation scale in strong-long-range systems is found to vanish as a power-law approaching the thermodynamic limit $\tau_{\text{fastest}} \propto N^{-q}$ with $q > 0$ (Bachelard and Kastner, 2013). Accordingly, signal propagation becomes increasingly faster as the system approaches the thermodynamic limit and hinders the traditional formulation of Lieb-Robinson bound. To circumvent such complications it is convenient to introduce rescaled time $\tau = tN^q$. In terms of this "proper" time variable the bound for $\alpha < d$ takes the same form as in the weak long-range regime, but with τ in spite of t on the r.h.s. of Eq. (115) (Storch *et al.*, 2015).

The aforementioned results for $\alpha < d$ produce the shortest signaling time t_{ss} between the edges of a system of size N to scale as $t_{\text{ss}} \gtrsim N^{\frac{2\alpha}{d}-2} \log N$, which leads to the possibility of a vanishing time for transmitting information between linearly distant sites of a strong long-range system. However, such fast signals have never been observed nor described, rather a size-independent signaling time was evidenced in several situations (Eisert *et al.*, 2013; Eldredge *et al.*, 2017; Hauke and Tagliacozzo, 2013). Moreover, for specific initial states strong long-range interactions may be inconsequential to signal propagation, due to the so-called shielding effect (Santos *et al.*, 2016).

Focusing on quadratic Hamiltonians a much tighter bound can be obtained, $t_{\text{ss}} \gtrsim N^{\frac{\alpha}{d}-1/2}$, which is saturated for $\alpha < d/2$ by the quantum state transfer protocol described in Ref. (Guo *et al.*, 2020). The same reference also provides a stricter bound for general interacting spin systems. It is worth noting that the Lieb-Robinson bound can be also used to predict the velocity of quantum information scrambling, whose importance lies at the edge between high-energy and condensed matter physics (Bentsen *et al.*, 2019a; Gärttner *et al.*, 2017; Maldacena *et al.*, 2016; Sekino and Susskind, 2008). In this context, the role of long-range interactions is particularly relevant due to their inclusion in most quantum mechanical models of black holes, possibly making these systems the fastest information scramblers in nature (Lashkari *et al.*, 2013).

Despite the fast propagation and scrambling of correlations due to long-range interactions, the growth of entanglement entropy after a sudden quench is strongly reduced. In particular, in the strong long-range regime ($\alpha < d$) it can become as slow as logarithmic, even in the absence of disorder (Buyskikh *et al.*, 2016; Pappalardi

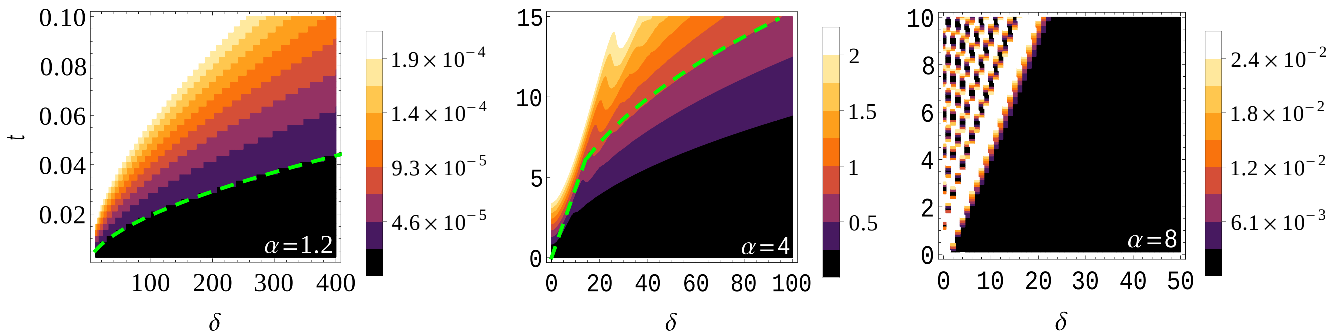

Figure 21 **Propagation patterns as a function of distance $\delta = d_{ij}$ between sites i, j and time t for different long-range exponents α.** Different models and physical quantities are shown in the different panels, but the overall picture remains the same. Left: The detection probability for a signal sent through a quantum channel between two sites at distance δ is shown for the long-range Ising chain (Eisert *et al.*, 2013). The green displays the power-law $\delta \propto t^{1.7}$. Center: Connected correlation functions between two sites at distance δ in a long-range field theory, see the effective action in Eq. (34) with $d = 1$ and $\alpha = 4$ (Rajabpour and Sotiriadis, 2015). The short-distance spreading resembles the conventional light-cone observed with local interactions, while for larger distances long-range effects appear, and power-law scaling is observed. The green dashed curve is a guide to the eye. Right: The mutual information between two lattice sites at distance δ in the KItaev chain described by the Hamiltonian in Eq. (48) with vanishing pairing and long-range hopping ($\alpha = 8$). The decay rate is large enough that only the light-cone is observed. Picture taken from Ref. (Storch *et al.*, 2015).

et al., 2018; Schachenmayer *et al.*, 2013). This peculiar phenomenon is connected with a suppression of the quasi-particle contribution to the von Neumann entanglement entropy, which is known to be governed by collective spin-excitations related with spin-squeezing (Pezzé and Smerzi, 2009; Sørensen and Mølmer, 2001; Tóth *et al.*, 2007). Extending to the dynamical case the bosonization procedure outlined in Sec. IV.G.1 (Lerose *et al.*, 2019c; Rückriegel *et al.*, 2012), it has been possible to show that the rate of divergence of semiclassical trajectories governs the transient growth of entanglement. This provides a very transparent and quantitative relationship between entanglement propagation measures (such as entropy, quantum Fisher information, spin squeezing) and chaos quantifiers (such as Lyapunov exponents and out-of-time-order correlations) in the semiclassical regime (Lerose and Pappalardi, 2020a,b). Fast entanglement growth is recovered only at criticality, corresponding to an unstable separatrix terminating onto a saddle point in phase space. Similarly, when the classical dynamics is chaotic (e.g. for kicked or multi-species models), the growth is fast, with a rate related to Lyapunov exponents. Interestingly, also long-but-finite-range interactions open up a finite layer of instability with fast entanglement growth, due to the presence of a chaotic dynamical phase (Lerose *et al.*, 2018, 2019c) Correlation spreading with van der Walls interactions and the presence of positional disorder in 2D was investigated in (Menu and Roscilde, 2020). Multifractality and localization of spin-wave excitations above a ferromagnetic ground state are observed. Also, the spreading of entanglement and correlations starting from a factorized state exhibits anomalous diffusion with variable dynamical exponent.

1. Experimental observation

The propagation of correlations and the violation of the local Lieb-Robinson bound have been observed in trapped ions quantum simulators for $0.6 \lesssim \alpha \lesssim 1.2$ (Jurcevic *et al.*, 2014; Richerme *et al.*, 2014). In Ref. (Jurcevic *et al.*, 2014), the authors have studied the dynamics following either a global or a local quench of a long-range XY Hamiltonian (see Eq. 8). The experimental system consists of a 15 ions chain, prepared in a product state where only the central spin is flipped with respect to the rest of the system. In this system the global magnetization $S_z = \sum_i \sigma_i^z$ is a conserved quantity, therefore the excitation can be described as a magnon quasiparticle that propagates from the center throughout the system. After the local quench, the authors observed that for $\alpha < 1$ the light cone calculated considering only the nearest-neighbor couplings did not capture well the dynamics of the system (see Fig. 22 a,b,c).

In Ref. (Richerme *et al.*, 2014), a global quench was performed under both Ising (5) and XY (8) Hamiltonians, measuring the evolution of the connected two-body correlations

$$C_{1,1+r}(t) = \left\langle \sigma_1^z(t)\sigma_{1+r}^z(t)\right\rangle - \left\langle \sigma_1^z(t)\right\rangle \left\langle \sigma_{1+r}^z(t)\right\rangle .$$

The light-cone boundary is extracted by measuring the time it takes a correlation of fixed amplitude ($C_{i,j} \sim 0.1C_{i,j}^{\max}$, where $C_{i,j}^{\max}$ is the largest connected correlation between two ions) to travel an ion–ion separation distance r. For strongly long-range interactions ($\alpha < 1$), accelerating information transfer is observed through the chain. This fast propagation of correlations is explained by the direct long-range coupling between distant spins. The increased propagation velocities quickly sur-

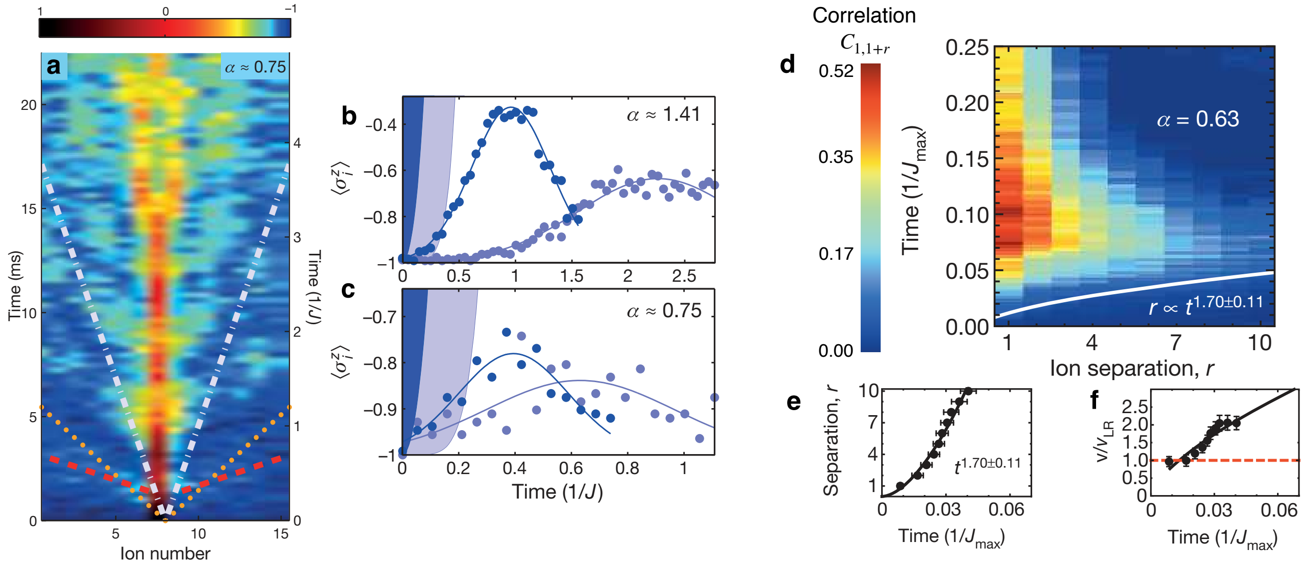

Figure 22 **Propagation of quantum information in long-range trapped ions systems.** **(a)** Single-site magnetization $\langle \sigma_i^z(t) \rangle$ as a function of time, following a quantum quench of the long-range XY Hamiltonian (8), with the central 8th ion initially flipped. Dashed (red) lines are fits to the observed magnon arrival times (see in **b**, bottom); dot-dashed white lines, light cone for averaged nearest-neighbour interactions; orange dots, after renormalization by the algebraic tail. The white lines are in clear disagreement with red lines. **(b-c)** Gaussian fits of magnon arrival time (red lines in **a**) for ion 6 (dark blue on the left) and 13 (light blue on the right) with $\alpha = 1.41$ (Top) and $\alpha = 0.75$, a nearest neighbour Lieb–Robinson bound captures most of the signal (shaded region) in the $\alpha = 1.41$ case and it does not for $\alpha = 0.75$. Adapted from Ref. (Jurcevic *et al.*, 2014). **(d)** Spatial and time-dependent correlations following a global quench of a long-range Ising Hamiltonian (5) with $\alpha = 0.63$. Correlation propagation velocity **(e)** . The curvature of the boundary shows an increasing propagation velocity **(f)**, quickly exceeding the short-range Lieb–Robinson velocity bound, v (red dashed line) (c). Solid lines give a power-law fit to the data, which slightly depends on the choice of fixed contour $C_{i,j}$. Adapted from Ref. (Richerme *et al.*, 2014).

pass the Lieb–Robinson velocity for a system with equivalent nearest-neighbour-only interactions, $v = 12eJ_{\max}$, where e is Euler's number and $J_{\max}$ is the maximum Ising coupling strength for a given spin–spin coupling matrix.

C. Kibble-Zurek mechanism

The correlation length of a quantum system diverges approaching its quantum critical points, while the dynamical gap vanishes. As a result, the dynamical scaling of the observables when the system is driven across the transition is reminiscent of the thermodynamic scaling at equilibrium. Yet, for such scaling to be displayed, the drive has to be slow enough that the dynamical evolution occurs in the vicinity of the equilibrium critical point.

Let us consider a critical system with an internal control parameter λ such that a (quantum) critical point occurs at $\lambda_c = 0$ ($\lambda = |T - T_c|/T_c$ for finite-temperature phase transitions). Conventionally, any slow enough drive of internal parameters $\lambda(t) = \delta \cdot t$ shall only produce adiabatic corrections $\sim \delta^2$ to the observables expectations with respect to the equilibrium value, as it can be deduced by simple thermodynamic arguments (Zwerger, 2008). However, when crossing an equilibrium critical point, the traditional adiabatic picture breaks down and the residual energy (heat) generated by the drive displays non-analytic behavior $E_{\text{res}} \approx \delta^\theta$ with $\theta < 2$ (Zurek, 1996). In most local systems such non-analytic scaling emerges due to the formation of topological defects according to the celebrated Kibble-Zurek mechanism, as confirmed by several condensed matter experiments, see Ref. (del Campo and Zurek, 2014) for a review.

In the quantum realm, the simplest example of defect production is furnished by the Landau-Zener problem, which describes a two-level system driven through an avoided level crossing (Damski, 2005; Landau and Lifshit's, 1991; Zener, 1932), but actual Kibble-Zurek scaling is only observed in quantum many-body systems in the thermodynamic limit (Dziarmaga, 2010; Zurek *et al.*, 2005). The heuristic scaling argument at the basis of the Kibble-Zurek mechanism can be proven to exactly apply to the nearest neighbor Ising model, i.e. the Hamiltonian (60) in the $\alpha \to \infty$ limit since that problem can be mapped to an infinite ensemble of Landau-Zener transitions (Dziarmaga, 2005).

In a general system, the Kibble-Zurek argument relies on the so-called adiabatic-impulse approximation, where the dynamical evolution of a system starting in its ordered ground-state a $t = -\infty$ is assumed to adiabatically follow the drive until the so-called freezing time

$-\hat{t}$. Beyond the "freezing" time the equilibration rate of the system becomes too small with respect to the drive velocity and the system state cannot follow the Hamiltonian modification, as it is approaching the quantum critical point at $t = 0$. Then, the dynamics is assumed to remain frozen at all times $t > -\hat{t}$ up to the crossing of the quantum critical point (at $t = 0$) and after; until the equilibration rate of the system grows back and the "un-freezing" time $\hat{t}'$, where adiabaticity is restored, is reached.

Once the system has unfrozen the state evolution will resume on the opposite side of the transition, where the Hamiltonian ground-state is supposed to break the Hamiltonian symmetry. Then, the dynamics will induce a transition between the symmetric and a symmetry-broken state. However, this transition will occur at finite correlation length $\hat{\xi}$, since the process only starts at $t \geq \hat{t}' = \hat{t}$, at least for a symmetric transition. The dynamics has thus modified the character of the continuous phase transition, making it rather similar to a first-order one, and the system will likely form topological defects, whose size would be roughly proportional to the (finite) correlation volume $\hat{\xi}^d$. Therefore, the total defect density scales according to $n_{\rm exc} \approx \hat{\xi}^{-d}$.

During the adiabatic stage of the dynamics, the system observables will acquire the equilibrium expectation of the instantaneous Hamiltonian and so does the minimal gap of the system $\Delta(t) = \Delta(\lambda(t))$. Then, a proper estimation of the drive strength on the system is $\dot{\Delta}/\Delta$ which has to be compared with the equilibration time Δ^{-1}, leading to the adiabatic condition

$$\dot{\Delta} \ll \Delta^2. \tag{116}$$

The freezing time $\hat{t}$ is defined by the breakdown of the adiabatic condition $\dot{\Delta}(\hat{t}) \simeq \Delta(\hat{t})^2$. Appling the critical scaling of the minimal gap with λ, one obtains the scaling of the freezing time $\hat{t} \approx \delta^{-\frac{z\nu}{1+z\nu}}$ and, accordingly, the freezing length scaling $\hat{\xi} \approx \delta^{-\frac{\nu}{1+z\nu}}$, which leads to the defect density expression

$$n_{\rm exc} \approx \hat{\xi}^{-d} \approx \delta^{\frac{d\nu}{1+z\nu}}. \tag{117}$$

The application of the traditional Kibble-Zurek picture is complicated by different effects depending on the strong or weak nature of long-range interactions. In the first case, the additional relevance of boundaries with respect to local systems produces clear difficulties in the definition of the topological defects. In the latter case, the presence of the competing scaling contributions discussed in Sec. IV.B.4 leads to novel scaling regimes, which are not encompassed by the Kibble-Zurek framework.

1. Kitaev chain

The appearance of multiple scaling contributions to the critical behavior of long-range quantum systems has been already exemplified in the study of the Kitaev chain in Sec. IV.B.4. In this sub-section, we are going to consider the effect of such multiple scalings on the universal dynamics.

The study of exactly solvable toy models is at the root of the current understanding of Kibble-Zurek scaling in general quantum systems. Indeed, first studies of defect formation in quantum systems have been pursued on the nearest neighbor Ising model, where finite-size scaling arguments led to the prediction

$$n_{\rm exc}^{\rm fss} \approx \delta^{\frac{1}{2z}} \tag{118}$$

which produces $n_{\rm exc} \approx \sqrt{\delta}$ in agreement with the Kibble-Zurek prediction in Eq. (117) since $z = \nu = 1$ in this case (Zurek *et al.*, 2005). Soon after this seminal investigation, an exact solution to the universal slow dynamics of the Ising model has been provided by mapping it to an infinite sum of Landau-Zener problems, each representing the dynamics of a single fermionic quasi-particle excitation (Dziarmaga, 2005).

Indeed, the dynamical evolution of quadratic fermions can be described in terms of the Bogoliubov amplitudes via the equation

$$i\frac{d}{dt}\begin{pmatrix} u_k \\ v_k \end{pmatrix} = \begin{pmatrix} \varepsilon_\alpha(k,t) & \Delta_\beta(k) \\ -\Delta_\beta(k) & \varepsilon_\alpha(k,t) \end{pmatrix} \begin{pmatrix} u_k \\ v_k \end{pmatrix}, \tag{119}$$

which generically represent an ensemble of two level systems, whose energy and coupling are given by the momentum space kinetic and pairing terms, respectively. Thus, the Kibble-Zurek dynamics of the Kitaev chain can be studied exactly and this solution is not limited to the nearest neighbour case, which represents the Ising model, but it can be extended to any form of the long-range couplings.

Let us, then, consider a slow variation of the chemical potential h in the Hamiltonian (43) with the usual slow drive form $h(t) = h_c + \delta t$, with the time spanning in the interval $t \in [-h_c/\delta, h_c/\delta]$. Then, in the small δ limit, the system is adiabatically ramped from a point deep in the topological phase $h = 0$ across the quantum phase transition and up into the trivial phase $h = 2h_c$. In the following we are going to focus on a ramp across the quantum phase transition occurring at $h_c = 1$.

Within this dynamical protocol the dynamical system in Eq. (119) reduces to the k dependent Landau-Zener problem (Damski, 2005; Landau and Lifshitz, 1969). Thus, the excitation probability of each Bogoliubov quasi-particle can be computed according to the Landau-Zener formula

$$\langle \gamma_k^\dagger \gamma_k \rangle = n_{\rm exc}(k) = \exp\left(-\frac{\pi}{\delta^2}\Delta_\beta(k)^2\right) + O(\delta^2 \Delta_\beta(k)^4). \tag{120}$$

The equation above only explicitly reports the leading term in the $k \to 0$ limit, which is the relevant one for the universal behavior. However, when considering a slow quench in a finite time interval $t \in [-h_c/\delta, h_c/\delta]$, the discontinuity in the drive derivative at the borders of the interval induces δ^2 corrections to the excitations probability (Defenu *et al.*, 2019b; Dziarmaga, 2010).

The excitation probability in Eq. (120) only depends on the pairing term in Hamiltonian (43), so that the universal slow dynamics is fully determined by the low-momentum scaling of the pairing coupling. Accordingly, the excitation density can be obtained by integrating Eq. (120) over the Brillouin zone

$$\int n_{\mathrm{exc}}(k)dk \approx \delta^{\frac{1}{2z_\Delta}} \tag{121}$$

where we have defined z_Δ from the scaling of the pairing coupling $\lim_{k\to 0}\Delta_\beta(k) \approx k^{z_\Delta}$. The result in Eq. (121) has been also employed to prove the validity of the Kibble-Zurek argument in Kitaev chains with long-range pairing terms (Dutta and Dutta, 2017) in addition to the purely local case (Dziarmaga, 2005).

Apart from the aforementioned results, which explicitly refer to quadratic Fermi systems, the application of adiabatic perturbation theory to slow quenches close to quantum critical points predicts the scaling of the defect density to agree with the Kibble-Zurek prediction $\theta = d\nu/(1 + z\nu)$ (Polkovnikov, 2005). Such prediction comes from the assumption that the scaling form of the critical propagator reproduces the equilibrium critical exponents. Since for $1d$ Fermi systems, one has $z\nu = 1$, the perturbative argument yields $d\nu/(z\nu + 1) = 1/2z$ in agreement with the finite-size scaling argument in Eq. (118). However, it was realized long ago (Dziarmaga, 2010) that the correspondence between the exact scaling in Eq. (121) and the perturbative prediction is tied to the relevance of the pairing term with respect to the momentum term in the scaling of the quasi-particle gap, see Eq. (54).

As outlined in Sec. IV.B.4, the presence of long-range (anisotropic) couplings in 1D Fermi systems may produce equilibrium scaling exponents dominated by the kinetic term in the gap scaling, see Eq. (77), differently from what occurs in short-range systems. Similarly, the introduction of non-local finite-range couplings in the Kitaev model has been known to produce a modified equilibrium scaling with a kinetic dominated dynamical critical exponent. The latter phenomenon is only found in the proximity of multi-critical points, where finite-range non-local couplings become relevant and are known to lead to a violation of the Kibble-Zurek result (Deng *et al.*, 2009; Divakaran *et al.*, 2009; Dziarmaga, 2010).

At variance, the anisotropic Kitaev model with weak long-range couplings in the $\alpha < \beta$ regime displays the aforementioned kinetic dominated scaling already at a second-order quantum critical point (Defenu *et al.*, 2019b). In particular, its dynamical phase diagram, depicted in Fig. 23(a) contains four different regions, two of them (green and white in Fig. 23(a)) fulfil the Kibble-Zurek prediction both with the nearest neighbours universal exponents ($\theta = 1/2$ in the white region) or with pairing dominated critical exponents ($\theta = (2\beta - 2)^{-1}$ green region in Fig. 23(a)). The conventional prediction $\theta = z\nu/(1 + z\nu)$ cannot be applied to the two red regions in Fig. 23(a), where $\alpha < \beta$, to the point that in the upper portion of the red region the nearest-neighbor prediction for the dynamics $\theta = 1/2$ remains valid deep in the regime where the equilibrium universal behavior is dominated by long-range interactions.

The absence of kinetic contributions to the critical dynamics only holds in the strict $\delta \to 0$ limit. So that non universal corrections still carry a sizeable contribution to the defect density from the power-law α as long $\delta \lesssim 1$ as it is shown in Fig. 23(b), where a full numerical computation of the defect density for various points in the (α, β) plane (reported in different colours and shapes, see the legends in Fig. 23) is compared with the analytical prediction in Eq. (120) (dashed lines). Such non-universal corrections are rapidly washed out in the slow drive limit, see Fig. 23(c), where the excitation probability at different α but with the same β collapse on each other.

It is worth noting that the agreement between the analytic prediction in Eq. (119) and the numerical result shown in Fig. 23(b) is limited by the δ^2 contributions to the excitation probability, which, in turn, are generated by the finite edge-points of the present dynamical protocol. Actually, for a slow linear quench in the infinite interval $t \in [-\infty, \infty]$ the result in Eq. (119) will remain valid independently on the δ value. Yet, in the present problem, a variation of $h \in [-\infty, +\infty]$ will lead to the crossing of two critical points and it will naturally lead to more complications.

In summary, several diverse predictions exist for the defect scaling after slow quenches in quantum many-body systems. In particular, the finite-size scaling argument in Eq. (118) and the traditional Kibble-Zurek result in Eq. (117) remain consistent with each other and with the exact solution for quadratic fermions, as long as $z\nu = 1$. This last condition always holds for the fermionic system described in Sec. IV.B, but this is not the case for the interacting field theories described in Sec. IV.A, where the dynamical critical exponent $z\nu$ depends on the decay exponent, see Fig. 12. In particular, the mean-field approximation produces the result $z\nu = 1/2$ for rotor models, in agreement with the result observed in the LMG model, which represents the $\alpha = 0$ limit of such theories. In the following, we are going to examine such extreme cases in detail and show how the Kibble-Zurek mechanism is modified by interactions in the strong long-range regime.

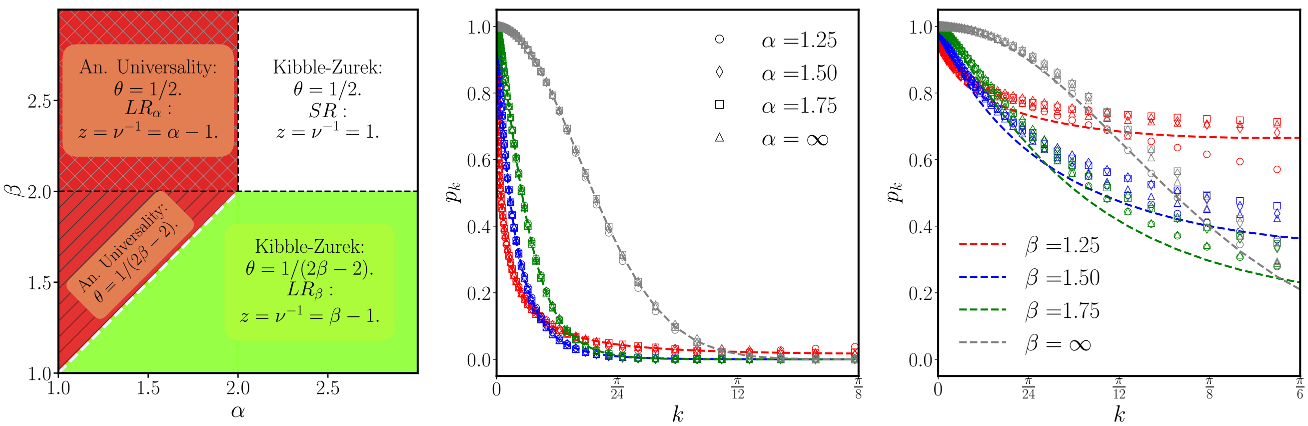

(a) Dynamical phase diagram (b) Excitations probability $\delta = 0.5$ (c) Excitations probability $\delta = 0.051$

Figure 23 **Kibble-Zurek mechanism in long-range Kitaev chains.** **(a)**: the dynamical phase diagram reporting the universal slow-dynamics exponents of the anisotropic Kitaev chain in the (α, β) plane. **(b,c)**: numerical analysis of Eq. (119) compared with the analytic formula in Eq. (120) for intermediate and small dynamical rates $\delta = 0.5, 0.05$. Each line represents a different value of $\beta = 1.25, 1.50, 1.75, \infty$ from bottom to top at small k. Different values of α are displayed by different symbols, see the legend in panel (b).

2. Lipkin-Meshkov-Glick model

In the following, the difficulty to reconcile the finite size scaling prediction in Eq. (118) with the perturbative result $\theta = d\nu/(1 + z\nu)$ (Polkovnikov, 2005) is exemplified by the study of the flat interactions case $\alpha = 0$ such as the LMG model, whose equilibrium behaviour has been described in Sec. IV.G. Apart from its prototypical role, the interest in the LMG model is motivated by the possibility to experimentally study slow dynamics in this system thanks to cold atoms into cavity experiments (Brennecke *et al.*, 2013), in spin-1 ferromagnetic BECs (Anquez *et al.*, 2016; Hoang *et al.*, 2016; Saito *et al.*, 2007; Xue *et al.*, 2018) as well as to its relation with the BCS model (Dusuel and Vidal, 2005b).

First numerical results on the scaling of the defect density after an adiabatic ramp crossing the quantum critical point of the LMG model could not be reproduced by the Kibble-Zurek formula in Eq. (117), but they displayed qualitative agreement with the finite-size scaling prediction in Eq. (118) (Caneva *et al.*, 2008). Yet, more intensive numerical studies unveiled a more complicated landscape where the adiabatic crossing of the equilibrium quantum critical point does not display any actual Kibble-Zurek scaling, but rather a universal behavior as a function of the scaled variable $\Lambda = N\,\delta$ (Acevedo *et al.*, 2014); while non-analytic corrections for the defect scaling was found for quenches up to the critical point (Hwang *et al.*, 2015).

This scenario can be safely reconstructed by the study of the effective critical theory depicted in Sec. IV.G.1. However, since the effective harmonic theory, which describes the fully-connected problem at order $1/N$, was obtained at equilibrium, it is first convenient to generalize the treatment to the dynamical case. Our goal is to consider the LMG problem with time-dependent coupling $h(t)$, with the system initially prepared at equilibrium at any initial time t_i and, then, manipulated across the quantum critical point. Thus, during the time evolution, the average expectation value of the global spin will change as the order parameter is modified by the dynamics as soon as $h(t) < h_c$. As a consequence, the assumption of small quantum depletion of the classical equilibrium expectation $\langle \boldsymbol{S} \rangle$, which is at the basis of the Holstein-Primakov expansion in Eqs. (104), (105) and (106), is dynamically disrupted by the macroscopic change in the order parameter.

A simple solution to this difficulty is obtained by considering a time-dependent classical expectation for the Holstein-Primakov expansion via the time-dependent spin-wave approximation introduced in Ref. (Rückriegel *et al.*, 2012). This solution strategy for the time-dependent fully-connected problem has already been employed to characterize the chaotic dynamical phase which emerges upon the inclusion of additional nearest-neighbor couplings on top of the LMG Hamiltonian (Lerose *et al.*, 2018, 2019c).

At leading order $1/N$ this procedure effectively decouples the classical evolution of the order parameter from the quantum fluctuations. Ramping the magnetic field slowly across the critical point $h(t) = h_c - \delta\, t$ for $t \in [-1/\delta, 1/\delta]$ is equivalent to dynamically modify the frequency of both classical field and the quantum fluctuations according to the equilibrium formulas (109) and (102). In principle, an accurate description of the ramp dynamics at finite δ would need the description of the back-action of the displacement of the classical observable from its equilibrium configuration into the dynamics of the quantum mode.

However, in the adiabatic limit $\delta \to 0$ we can employ the classical adiabatic theorem (Landau and Lifshitz, 1976) to conclude that the classical trajectory will remain close to the instantaneous solution $\theta(t)-\theta_{\mathrm{eq}} \approx \delta^2$ and $\varphi(t)-\varphi_{\mathrm{eq}} \approx \delta^2$, where the equilibrium contributions are $\varphi_{\mathrm{eq}} = 0$ and θ_{eq} is given in Eq. (101). Yet, based on the previous discussion, the classical δ^2 correction is going to be superseded by the one arising from quantum fluctuations. Indeed, quantum fluctuations in the LMG problem are effectively described by a single harmonic mode adiabatically ramped across its fully degenerate quantum critical point.

Interestingly, none of the results on defect scaling, presented at the beginning of Sec. V.C, apply to the present problem since the general result derived by dynamical perturbation theory does not apply to Bose quasiparticles (de Grandi and Polkovnikov, 2010). In fact, it was first noticed by asymptotic expansion that a quasistatic transformation of an harmonic oscillator with linear time scaling of its frequency across the fully degenerate point $\omega(t)^2 \approx (\delta t)^2$ produces non-adiabatic corrections which do not vanish in the $\delta \to 0$ limit (Bachmann *et al.*, 2017). Clearly, this result does not directly apply to the LMG case, since for a linear scaling of the control parameter $\lambda(t) = h(t)-h_c = \delta t$ the dynamical frequency for the spin wave model reads

$$\omega(t)^2 \approx \delta|t| \tag{122}$$

at leading order in the small-time δ expansion. Based on the conventional adiabatic argument $\dot{\omega}(t) \ll \omega(t)^2$ the faster the drive vanishes across the fully-degenerate point, the stronger non-adiabatic effects shall be. Then, one may in principle expect the linear drive in Eq. (122) to be more adiabatic than the $\sim t^2$ case studied in Ref. (Bachmann *et al.*, 2017) and to present a different non-adiabatic scaling.

In general, the characterization of slow dynamics for different kinds of excitations and dynamical scaling is very relevant to the problem of long-range interactions. Indeed, we have already shown that the quantum long-range Ising model in Eq. (60) varies as a function of α from a critical point with Fermi quasi-particles ($\alpha > \alpha_*$) to a purely bosonic effective field theory ($\alpha < \frac{5}{3}d$). In the first case ($\alpha > \alpha_*$), the validity of the Kibble-Zurek argument follows from the derivation in Ref. (Dziarmaga, 2005), which generally applies to critical systems with Fermi quasi-particles. In the intermediate case ($\alpha_* > \alpha > \frac{5}{3}d$) non-analytic scaling $\sim \delta^\theta$ follow from the dynamical perturbation theory result in Ref. (Polkovnikov, 2005). However, this picture cannot be applied to Bose quasi-particles, whose large occupation numbers hinder the applicability of adiabatic perturbation theory (de Grandi and Polkovnikov, 2010).

Then, the Kibble-Zurek scaling of mean-field systems, such as the LMG, whose excitation spectrum is described by free Bosons, needs a tailored framework to be understood (Defenu *et al.*, 2018). In this perspective, it is worth considering a single dynamically driven Harmonic mode with Hamiltonian

$$H(t) = \frac{1}{2}\left(p^2 + \omega(t)^2 x^2\right), \tag{123}$$

which faithfully describes the dynamics in Eq. (96), when adiabatic δ^2 corrections coming from the classical dynamics of the order parameter are neglected (Defenu *et al.*, 2018), see also Eq. (96).

For any time-dependent frequency a complete set of time-dependent states $\psi_n(x,t)$ can be constructed, whose occupation is conserved by the dynamics (Lewis, 1967; Lewis Jr., 1968; Lewis Jr. and Riesenfeld, 1969). In order to determine the excitation density and the ground state fidelity with respect to the instantaneous equilibrium solution of the problem, we define the adiabatic basis $\psi_n^{\mathrm{ad}}(x,t)$, which is obtained taking the conventional time-independent Harmonic oscillator eigenstates and replacing the constant frequency with the time-dependent one (Dabrowski and Dunne, 2016). Accordingly, one can expand the exact time-dependent state in terms of the adiabatic basis $\psi(x,t) = \sum c_n(t)\psi_n^{\mathrm{ad}}(x,t)$, leading to the excitation density $n_{\mathrm{exc}}(t) = \sum_{n\in 2\mathbb{N}} n|c_n|^2$, the adiabatic ground-state fidelity $f(t) = |c_0|^2$ and the residual heat $Q(t) = \omega(t)n_{\mathrm{exc}}(t)$ expressions.

According to the behaviour of these observables in the adiabatic limit $\delta \to 0$ the dynamical evolution described by Eq. (123) presents three regimes

1. Perturbative regime ($Q \sim \delta^2$).
2. Kibble-Zurek regime ($Q \sim \delta^{\frac{z\nu}{1+z\nu}}$, half-ramp).
3. Non-adiabatic regime ($Q \sim O(1)$, full ramp).

Regime (1) occurs for a finite minimal frequency at the critical point $\lim_{t\to 0}\omega(t) = \omega_0 \neq 0$: there the adiabatic perturbation theory result produces the analytic δ^2 corrections predicted by dynamical perturbation theory. Regime (2) is realized in a dynamics terminating at the quantum critical point $\omega_0 = 0$, where non-analytic corrections appear, which are encompassed by the Kibble-Zurek argument. The actual crossing of the quantum critical point only occurs in regime (3) and the actual non-adiabatic regime, is realized, leading to rate-independent corrections to the adiabatic observables, as it will be seen in the following.

For a finite thermodynamic system, we expect the dynamical gap not to completely vanish at the critical point, but to present a finite correction vanishing according to finite size scaling $t_0 \approx N^{-1/\nu_*}$, where $\nu_* = 3/2$ according to Eq. (110). Then, the residual scaled frequency only depends on the parameters combination $\Lambda = N\delta$ and,

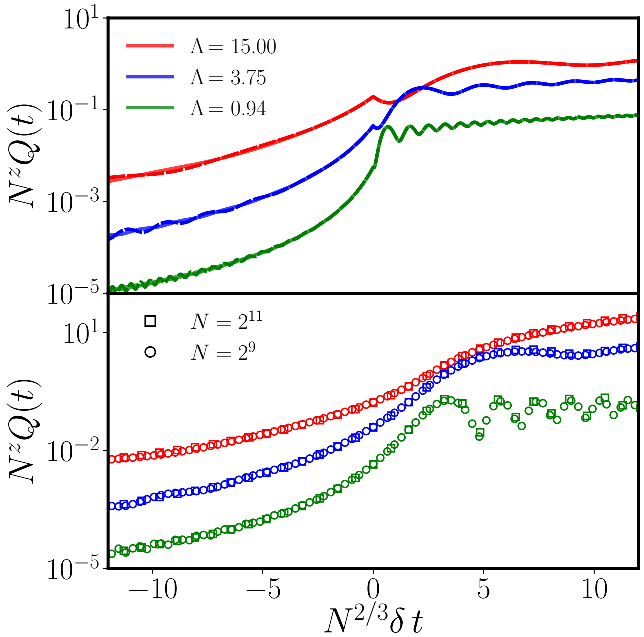

Figure 24 We present the heat curves obtained respectively via the effective model in Eq. (123) (upper panel) and via the full numerical solution of the time-dependent LMG model in Eq. (96) with time-dependent coupling $J = h_c - \delta\, t$ performed in Ref. (Acevedo *et al.*, 2014) (lower panel). Each colour represents a different value of $\Lambda = N\delta = 15, 3.75, 0.94$ from top to bottom with $N = 2^9$ and $N = 2^{11}$ (dashed and solid lines in the upper panel). Both the heat and the time variables have been rescaled following the notation of Ref. (Acevedo *et al.*, 2014). As expected, the curves at different sizes but same Λ collapse both in the theory and in the exact simulations. Moreover, the similarity between the theoretical model and the numerics is remarkable. Despite the effective model in Eq. (123) is just an effective model, which does not account for the mean-field energy shift, it captures quantitative features such as the initial smooth increase and the oscillations of the residual energy. We thank the authors of Ref. (Acevedo *et al.*, 2014) for sharing the numerical data displayed in the lower panel.

since the minimal scaled frequency reads $\tilde{\omega}^2(0) \approx \Lambda^{-2/3}$, it follows that the thermodynamic limit ($N \to \infty$) and the adiabatic one ($\delta \to 0$) do not commute. Rather, the same dynamical evolution for thermodynamical observables occurs for different sizes and drive rates as long as the combination Λ remains fixed. The universal behavior evidenced for the present harmonic effective model faithfully reproduces exact numerical computations. Indeed, a comparison between the analytic and numerical analyses of the LMG model is shown in Fig. 24 proving that the "anomalous" scaling described in Ref. (Acevedo *et al.*, 2014) is perfectly justified by the effective model studied here and introduced in Ref. (Defenu *et al.*, 2018).

3. Structural transitions

Ion crystals and, in general, structural transitions occurring in non-local systems with competing interactions have first triggered the theoretical interest in the Kibble-Zurek scaling of non-homogeneous systems (Chiara *et al.*, 2010; Del Campo *et al.*, 2010; Zurek, 2009). In presence of inhomogeneity, the critical point occurs at different moments in the different regions of the system, restoring adiabaticity for dynamical transition where critical excitations propagate faster than the phase boundaries. A straightforward enough argument to justify the previous picture is found by generalizing the scaling theory outlined at the beginning of Sec. V.C to the non-homogeneous case.

We consider a both spatial and time dependent control parameter $\lambda(x,t)$, such that the critical front occurs at $\lambda(x,t) \approx 0$, while in general one has

$$\lambda(x,t) = \alpha(x - v_{\rm p} t) \tag{124}$$

where $v_{\rm p} > 0$ is the velocity of the phase front. Locally, the inhomogeneous control parameter in Eq. (124) resembles the homogeneous case with ramp rate $\delta = \alpha\, v_{\rm p}$. Accordingly, all the locations of the systems where $\lambda(x,t) < 0$ already lie in the symmetry broken phase and, then, they can communicate the orientation of the order parameter across the phase boundary at $\lambda(x,t) \approx 0$ towards the symmetric regions of the system where $\lambda(x,t) > 0$. The maximal velocity $\hat{v}_{\rm p}$ at which this communication occurs can be found via the relation $\hat{v}_{\rm p} = \hat{\xi}/\hat{t}$. As long as $v_{\rm p} \gg \hat{v}_{\rm p}$ inhomogeneity is not relevant, since the regions on the opposite side of the phase front are effectively decoupled. On the contrary, defect formation is suppressed for $v_{\rm p} \ll \hat{v}_{\rm p}$ due to the symmetry broken regions of the system coordinating with the ones at $\lambda(x,t) > 0$.

Following the discussion above one can use the conventional scaling relations for the homogeneous Kibble-Zurek mechanism to obtain $\hat{v}_{\rm p} \sim \delta^{\frac{(z-1)\nu}{z\nu+1}} \sim \alpha^{\frac{(z-1)\nu}{\nu+1}}$, which, in turns, leads to the "critical" ramp rate

$$\hat{\delta} \sim \alpha^{\frac{z\nu+1}{1+\nu}}. \tag{125}$$

At rates $\delta \gg \hat{\delta}$ the system effectively behaves as homogeneous and the traditional results for the excitations density are retrieved, conversely in the slow drive limit $\delta \ll \hat{\delta}$ inhomogeneity becomes relevant and can alter the universal Kibble-Zurek scaling. Accordingly, in the homogeneous limit the critical rate vanishes $\lim_{\alpha\to 0}\hat{\delta} = 0$. Several examples of non-homogeneous Kibble-Zurek mechanism can be found in the literature (Collura and Karevski, 2010; Dziarmaga and Rams, 2010; Schaller, 2008; Zurek and Dorner, 2008).

Thanks to their tuneability(Lemmer *et al.*, 2015), trapped ion platforms played a crucial role both in the theoretical and experimental investigations of defects formation in the non-homogeneous realm (Lemmer *et al.*, 2015; Schneider *et al.*, 2012). By adiabatically altering the trapping parameters, it is possible to drive the system across the structural transition briefly outlined in Sec. IV.F (Baltrusch *et al.*, 2012). However, such a procedure will naturally generate localized defects in agreement with the Kibble-Zurek theory (Schneider *et al.*, 2012). A similar phenomenology is also expected for sudden quenches across the boundary of the structural transition (Del Campo *et al.*, 2010; Landa *et al.*, 2010). Moreover, the dynamics of local defects in Coulomb crystals have been proposed to realize the Frenkel-Kontorova model (Cormick and Morigi, 2012; Pruttivarasin *et al.*, 2011).

The experimental exploration of the quantum dynamics and formation of kinks in Coulomb crystals (Pyka *et al.*, 2013; Ulm *et al.*, 2013) has shown good agreement with the theory expectation (Landa *et al.*, 2010), providing a flexible tool to investigate defect formation according to the inhomogenous Kibble-Zurek mechanism (Chiara *et al.*, 2010; Del Campo *et al.*, 2010).

4. Cavity systems

Quench experiments based on quantum gases in optical cavities (Baumann *et al.*, 2011; Klinder *et al.*, 2015b) have also been interpreted within the framework of the Kibble Zurek mechanism (del Campo and Zurek, 2014; Kibble, 2001; Zurek, 1985). The global character of the cavity-mediated interaction inhibits the formation of domains and thus also of defects during the crossing of this second-order phase transition. However, remnants of the Kibble Zurek mechanism can be found in hysteretic behavior and the symmetry breaking itself.

In the case of a retarded cavity-mediated interaction, i.e. where the cavity linewidth κ is comparable to the recoil frequency ω_r, pronounced dynamical hysteresis has been observed when crossing the self-organization phase transition (Klinder *et al.*, 2015b), see Fig. 25. The intra-cavity light field, corresponding to the order parameter, shows a hysteresis loop that encloses an area exhibiting a power-law dependence upon the duration of the quench across the phase transition. Real-time observation of the intra-cavity field thus allows identifying at which coupling strength the system effectively freezes its dynamics, depending on the quench rate. A simple power-law model allows to extract dynamical exponents $z\nu$. However, a deeper interpretation would require a comprehensive extension of the concept of universality to driven-dissipative systems (Klinder *et al.*, 2015b; Sieberer *et al.*, 2013). In particular, it should be noted that these experimental observations appear not to follow the theoretical predictions outlined in Sec. V.C.2 and in Refs. (Acevedo *et al.*, 2014; Defenu *et al.*, 2018) for isolated quantum systems.

In the limit of large cavity line width with respect to the atomic recoil frequency (Baumann *et al.*, 2011),

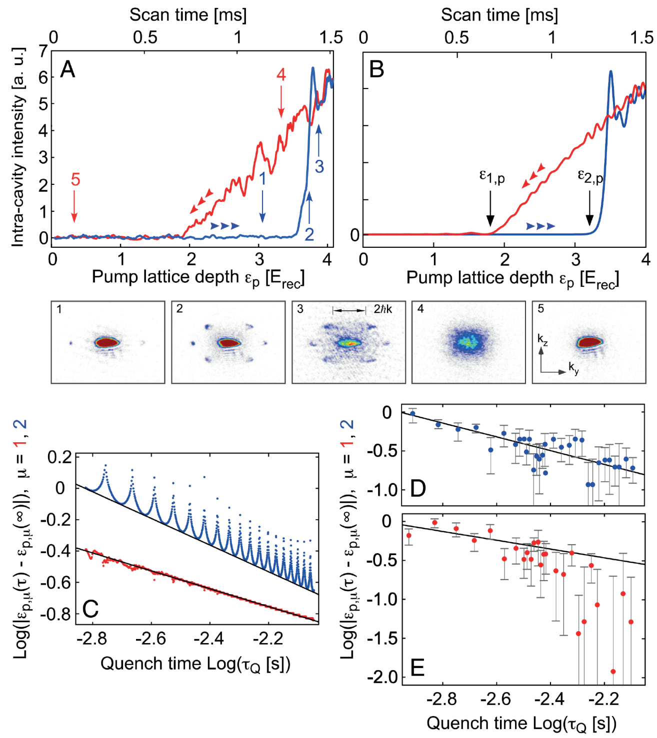

Figure 25 **Dynamical critical behavior at the self-organization phase transition.** (**A**) Intracavity intensity while the transverse pump lattice depth ϵ_p is ramped up (blue) and down (red) in ramps of 1.5 ms, each. Below, momentum spectra (1–5) are shown, recorded at increasing times during the ϵ_p-ramp, indicated by the numbered arrows in **A**. **B** Mean-field calculation according to **A** neglecting collisional interactions and assuming an infinite system. The points $\epsilon_{p,1}$ and $\epsilon_{p,2}$ indicate the upper and lower critical lattice depths. **C** Mean-field calculations of $\epsilon_{p,1}$ and $\epsilon_{p,2}$ as a function of quench time, resulting in exponents of $(n_1, n_2) = (-0.57, 0.85)$ for power law fits. **D,E** Experimentally determined dependence of the upper and lower critical lattice depths on the quench time, together with solid lines reproducing the power law dependences of **C**. Figure reproduced from (Klinder *et al.*, 2015b).

the hysteresis loop is vanishing (Klinder *et al.*, 2015b), but the effect of the quench rate can be observed in the discrete symmetry breaking described in Sec. IV.G.3. The finite size of the system naturally leads to a small symmetry-breaking field, completely dominating the symmetry-breaking process in the limit of adiabatically crossing the phase transition. However, for a finite quench rate, the approach to the phase transition can be again divided into a quasi-adiabatic regime, where the system follows the control parameter, and an impulse regime, where the system is effectively frozen. For increasing quench rates of the transverse pump power, the coupling strength separating these two regimes is decreasing, as captured by Zurek's equation (Zurek *et al.*, 2005) $|\dot{\zeta}/\zeta| = \Delta/\hbar$, with $\zeta = (\Lambda_c - \Lambda)/\Lambda_c$ describing the distance to the critical point (see also Section II.B.3) and the energy gap between ground and first excited state

$\Delta = \hbar\omega_0\sqrt{1-\Lambda^2/\Lambda_c^2}$. Accordingly, in the experiments, the symmetry breaking for large quench rates becomes dominated by (quantum) fluctuations and increasingly independent of the symmetry breaking field. Quantitative agreement of the observations with the model was found (Baumann *et al.*, 2011).

D. Dynamical Phase Transitions

One of the most relevant scaling phenomena in the far out-of-equilibrium realm is provided by dynamical phase transitions (Mori *et al.*, 2018; Zvyagin, 2016). In particular, after the sudden quench of a control parameter dynamical phase transitions may be classified into two main families. The first family displays a (possibly local) order parameter $A(t)$, whose long-time Cesaro's average $\bar{A}$, defined according to Eq. (112), characterises different steady states (Eckstein and Kollar, 2008; Eckstein *et al.*, 2009; Halimeh *et al.*, 2017; Lang *et al.*, 2018; Moeckel and Kehrein, 2008; Sciolla and Biroli, 2010). While this phenomenon is naturally observed for quenches across equilibrium symmetry breaking transitions, diverse dynamical phases may also arise in quantum systems, which do not possess any finite-temperature phase transition. There, following a sudden quench, the order parameter $A(t)$ always equilibrates to its normal phase expectation in the long time limit ($\bar{A} = 0$ for ferromagnetic systems), but the dynamical phase transition can be observed in a sudden change in the scaling approach to equilibrium (Altman and Auerbach, 2002; Barmettler *et al.*, 2009; Heyl, 2014; Lang *et al.*, 2018).

Experimental evidence of this first kind of dynamical transitions has been found in a linear chain of trapped $^{171}\mathrm{Yb}^+$ ion spins stored in a Paul trap (Zhang *et al.*, 2017b). The system was initialized in the ferromagnetic product state $|\psi_0\rangle = |\downarrow\downarrow\downarrow \ldots \downarrow\rangle_x$ and, then, evolved according to the long-range Ising Hamiltonian in Eq. (60). The dynamical quantum phase transition occurs when the ratio $h/J_0 \sim 1$, where J_0 is the strength of long-range interactions ($V_r \propto J_0/r^\alpha$) and the order parameter changes abruptly from ferromagnetic to paramagnetic order. The observation of the dynamical transition has been obtained by measuring the late time average of the two-body correlator defined as:

$$C_2 = \frac{1}{N^2}\sum_{ij}\langle\sigma_i^x\sigma_j^x\rangle, \tag{126}$$

after the quantum quench.

The measured late time correlator C_2 features a "dip" at the critical point that sharpens scaling up the system size N up to 53 $^{171}\mathrm{Yb}^+$ qubits, as shown in Fig. 26(c). Additional evidence of the occurrence of the dynamical phase transition can be also observed in higher-order correlations, such as the distribution of domain sizes throughout the entire chain, shown in Fig. 26(d). The occurrence of the dynamical phase transition is observed in the decreased probabilities of observing long strings of aligned ions at the critical point $h/J_0 \sim 1$. This is shown by measuring the mean largest domain size as a function of the transverse field strength, for late times and repeated experimental shots, which feature a sharp transition at the critical point. Another recent experimental realization of dynamical phase transitions within the LMG model was reported in Ref. (Muniz *et al.*, 2020). The experiment was performed with large ensembles of $^{88}\mathrm{Sr}$ atoms in an optical cavity where magnetic interactions can be accurately tuned (Norcia *et al.*, 2018) and reports the observation of distinct dynamical phases of matter in this system. A similar setup has been proposed also for the observation of dynamical phases of the celebrated BCS model in superconductivity as a function of system parameters and the prepared initial states (Lewis-Swan *et al.*, 2021).

The second family of dynamical phase transitions features periodic non analyticities in the Loschmidt return rate (Heyl *et al.*, 2013). It is convenient to define the return probability to the initial state $|\psi_0\rangle$ after a quantum quench under the Hamiltonian H as $\mathcal{G}(t) = \langle\psi_0| e^{-iHt} |\psi_0\rangle$. This quantity exhibits non-analycities that are formally analogous to the ones of the partition function of the corresponding equilibrium system, defined as $Z = \mathrm{Tr}(e^{-H/k_BT})$ (Heyl *et al.*, 2013). Along this analogy, the complex counterpart of the thermodynamic free energy density $f = -N^{-1}k_BT\log(Z)$ is the rate function $\lambda(t) = -N^{-1}\log[\mathcal{G}(t)]$. This quantity, in the thermodynamic limit, exhibits dynamical real-time nonanalyticities that play an analogous role as the non-analytic behavior of the free energy density of a thermodynamic system at equilibrium.

As a consequence of the above statements, the non-analyticities in the return rate signal the occurrence of dynamical quantum phase transitions at certain critical evolution times after the sudden quench. These phenomena recently generated a high degree of interest both from the theoretical (Heyl, 2018; Mori *et al.*, 2018) and experimental physics communities (Fläschner *et al.*, 2018a; Jurcevic *et al.*, 2017). The first theoretical description of dynamical phase transitions in the return rates has been shown in the case of the nearest-neighbor transverse-field Ising chain. There, non-analytic cusps in the return rate could be only observed after a sudden quench across the equilibrium critical point. It was shown by several subsequent examples that dynamical crossing an equilibrium phase boundary may not produce the aforementioned cusps in the return rates while sudden quenches within the same phase may produce type-II dynamical phase transitions (Andraschko and Sirker, 2014; Vajna and Dóra, 2014).

Therefore, the dynamical critical point for the appearance of type-II dynamical phase transitions does not need to coincide with the quantum critical point of the system

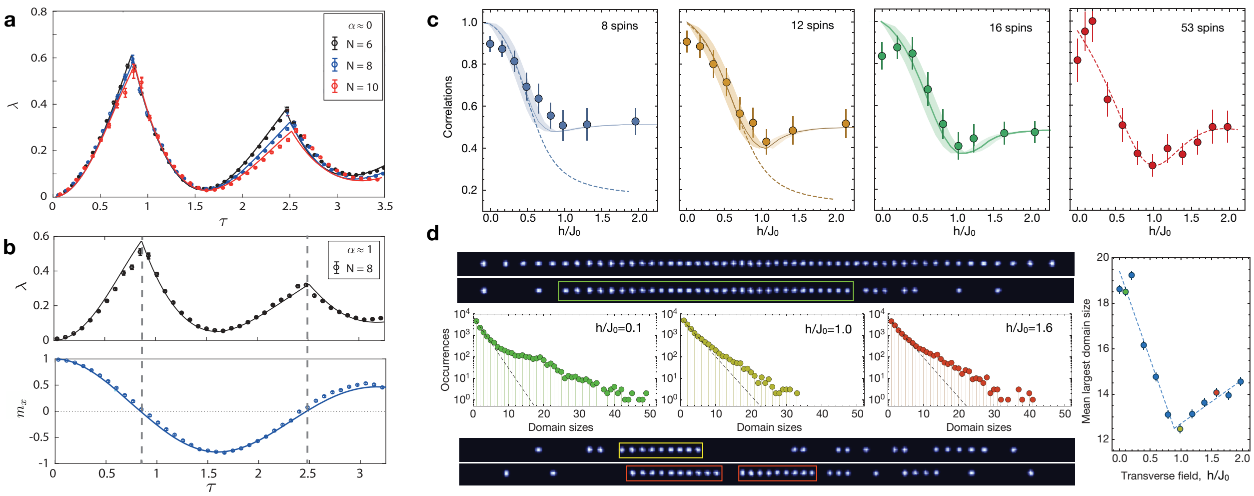

Figure 26 **Dynamical phase transitions:** Type I **(a-b)** and type II **(c-d)**. **(a)** Measured rate function λ for three different system sizes at $h/J_0 \approx 2.38$, with $\tau = th$ being the dimensionless time. The kinks in the evolution become sharper for larger N. Here the rate function is defined based on the return probability to the ground state manifold, namely $\lambda(t) = N^{-1}\log(P_{|\psi_0\rangle} + P_{|-\psi_0\rangle})$, where $|-\psi_0\rangle = |\uparrow\uparrow\uparrow\cdots\uparrow\rangle_x$. **(b)** Comparison between rate function $\lambda(t)$ and magnetization evolution $m_x(t)$. The inversion of the magnetization sign corresponds to the nonanalyticity of the rate function $\lambda(t)$. Solid lines are exact numerical predictions based on experimental parameters ($h/J_0 = 2$). Adapted from Ref. (Jurcevic *et al.*, 2017). **(c)** Long-time averaged values of the two-body correlations C_2, for different numbers of spins in the chain. Solid lines in are exact numerical solutions to the Schrödinger equation, and the shaded regions take into account uncertainties from experimental Stark shift calibration errors. Dashed lines in for $N = 12, 16$ are calculations using a canonical (thermal) ensemble with an effective temperature corresponding to the initial energy density. **(d)** Domain statistics and reconstructed single-shot images of 53 spins. Top and bottom: reconstructed images based on binary detection of spin state. The top image shows a chain of 53 ions in bright spin states. The other three images show 53 ions in combinations of bright and dark spin states. Center: statistics of the sizes of domains for three different values of h/J_0, plotted on a logarithmic scale. Dashed lines are fit to exponential functions, which could be expected for an infinite-temperature thermal state. Long tails of deviations are clearly visible and vary depending on h/J_0. Right: mean of the largest domain sizes in every single experimental shot. Dashed lines represent a piecewise linear fit, used to extract the transition point. The green, yellow, and red data points correspond to the transverse fields shown in the domain statistics data on the left-center figure. Adapted from Ref. (Zhang *et al.*, 2017b).

at equilibrium. Further proof of this distinction comes from the strong dependence of the dynamical critical point on the initial state of the system (Halimeh *et al.*, 2017; Lang *et al.*, 2018). In this perspective, long-range interactions have been shown to produce several additional dynamical phases with respect to the simple nearest neighbors case (Defenu *et al.*, 2019a; Halimeh and Zauner-Stauber, 2017; Homrighausen *et al.*, 2017; Uhrich *et al.*, 2020). It is, thus, not surprising that the first observation of type-II dynamical phase transitions has been detected in a trapped ion simulation of the long-range Ising Hamiltonian in Eq. (60).

The simulation was performed with a linear chain of trapped $^{40}Ca^{+}$ ion spins (Jurcevic *et al.*, 2017). The system is prepared in the classical eigenstate which minimizes the ferromagnetic interactions $|\psi_0\rangle = |\downarrow\downarrow\downarrow \ldots \downarrow\rangle_x$, then a finite transverse field is suddenly switched on (quenched), such that the Hamiltonian in Eq. (60) lies in the $h > J_0$, with J_0 being the average nearest-neighbor spin-spin coupling. Fig. 26(a) displays the return rate λ, which exhibits clear non-analyticities at the critical times t_c. As expected, the Löschmidt echo cusps also correspond with the zero crossings of the order parameter at the critical times t_c, see Fig. 26(b).

The correspondence between the zero crossings of the order parameter and the cusps of the return rate $\lambda(t)$ is not the only relation between the two families of dynamical phase transitions. Indeed, the dynamical critical points for type-I and type-II transitions were shown to coincide (Halimeh *et al.*, 2017; Žunkovič *et al.*, 2018). More in general, the fundamental relations between thermodynamic equilibrium phases and their dynamical counterparts has been extensively explored not only in terms of order parameters (Ajisaka *et al.*, 2014; Heyl, 2018; Titum *et al.*, 2019; Žunkovič *et al.*, 2018), but also with respect to scaling and universality (Heyl, 2015), discrete or continuous symmetry breaking (Huang *et al.*, 2019; Weidinger *et al.*, 2017; Žunkovič *et al.*, 2016) and nature of the quasi-particles (Syed *et al.*, 2021).

Free-fermionic systems, described by the Kitaev Hamiltonians studied in Sec. IV.B, played a prominent role both in the experimental and theoretical study of dynamical phase transitions. Indeed, despite the absence of a local order parameter in the equilibrium topological phase transition of the Kitaev chain, dynamical phase transitions also occur in these models (Bhattacharya and

Dutta, 2017a,b; Budich and Heyl, 2016; Vajna and Dóra, 2015), where they have been also experimentally observed (Fläschner *et al.*, 2018b). The possibility of analytically solving free-fermionic models also in presence of long-range hopping or pairing produced a comprehensive understanding of how additional dynamical phases can be influenced by corrections to scaling in the spectrum as well as its relation with the results for the Ising model (Defenu *et al.*, 2019a). Despite the absence of any local order parameter in free-fermi systems, a relation between the occurrence of cusps in the Loschmidt echo and the zero crossings of the (non-local) string order parameter (Uhrich *et al.*, 2020)

Despite its close relation to the Kitaev chain, see Sec. IV.B.3, the long-range Ising model presents a more complex phenomenology with respect to the Kitaev chain. This occurrence is related to the appearance of domain-wall confinement due to long-range interactions in the Ising model (Liu *et al.*, 2019), these confined excitations behave like Stark-localized particles in an effective confining potential (Lerose *et al.*, 2020), see also the next section. This domain-wall coupling was found to be the reason for the appearance of anomalous cusps in quantum quenches at sufficiently small transverse-field strengths (Halimeh *et al.*, 2020; Halimeh and Zauner-Stauber, 2017), while the absence of quasiparticles coupling in the Kitaev chain disrupts the anomalous phase (Defenu *et al.*, 2019a).

Critical quenches, where the post-quench Hamiltonian is critical are known to yield long-time universal scaling behavior following the mechanism of aging (Chiocchetta *et al.*, 2017). These kinds of phenomena are strongly influenced by long-range interactions as studied in (Halimeh and Maghrebi, 2021). In particular, in the LMG model, depending on the type of quench, three behaviors where both the short-time dynamics and the stationary state at long times are effectively thermal, quantum, and genuinely non-equilibrium were identified. Each stationary state is characterized by distinct universality classes and static and dynamical critical exponents (Titum and Maghrebi, 2020).

E. Confinement

As previously shown in section V.B, long-range interactions can give rise to the fast-spreading of correlations. However, focusing on trapped ions systems in this section we will review a different regime in which long-range interactions allow the observation of confinement.

In general, spin models can be engineered to exhibit confinement of correlations and meson production. Ref. (Kormos *et al.*, 2017), studied the case of a global quench with the nearest-neighbor Ising Hamiltonian

$$H = -J \sum_i \sigma_i^x \sigma_{i+1}^x + h_z \sum \sigma_i^z + h_x \sum \sigma_i^x \tag{127}$$

with both transverse h_z and longitudinal field h_x. In this case, the dynamics produces confinement of quasiparticles and magnetization oscillations with frequencies related to the mass/energy differences between the bound states most involved in the dynamics. In this setting, the quasiparticle excitation is mapped to domain walls whose separation is energetically suppressed by the longitudinal field, which causes the appearance of a ladder of discrete meson states in the low-energy spectrum of the system (James *et al.*, 2019). Remarkably, after a quantum quench in this system, both correlation spreading and energy flow (Mazza *et al.*, 2019) are suppressed, even if the system is non-integrable and non-disordered.

A similar phenomenology can be also observed in long-range spin systems described by Hamiltonian (60), as theorized in Ref. (Liu *et al.*, 2019) for low energy states and $\alpha < 3$ [see Figs. 27(b)-(c)] and in Ref. (Lerose *et al.*, 2019b) for highly excited states for $\alpha < 2$ [see Fig. 27(d)]. Interestingly, the confining potential induced by the long-range tail of the interaction on the domain walls acts, to a first approximation, as an effective longitudinal field that constrains the evolution of the spin excitations, see Fig. 27(a). Therefore, in the regime in which the transverse field h_z is smaller than the spin-spin interaction J_0, long-range interactions cause a phenomenology analogous to the one found in the Hamiltonian in Eq. (127): the presence of bounds states results in the slow spread of correlations and magnetization oscillations.

The latter has been observed experimentally for a chain of up to 38 ions (Tan *et al.*, 2021), showing a mass scaling in agreement with theory in the low energy part of the spectrum. In the same work, a smaller chain of 11 ions was used to probe the first few bound states by preparing different initial product states and measuring the magnetization $\langle \sigma_i^z(t) \rangle$ at the center of the chain (for 0 initial domain walls) or next to the boundaries of the initial domain (for 2 initial domain walls). The initial states have been chosen to maximize the matrix elements of the magnetization between the prepared state i and the adjacent higher-energy bound state $i+1$, allowing to extract the energy gap between these two states, see Fig. 27(d). Similarly, the slow spread of correlations has been observed by measuring two-body correlations of the central spin with the rest of the system, resulting in a much slower correlation spread compared to the nearest neighbor Ising chain, see Fig. 27(e).

The possibility to engineer mesons in long-range interacting spin systems has sparked an increasing body of theoretical works on the existence of string breaking in a specific range of parameters (Verdel *et al.*, 2020) and mesons collisions (Karpov *et al.*, 2020; Surace and Lerose, 2021).

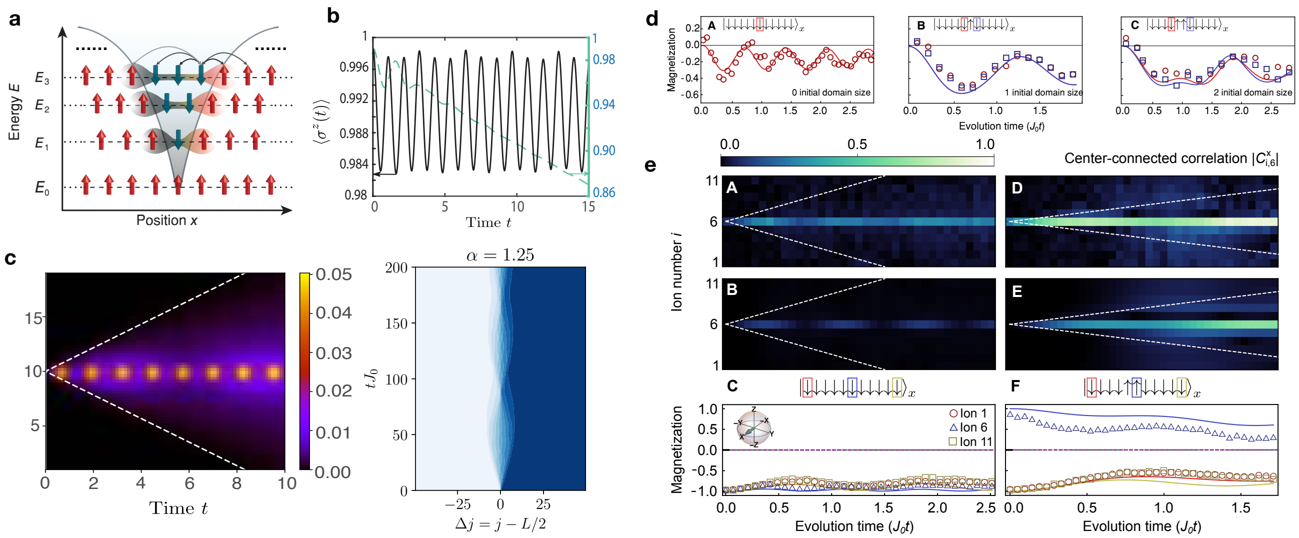

Figure 27 **Confinement in long-range spin systems (a)** Magnetic domain walls in Ising spin chains can experience an effective confining potential that increases with distance, analogously to the strong nuclear force. This potential results in meson-like domain wall bound states (labeled E_1 to E_3) that influence the post-quench dynamics. Adapted from Ref. (Tan *et al.*, 2021). **(b)** Magnetization oscillation $\langle\sigma_z(t)\rangle$ (black line) versus time after quenching to $\alpha = 2.3$, $B_z = 0.27J_0$, for $N = 20$. The dashed green lines show the magnetization for the TFIM with nearest neighbor interactions only. Numerical calculations adapted from Ref. (Liu *et al.*, 2019). **(c)** Left: Confinement of correlation in long-range system for $\alpha = 2.3$ starting from the polarized state $|\downarrow\downarrow\ldots\downarrow\rangle$, adapted from Ref. (Liu *et al.*, 2019). Right: Confinement of correlation in long-range system for $\alpha = 1.25$ starting from the highly excited state $|\downarrow\downarrow\ldots\downarrow\uparrow\uparrow\ldots\uparrow\rangle$, adapted from Ref. (Lerose *et al.*, 2019b). **(d)** Magnetization oscillations ($\alpha \sim 1.1$) starting from low energy product states to probe the first three mesons' masses. Adapted from Ref. (Tan *et al.*, 2021). **(e)** Confinement dynamics at $B_z/J_0 \approx 0.75, L = 11, \alpha \sim 1.1$). The top row shows the absolute value of experimental center-connected correlations $|C^x_{i,6}(t)|$ averaged over 2000 experiments. The middle row shows $|C^x_{i,6}(t)|$ calculated by solving the Schrödinger equation. Dashed white lines show correlation propagation bounds (light cones) in the limit $\alpha \to \infty$ (nearest-neighbor interactions). The bottom row shows measured individual-spin magnetizations along their initialization axes, $\langle\sigma^z_i(t)\rangle$, averaged over 2000 experiments. Symbols represent magnetization data and solid colored curves represent theoretical magnetizations calculated by solving the Schrödinger equation. Purple (green) dashed lines represent thermal expectation values calculated from a canonical (microcanonical) ensemble averaged over the three displayed spins. Adapted from Ref. (Tan *et al.*, 2021).

F. Other dynamical phenomena

1. Many-body localization

Long-range interacting quantum systems have been explored also in different settings, including disordered fields or interactions or in a Floquet setting, where the system is subjected to a periodic drive. In presence of disorder, long-range interacting quantum systems can exhibit many-body localization (MBL), where the system fails to thermalize at long times owing to the existence of an extensive set of quasi-local integrals of motion (Abanin *et al.*, 2019; Nandkishore and Huse, 2015). However, sufficiently long-range interactions can destroy many-body localization as shown in (Pino, 2014; Yao *et al.*, 2014). In this perspective, as it occurred for the XXZ model in Secs. IV.C and IV.D, it is important to differentiate between the case of long-range exchange couplings, i.e. hopping terms in the Hubbard model representation, and long-range density-density interactions, i.e. Ising interactions in the spin formalism.

In particular, for long-range hopping terms, analytical arguments have been used to predict the boundary $\alpha < 3d/2$ (Burin, 2015a) as a condition for delocalization in long-range spin systems governed by an XY Hamiltonian, while in the case of long-range Ising interactions, the boundary value has been found to be $\alpha_* = 2d$ (Burin, 2015b). Within this framework, the relaxation rates of local excitations in dipolar disordered systems have been studied in two and three dimensions in Ref. (Nandkishore and Gopalakrishnan, 2021) as a function of frequency and temperature. Again, in the case of a long-range spin exchange, Ref. (Safavi-Naini *et al.*, 2019a) shows numerical evidence that an XY model is delocalized for $\alpha < 1$ in one dimension, in contrast with the $\alpha_* = 1.5$ result of Ref. (Burin, 2015a). This different prediction might be due to how dominant finite size effects are for system sizes that can be simulated exactly. In this respect, (Maksymov and Burin, 2020) studied the scaling with the size of critical disorder for $\alpha < 3/2d$. (Nandkishore and Sondhi, 2017) use bosonization arguments to show that MBL can arise in one-dimensional systems with $\sim r$ interactions and speculate that MBL can be observed in two-dimensional systems with $\log(r)$ interactions, and in three-dimensional systems with $1/r$ interactions. Interestingly, MBL has been predicted with mean-field analysis (Roy and Logan, 2019) on the disordered XXZ model with different power-law exponents for $\beta < 1/2$ and $\beta < \alpha$, where α is the decay exponent long-range exchange couplings and β the one of long-range Ising interactions. MBL has also been found numerically in all-to-all systems (Sierant *et al.*, 2019) and fermionic system with long-range hopping (Nag and Garg, 2019).

An important feature of MBL in the presence of long-range density-density interactions is algebraic localization of the quasi-local integrals of motion (LIOMs) which characterize the MBL phase (De Tomasi, 2019; Pino, 2014). Conversely, in short-range interacting systems, LIOMs are exponentially localized and entanglement entropy grows logarithmically. However, since in MBL long-range systems LIOMs are algebraically localized one expects that entanglement entropy grows polynomially (Safavi-Naini *et al.*, 2019b). In particular, (Deng *et al.*, 2020) showed that in a variety of models (XY, XXZ, and Extended Hubbard Model) with power-law interactions there is a universal power-law growth of the entanglement entropy at the MBL transition. Experimental signatures of many-body localization in long-range systems, such as memory of the initial states (Smith *et al.*, 2016) confirmed numerically by Ref. (Wu and Das Sarma, 2016), and slow growth of the second-order Renyi entropy (Brydges *et al.*, 2019), have been observed in trapped ion chains up to 20 qubits.

More recently, disorder-free, "stark" MBL (van Nieuwenburg *et al.*, 2019; Schulz *et al.*, 2019) has been predicted to be more resilient than “standard” MBL to long-range exchange couplings (Bhakuni and Sharma, 2020). This phenomenon has been later connected to the Hilbert space shattering caused by conservation laws (Khemani *et al.*, 2020; Moudgalya *et al.*, 2021). Signatures of this type of disorder-free MBL have been observed in a trapped-ion chain of up to 25 qubits with long-range interactions decaying with $\alpha \sim 1.3$ and a strong effective magnetic field gradient (Morong *et al.*, 2021). As mentioned in section II.A.1, a large magnetic field makes the Ising model an effective XY model with long-range exchange couplings, and, in this case, the LIOMs are given by the Wannier-Stark states. Conversely, in the case of long-range density-density interactions, one expects Hilbert-space fragmentation, which was also studied in short-range interacting disordered spinless fermions (Bar Lev *et al.*, 2015; De Tomasi *et al.*, 2019). In particular, in Hubbard models with polar interactions and nearest-neighbor hoppings (Li *et al.*, 2021) the power-law tail plays a crucial role because it induces Hilbert-space shattering and MBL-like localization in absence of any disorder, even for moderate ratios of the polar interactions versus hopping. This is not the case of models with both nearest-neighbor hopping and density-density interactions, where Hilbert-space fragmentation does not lead to disorder-free MBL (De Tomasi *et al.*, 2019).

2. Periodic drive

Quantum many-body systems with both disorder and interactions have been recently used to observe new phases of matter in periodically driven (Floquet) systems (Else *et al.*, 2016; von Keyserlingk *et al.*, 2016; Khemani *et al.*, 2016; Yao and Nayak, 2018) in which discrete-time translational symmetry is spontaneously broken. The observation of time-crystalline behavior has been achieved in a periodically driven 1D trapped ion chain with on-site static disorder (Zhang *et al.*, 2017a) and a 3D disordered sample of NV-centers with dipolar interaction (Choi *et al.*, 2017). However, it has been later shown numerically (Khemani *et al.*, 2019) that both realizations did not realize a genuine discrete time crystal where MBL prevents the system to heat to infinite temperature, but rather a pre-thermal (trapped ions) and critical (NV-centers) time crystal. Recently, genuine MBL time crystals have been realized in systems with disordered interactions in a system of 9 ^{13}C nuclear spins coupled to a single NV center (Randall *et al.*, 2021) and in the Google quantum computer (Mi *et al.*, 2022) using 20 superconducting qubits with fully programmable interactions. In the same spirit, quasi-periodic Floquet drives have been predicted (Friedman *et al.*, 2022) to realize an emergent dynamical symmetry-protected topological phase (EDSPT) that has been experimentally realized with 10 atomic ions in Ref. (Dumitrescu *et al.*, 2021).

Long-range interactions do play a special role in the case of pre-thermal discrete time crystals, where the temporal and spatial long-range order is exhibited only for low energy initial states (Machado *et al.*, 2020). The pre-thermal discrete time crystal has been observed and characterized experimentally in a trapped ions chain of up to 25 spins (Kyprianidis *et al.*, 2021). Limit cycles and time crystalline behavior has been predicted and experimentally observed also in periodically driven many-body cavity QED systems (Cosme *et al.*, 2018; Georges *et al.*, 2021; Keßler *et al.*, 2019, 2020). In addition, even without providing a time-dependent external drive, many-body cavity QED systems can feature non-stationary periodically evolving states that emerge due to the competition between dissipative and coherent processes in long-range interacting systems, as has been recently experimentally observed (Dogra *et al.*, 2019) and theoretically analyzed (Buča and Jaksch, 2019; Chiacchio and Nunnenkamp, 2019).

Time crystals and, in general, Floquet dynamics has been also found to be a source of dynamical phase transition (Kosior and Sacha, 2018; Yang *et al.*, 2019). Indeed, novel dynamical transitions can be engineered by periodic driving. In the particular case of the long-range Ising model, the periodic drive can stabilize phases, dubbed Kapitza phases, with magnetic ordering without an equilibrium counterpart (Lerose *et al.*, 2019a). Moreover, in the study of the quantum Ising chain, long-range interactions have been shown to induce a huge variety of different "higher-order" discrete time crystal phases, where the periodicity of the response is a multiple nT of the external drive period T (Collura *et al.*, 2021; Giachetti *et al.*, 2022; Pizzi *et al.*, 2021). It is worth noting that a similar structure of the time-crystal phases has been also predicted to occur in periodically driven BCS superconductors (Ojeda Collado *et al.*, 2021).

VI. CONCLUSION AND OUTLOOK

In this paper, we have reviewed the main atomic, molecular and optical (AMO) systems in which long-range interactions are naturally present, **and** we have also emphasized the fact that in many of such systems the range of the interaction can be controlled and varied giving rise to tunable values of α. This can be seen in the spirit of quantum simulations, where one has a high degree of control over the system and on its crucial properties.

We have discussed in the main text most of the quantum models that it is possible to **currently** simulate, focusing in particular on lattice and spin models. A variety of spin models such as quantum Ising, XX, and XXZ models (and their variants) with tunable long-range interactions can be implemented. These spin models alongside bosonic and fermionic models with long-range density-density interactions provide an ample arena of models in which the long-rangedness of the interactions plays a key role. If remarkable progress has been done in the simulations of quantum long-range lattice models, many more models have yet to find their way, such as bosonic and fermionic models with long-range hopping (a task presently hard to be implemented) and long-range multi-body and multi-spin terms (Andrade *et al.*, 2021).

In particular, in experimental AMO systems, the main challenges are centered on gaining more tunability of the spin-spin interactions through individual atom control. For example, trapped-ion systems are routinely used as quantum computing platforms (Bruzewicz *et al.*, 2019; Pino *et al.*, 2021; Wright *et al.*, 2019) where individual qubit control and detection are necessary ingredients to exploit the long-range connectivity of pairwise quantum logic gate operations. Leveraging on the same technological advances, trapped-ion simulators are posed to explore a wider range of physical models where long-range interactions and high connectivity play crucial roles, ranging from high energy physics (Martinez *et al.*, 2016; Muschik *et al.*, 2017), spin-boson models (Gorman *et al.*, 2018; Safavi-Naini *et al.*, 2018), to quantum glasses (Rademaker and Abanin, 2020).

Also, many-body cavity QED systems have just demonstrated the first results on tuning the interaction range. In the next step, the resulting many-body phases, phase transition, and associated phenomena including the Brazovskii transition, glassiness, or frustration have to be explored. Having these tunable range interactions compete with short-range collisional interactions will allow to enter strongly correlated regimes and to explore the rich universe of extended Hubbard models.

Long-range couplings induce a dispersion relation $\propto k^\sigma$ as opposed to the standard relation $\propto k^2$ in short-range systems. Given this nature of the dispersion relation in long-range systems, one can expect – and find in some cases with microscopic calculations – that the effective low-energy model features fractional derivatives (or fractional Laplacians) altering the scaling of the observables in the system. While this modified scaling is – at least partially – understood for $O(\mathcal{N})$ systems (Defenu *et al.*, 2020), its counterpart in interacting lattice systems remains to be thoroughly investigated (Botzung *et al.*, 2021; Ferraretto and Salasnich, 2019; Iglói *et al.*, 2018; Lepori *et al.*, 2016).

Interestingly, relevant non-analytic momentum terms in quantum long-range models induce an universal behavior which effectively corresponds to the one of a classical model in the fractional $d + z$ dimension, with $z < 1$ (Defenu *et al.*, 2017b). For this reason, the spatial dimensionality does not appear to play a crucial role in long-range systems as it does in the local case, since long-range couplings alter the spectral dimension of the bare theory (Leuzzi *et al.*, 2008a; Millán *et al.*, 2021). A similar effect may be also expected in the strong long-range regime, where the spectral dimension is not defined, but the spectral properties are still expected to rule the universal behaviour both at and out of equilibrium. Nevertheless, the connection between those spectral properties and universal aspects of celebrated phenomena such as ensemble in-equivalence, negative specific heats and quasi-stationary states largely remain to be explored and exploited (Defenu, 2021; Kastner, 2010).

Several recent results not fully established in the long-range literature have not been discussed in details. The choice of topics has been motivated by the goal to advocate for the inclusion of long-range physics, and quantum long-range systems in particular, in university-taught courses. The (not exhaustive) list of topics we did not discuss includes the well established interplay between long-range couplings and disorder (Katzgraber *et al.*, 2009; Kotliar *et al.*, 1983; Leuzzi *et al.*, 2008b), recently studied in the perspective of long-range interactions (Millán *et al.*, 2021). Also, the presence of long-range correlated noise in quantum computing devices (Aharonov *et al.*, 2006), has been reconsidered in the context of studies on long-range systems (Biella *et al.*, 2013; Chávez *et al.*, 2019; Seetharam *et al.*, 2022). Finally, examples of quantum circuits, where long-range couplings or disorder generate peculiar scaling of entanglement (Block *et al.*, 2022; Minato *et al.*, 2022; Xu, 2022), promising to induce further excitement on applications of long-range interactions, were not substantially covered in our review. Nevertheless, a careful reading of the previous papers shows that the information provided in the present work should put the interested reader in condition to fully understand the phenomena typically discussed in such recent areas of research.

The analysis of the different systems presented in this review ultimately shows then that long-range interactions provide an "ingredient" that we can control and use for different purposes. On the one hand, they can be exploited to control the stationary states and the thermalization properties. On the other hand, they may affect the phase diagram and the universality properties. Additionally, they can be a resource in the quantum control of the system, providing a useful knob to control the dynamics and the implementation of quantum information tasks, where they can be used to improve the efficiency of control gates and the unitary dynamics needed to modify in the desired way the quantum state of the system.

Long-range properties can be also exploited in typical quantum simulations contexts, as highlighted in the simulation of dynamical gauge field theory with AMO systems (Bañuls *et al.*, 2020; Davoudi *et al.*, 2020, 2021), where a suitably tailored long-range interactions can be used to simulate the effect of dynamical gauge fields. Similarly, they can play a role in the study of quantum devices and the thermodynamic aspects of quantum registers.

The study of the possible uses of long-range interactions in quantum simulators and devices is only at the beginning and it will benefit from (and motivate in turn) progress in systems in which the long-range nature of the interactions can be controlled, as in the mode control of long-range interactions with trapped ions. Several systems in which long-range interactions may play a crucial role remain to be fully investigated, such as ultracold fermionic gases with long-range interactions. We envision a significant interplay between the study of new equilibrium phases and dynamical regimes in quantum long-range systems and the focused embodiment of systems with long-range coupling in quantum devices and simulators. We hope that the present review may trigger such combined studies to fully exploit the richness of quantum long-range systems.

ACKNOWLEDGEMENTS

We thank all our colleagues within the long-range community that engaged us in many fruitful interactions and discussions over the years. In particular, we acknowledge useful correspondence on the content of this review with O. L. Acevedo, A. Lerose, G. Morigi, and L. Quiroga. We acknowledge A. Daley, D. O'Dell, L. Dell'Anna, Z.-X. Gong, J. A. S. Lourenço, M. Maghrebi, G. Morigi, D. Mukamel, G. Pupillo, A. M. Rey, L. Santos, J. Schachenmayer, P. Schauss, R. Nandkishore for their valuable feedback and careful reading of the manuscript. This work is supported by the Deutsche Forschungsgemeinschaft (DFG, German Research Foundation) under Germany's Excellence Strategy EXC2181/1-390900948 (the Heidelberg STRUCTURES Excellence Cluster). T.D. acknowledges funding from the Swiss National Science Foundation SNF: NCCR QSIT and the project "Cavity-assisted pattern recognition" (Project No. IZBRZ2 186312), and funding from EU Horizon 2020: ITN grant ColOpt (Project No. 721465). T.M. acknowledges CNPq for support through Bolsa de produtividade em Pesquisa n.311079/2015-6 and the Serrapilheira Institute (grant number Serra-1812-27802). A.T. and S.R. acknowledge support by the MISTI GlobalSeed Funds MIT-FVG Collaboration Grant "NV centers for the test of the Quantum Jarzynski Equality (NVQJE)". G.P. acknowledges the NSF CAREER Award (Award No. PHY-2144910), the Army Research Office (W911NF21P0003), the Office of Naval Research (N00014-20-1-2695, N00014-22-1-2282) and the DOE Office of Science, under Award no. DE SC0021143.

REFERENCES

Abanin, D. A., E. Altman, I. Bloch, and M. Serbyn (2019), Rev. Mod. Phys. **91**, 021001.

Abanov, A., V. Kalatsky, V. L. Pokrovsky, and W. M. Saslow (1995), Phys. Rev. B **51**, 1023.

Abreu, B., F. Cinti, and T. Macrì (2020), arXiv:2009.10203.

Acevedo, O. L., L. Quiroga, F. J. Rodr i guez, and N. F. Johnson (2014), Phys. Rev. Lett. **112** (3), 030403.

Adelhardt, P., J. A. Koziol, A. Schellenberger, and K. P. Schmidt (2020), Phys. Rev. B **102**, 174424.

Aharonov, D., A. Kitaev, and J. Preskill (2006), Phys. Rev. Lett. **96**, 050504.

Ajisaka, S., F. Barra, and B. Žunkovič (2014), New J. Phys. **16** (3), 033028.

Albash, T., and D. A. Lidar (2018), Rev. Mod. Phys. **90**, 015002.

Alecce, A., and L. Dell'Anna (2017), Phys. Rev. B **95**, 195160.

Altman, E., and A. Auerbach (2002), Phys. Rev. Lett. **89**, 250404.

Amico, L., R. Fazio, A. Osterloh, and V. Vedral (2008), Rev. Mod. Phys. **80**, 517.

Ancilotto, F., M. Rossi, and F. Toigo (2013), Phys. Rev. A **88**, 033618.

Andelman, D., F. Broçhard, and J.-F. Joanny (1987), J. Chem. Phys. **86** (6), 3673.

Anderegg, L., L. W. Cheuk, Y. Bao, S. Burchesky, W. Ketterle, K.-K. Ni, and J. M. Doyle (2019), Science **365** (6458), 1156.

Anderson, P. W., and G. Yuval (1969), Phys. Rev. Lett. **23**, 89.

Anderson, P. W., G. Yuval, and D. R. Hamann (1970), Phys. Rev. B **1**, 4464.

Andrade, B., Z. Davoudi, T. Graß, M. Hafezi, G. Pagano, and A. Seif (2021), arXiv:2108.01022 [quant-ph].

Andraschko, F., and J. Sirker (2014), Phys. Rev. B **89**, 125120.

Andreev, A. F., and I. M. Lifshitz (1969), Soviet Physics JETP **29** (6), 2057.

Angelini, M. C., G. Parisi, and F. Ricci-Tersenghi (2014), Phys. Rev. E **89**, 062120.

Angelone, A., F. Mezzacapo, and G. Pupillo (2016), Phys. Rev. Lett. **116**, 135303.

Angelone, A., T. Ying, F. Mezzacapo, G. Masella, M. Dalmonte, and G. Pupillo (2020), Phys. Rev. A **101**, 063603.

Anquez, M., B. A. Robbins, H. M. Bharath, M. Boguslawski, T. M. Hoang, and M. S. Chapman (2016), Phys. Rev. Lett. **116**, 155301.

Antenucci, F., M. Ibáñez Berganza, and L. Leuzzi (2015), Phys. Rev. B **92**, 014204.

Antoni, M., and S. Ruffo (1995), Phys. Rev. E **52** (3), 2361.

Antoniazzi, A., F. Califano, D. Fanelli, and S. Ruffo (2007), Phys. Rev. Lett. **98**, 150602.

Astrakharchik, G. E., J. Boronat, I. L. Kurbakov, and Y. E. Lozovik (2007), Phys. Rev. Lett. **98**, 060405.

Astrakharchik, G. E., and M. D. Girardeau (2011), Phys. Rev. B **83**, 153303.

Bachelard, R., T. Dauxois, G. De Ninno, S. Ruffo, and F. Staniscia (2011), Phys. Rev. E **83**, 061132.

Bachelard, R., and M. Kastner (2013), Phys. Rev. Lett. **110**, 170603.

Bachmann, S., M. Fraas, and G. M. Graf (2017), Ann. Henri Poincaré **18** (5), 1755.

Baillie, D., and P. B. Blakie (2018), Phys. Rev. Lett. **121**, 195301.

Baillie, D., R. M. Wilson, R. N. Bisset, and P. B. Blakie (2016), Phys. Rev. A **94**, 021602.

Baillie, D., R. M. Wilson, and P. B. Blakie (2017), Phys. Rev. Lett. **119**, 255302.

Bakhtiari, M. R., A. Hemmerich, H. Ritsch, and M. Thorwart (2015), Phys. Rev. Lett. **114** (12), 123601.

Balewski, J. B., A. T. Krupp, A. Gaj, S. Hofferberth, R. Löw, and T. Pfau (2014), New J. Phys. **16** (6), 063012.

Balog, I., G. Tarjus, and M. Tissier (2014), J. Stat. Mech.: Theory Exp. **2014** (10), 10017.

Baltrusch, J. D., C. Cormick, and G. Morigi (2012), Phys. Rev. A **86** (3), 53.

Bañuls, M. C., R. Blatt, J. Catani, A. Celi, J. I. Cirac, M. Dalmonte, L. Fallani, K. Jansen, M. Lewenstein, S. Montangero, C. A. Muschik, B. Reznik, E. Rico, L. Tagliacozzo, K. Van Acoleyen, F. Verstraete, U.-J. Wiese, M. Wingate, J. Zakrzewski, and P. Zoller (2020), Eur. Phys. J. D **74** (8), 165.

Bapst, V., and G. Semerjian (2012), J. Stat. Mech.: Theory Exp. **2012** (06), P06007.

Bar Lev, Y., G. Cohen, and D. R. Reichman (2015), Phys. Rev. Lett. **114**, 100601.

Baranov, M. A., M. Dalmonte, G. Pupillo, and P. Zoller (2012), Chemical Reviews **112** (9), 5012.

Barci, D. G., L. Ribeiro, and D. A. Stariolo (2013), Phys. Rev. E **87** (6), 85.

Barci, D. G., and D. A. Stariolo (2007), Phys. Rev. Lett. **98** (20), 200604.

Barci, D. G., and D. A. Stariolo (2009), Phys. Rev. B **79** (7), 075437.

Barci, D. G., and D. A. Stariolo (2011), Phys. Rev. B **84** (9), 094439.

Barmettler, P., M. Punk, V. Gritsev, E. Demler, and E. Altman (2009), Phys. Rev. Lett. **102**, 130603.

Barré, J., and B. Gonçalves (2007), Physica A **386** (1), 212.

Barré, J., D. Mukamel, and S. Ruffo (2001), Phys. Rev. Lett. **87**, 030601.

Barredo, D., H. Labuhn, S. Ravets, T. Lahaye, A. Browaeys, and C. S. Adams (2015), Phys. Rev. Lett. **114**, 113002.

Barredo, D., S. de Léséleuc, V. Lienhard, T. Lahaye, and A. Browaeys (2016), Science **354** (6315), 1021.

Bates, F. S., and G. H. Fredrickson (1990), Annu. Rev. Phys. Chem. **41**, 525.

Baumann, K., C. Guerlin, F. Brennecke, and T. Esslinger (2010), Nature **464** (7293), 1301.

Baumann, K., R. Mottl, F. Brennecke, and T. Esslinger (2011), Phys. Rev. Lett. **107** (14), 140402.

Baus, M., and J.-P. Hansen (1980), Physics Reports **59** (1), 1.

Bause, R., A. Kamijo, X.-Y. Chen, M. Duda, A. Schindewolf, I. Bloch, and X.-Y. Luo (2021), arXiv:2106.10089 [cond-mat.quant-gas].

Béguin, L., A. Vernier, R. Chicireanu, T. Lahaye, and A. Browaeys (2013), Phys. Rev. Lett. **110** (26), 263201.

Behan, C., L. Rastelli, S. Rychkov, and B. Zan (2017), Phys. Rev. Lett. **118** (24), 1819.

Benatti, F., and R. Floreanini (2005), Int. J. Mod. Phys. A **19** (19), 3063.

Bentsen, G., Y. Gu, and A. Lucas (2019a), Proceedings of the National Academy of Sciences **116** (14), 6689.

Bentsen, G., T. Hashizume, A. S. Buyskikh, E. J. Davis, A. J. Daley, S. S. Gubser, and M. Schleier-Smith (2019b), Phys. Rev. Lett. **123**, 130601.

Berganza, M. I. n., and L. Leuzzi (2013), Phys. Rev. B **88**, 144104.

Berges, J., N. Tetradis, and C. Wetterich (2002), Phys. Rep. **363** (4-6), 223.

Bermudez, A., and M. B. Plenio (2012), Phys. Rev. Lett. **109**, 010501.

Bermudez, A., L. Tagliacozzo, G. Sierra, and P. Richerme (2017), Phys. Rev. B **95** (2), 024431.

Bernien, H., S. Schwartz, A. Keesling, H. Levine, A. Omran, H. Pichler, S. Choi, A. S. Zibrov, M. Endres, M. Greiner, V. Vuletić, and M. D. Lukin (2017), Nature **551** (7682), 579.

Bhakuni, D. S., and A. Sharma (2020), Phys. Rev. B **102**, 085133.

Bhattacharya, U., and A. Dutta (2017a), Phys. Rev. B **96**, 014302.

Bhattacharya, U., and A. Dutta (2017b), Phys. Rev. B **95**, 184307.

Biella, A., F. Borgonovi, R. Kaiser, and G. L. Celardo (2013), EPL (Europhysics Letters) **103** (5), 57009, arXiv:1304.5451 [cond-mat.mes-hall].

Bienias, P., J. Douglas, A. Paris-Mandoki, P. Titum, I. Mirgorodskiy, C. Tresp, E. Zeuthen, M. J. Gullans, M. Manzoni, S. Hofferberth, D. Chang, and A. V. Gorshkov (2020), Phys. Rev. Research **2**, 033049.

Bighin, G., N. Defenu, I. Nándori, L. Salasnich, and A. Trombettoni (2019), Phys. Rev. Lett. **123**, 100601.

Binder, K. (1985), Zeitschrift fur Physik B Condensed Matter **61** (1), 13.

Birkl, G., S. Kassner, and H. Walther (1992), Nature (London) **357** (6376), 310.

Bismut, G., B. Laburthe-Tolra, E. Maréchal, P. Pedri, O. Gorceix, and L. Vernac (2012), Phys. Rev. Lett. **109**, 155302.

Black, A. T., H. W. Chan, and V. Vuletić (2003), Phys. Rev. Lett. **91** (20), 203001.

Blanchard, T., M. Picco, and M. A. Rajabpour (2013), EPL (Europhysics Letters) **101** (5), 56003.

Blaß, B., H. Rieger, G. m. H. Roósz, and F. Iglói (2018), Phys. Rev. Lett. **121**, 095301.

Blatt, R., and C. F. Roos (2012), Nat. Phys. **8** (4), 277.

Blatt, R., and D. Wineland (2008), Nature **453** (7198), 1008.

Blinc, R., and A. P. Levanyuk (1986), *Incommensurate Phases in Dielectrics*, Modern Problems in Condensed Matter Sciences 14 (North-Holland).

Bloch, I., J. Dalibard, and W. Zwerger (2008a), Rev. Mod. Phys. **80** (3), 885.

Bloch, I., J. Dalibard, and W. Zwerger (2008b), Reviews of Modern Physics **80** (3), 885.

Block, M., Y. Bao, S. Choi, E. Altman, and N. Y. Yao (2022), Phys. Rev. Lett. **128**, 010604.

Bluemel, R., J. M. Chen, E. Peik, W. Quint, and W. Schleich (1988), Nature (London) **334**, 309.

Bluvstein, D., A. Omran, H. Levine, A. Keesling, G. Semeghini, S. Ebadi, T. T. Wang, A. A. Michailidis, N. Maskara, W. W. Ho, S. Choi, M. Serbyn, M. Greiner, V. Vuletić, and M. D. Lukin (2021), Science **371** (6536), 1355.

Bohn, J. L., A. M. Rey, and J. Ye (2017), Science **357** (6355), 1002.

Bohrdt, A., A. Omran, E. Demler, S. Gazit, and F. Grusdt (2020), Phys. Rev. Lett. **124**, 073601.

Boninsegni, M., N. Prokof'ev, and B. Svistunov (2006), Phys. Rev. Lett. **96**, 070601.

Boninsegni, M., and N. V. Prokof'ev (2012), Rev. Mod. Phys. **84**, 759.

Borish, V., O. Marković, J. A. Hines, S. V. Rajagopal, and M. Schleier-Smith (2020), Phys. Rev. Lett. **124**, 063601.

Borzi, R. A., S. A. Grigera, J. Farrell, R. S. Perry, S. J. S. Lister, S. L. Lee, D. A. Tennant, Y. Maeno, and A. P. Mackenzie (2007), Science **315** (5809), 214.

Bose, S. (2007), Contemporary Physics **48** (1), 13.

Botet, R., and R. Jullien (1983), Phys. Rev. B **28**, 3955.

Botet, R., R. Jullien, and P. Pfeuty (1982), Phys. Rev. Lett. **49** (7), 478.

Böttcher, F., J.-N. Schmidt, J. Hertkorn, K. S. H. Ng, S. D. Graham, M. Guo, T. Langen, and T. Pfau (2020), arXiv e-prints , arXiv:2007.06391arXiv:2007.06391 [cond-mat.quant-gas].

Böttcher, F., J.-N. Schmidt, J. Hertkorn, K. S. H. Ng, S. D. Graham, M. Guo, T. Langen, and T. Pfau (2021), Reports on Progress in Physics **84** (1), 012403.

Botzung, T., D. Hagenmüller, G. Masella, J. Dubail, N. Defenu, A. Trombettoni, and G. Pupillo (2021), Phys. Rev. B **103**, 155139.

Botzung, T., G. Pupillo, P. Simon, R. Citro, and E. Ercolessi (2019), arXiv e-prints , arXiv:1909.12168arXiv:1909.12168 [cond-mat.str-el].

Brankov, I. G., V. A. Zagrebnov, and I. S. Tonchev (1975), Theoretical and Mathematical Physics **22** (1), 13.

Bravyi, S., M. B. Hastings, and F. Verstraete (2006), Phys. Rev. Lett. **97**, 050401.

Brazovskii, S. A. (1975), Zh. Eksp. Teor. Fiz. **68** (1), 175.

Brennecke, F., R. Mottl, K. Baumann, R. Landig, T. Donner, and T. Esslinger (2013), Proc. Natl. Acad. Sci. **110** (29), 11763.

Brézin, E., and J. Zinn-Justin (1976), Phys. Rev. Lett. **36** (13), 691.

Britton, J. W., B. C. Sawyer, A. C. Keith, C. C. J. Wang, J. K. Freericks, H. Uys, M. J. Biercuk, and J. J. Bollinger (2012), Nature **484** (7395), 489.

Browaeys, A., and T. Lahaye (2020), Nature Physics **16** (2), 132.

Brown, L. S., and G. Gabrielse (1986), Rev. Mod. Phys. **58**, 233.

Brunelli, M., L. Fusco, R. Landig, W. Wieczorek, J. Hoelscher-Obermaier, G. Landi, F. L. Semião, A. Ferraro, N. Kiesel, T. Donner, G. De Chiara, and M. Paternostro (2018), Phys. Rev. Lett. **121** (16), 160604.

Bruno, P. (2001), Phys. Rev. Lett. **87**, 137203.

Bruun, G. M., and D. R. Nelson (2014), Phys. Rev. B **89** (9), 609.

Bruun, G. M., and E. Taylor (2008), Phys. Rev. Lett. **101** (24), 610.

Bruzewicz, C. D., J. Chiaverini, R. McConnell, and J. M. Sage (2019), Applied Physics Reviews **6** (2), 021314.

Brydges, T., A. Elben, P. Jurcevic, B. Vermersch, C. Maier, B. P. Lanyon, P. Zoller, R. Blatt, and C. F. Roos (2019), Science (New York, N.Y.) **364** (6437), 260.

Buča, B., and D. Jaksch (2019), Phys. Rev. Lett. **123** (26), 260401.

Büchler, H. P., E. Demler, M. Lukin, A. Micheli, N. Prokof'ev, G. Pupillo, and P. Zoller (2007), Phys. Rev. Lett. **98**, 060404.

Budich, J. C., and M. Heyl (2016), Phys. Rev. B **93**, 085416.

Burin, A. L. (2015a), Phys. Rev. B **92**, 104428.

Burin, A. L. (2015b), Phys. Rev. B **91**, 094202.

Bustingorry, S., E. Jagla, and J. Lorenzana (2005), Acta Materialia **53** (19), 5183.

Buyskikh, A. S., M. Fagotti, J. Schachenmayer, F. Essler, and A. J. Daley (2016), Phys. Rev. A **93** (5), 053620.

Caballero-Benitez, S. F., and I. B. Mekhov (2015), Phys. Rev. Lett. **115** (24), 243604.

Calabrese, P., and J. Cardy (2004), J. Stat. Mech.: Theory Exp. **2004** (6), 06002.

Calabrese, P., and J. Cardy (2006), Phys. Rev. Lett. **96** (13), 136801.

Camacho-Guardian, A., R. Paredes, and S. F. Caballero-Benítez (2017), Phys. Rev. A **96**, 051602.

Campa, A., T. Dauxois, D. Fanelli, and S. Ruffo (2014), *Physics of Long-Range Interacting Systems* (Oxford Univ. Press).

Campa, A., T. Dauxois, and S. Ruffo (2009), Phys. Rep. **480** (3-6), 57.

del Campo, A., and W. H. Zurek (2014), Int. J. Mod. Phys. A **29**.

Caneva, T., R. Fazio, and G. E. Santoro (2008), Phys. Rev. B **78** (10), 10.1103/physrevb.78.104426.

Cannas, S. A., M. F. Michelon, D. A. Stariolo, and F. A. Tamarit (2006), Phys. Rev. B **73**, 184425.

Capati, M., S. Caprara, C. di Castro, M. Grilli, G. Seibold, and J. Lorenzana (2015), Nat. Comm. **6**, 7691.

Cappelli, A., L. Maffi, and S. Okuda (2019), Journal of High Energy Physics **2019** (1), 161.

Capponi, S., D. Poilblanc, and T. Giamarchi (2000), Phys. Rev. B **61**, 13410.

Cardy, J. (1996), *Scaling and Renormalization in Statistical Physics* (Cambridge University Press).

Cardy, J. L. (1999), J. Phys. A: Math. Gen. **14** (6), 1407.

Carr, L. D., D. DeMille, R. V. Krems, and J. Ye (2009), New J. Phys. **11** (5), 055049.
Cartarius, F., G. Morigi, and A. Minguzzi (2014), Phys. Rev. A **90**, 053601.
Casula, M., S. Sorella, and G. Senatore (2006), Phys. Rev. B **74**, 245427.
Ceperley, D. M. (1995), Rev. Mod. Phys. **67**, 279.
Cescatti, F., M. Ibáñez-Berganza, A. Vezzani, and R. Burioni (2019), Phys. Rev. B **100** (5), 054203.
Chávez, N. C., F. Mattiotti, J. A. Méndez-Bermúdez, F. Borgonovi, and G. L. Celardo (2019), The European Physical Journal B **92** (7), 10.1140/epjb/e2019-100016-3.
Chayes, L., N. Crawford, D. Ioffe, and A. Levit (2008), J. Stat. Phys. **133** (1), 131.
Chen, C.-F., and A. Lucas (2019), Phys. Rev. Lett. **123**, 250605.
Chen, Y., Z. Yu, and H. Zhai (2016), Phys. Rev. A **93** (4), 041601.
Chiacchio, E. I. R., and A. Nunnenkamp (2018), Phys. Rev. A **98** (2), 023617.
Chiacchio, E. I. R., and A. Nunnenkamp (2019), Phys. Rev. Lett. **122** (19), 193605, arXiv:1901.06996.
Chiara, G. D., A. d. Campo, G. Morigi, M. B. Plenio, and A. Retzker (2010), New J. Phys. **12** (11), 115003.
Chiocchetta, A., A. Gambassi, S. Diehl, and J. Marino (2017), Phys. Rev. Lett. **118**, 135701.
Chitov, G. Y. (2018), Phys. Rev. B **97**, 085131.
Choi, S., J. Choi, R. Landig, G. Kucsko, H. Zhou, J. Isoya, F. Jelezko, S. Onoda, H. Sumiya, V. Khemani, C. von Keyserlingk, N. Y. Yao, E. Demler, and M. D. Lukin (2017), Nature **543** (7644), 221.
Chomaz, L., S. Baier, D. Petter, M. J. Mark, F. Wächtler, L. Santos, and F. Ferlaino (2016), Phys. Rev. X **6**, 041039.
Chomaz, L., R. M. W. van Bijnen, D. Petter, G. Faraoni, S. Baier, J. H. Becher, M. J. Mark, F. Wächtler, L. Santos, and F. Ferlaino (2018), Nature Physics **14** (5), 442.
Chomaz, L., I. Ferrier-Barbut, F. Ferlaino, B. Laburthe-Tolra, B. L. Lev, and T. Pfau (2022), arXiv e-prints arXiv:2201.02672.
Christensen, J. E., D. Hucul, W. C. Campbell, and E. R. Hudson (2020), npj Quantum Information **6** (1), 35.
Cidrim, A., F. E. A. dos Santos, E. A. L. Henn, and T. Macrì (2018), Phys. Rev. A **98**, 023618.
Cinti, F., A. Cappellaro, L. Salasnich, and T. Macrì (2017), Phys. Rev. Lett. **119**, 215302.
Cinti, F., P. Jain, M. Boninsegni, A. Micheli, P. Zoller, and G. Pupillo (2010), Phys. Rev. Lett. **105**, 135301.
Cinti, F., and T. Macrì (2019), Condens. Matter **4** (93).
Cinti, F., T. Macrì, W. Lechner, G. Pupillo, and T. Pohl (2014), Nat. Comm. **5** (1), 3235.
Cirac, J. I., M. Lewenstein, K. Mølmer, and P. Zoller (1998), Phys. Rev. A **57**, 1208.
Codello, A., N. Defenu, and G. D'Odorico (2015), Phys. Rev. D **91** (10), 105003.
Collura, M., A. De Luca, D. Rossini, and A. Lerose (2021), arXiv , 2110.14705.
Collura, M., and D. Karevski (2010), Phys. Rev. Lett. **104**, 200601.
Colonna-Romano, L., H. Gould, and W. Klein (2014), Phys. Rev. E **90**, 042111.
Cormick, C., and G. Morigi (2012), Phys. Rev. Lett. **109**, 053003.
Cosme, J. G., C. Georges, A. Hemmerich, and L. Mathey (2018), Phys. Rev. Lett. **121** (15), 153001.
Covey, J. P., I. S. Madjarov, A. Cooper, and M. Endres (2019), Phys. Rev. Lett. **122**, 173201.
Cowley, M. D., and R. E. Rosensweig (1967), Journal of Fluid Mechanics **30**, 671.
Cross, M. C., and P. C. Hohenberg (1993), Rev. Mod. Phys. **65**, 851.
Dabrowski, R., and G. V. Dunne (2016), Phys. Rev. D **94** (6), 443.
Dalmonte, M., W. Lechner, Z. Cai, M. Mattioli, A. M. Läuchli, and G. Pupillo (2015), Phys. Rev. B **92**, 045106.
Dalmonte, M., G. Pupillo, and P. Zoller (2010), Phys. Rev. Lett. **105**, 140401.
Damski, B. (2005), Phys. Rev. Lett. **95** (3), 1301.
Dauxois, T., V. Latora, A. Rapisarda, S. Ruffo, and A. Torcini (2002), *Dynamics and Thermodynamics of Systems with Long-Range Interactions*, edited by T. Dauxois, S. Ruffo, E. Arimondo, and M. Wilkens (Springer Berlin Heidelberg, Berlin, Heidelberg).
Dauxois, T., S. Ruffo, E. Arimondo, and M. Wilkens (2002), *Dynamics and Thermodynamics of Systems With Long Range Interactions*, Vol. 602 (Springer-Verlag Berlin Heidelberg).
Davis, E., G. Bentsen, and M. Schleier-Smith (2016), Phys. Rev. Lett. **116**, 053601.
Davis, E. J., G. Bentsen, L. Homeier, T. Li, and M. H. Schleier-Smith (2019), Phys. Rev. Lett. **122**, 010405.
Davis, E. J., A. Periwal, E. S. Cooper, G. Bentsen, S. J. Evered, K. Van Kirk, and M. H. Schleier-Smith (2020), Phys. Rev. Lett. **125**, 060402.
Davoudi, Z., M. Hafezi, C. Monroe, G. Pagano, A. Seif, and A. Shaw (2020), Phys. Rev. Research **2**, 023015.
Davoudi, Z., N. M. Linke, and G. Pagano (2021), arXiv:2104.09346 [quant-ph].
de Oliveira, T. R., C. Charalambous, D. Jonathan, M. Lewenstein, and A. Riera (2018), New J. Phys. **20** (3), 033032.
De Tomasi, G. (2019), Phys. Rev. B **99**, 054204.
De Tomasi, G., D. Hetterich, P. Sala, and F. Pollmann (2019), Phys. Rev. B **100**, 214313.
Defenu, N. (2021), Proceedings of the National Academy of Sciences **118** (30), e2101785118, https://www.pnas.org/doi/pdf/10.1073/pnas.2101785118.
Defenu, N., A. Codello, S. Ruffo, and A. Trombettoni (2020), Journal of Physics A Mathematical General **53** (14), 143001.
Defenu, N., T. Enss, and J. C. Halimeh (2019a), Phys. Rev. B **100**, 014434.
Defenu, N., T. Enss, M. Kastner, and G. Morigi (2018), Phys. Rev. Lett. **121**, 240403.
Defenu, N., G. Morigi, L. Dell'Anna, and T. Enss (2019b), Phys. Rev. B **100**, 184306.
Defenu, N., A. Trombettoni, and A. Codello (2015), Phys. Rev. E **92** (5), 289.
Defenu, N., A. Trombettoni, I. Nándori, and T. Enss (2017a), Phys. Rev. B **96** (17), 1144.
Defenu, N., A. Trombettoni, and S. Ruffo (2016), Phys. Rev. B **94**, 224411.
Defenu, N., A. Trombettoni, and S. Ruffo (2017b), Phys. Rev. B **96** (10), 1.
Defenu, N., A. Trombettoni, and D. Zappalà (2021), Nuclear Physics B **964**, 115295.
Dehmelt, H. (1967), Adv. At. Mol. Phys. **3**, 53.
Del Campo, A., G. De Chiara, G. Morigi, M. B. Plenio, and A. Retzker (2010), Phys. Rev. Lett. **105** (7), 1301.

Delamotte, B. (2011), in *Order, Disorder and Criticality* (WORLD SCIENTIFIC) pp. 1–77.

Deng, S., G. Ortiz, and L. Viola (2009), Phys. Rev. B **80**, 241109.

Deng, X., G. Masella, G. Pupillo, and L. Santos (2020), Phys. Rev. Lett. **125**, 010401.

Díaz-Méndez, R., F. Mezzacapo, F. Cinti, W. Lechner, and G. Pupillo (2015), Phys. Rev. E **92**, 052307.

Díaz-Méndez, R., F. Mezzacapo, W. Lechner, F. Cinti, E. Babaev, and G. Pupillo (2017), Phys. Rev. Lett. **118**, 067001.

Dicke, R. H. (1954), Phys. Rev. **93**, 99.

Dickstein, A. J., S. Erramilli, R. E. Goldstein, D. P. Jackson, and S. A. Langer (1993), Science **261** (5124), 1012.

Dimer, F., B. Estienne, A. S. Parkins, and H. J. Carmichael (2007), Phys. Rev. A **75** (1), 013804.

Divakaran, U., V. Mukherjee, A. Dutta, and D. Sen (2009), J. Stat. Mech.: Theory Exp. **2009** (2), 02007.

Dogra, N., F. Brennecke, S. D. Huber, and T. Donner (2016), Phys. Rev. A **94** (2), 023632.

Dogra, N., M. Landini, K. Kroeger, L. Hruby, T. Donner, and T. Esslinger (2019), Science **366** (6472), 1496.

Dorogovtsev, S. N., A. V. Goltsev, and J. F. F. Mendes (2008), Rev. Mod. Phys. **80**, 1275.

Douglas, J. S., H. Habibian, C. L. Hung, A. V. Gorshkov, H. J. Kimble, and D. E. Chang (2015), Nat. Phot. **9** (5), 326.

Dubin, D. H. E., and T. M. O'Neil (1999), Rev. Mod. Phys. **71**, 87.

Dukelsky, J., S. Pittel, and G. Sierra (2004), Rev. Mod. Phys. **76**, 643.

Dumitrescu, P. T., J. Bohnet, J. Gaebler, A. Hankin, D. Hayes, A. Kumar, B. Neyenhuis, R. Vasseur, and A. C. Potter (2021), "Realizing a dynamical topological phase in a trapped-ion quantum simulator," .

Dupuis, N., L. Canet, A. Eichhorn, W. Metzner, J. M. Pawlowski, M. Tissier, and N. Wschebor (2020), arXiv e-prints , arXiv:2006.04853arXiv:2006.04853 [cond-mat.stat-mech].

Dusuel, S., and J. Vidal (2004), arXiv.org **arXiv:cond-mat**.

Dusuel, S., and J. Vidal (2005a), Phys. Rev. B **71** (22), 48.

Dusuel, S., and J. Vidal (2005b), Phys. Rev. A **71**, 060304.

Dutta, A., G. Aeppli, B. K. Chakrabarti, U. Divakaran, T. F. Rosenbaum, and D. Sen (2015), *Quantum Phase Transitions in Transverse Field Spin Models: From Statistical Physics to Quantum Information* (Cambridge University Press).

Dutta, A., and J. K. Bhattacharjee (2001a), Phys. Rev. B **64**, 184106.

Dutta, A., and J. K. Bhattacharjee (2001b), Phys. Rev. B **64** (18), 2076.

Dutta, A., and A. Dutta (2017), Phys. Rev. B **96** (12), 1301.

Dyson, F. J. (1969), Comm. Math. Phys. **12** (2), 91.

Dziarmaga, J. (2005), Phys. Rev. Lett. **95** (24), 245701.

Dziarmaga, J. (2010), Advances in Physics **59** (6), 1063.

Dziarmaga, J., and M. M. Rams (2010), New J. Phys. **12** (5), 055007.

Ebadi, S., T. T. Wang, H. Levine, A. Keesling, G. Semeghini, A. Omran, D. Bluvstein, R. Samajdar, H. Pichler, W. W. Ho, S. Choi, S. Sachdev, M. Greiner, V. Vuletić, and M. D. Lukin (2021), Nature **595** (7866), 227.

Eckstein, M., and M. Kollar (2008), Phys. Rev. Lett. **100**, 120404.

Eckstein, M., M. Kollar, and P. Werner (2009), Phys. Rev. Lett. **103**, 056403.

Eisert, J., M. Cramer, and M. B. Plenio (2010), Rev. Mod. Phys. **82**, 277.

Eisert, J., M. Van Den Worm, S. R. Manmana, and M. Kastner (2013), Phys. Rev. Lett. **111** (26), 260401.

El-Showk, S., M. Paulos, D. Poland, S. Rychkov, D. Simmons-Duffin, and A. Vichi (2014), Phys. Rev. Lett. **112** (1), 141601.

Eldredge, Z., Z.-X. Gong, J. T. Young, A. H. Moosavian, M. Foss-Feig, and A. V. Gorshkov (2017), Phys. Rev. Lett. **119**, 170503.

Else, D. V., B. Bauer, and C. Nayak (2016), Phys. Rev. Lett. **117**, 090402.

Else, D. V., F. Machado, C. Nayak, and N. Y. Yao (2020), Phys. Rev. A **101**, 022333.

Emary, C., and T. Brandes (2003), Phys. Rev. E **67** (6), 066203.

Endres, M., H. Bernien, A. Keesling, H. Levine, E. R. Anschuetz, A. Krajenbrink, C. Senko, V. Vuletic, M. Greiner, and M. D. Lukin (2016), Science **354** (6315), 1024.

van Enter, A. C. D. (1982), Phys. Rev. B **26**, 1336.

Enzer, D. G., M. M. Schauer, J. J. Gomez, M. S. Gulley, M. H. Holzscheiter, P. G. Kwiat, S. K. Lamoreaux, C. G. Peterson, V. D. Sandberg, D. Tupa, A. G. White, R. J. Hughes, and D. F. V. James (2000), Phys. Rev. Lett. **85**, 2466.

Essler, F. H. L., S. Evangelisti, and M. Fagotti (2012), Phys. Rev. Lett. **109**, 247206.

Faber, T. E. (1958), Proceedings of the Royal Society of London Series A **248** (1255), 460.

Fano, G., F. Ortolani, A. Parola, and L. Ziosi (1999), Phys. Rev. B **60**, 15654.

Feng, L., W. L. Tan, A. De, A. Menon, A. Chu, G. Pagano, and C. Monroe (2020), Phys. Rev. Lett. **125**, 053001.

Fernández-Vidal, S., G. De Chiara, J. Larson, and G. Morigi (2010), Phys. Rev. A **81** (4), 043407.

Ferraretto, M., and L. Salasnich (2019), Phys. Rev. A **99**, 013618.

Festa, L., N. Lorenz, L.-M. Steinert, Z. Chen, P. Osterholz, R. Eberhard, and C. Gross (2021), arXiv:2103.14383 [physics.atom-ph].

Fey, S., S. C. Kapfer, and K. P. Schmidt (2019), Phys. Rev. Lett. **122**, 017203.

Fey, S., and K. P. Schmidt (2016), Phys. Rev. B **94** (7), 2087.

Feynman, R. P. (1954), Phys. Rev. **94**, 262.

Fisher, M. E. (2002), Rep. Prog. Phys. **30** (2), 615.

Fisher, M. E., and M. N. Barber (1972), Phys. Rev. Lett. **28**, 1516.

Fisher, M. E., S.-k. Ma, and B. G. Nickel (1972), Phys. Rev. Lett. **29**, 917.

Fisher, M. E., R. Pynn, and A. Skjeltorp (1984), *Multicritical Phenomena: Proceedings of a NATO Advanced Study Institute on Multicritical Phenomena, held April 10–21, 1983, in Geilo, Norway*, 1st ed., NATO ASI Series 106 (Springer US).

Fisher, M. E., and W. Selke (1980), Phys. Rev. Lett. **44**, 1502.

Fishman, S., G. De Chiara, T. Calarco, and G. Morigi (2008), Phys. Rev. B **77**, 064111.

Fläschner, N., D. Vogel, M. Tarnowski, B. S. Rem, D. S. Lühmann, M. Heyl, J. C. Budich, L. Mathey, K. Sengstock, and C. Weitenberg (2018a), Nature Physics **14** (3), 265.

Fläschner, N., D. Vogel, M. Tarnowski, B. S. Rem, D. S. Lühmann, M. Heyl, J. C. Budich, L. Mathey, K. Sengstock, and C. Weitenberg (2018b), Nature Physics **14** (3), 265.
Flores-Sola, E., B. Berche, R. Kenna, and M. Weigel (2016a), Phys. Rev. Lett. **116**, 115701.
Flores-Sola, E., B. Berche, R. Kenna, and M. Weigel (2016b), Phys. Rev. Lett. **116** (11), 115701.
Flores-Sola, E. J., B. Berche, R. Kenna, and M. Weigel (2015), Eur. Phys. J. B **88** (1), 28.
Foss-Feig, M., Z.-X. Gong, C. W. Clark, and A. V. Gorshkov (2015a), Phys. Rev. Lett. **114**, 157201.
Foss-Feig, M., Z.-X. Gong, C. W. Clark, and A. V. Gorshkov (2015b), Phys. Rev. Lett. **114** (15), 157201.
Fradkin, E. (2013), *Field Theories of Condensed Matter Physics*, 2nd ed. (Cambridge University Press).
Fradkin, E., and S. A. Kivelson (1999), Phys. Rev. B **59**, 8065.
Fraxanet, J., U. Bhattacharya, T. Grass, D. Rakshit, M. Lewenstein, and A. Dauphin (2021), Phys. Rev. Research **3**, 013148.
Frérot, I., P. Naldesi, and T. Roscilde (2017), Phys. Rev. B **95**, 245111.
Frérot, I., P. Naldesi, and T. Roscilde (2018), Phys. Rev. Lett. **120**, 050401.
Friedberg, R., T. Lee, and H. Ren (1993), Annals of Physics **228** (1), 52.
Friedenauer, A., H. Schmitz, J. T. Glueckert, D. Porras, and T. Schaetz (2008), Nature Physics **4** (10), 757.
Friedman, A. J., B. Ware, R. Vasseur, and A. C. Potter (2022), Phys. Rev. B **105**, 115117.
Fröhlich, J., and T. Spencer (1983), Communications in Mathematical Physics **88** (2), 151 .
Fukui, K., and S. Todo (2009), Journal of Computational Physics **228** (7), 2629.
Gabardos, L., B. Zhu, S. Lepoutre, A. M. Rey, B. Laburthe-Tolra, and L. Vernac (2020), Phys. Rev. Lett. **125**, 143401.
Gabrielli, A., M. Joyce, and B. Marcos (2010), Phys. Rev. Lett. **105** (21), 10.1103/physrevlett.105.210602.
Gadway, B., and B. Yan (2016), Journal of Physics B: Atomic, Molecular and Optical Physics **49** (15), 152002.
Gaetan, A., Y. Miroshnychenko, T. Wilk, A. Chotia, M. Viteau, D. Comparat, P. Pillet, A. Browaeys, and P. Grangier (2009), Nat Phys **5** (2), 115.
Gambetta, F. M., C. Zhang, M. Hennrich, I. Lesanovsky, and W. Li (2020), Phys. Rev. Lett. **125**, 133602.
Gardiner, C., and P. Zoller (2004), *Quantum Noise: A Handbook of Markovian and Non-Markovian Quantum Stochastic Methods with Applications to Quantum Optics* (Springer-verlag, Berlin).
Gärttner, M., J. G. Bohnet, A. Safavi-Naini, M. L. Wall, J. J. Bollinger, and A. M. Rey (2017), Nature Physics **13** (8), 781.
Geier, S., N. Thaicharoen, C. Hainaut, T. Franz, A. Salzinger, A. Tebben, D. Grimshandl, G. Zürn, and M. Weidemüller (2021), arXiv:2105.01597 [cond-mat.quant-gas].
P. G. de Gennes, J. P. (1993), *The physics of liquid crystals*, 2nd ed., The International series of monographs on physics 83 Oxford science publications (Clarendon Press; Oxford University Press).
Georges, C., J. G. Cosme, H. Keßler, L. Mathey, and A. Hemmerich (2021), New J. Phys. **23** (2), 023003.
Georgescu, I. M., S. Ashhab, and F. Nori (2014), Rev. Mod. Phys. **86**, 153.
Giachetti, G., N. Defenu, S. Ruffo, and A. Trombettoni (2021a), Phys. Rev. Lett. **127**, 156801.
Giachetti, G., N. Defenu, S. Ruffo, and A. Trombettoni (2021b), EPL (Europhysics Letters) **133** (5), 57004.
Giachetti, G., A. Solfanelli, L. Correale, and N. Defenu (2022), arXiv , 2203.16562.
Giamarchi, T. (2004), *Quantum Physics in One Dimension*, illustrated edition ed., The international series of monographs on physics 121 (Clarendon; Oxford University Press).
Gibberd, R. W. (1974), Australian Journal of Physics **27**, 241.
Gil, L. I. R., R. Mukherjee, E. M. Bridge, M. P. A. Jones, and T. Pohl (2014), Phys. Rev. Lett. **112**, 103601.
Gillman, E., F. Carollo, and I. Lesanovsky (2020), Phys. Rev. Lett. **125**, 100403.
Giovanazzi, S., D. O'Dell, and G. Kurizki (2002), Phys. Rev. Lett. **88**, 130402.
Giuliani, A., V. Mastropietro, and S. Rychkov (2021), Journal of High Energy Physics **2021** (1), 26.
Glaetzle, A. W., R. M. W. van Bijnen, P. Zoller, and W. Lechner (2017), Nat. Comm. **8**, 15813.
Glaetzle, A. W., M. Dalmonte, R. Nath, I. Rousochatzakis, R. Moessner, and P. Zoller (2014), Phys. Rev. X **4**, 041037.
Glick, A. J., H. J. Lipkin, and N. Meshkov (1965), Nuclear Physics **62** (2), 211.
Goldschmidt, E. A., T. Boulier, R. C. Brown, S. B. Koller, J. T. Young, A. V. Gorshkov, S. L. Rolston, and J. V. Porto (2016), Phys. Rev. Lett. **116**, 113001.
Gong, Z.-X., M. Foss-Feig, F. G. S. L. Brandão, and A. V. Gorshkov (2017), Phys. Rev. Lett. **119**, 050501.
Gong, Z.-X., M. Foss-Feig, S. Michalakis, and A. V. Gorshkov (2014), Phys. Rev. Lett. **113** (3), 030602.
Gong, Z. X., M. F. Maghrebi, A. Hu, M. Foss-Feig, P. Richerme, C. Monroe, and A. V. Gorshkov (2016a), Phys. Rev. B **93** (20), 205115.
Gong, Z.-X., M. F. Maghrebi, A. Hu, M. L. Wall, M. Foss-Feig, and A. V. Gorshkov (2016b), Phys. Rev. B **93**, 041102.
Gonzalez-Lazo, E., M. Heyl, M. Dalmonte, and A. Angelone (2021), arXiv:2104.15070 [cond-mat.stat-mech].
Gopalakrishnan, S., B. Lev, and P. Goldbart (2010), Phys. Rev. A **82** (4), 043612.
Gopalakrishnan, S., B. L. Lev, and P. M. Goldbart (2009), Nature Physics **5** (11), 845.
Gopalakrishnan, S., B. L. Lev, and P. M. Goldbart (2011), Phys. Rev. Lett. **107** (27), 604.
Góral, K., L. Santos, and M. Lewenstein (2002), Phys. Rev. Lett. **88**, 170406.
Gori, G., M. Michelangeli, N. Defenu, and A. Trombettoni (2017), Phys. Rev. E **96** (1), 283.
Gorman, D. J., B. Hemmerling, E. Megidish, S. A. Moeller, P. Schindler, M. Sarovar, and H. Haeffner (2018), Phys. Rev. X **8**, 011038.
Gracey, J. A. (2015), Phys. Rev. D **92**, 025012.
de Grandi, C., and A. Polkovnikov (2010), in *Quantum Quenching, Annealing and Computation* (Springer Berlin Heidelberg, Berlin, Heidelberg) pp. 75–114.
Grassberger, P. (2013), J. Stat. Phys. **153** (2), 289.
Gräter, M., and C. Wetterich (1995), Phys. Rev. Lett. **75** (3), 378.
Greer, A. L. (2000), Nature **404** (6774), 134.
Greiner, M., O. Mandel, T. Esslinger, T. W. Hänsch, and I. Bloch (2002), Nature **415** (6867), 39.

Greiter, M., V. Schnells, and R. Thomale (2014), Annals of Physics **351**, 1026.

Gross, E. P. (1957), Phys. Rev. **106**, 161.

Guardado-Sanchez, E., P. T. Brown, D. Mitra, T. Devakul, D. A. Huse, P. Schauß, and W. S. Bakr (2018), Phys. Rev. X **8**, 021069.

Guardado-Sanchez, E., B. M. Spar, P. Schauss, R. Belyansky, J. T. Young, P. Bienias, A. V. Gorshkov, T. Iadecola, and W. S. Bakr (2021), Phys. Rev. X **11**, 021036.

Guo, A. Y., M. C. Tran, A. M. Childs, A. V. Gorshkov, and Z.-X. Gong (2020), Phys. Rev. A **102**, 010401.

Guo, Y., V. D. Vaidya, R. M. Kroeze, R. A. Lunney, B. L. Lev, and J. Keeling (2019), Phys. Rev. A **99** (5), 053818.

Gupta, R., and C. F. Baillie (1992), Phys. Rev. B **45** (6), 2883, publisher: American Physical Society.

Gupta, R., J. DeLapp, G. G. Batrouni, G. C. Fox, C. F. Baillie, and J. Apostolakis (1988), Phys. Rev. Lett. **61** (17), 1996, publisher: American Physical Society.

Gupta, S., A. Campa, and S. Ruffo (2012a), Phys. Rev. E **86**, 061130.

Gupta, S., M. Potters, and S. Ruffo (2012b), Phys. Rev. E **85**, 066201.

Gyongyosi, L., and S. Imre (2019), Computer Science Review **31**, 51.

Habibian, H., A. Winter, S. Paganelli, H. Rieger, and G. Morigi (2013), Phys. Rev. Lett. **110** (7), 075304.

Hadzibabic, Z., P. Krüger, M. Cheneau, B. Battelier, and J. Dalibard (2006), Nature (London) **441**, 1118.

Halimeh, J. C., and M. F. Maghrebi (2021), Phys. Rev. E **103**, 052142.

Halimeh, J. C., M. Van Damme, V. Zauner-Stauber, and L. Vanderstraeten (2020), Phys. Rev. Research **2**, 033111.

Halimeh, J. C., and V. Zauner-Stauber (2017), Phys. Rev. B **96**, 134427.

Halimeh, J. C., V. Zauner-Stauber, I. P. McCulloch, I. de Vega, U. Schollwöck, and M. Kastner (2017), Phys. Rev. B **95**, 024302.

Happer, W. (1972), Rev. Mod. Phys. **44**, 169.

Harty, T., D. Allcock, C. Ballance, L. Guidoni, H. Janacek, N. Linke, D. Stacey, and D. Lucas (2014), Phys. Rev. Lett. **113** (22).

Harty, T. P., M. A. Sepiol, D. T. C. Allcock, C. J. Ballance, J. E. Tarlton, and D. M. Lucas (2016), Phys. Rev. Lett. **117**, 140501.

Hasenbusch, M., M. Marcu, and K. Pinn (1992), Nuclear Physics B Proceedings Supplements **26**, 598.

Hastings, M. B., and T. Koma (2006), Commun. Math. Phys. **265**, 781.

Hauke, P., and L. Tagliacozzo (2013), Phys. Rev. Lett. **111** (20), 207202.

Hazzard, K. R. A., S. R. Manmana, M. Foss-Feig, and A. M. Rey (2013), Phys. Rev. Lett. **110**, 075301.

Hazzard, K. R. A., M. van den Worm, M. Foss-Feig, S. R. Manmana, E. G. Dalla Torre, T. Pfau, M. Kastner, and A. M. Rey (2014), Phys. Rev. A **90**, 063622.

Henkel, N., F. Cinti, P. Jain, G. Pupillo, and T. Pohl (2012), Phys. Rev. Lett. **108**, 265301.

Henkel, N., R. Nath, and T. Pohl (2010), Phys. Rev. Lett. **104**, 195302.

Hepp, K., and E. H. Lieb (1973), Annals of Physics **76** (2), 360.

Hermes, S., T. J. G. Apollaro, S. Paganelli, and T. Macrì (2020), Phys. Rev. A **101**, 053607.

Hernández-Santana, S., C. Gogolin, J. I. Cirac, and A. Acín (2017), Phys. Rev. Lett. **119**, 110601.

Hertkorn, J., J.-N. Schmidt, F. Böttcher, M. Guo, M. Schmidt, K. S. H. Ng, S. D. Graham, H. P. Büchler, T. Langen, M. Zwierlein, and T. Pfau (2021), Phys. Rev. X **11**, 011037.

Heyl, M. (2014), Phys. Rev. Lett. **113**, 205701.

Heyl, M. (2015), Phys. Rev. Lett. **115**, 140602.

Heyl, M. (2018), Reports on Progress in Physics **81** (5), 054001.

Heyl, M., A. Polkovnikov, and S. Kehrein (2013), Phys. Rev. Lett. **110** (13), 135704.

Himbert, L., C. Cormick, R. Kraus, S. Sharma, and G. Morigi (2019), Phys. Rev. A **99** (4), 043633.

Hoang, T. M., H. M. Bharath, M. J. Boguslawski, M. Anquez, B. A. Robbins, and M. S. Chapman (2016), Proceedings of the National Academy of Sciences **113** (34), 9475, https://www.pnas.org/content/113/34/9475.full.pdf.

Hohenberg, P. C. (1967), Phys. Rev. **158**, 383.

Hohenberg, P. C., and J. B. Swift (1995), Phys. Rev. E **52**, 1828.

Holovatch, Y., and M. Shpot (1992), J. Stat. Phys. **66** (3-4), 867.

Holstein, T., and H. Primakoff (1940), Phys. Rev. **58** (12), 1098.

Holzhey, C., F. Larsen, and F. Wilczek (1994), Nuclear Physics B **424** (3), 443.

Homrighausen, I., N. O. Abeling, V. Zauner-Stauber, and J. C. Halimeh (2017), Phys. Rev. B **96**, 104436.

Honkonen, J. (1990), Journal of Physics A Mathematical General **23** (5), 825.

Horak, P., and H. Ritsch (2001), Phys. Rev. A **63** (2), 023603.

Horita, T., H. Suwa, and S. Todo (2017), Phys. Rev. E **95** (1), 012143.

Hruby, L., N. Dogra, M. Landini, T. Donner, and T. Esslinger (2018), Proc. Natl. Acad. Sci. **115** (13), 3279.

Huang, Y.-P., D. Banerjee, and M. Heyl (2019), Phys. Rev. Lett. **122**, 250401.

Hughes-Hallett, D., A. M. Gleason, W. G. McCallum, D. O. Lomen, D. Lovelock, J. Tecosky-Feldman, T. W. Tucker, D. E. Flath, J. Thrash, K. R. Rhea, A. Pasquale, S. P. Gordon, D. Quinney, and P. Frazer Lock (2008), *Calculus: Single Variable*, 5th ed. (Wiley).

Hung, C.-L., A. González-Tudela, J. I. Cirac, and H. J. Kimble (2016), Proceedings of the National Academy of Sciences **113** (34), E4946.

Hung, C.-L., X. Zhang, N. Gemelke, and C. Chin (2010), Phys. Rev. Lett. **104** (16), 160403.

Hwang, M. J., R. Puebla, and M. B. Plenio (2015), Phys. Rev. Lett. **115** (18), 180404.

Iglói, F., B. Blaß, G. m. H. Roósz, and H. Rieger (2018), Phys. Rev. B **98**, 184415.

Imry, Y. (1974), Phys. Rev. Lett. **33**, 1304.

Isenhower, L., E. Urban, X. L. Zhang, A. T. Gill, T. Henage, T. A. Johnson, T. G. Walker, and M. Saffman (2010), Phys. Rev. Lett. **104**, 010503.

Ising, E. (1925), Zeitschrift für Physik **31** (1), 253.

Islam, R., C. Senko, W. C. Campbell, S. Korenblit, J. Smith, A. Lee, E. E. Edwards, C. C. J. Wang, J. K. Freericks, and C. Monroe (2013), Science **340** (6132), 583.

Ispolatov, I., and E. G. D. Cohen (2001), Physica A **295** (3), 475.

Jacobs, L., and R. Savit (1983), Annals of the New York Academy of Sciences **410** (1), 281.

Jäger, S. B., L. Dell'Anna, and G. Morigi (2020), Phys. Rev. B **102**, 035152.

Jaksch, D., J. I. Cirac, P. Zoller, S. L. Rolston, R. Côté, and M. D. Lukin (2000), Phys. Rev. Lett. **85**, 2208.

Jakubczyk, P., N. Dupuis, and B. Delamotte (2014), Phys. Rev. E **90** (6), 062105.

Jakubczyk, P., and W. Metzner (2017), Phys. Rev. B **95**, 085113.

James, A. J. A., R. M. Konik, and N. J. Robinson (2019), Phys. Rev. Lett. **122**, 130603.

Jaschke, D., K. Maeda, J. D. Whalen, M. L. Wall, and L. D. Carr (2017), New J. Phys. **19** (3), 033032.

Jau, Y. Y., A. M. Hankin, T. Keating, I. H. Deutsch, and G. W. Biedermann (2016), Nature Physics **12** (1), 71.

Johnson, J. E., and S. L. Rolston (2010), Phys. Rev. A **82**, 033412.

Jordan, E., K. A. Gilmore, A. Shankar, A. Safavi-Naini, J. G. Bohnet, M. J. Holland, and J. J. Bollinger (2019), Phys. Rev. Lett. **122**, 053603.

José, J. V., Ed. (2013), *40 Years of Berezinskii-Kosterlitz-Thouless Theory* (World Scientific, Singapore).

Joyce, G. S. (1966), Phys. Rev. **146**, 349.

Jozsa, R., and N. Linden (2003), Proceedings of the Royal Society of London Series A **459** (2036), 2011, arXiv:quant-ph/0201143 [quant-ph].

Jurcevic, P., B. P. Lanyon, P. Hauke, C. Hempel, P. Zoller, R. Blatt, and C. F. Roos (2014), Nature **511** (7508), 202.

Jurcevic, P., H. Shen, P. Hauke, C. Maier, T. Brydges, C. Hempel, B. P. Lanyon, M. Heyl, R. Blatt, and C. F. Roos (2017), Phys. Rev. Lett. **119**, 080501.

Kac, M., G. E. Uhlenbeck, and P. C. Hemmer (1963), Journal of Mathematical Physics **4** (2), 216.

Kanungo, S. K., J. D. Whalen, Y. Lu, M. Yuan, S. Dasgupta, F. B. Dunning, K. R. A. Hazzard, and T. C. Killian (2021), arXiv:2101.02871 [physics.atom-ph].

Karpov, P. I., G. Y. Zhu, M. P. Heller, and M. Heyl (2020), arXiv:2011.11624 [cond-mat.quant-gas].

Kashuba, A., and V. L. Pokrovsky (1993), Phys. Rev. Lett. **70** (20), 3155.

Kastner, M. (2010), Phys. Rev. Lett. **104** (24), 240403.

Kastner, M. (2011), Phys. Rev. Lett. **106** (13), 130601.

Katzgraber, H. G., D. Larson, and A. P. Young (2009), Phys. Rev. Lett. **102** (17), 177205.

Kaubruegger, R., P. Silvi, C. Kokail, R. van Bijnen, A. M. Rey, J. Ye, A. M. Kaufman, and P. Zoller (2019), Phys. Rev. Lett. **123**, 260505.

Kaufmann, H., S. Ulm, G. Jacob, U. Poschinger, H. Landa, A. Retzker, M. B. Plenio, and F. Schmidt-Kaler (2012), Phys. Rev. Lett. **109**, 263003.

Kawaguchi, Y., and M. Ueda (2012), Physics Reports **520** (5), 253, spinor Bose–Einstein condensates.

Keesling, A., A. Omran, H. Levine, H. Bernien, H. Pichler, S. Choi, R. Samajdar, S. Schwartz, P. Silvi, S. Sachdev, P. Zoller, M. Endres, M. Greiner, V. Vuletić, and M. D. Lukin (2019), Nature **568** (7751), 207.

Keller, T., S. B. Jager, and G. Morigi (2017), J. Stat. Mech.: Theory Exp. **2017**, 064002.

Keßler, H., J. G. Cosme, M. Hemmerling, L. Mathey, and A. Hemmerich (2019), Phys. Rev. A **99** (5), 053605.

Keßler, H., P. Kongkhambut, C. Georges, L. Mathey, J. G. Cosme, and A. Hemmerich (2020), arXiv preprint arXiv:2012.08885 arXiv:2012.08885.

von Keyserlingk, C. W., V. Khemani, and S. L. Sondhi (2016), Phys. Rev. B **94**, 085112.

Khemani, V., M. Hermele, and R. Nandkishore (2020), Phys. Rev. B **101**, 174204.

Khemani, V., A. Lazarides, R. Moessner, and S. L. Sondhi (2016), Phys. Rev. Lett. **116**, 250401.

Khemani, V., R. Moessner, and S. L. Sondhi (2019), arXiv:1910.10745 [cond-mat.str-el].

Kibble, T. W. B. (2001), J. Phys. A: Math. Gen. **9** (8), 1387.

Kim, K., M.-S. Chang, R. Islam, S. Korenblit, L.-M. Duan, and C. Monroe (2009), Phys. Rev. Lett. **103**, 120502.

Kirton, P., M. M. Roses, J. Keeling, and E. G. Dalla Torre (2019), Advanced Quantum Technologies **2** (1-2), 1800043.

Kitaev, A., V. Lebedev, and M. Feigel'man (2009), AIP Conference Proceedings 10.1063/1.3149495.

Kitaev, A. Y. (2001), Physics Uspekhi **44** (10S), 131.

Kivelson, S. A., I. P. Bindloss, E. Fradkin, V. Oganesyan, J. M. Tranquada, A. Kapitulnik, and C. Howald (2003), Rev. Mod. Phys. **75**, 1201.

Kivelson, S. A., E. Fradkin, and V. J. Emery (1998), Nature **393** (6685), 550.

Kleinert, H. (2001), *Critical Poperties of Phi4 Theories* (World Scientific Publishing).

Klinder, J., H. Keßler, M. R. Bakhtiari, M. Thorwart, and A. Hemmerich (2015a), Phys. Rev. Lett. **115** (23), 230403.

Klinder, J., H. Keßler, M. Wolke, L. Mathey, and A. Hemmerich (2015b), Proc. Natl. Acad. Sci. **112** (11), 3290.

Klinovaja, J., P. Stano, A. Yazdani, and D. Loss (2013), Phys. Rev. Lett. **111**, 186805.

Knight, P. L., E. A. Hinds, M. B. Plenio, D. J. Wineland, M. Barrett, J. Britton, J. Chiaverini, B. DeMarco, W. M. Itano, B. Jelenković, C. Langer, D. Leibfried, V. Meyer, T. Rosenband, and T. Schätz (2003), Philosophical Transactions of the Royal Society of London. Series A: Mathematical, Physical and Engineering Sciences **361** (1808), 1349.

Koffel, T., M. Lewenstein, and L. Tagliacozzo (2012), Phys. Rev. Lett. **109** (26), 267203.

Kohn, W. (1964), Phys. Rev. **133**, A171.

Kollár, A. J., A. T. Papageorge, V. D. Vaidya, Y. Guo, J. Keeling, and B. L. Lev (2017), Nat. Comm. **8** (1), 14386.

Kormos, M., M. Collura, G. Takács, and P. Calabrese (2017), Nature Physics **13** (3), 246.

Kosior, A., and K. Sacha (2018), Phys. Rev. A **97**, 053621.

Kosterlitz, J. M. (1974), J. Phys. C **7**, 1046.

Kosterlitz, J. M. (2017), Rev. Mod. Phys. **89**, 040501.

Kosterlitz, J. M., and D. J. Thouless (1973), J. Phys. C **6** (7), 1181.

Kotliar, G., P. W. Anderson, and D. L. Stein (1983), Phys. Rev. B **27**, 602.

Koziol, J., S. Fey, S. C. Kapfer, and K. P. Schmidt (2019), Phys. Rev. B **100**, 144411.

Koziol, J., A. Langheld, S. C. Kapfer, and K. P. Schmidt (2021), arXiv:2103.09469 [cond-mat.stat-mech].

Krieg, J., and P. Kopietz (2017), Phys. Rev. E **96**, 042107.

Kroeze, R. M., Y. Guo, V. D. Vaidya, J. Keeling, and B. L. Lev (2018), Phys. Rev. Lett. **121** (16), 163601.

Kunimi, M., and Y. Kato (2012), Phys. Rev. B **86**, 060510.

Kunz, H., and C. E. Pfister (1976), Communications in Mathematical Physics **46** (3), 245.

Kuwahara, T., and K. Saito (2020), Phys. Rev. X **10**, 031010.

Kwaśnicki, M. (2017), Fractional Calculus and Applied Analysis **20** (1), 7.

Kyprianidis, A., F. Machado, W. Morong, P. Becker, K. S. Collins, D. V. Else, L. Feng, P. W. Hess, C. Nayak, G. Pagano, N. Y. Yao, and C. Monroe (2021), Science

372 (6547), 1192.

Labuhn, H., D. Barredo, S. Ravets, S. de Léséleuc, T. Macrì, T. Lahaye, and A. Browaeys (2016), Nature **534** (7609), 667.

Ladd, T. D., F. Jelezko, R. Laflamme, Y. Nakamura, C. Monroe, and J. L. O'Brien (2010), Nature **464**, 45.

Laghi, D., T. Macrì, and A. Trombettoni (2017), Phys. Rev. A **96**, 043605.

Lahaye, T., C. Menotti, L. Santos, M. Lewenstein, and T. Pfau (2009), Rep. Prog. Phys. **72** (12), 126401.

Landa, H., S. Marcovitch, A. Retzker, M. B. Plenio, and B. Reznik (2010), Phys. Rev. Lett. **104**, 043004.

Landau, L. D., and E. M. Lifshit's (1991), *Quantum mechanics : non-relativistic theory* (Butterworth-Heinemann).

Landau, L. D., and E. M. Lifshitz (1969), *Statistical physics. Pt.1* (Butterworth-Heinemann).

Landau, L. D., and E. M. Lifshitz (1976), *Mechanics, Third Edition: Volume 1 (Course of Theoretical Physics)*, 3rd ed. (Butterworth-Heinemann).

Landig, R., F. Brennecke, R. Mottl, T. Donner, and T. Esslinger (2015), Nat. Comm. **6** (1), 7046.

Landig, R., L. Hruby, N. Dogra, M. Landini, R. Mottl, T. Donner, and T. Esslinger (2016), Nature **532** (7600), 476.

Landini, M., N. Dogra, K. Kroeger, L. Hruby, T. Donner, and T. Esslinger (2018), Phys. Rev. Lett. **120** (22), 223602.

Lang, J., B. Frank, and J. C. Halimeh (2018), Phys. Rev. Lett. **121**, 130603.

Lang, J., F. Piazza, and W. Zwerger (2017), New J. Phys. **19** (12), 123027.

Larkin, A. I., and S. A. Pikin (1969), J. Exp. Theor. Phys. **29**, 891.

Larson, J., B. Damski, G. Morigi, and M. Lewenstein (2008), Phys. Rev. Lett. **100** (5), 050401.

Lashkari, N., D. Stanford, M. Hastings, T. Osborne, and P. Hayden (2013), J. High Energ. Phys. **2013**, 22.

Last, Y. (1996), Journal of Functional Analysis **142** (2), 406.

Latella, I., A. Pérez-Madrid, A. Campa, L. Casetti, and S. Ruffo (2015), Phys. Rev. Lett. **114**, 230601.

Lechner, W., H.-P. Büchler, and P. Zoller (2014), Phys. Rev. Lett. **112** (25), 255301.

Lechner, W., P. Hauke, and P. Zoller (2015), Science Advances **1** (9), 10.1126/sciadv.1500838.

Lee, A.-C., D. Baillie, R. N. Bisset, and P. B. Blakie (2018), Phys. Rev. A **98**, 063620.

Lee, R. M., and N. D. Drummond (2011), Phys. Rev. B **83**, 245114.

Lee, S. K., J. Cho, and K. S. Choi (2015), New J. Phys. **17** (11), 113053.

Lee, W., M. Kim, H. Jo, Y. Song, and J. Ahn (2019), Phys. Rev. A **99**, 043404.

Leibfried, D., R. Blatt, C. Monroe, and D. Wineland (2003a), Rev. Mod. Phys. **75**, 281.

Leibfried, D., B. DeMarco, V. Meyer, D. Lucas, M. Barrett, J. Britton, W. M. Itano, B. Jelenković, C. Langer, T. Rosenband, and et al. (2003b), Nature **422** (6930), 412.

Lemmer, A., C. Cormick, C. T. Schmiegelow, F. Schmidt-Kaler, and M. B. Plenio (2015), Phys. Rev. Lett. **114**, 073001.

Léonard, J., A. Morales, P. Zupancic, T. Donner, and T. Esslinger (2017a), Science **358** (6369), 1415.

Léonard, J., A. Morales, P. Zupancic, T. Esslinger, and T. Donner (2017b), Nature **543** (7643), 87.

Lepori, L., and L. Dell'Anna (2017), New J. Phys. **19** (10), 103030.

Lepori, L., A. Trombettoni, and D. Vodola (2017), J. Stat. Mech. **2017** (3), 033102.

Lepori, L., D. Vodola, G. Pupillo, G. Gori, and A. Trombettoni (2016), Annals of Physics **374**, 35.

Lepoutre, S., J. Schachenmayer, L. Gabardos, B. Zhu, B. Naylor, E. Maréchal, O. Gorceix, A. M. Rey, L. Vernac, and B. Laburthe-Tolra (2019), Nat. Comm. **10** (1), 1714.

Lerose, A., J. Marino, A. Gambassi, and A. Silva (2019a), Phys. Rev. B **100**, 104306.

Lerose, A., J. Marino, B. Žunkovič, A. Gambassi, and A. Silva (2018), Phys. Rev. Lett. **120** (13), 130603.

Lerose, A., and S. Pappalardi (2020a), Phys. Rev. A **102**, 032404.

Lerose, A., and S. Pappalardi (2020b), Phys. Rev. Research **2**, 012041.

Lerose, A., F. M. Surace, P. P. Mazza, G. Perfetto, M. Collura, and A. Gambassi (2020), Phys. Rev. B **102**, 041118.

Lerose, A., B. Žunkovič, A. Silva, and A. Gambassi (2019b), Phys. Rev. B **99**, 121112.

Lerose, A., B. Žunkovič, J. Marino, A. Gambassi, and A. Silva (2019c), Phys. Rev. B **99** (4), 10.1103/physrevb.99.045128.

Leroux, I. D., M. H. Schleier-Smith, and V. Vuletić (2010), Phys. Rev. Lett. **104**, 073602.

Lesanovsky, I., and J. P. Garrahan (2013), Phys. Rev. Lett. **111**, 215305.

Lesanovsky, I., K. Macieszczak, and J. P. Garrahan (2019), Quantum Science and Technology **4** (2), 02LT02.

de Léséleuc, S., V. Lienhard, P. Scholl, D. Barredo, S. Weber, N. Lang, H. P. Büchler, T. Lahaye, and A. Browaeys (2019), Science **365** (6455), 775.

Letscher, F., O. Thomas, T. Niederprüm, M. Fleischhauer, and H. Ott (2017), Phys. Rev. X **7**, 021020.

Leuzzi, L., G. Parisi, F. Ricci-Tersenghi, and J. J. Ruiz-Lorenzo (2008a), Phys. Rev. Lett. **101**, 107203.

Leuzzi, L., G. Parisi, F. Ricci-Tersenghi, and J. J. Ruiz-Lorenzo (2008b), Phys. Rev. Lett. **101**, 107203.

Levi, E., R. Gutiérrez, and I. Lesanovsky (2016), Journal of Physics B: Atomic, Molecular and Optical Physics **49** (18), 184003.

Levin, Y., R. Pakter, F. B. Rizzato, T. N. Teles, and F. P. Benetti (2014), Physics Reports **535** (1), 1.

Lewenstein, M., A. Sanpera, V. Ahufinger, B. Damski, A. Sen, and U. Sen (2007), Advances in Physics **56** (2), 243.

Lewin, M., and E. H. Lieb (2015), Phys. Rev. A **91** (2), 022507.

Lewis, H. R. (1967), Phys. Rev. Lett. **18** (13), 510.

Lewis Jr., H. R. (1968), J. Math. Phys. **9** (11), 1976.

Lewis Jr., H. R., and W. B. Riesenfeld (1969), J. Math. Phys. **10** (8), 1458.

Lewis-Swan, R. J., D. Barberena, J. R. K. Cline, D. J. Young, J. K. Thompson, and A. M. Rey (2021), Phys. Rev. Lett. **126**, 173601.

Li, J. R., J. Lee, W. Huang, S. Burchesky, B. Shteynas, F. Ç. Topi, A. O. Jamison, and W. Ketterle (2017), Nature **543** (7643), 91.

Li, W., A. Dhar, X. Deng, K. Kasamatsu, L. Barbiero, and L. Santos (2020), Phys. Rev. Lett. **124**, 010404.

Li, W., T. Pohl, J. M. Rost, S. T. Rittenhouse, H. R. Sadeghpour, J. Nipper, B. Butscher, J. B. Balewski, V. Bendkowsky, R. Löw, and T. Pfau (2011), Science **334** (6059), 1110, https://www.science.org/doi/pdf/10.1126/science.1211255.

Li, W.-H., X. Deng, and L. Santos (2021), arXiv:2103.13780 [cond-mat.quant-gas].

Li, Y., A. Geißler, W. Hofstetter, and W. Li (2018), Phys. Rev. A **97**, 023619.

Li, Y., L. He, and W. Hofstetter (2013), Phys. Rev. A **87** (5), 051604.

Lieb, E. H., and D. W. Robinson (1972a), Comm. Math. Phys. **28**, 251.

Lieb, E. H., and D. W. Robinson (1972b), Comm. Math. Phys. **28** (3), 251 .

Lienhard, V., S. de Léséleuc, D. Barredo, T. Lahaye, A. Browaeys, M. Schuler, L.-P. Henry, and A. M. Läuchli (2018), Phys. Rev. X **8**, 021070.

Lienhard, V., P. Scholl, S. Weber, D. Barredo, S. de Léséleuc, R. Bai, N. Lang, M. Fleischhauer, H. P. Büchler, T. Lahaye, and A. Browaeys (2020), Phys. Rev. X **10**, 021031.

Likos, C. N. (2001), Physics Reports **348** (4), 267 .

Likos, C. N., A. Lang, M. Watzlawek, and H. Löwen (2001), Phys. Rev. E **63**, 031206.

Likos, C. N., B. M. Mladek, D. Gottwald, and G. Kahl (2007), The Journal of Chemical Physics **126** (22), 224502.

Lilly, M. P., K. B. Cooper, J. P. Eisenstein, L. N. Pfeiffer, and K. W. West (1999), Phys. Rev. Lett. **82**, 394.

Lima, A. R. P., and A. Pelster (2011), Phys. Rev. A **84**, 041604.

Lin, R., L. Papariello, P. Molignini, R. Chitra, and A. U. J. Lode (2019), Phys. Rev. A **100** (1), 013611.

Lin, Y., J. P. Gaebler, T. R. Tan, R. Bowler, J. D. Jost, D. Leibfried, and D. J. Wineland (2013), Phys. Rev. Lett. **110**, 153002.

Linden, N., S. Popescu, A. J. Short, and A. Winter (2009), Phys. Rev. E **79** (6), 061103.

Lipkin, H. J., N. Meshkov, and A. J. Glick (1965), Nuclear Physics **62** (2), 188.

Lipowsky, R. (1987), Ferroelectrics **73** (1), 69.

Lipowsky, R., and W. Speth (1983), Phys. Rev. B **28** (7), 3983.

Liu, F., R. Lundgren, P. Titum, G. Pagano, J. Zhang, C. Monroe, and A. V. Gorshkov (2019), Phys. Rev. Lett. **122**, 150601.

Lourenço, J. A. S., G. Higgins, C. Zhang, M. Hennrich, and T. Macrì (2021), "Non-hermitian dynamics and $\mathcal{PT}$-symmetry breaking in interacting mesoscopic rydberg platforms," arXiv:2111.04378 [cond-mat.quant-gas].

Lu, M., N. Q. Burdick, and B. L. Lev (2012), Phys. Rev. Lett. **108**, 215301.

Lu, Z.-K., Y. Li, D. S. Petrov, and G. V. Shlyapnikov (2015), Phys. Rev. Lett. **115** (7), 1191.

Luijten, E., and H. W. J. Blöte (1996), Phys. Rev. Lett. **76**, 1557.

Luijten, E., and H. W. J. Blöte (1997), Phys. Rev. B **56**, 8945.

Luijten, E., and H. W. J. Blöte (2002), Phys. Rev. Lett. **89** (2), 1.

Lukin, M. D., M. Fleischhauer, R. Cote, L. M. Duan, D. Jaksch, J. I. Cirac, and P. Zoller (2001), Phys. Rev. Lett. **87**, 037901.

Lynden-Bell, D. (1999), Physica A **263** (1-4), 293.

Machado, F., D. V. Else, G. D. Kahanamoku-Meyer, C. Nayak, and N. Y. Yao (2020), Phys. Rev. X **10**, 011043.

Macrì, T., F. Maucher, F. Cinti, and T. Pohl (2013), Phys. Rev. A **87**, 061602.

Macrì, T., and T. Pohl (2014), Phys. Rev. A **89**, 011402.

Macrì, T., S. Saccani, and F. Cinti (2014), Journal of Low Temperature Physics **177** (1), 59.

Macrì, T., A. Smerzi, and L. Pezzè (2016), Phys. Rev. A **94**, 010102.

Maghrebi, M. F., Z.-X. Gong, M. Foss-Feig, and A. V. Gorshkov (2016), Phys. Rev. B **93**, 125128.

Maghrebi, M. F., Z.-X. Gong, and A. V. Gorshkov (2017), Phys. Rev. Lett. **119** (2), 023001.

Maier, P. G., and F. Schwabl (2004), Phys. Rev. B **70**, 134430.

Maity, S., U. Bhattacharya, and A. Dutta (2019), Journal of Physics A: Mathematical and Theoretical **53** (1), 013001.

Majer, J., J. M. Chow, J. M. Gambetta, J. Koch, B. R. Johnson, J. A. Schreier, L. Frunzio, D. I. Schuster, A. A. Houck, A. Wallraff, A. Blais, M. H. Devoret, S. M. Girvin, and R. J. Schoelkopf (2007), Nature **449** (7161), 443.

Maksymov, A. O., and A. L. Burin (2020), Phys. Rev. B **101**, 024201.

Malard, M. (2013), Brazilian Journal of Physics **43** (3), 182.

Maldacena, J., S. H. Shenker, and D. Stanford (2016), Journal of High Energy Physics **2016** (8), 106.

Manzano, D. (2020), AIP Advances **10** (2), 025106.

Marino, J. (2021), "Universality class of ising critical states with long-range losses," arXiv:2108.12422 [cond-mat.stat-mech].

Martinez, E. A., C. A. Muschik, P. Schindler, D. Nigg, A. Erhard, M. Heyl, P. Hauke, M. Dalmonte, T. Monz, P. Zoller, and R. Blatt (2016), Nature **534** (7608), 516.

Maschler, C., I. B. Mekhov, and H. Ritsch (2008), Eur. Phys. J. D **46** (3), 545.

Masella, G., A. Angelone, F. Mezzacapo, G. Pupillo, and N. V. Prokof'ev (2019), Phys. Rev. Lett. **123**, 045301.

Matsuda, K., L. De Marco, J.-R. Li, W. G. Tobias, G. Valtolina, G. Quéméner, and J. Ye (2020), Science **370** (6522), 1324.

Matsuta, T., T. Koma, and S. Nakamura (2017), Annales Henri Poincaré **18** (2), 519.

Mattioli, M., M. Dalmonte, W. Lechner, and G. Pupillo (2013), Phys. Rev. Lett. **111**, 165302.

Matveeva, N., and S. Giorgini (2014), Phys. Rev. A **90** (5), 053620.

Maucher, F., N. Henkel, M. Saffman, W. Królikowski, S. Skupin, and T. Pohl (2011), Phys. Rev. Lett. **106**, 170401.

Mazza, P. P., G. Perfetto, A. Lerose, M. Collura, and A. Gambassi (2019), Phys. Rev. B **99**, 180302.

Mazza, P. P., R. Schmidt, and I. Lesanovsky (2020), Phys. Rev. Lett. **125**, 033602.

McDonald, J.-P. H. I. (2013), Academic Press.

Ohl de Mello, D., D. Schäffner, J. Werkmann, T. Preuschoff, L. Kohfahl, M. Schlosser, and G. Birkl (2019), Phys. Rev. Lett. **122**, 203601.

Mendoza-Coto, A., D. G. Barci, and D. A. Stariolo (2017), Phys. Rev. B **95**, 144209.

Mendoza-Coto, A., R. Cenci, G. Pupillo, R. Díaz-Méndez, and E. Babaev (2021a), Soft Matter **17**, 915.

Mendoza-Coto, A., L. Nicolao, and R. Díaz-Méndez (2019), Scientific Reports **9** (1), 10.1038/s41598-018-38465-8.

Mendoza-Coto, A., and D. A. Stariolo (2012), Phys. Rev. E **86** (5), 051130.

Mendoza-Coto, A., D. A. Stariolo, and L. Nicolao (2015a), Phys. Rev. Lett. **114** (11), 116101.

Mendoza-Coto, A., D. A. Stariolo, and L. Nicolao (2015b), Phys. Rev. Lett. **114**, 116101.

Mendoza-Coto, A., R. Turcati, V. Zampronio, R. Díaz-Méndez, T. Macrì, and F. Cinti (2021b), "Exploring quantum quasicrystal patterns: a variational study," arXiv:2110.12299 [cond-mat.quant-gas].

Menu, R., and T. Roscilde (2020), Phys. Rev. Lett. **124**, 130604.

Mermin, N. D., and H. Wagner (1966), Phys. Rev. Lett. **17**, 1133.

Meshkov, N., A. J. Glick, and H. J. Lipkin (1965), Nuclear Physics **62** (2), 199.

Meyer, J. S., K. A. Matveev, and A. I. Larkin (2007), Phys. Rev. Lett. **98**, 126404.

Mi, X., M. Ippoliti, C. Quintana, A. Greene, Z. Chen, J. Gross, F. Arute, K. Arya, J. Atalaya, R. Babbush, J. C. Bardin, J. Basso, A. Bengtsson, A. Bilmes, A. Bourassa, L. Brill, M. Broughton, B. B. Buckley, D. A. Buell, B. Burkett, N. Bushnell, B. Chiaro, R. Collins, W. Courtney, D. Debroy, S. Demura, A. R. Derk, A. Dunsworth, D. Eppens, C. Erickson, E. Farhi, A. G. Fowler, B. Foxen, C. Gidney, M. Giustina, M. P. Harrigan, S. D. Harrington, J. Hilton, A. Ho, S. Hong, T. Huang, A. Huff, W. J. Huggins, L. B. Ioffe, S. V. Isakov, J. Iveland, E. Jeffrey, Z. Jiang, C. Jones, D. Kafri, T. Khattar, S. Kim, A. Kitaev, P. V. Klimov, A. N. Korotkov, F. Kostritsa, D. Landhuis, P. Laptev, J. Lee, K. Lee, A. Locharla, E. Lucero, O. Martin, J. R. McClean, T. McCourt, M. McEwen, K. C. Miao, M. Mohseni, S. Montazeri, W. Mruczkiewicz, O. Naaman, M. Neeley, C. Neill, M. Newman, M. Y. Niu, T. E. O'Brien, A. Opremcak, E. Ostby, B. Pato, A. Petukhov, N. C. Rubin, D. Sank, K. J. Satzinger, V. Shvarts, Y. Su, D. Strain, M. Szalay, M. D. Trevithick, B. Villalonga, T. White, Z. J. Yao, P. Yeh, J. Yoo, A. Zalcman, H. Neven, S. Boixo, V. Smelyanskiy, A. Megrant, J. Kelly, Y. Chen, S. L. Sondhi, R. Moessner, K. Kechedzhi, V. Khemani, and P. Roushan (2022), Nature **601** (7894), 531.

Micheli, A., G. Pupillo, H. P. Büchler, and P. Zoller (2007), Phys. Rev. A **76**, 043604.

Millán, A. P., G. Gori, F. Battiston, T. Enss, and N. Defenu (2021), Phys. Rev. Research **3**, 023015.

Minato, T., K. Sugimoto, T. Kuwahara, and K. Saito (2022), Phys. Rev. Lett. **128**, 010603.

Mishra, C., L. Santos, and R. Nath (2020), Phys. Rev. Lett. **124**, 073402.

Mivehvar, F., S. Ostermann, F. Piazza, and H. Ritsch (2018), Phys. Rev. Lett. **120** (12), 123601.

Mivehvar, F., F. Piazza, T. Donner, and H. Ritsch (2021), Advances in Physics **70** (1), 1.

Moeckel, M., and S. Kehrein (2008), Phys. Rev. Lett. **100**, 175702.

Mokhberi, A., M. Hennrich, F. Schmidt-Kaler, L. F. Dimauro, H. Perrin, and S. F. Yelin (2020), *Advances In Atomic, Molecular, and Optical Physics*, Vol. 69 (Academic Press).

Monroe, C., W. C. Campbell, L.-M. Duan, Z.-X. Gong, A. V. Gorshkov, P. W. Hess, R. Islam, K. Kim, N. M. Linke, G. Pagano, P. Richerme, C. Senko, and N. Y. Yao (2021), Rev. Mod. Phys. **93**, 025001.

Monroe, C., D. M. Meekhof, B. E. King, S. R. Jefferts, W. M. Itano, D. J. Wineland, and P. Gould (1995), Phys. Rev. Lett. **75**, 4011.

Monthus, C. (2015), J. Stat. Mech.: Theory Exp. **2015** (5), 05026.

Morales, A., P. Zupancic, J. Léonard, T. Esslinger, and T. Donner (2018), Nature Materials **17** (8), 686.

Morgado, M., and S. Whitlock (2020), arXiv:2011.03031.

Mori, T., T. N. Ikeda, E. Kaminishi, and M. Ueda (2018), Journal of Physics B: Atomic, Molecular and Optical Physics **51** (11), 112001.

Morigi, G., and S. Fishman (2004), Phys. Rev. Lett. **93**, 170602.

Morong, W., F. Liu, P. Becker, K. S. Collins, L. Feng, A. Kyprianidis, G. Pagano, T. You, A. V. Gorshkov, and C. Monroe (2021), Nature **599** (7885), 393.

Moroni, S., and M. Boninsegni (2014), Phys. Rev. Lett. **113**, 240407.

Moses, S. A., J. P. Covey, M. T. Miecnikowski, D. S. Jin, and J. Ye (2017), Nature Physics **13** (1), 13.

Mottl, R., F. Brennecke, K. Baumann, R. Landig, T. Donner, and T. Esslinger (2012), Science **336** (6088), 1570.

Moudgalya, S., A. Prem, R. Nandkishore, N. Regnault, and B. A. Bernevig (2021), "Thermalization and its absence within krylov subspaces of a constrained hamiltonian," in *Memorial Volume for Shoucheng Zhang*, Chap. Chapter 7, pp. 147–209.

Mukamel, D. (2008), *Statistical Mechanics of Systems with Long-Range Interactions*, Long-Range Interacting Systems Lecture Notes of the Les Houches Summer School: Volume 90, August 2008 (Oxford Univ. Press).

Mukamel, D., S. Ruffo, and N. Schreiber (2005), Phys. Rev. Lett. **95** (24), 240604.

Müller, M., L. Liang, I. Lesanovsky, and P. Zoller (2008), New J. Phys. **10** (9), 093009.

Muniz, J. A., D. Barberena, R. J. Lewis-Swan, D. J. Young, J. R. K. Cline, A. M. Rey, and J. K. Thompson (2020), Nature **580** (7805), 602.

Murthy, P. A., I. Boettcher, L. Bayha, M. Holzmann, D. Kedar, M. Neidig, M. G. Ries, A. N. Wenz, G. Zürn, and S. Jochim (2015), Phys. Rev. Lett. **115**, 010401.

Muschik, C., M. Heyl, E. Martinez, T. Monz, P. Schindler, B. Vogell, M. Dalmonte, P. Hauke, R. Blatt, and P. Zoller (2017), New J. Phys. **19** (10), 103020.

Mussardo, G. (2009), *Statistical Field Theory: An Introduction to Exactly Solved Models in Statistical Physics*, Oxford Graduate Texts (Oxford University Press).

Myerson, A. H., D. J. Szwer, S. C. Webster, D. T. C. Allcock, M. J. Curtis, G. Imreh, J. A. Sherman, D. N. Stacey, A. M. Steane, and D. M. Lucas (2008), Phys. Rev. Lett. **100**, 200502.

Nachtergaele, B., Y. Ogata, and R. Sims (2006), J. Stat. Phys. **124** (1), 1.

Nadj-Perge, S., I. K. Drozdov, J. Li, H. Chen, S. Jeon, J. Seo, A. H. MacDonald, B. A. Bernevig, and A. Yazdani (2014), Science **346** (6209), 602.

Nag, S., and A. Garg (2019), Phys. Rev. B **99**, 224203.

Nagy, D., G. Kónya, G. Szirmai, and P. Domokos (2010), Phys. Rev. Lett. **104** (13), 130401.

Nagy, D., G. Szirmai, and P. Domokos (2008), Eur. Phys. J. D **48** (1), 127.

Nagy, D., G. Szirmai, and P. Domokos (2011), Phys. Rev. A **84** (4), 043637.

Nakamura, M. (2000), Phys. Rev. B **61**, 16377.

Nandkishore, R., and S. Gopalakrishnan (2021), Phys. Rev. B **103**, 134423.

Nandkishore, R., and D. A. Huse (2015), Annu. Rev. Condens. Matter Phys. **6** (1), 15.

Nandkishore, R. M., and S. L. Sondhi (2017), Phys. Rev. X **7**, 041021.

Natale, G., R. M. W. van Bijnen, A. Patscheider, D. Petter, M. J. Mark, L. Chomaz, and F. Ferlaino (2019), Phys.

Rev. Lett. **123**, 050402.
Nath, R., M. Dalmonte, A. W. Glaetzle, P. Zoller, F. Schmidt-Kaler, and R. Gerritsma (2015), New J. Phys. **17** (6), 065018.
Nelson, D. R., and J. M. Kosterlitz (1977), Phys. Rev. Lett. **39**, 1201.
Newman, C. M., and L. S. Schulman (1977), Journal of Mathematical Physics **18** (1), 23.
Neyenhuis, B., J. Zhang, P. W. Hess, J. Smith, A. C. Lee, P. Richerme, Z.-X. Gong, A. V. Gorshkov, and C. Monroe (2017), Science Advances **3** (8), e1700672.
Nezhadhaghighi, M. G., and M. A. Rajabpour (2014), Phys. Rev. B **90**, 205438.
van Nieuwenburg, E., Y. Baum, and G. Refael (2019), Proceedings of the National Academy of Sciences **116** (19), 9269.
Nishimori, H., and G. Ortiz (2015), *Elements of phase transitions and critical phenomena* (Oxford University Press).
Nisoli, C., and A. R. Bishop (2014), Phys. Rev. Lett. **112**, 070401.
Noek, R., G. Vrijsen, D. Gaultney, E. Mount, T. Kim, P. Maunz, and J. Kim (2013), Opt. Lett. **38** (22), 4735.
Norcia, M. A., R. J. Lewis-Swan, J. R. K. Cline, B. Zhu, A. M. Rey, and J. K. Thompson (2018), Science **361** (6399), 259.
Norcia, M. A., C. Politi, L. Klaus, E. Poli, M. Sohmen, M. J. Mark, R. Bisset, L. Santos, and F. Ferlaino (2021), arXiv:2102.05555 [cond-mat.quant-gas].
Nussenzveig, H. (1973), *Introduction to Quantum Optics*, Documents on Modern Physics: Gordon and Breach (Gordon and Breach Science Publishers).
O'Dell, D., S. Giovanazzi, G. Kurizki, and V. M. Akulin (2000), Phys. Rev. Lett. **84**, 5687.
O'Dell, D. H. J., S. Giovanazzi, and G. Kurizki (2003), Phys. Rev. Lett. **90**, 110402.
Ojeda Collado, H. P., G. Usaj, C. A. Balseiro, D. H. Zanette, and J. Lorenzana (2021), Phys. Rev. Research **3**, L042023.
Orioli, A. P. n., A. Signoles, H. Wildhagen, G. Günter, J. Berges, S. Whitlock, and M. Weidemüller (2018), Phys. Rev. Lett. **120**, 063601.
Ortix, C., J. Lorenzana, and C. D. Castro (2008), J. Phys.: Condens. Matter **20** (43), 434229.
Ospelkaus, C., U. Warring, Y. Colombe, K. R. Brown, J. M. Amini, D. Leibfried, and D. J. Wineland (2011), Nature **476** (7359), 181.
Öztop, B., M. Bordyuh, Ö. E. Müstecaplıoğlu, and H. E. Türeci (2012), New J. Phys. **14** (8), 085011.
Öztop, B., Ö. E. Müstecaplıoğlu, and H. E. Türeci (2013), Laser Physics **23** (2), 025501.
P. M. Chaikin, T. C. L. (1995), *Principles of condensed matter physics*, 1st ed. (Cambridge University Press).
Pagano, G., P. W. Hess, H. B. Kaplan, W. L. Tan, P. Richerme, P. Becker, A. Kyprianidis, J. Zhang, E. Birckelbaw, M. R. Hernandez, Y. Wu, and C. Monroe (2018), Quantum Science and Technology **4** (1), 014004.
Pan, F., and J. P. Draayer (1999), Physics Letters B **451** (1-2), 1.
Pan, W., R. R. Du, H. L. Stormer, D. C. Tsui, L. N. Pfeiffer, K. W. Baldwin, and K. W. West (1999), Phys. Rev. Lett. **83**, 820.
Pappalardi, S., A. Russomanno, B. Žunkovič, F. Iemini, A. Silva, and R. Fazio (2018), Phys. Rev. B **98**, 134303.
Park, J. W., S. A. Will, and M. W. Zwierlein (2015), Phys. Rev. Lett. **114** (20), 205302.
Parker, C. V., P. Aynajian, E. H. da Silva Neto, A. Pushp, S. Ono, J. Wen, Z. Xu, G. Gu, and A. Yazdani (2010), Nature **468** (7324), 677.
Parker, N. G., C. Ticknor, A. M. Martin, and D. H. J. O'Dell (2009), Phys. Rev. A **79**, 013617.
Patrick, K., T. Neupert, and J. K. Pachos (2017), Phys. Rev. Lett. **118** (26), 267002.
Patscheider, A., B. Zhu, L. Chomaz, D. Petter, S. Baier, A.-M. Rey, F. Ferlaino, and M. J. Mark (2020), Phys. Rev. Research **2**, 023050.
Paul, W. (1990), Rev. Mod. Phys. **62**, 531.
de Paz, A., A. Sharma, A. Chotia, E. Maréchal, J. H. Huckans, P. Pedri, L. Santos, O. Gorceix, L. Vernac, and B. Laburthe-Tolra (2013), Phys. Rev. Lett. **111**, 185305.
Pehlivan, Y., A. B. Balantekin, T. Kajino, and T. Yoshida (2011), Phys. Rev. D **84**, 065008.
Pelissetto, A., and E. Vicari (2002), Physics Reports **368** (6), 549.
Periwal, A., E. S. Cooper, P. Kunkel, J. F. Wienand, E. J. Davis, and M. Schleier-Smith (2021), arXiv:2106.04070 [quant-ph].
Peter, D., N. Y. Yao, N. Lang, S. D. Huber, M. D. Lukin, and H. P. Büchler (2015), Phys. Rev. A **91**, 053617.
Petter, D., G. Natale, R. M. W. van Bijnen, A. Patscheider, M. J. Mark, L. Chomaz, and F. Ferlaino (2019), Phys. Rev. Lett. **122**, 183401.
Petter, D., A. Patscheider, G. Natale, M. J. Mark, M. A. Baranov, R. v. Bijnen, S. M. Roccuzzo, A. Recati, B. Blakie, D. Baillie, L. Chomaz, and F. Ferlaino (2020), arXiv:2005.02213 [cond-mat.quant-gas].
Pezzé, L., and A. Smerzi (2009), Phys. Rev. Lett. **102**, 100401.
Piacente, G., I. V. Schweigert, J. J. Betouras, and F. M. Peeters (2004), Phys. Rev. B **69**, 045324.
Piazza, F., and P. Strack (2014), Phys. Rev. A **90** (4), 043823.
Piazza, F., P. Strack, and W. Zwerger (2013), Annals of Physics **339**, 135.
Picco, M. (2012), arXiv: , 1207.1018.
Pino, J. M., J. M. Dreiling, C. Figgatt, J. P. Gaebler, S. A. Moses, M. S. Allman, C. H. Baldwin, M. Foss-Feig, D. Hayes, K. Mayer, C. Ryan-Anderson, and B. Neyenhuis (2021), Nature **592** (7853), 209.
Pino, M. (2014), Phys. Rev. B **90**, 174204.
Pistorius, T., J. Kazemi, and H. Weimer (2020), Phys. Rev. Lett. **125**, 263604.
Pizzi, A., J. Knolle, and A. Nunnenkamp (2021), Nature Communications **12** (1), 2341.
Poderoso, F. C., J. J. Arenzon, and Y. Levin (2011), Phys. Rev. Lett. **106** (6), 067202.
Podolsky, D. (2016), Phys. Rev. X **6** (3), 10.1103/PhysRevX.6.031025.
Poilblanc, D., S. Yunoki, S. Maekawa, and E. Dagotto (1997), Phys. Rev. B **56**, R1645.
Poland, D., S. Rychkov, and A. Vichi (2019), Rev. Mod. Phys. **91**, 015002.
Polchinski, J. (1984), Nuclear Physics B **231** (2), 269.
Polkovnikov, A. (2005), Phys. Rev. B **72** (16), 161201.
Pomeau, Y., and S. Rica (1994), Phys. Rev. Lett. **72**, 2426.
Porras, D., and J. I. Cirac (2004), Phys. Rev. Lett. **92**, 207901.
Portmann, O., A. Gölzer, N. Saratz, O. V. Billoni, D. Pescia, and A. Vindigni (2010), Phys. Rev. B **82** (18), 184409.
Pozrikidis, C. (2016), *The Fractional Laplacian* (Taylor & Francis).

Pruttivarasin, T., M. Ramm, I. Talukdar, A. Kreuter, and H. Häffner (2011), New J. Phys. **13** (7), 075012.

Pupillo, G., A. Griessner, A. Micheli, M. Ortner, D.-W. Wang, and P. Zoller (2008), Phys. Rev. Lett. **100**, 050402.

Pupillo, G., A. Micheli, M. Boninsegni, I. Lesanovsky, and P. Zoller (2010), Phys. Rev. Lett. **104**, 223002.

Pupillo, G., P. c. v. Ziherl, and F. Cinti (2020), Phys. Rev. B **101**, 134522.

Pyka, K., J. Keller, H. L. Partner, R. Nigmatullin, T. Burgermeister, D. M. Meier, K. Kuhlmann, A. Retzker, M. B. Plenio, W. H. Zurek, A. Del Campo, and T. E. Mehlstäubler (2013), Nat. Comm. **4** (1), 1387.

Rademaker, L., and D. A. Abanin (2020), Phys. Rev. Lett. **125**, 260405.

Rajabpour, M. A., and S. Sotiriadis (2015), Phys. Rev. B **91** (4), 045131.

Raju, A., C. B. Clement, L. X. Hayden, J. P. Kent-Dobias, D. B. Liarte, D. Z. Rocklin, and J. P. Sethna (2019), Phys. Rev. X **9**, 021014.

Randall, J., C. E. Bradley, F. V. van der Gronden, A. Galicia, M. H. Abobeih, M. Markham, D. J. Twitchen, F. Machado, N. Y. Yao, and T. H. Taminiau (2021), Science **374** (6574), 1474, https://www.science.org/doi/pdf/10.1126/science.abk0603.

Ravets, S., H. Labuhn, D. Barredo, L. Béguin, T. Lahaye, and A. Browaeys (2014), Nature Physics **10** (12), 914.

Reimann, P. (2008), Phys. Rev. Lett. **101**, 190403.

Ribeiro, P., J. Vidal, and R. Mosseri (2007), Phys. Rev. Lett. **99**, 050402.

Richerme, P., Z.-X. Gong, A. Lee, C. Senko, J. Smith, M. Foss-Feig, S. Michalakis, A. V. Gorshkov, and C. Monroe (2014), Nature **511** (7508), 198.

Ritsch, H., P. Domokos, F. Brennecke, and T. Esslinger (2013), Rev. Mod. Phys. **85** (2), 553.

Roccuzzo, S. M., A. Gallemí, A. Recati, and S. Stringari (2020), Phys. Rev. Lett. **124**, 045702.

Roos, C. F., D. Leibfried, A. Mundt, F. Schmidt-Kaler, J. Eschner, and R. Blatt (2000), Phys. Rev. Lett. **85**, 5547.

Rossotti, S., M. Teruzzi, D. Pini, D. E. Galli, and G. Bertaina (2017), Phys. Rev. Lett. **119**, 215301.

Roy, S., and D. E. Logan (2019), SciPost Phys. **7**, 42.

Rückriegel, A., A. Kreisel, and P. Kopietz (2012), Phys. Rev. B **85** (5), 054422.

Ruffo, S. (1994), *Transport, Chaos And Plasma Physics*, edited by S. Benkadda, F. Doveil, and Y. Elskens (World Scientific, Singapore).

Saccani, S., S. Moroni, and M. Boninsegni (2012), Phys. Rev. Lett. **108**, 175301.

Sachdev, S. (1999), *Quantum Phase Transitions* (Cambridge Univ. Press, Cambridge).

Safavi-Naini, A., R. J. Lewis-Swan, J. G. Bohnet, M. Gärttner, K. A. Gilmore, J. E. Jordan, J. Cohn, J. K. Freericks, A. M. Rey, and J. J. Bollinger (2018), Phys. Rev. Lett. **121**, 040503.

Safavi-Naini, A., M. L. Wall, O. L. Acevedo, A. M. Rey, and R. M. Nandkishore (2019a), Phys. Rev. A **99**, 033610.

Safavi-Naini, A., M. L. Wall, O. L. Acevedo, A. M. Rey, and R. M. Nandkishore (2019b), Phys. Rev. A **99**, 033610.

Saffman, M., T. G. Walker, and K. Mølmer (2010), Rev. Mod. Phys. **82** (3), 2313.

Saito, H., Y. Kawaguchi, and M. Ueda (2007), Phys. Rev. A **76**, 043613.

Sak, J. (1973), Phys. Rev. B **8** (1), 281.

Samajdar, R., W. W. Ho, H. Pichler, M. D. Lukin, and S. Sachdev (2021), Proceedings of the National Academy of Sciences **118** (4), 10.1073/pnas.2015785118.

Santos, L., G. V. Shlyapnikov, and M. Lewenstein (2003), Phys. Rev. Lett. **90**, 250403.

Santos, L. F., F. Borgonovi, and G. L. Celardo (2016), Phys. Rev. Lett. **116** (25), 250402.

Saratz, N., A. Lichtenberger, O. Portmann, U. Ramsperger, A. Vindigni, and D. Pescia (2010), Phys. Rev. Lett. **104**, 077203.

Scardicchio, A., and T. Thiery (2017), arXiv:1710.01234 [cond-mat.dis-nn].

Schachenmayer, J., B. P. Lanyon, C. F. Roos, and A. J. Daley (2013), Phys. Rev. X **3** (3), 031015.

Schachenmayer, J., A. Pikovski, and A. M. Rey (2015a), New J. Phys. **17** (6), 065009.

Schachenmayer, J., A. Pikovski, and A. M. Rey (2015b), Phys. Rev. X **5**, 011022.

Schaller, G. (2008), Phys. Rev. A **78**, 032328.

Schauss, P. (2018), Quantum Science and Technology **3** (2), 023001.

Schauß, P., M. Cheneau, M. Endres, T. Fukuhara, S. Hild, A. Omran, T. Pohl, C. Gross, S. Kuhr, and I. Bloch (2012), Nature **491** (7422), 87.

Schauß, P., J. Zeiher, T. Fukuhara, S. Hild, M. Cheneau, T. Macrì, T. Pohl, I. Bloch, and C. Gross (2015), Science **347** (6229), 1455.

Schempp, H., G. Günter, S. Wüster, M. Weidemüller, and S. Whitlock (2015), Phys. Rev. Lett. **115** (9), 093002.

Schiffer, J. P. (1993), Phys. Rev. Lett. **70**, 818.

Schneider, C., D. Porras, and T. Schaetz (2012), Rep. Prog. Phys. **75** (2).

Schnyder, A. P., S. Ryu, A. Furusaki, and A. W. W. Ludwig (2008), Phys. Rev. B **78**, 195125.

Scholl, P., M. Schuler, H. J. Williams, A. A. Eberharter, D. Barredo, K.-N. Schymik, V. Lienhard, L.-P. Henry, T. C. Lang, T. Lahaye, A. M. Läuchli, and A. Browaeys (2020), arXiv:2012.12268 [quant-ph].

Scholl, P., H. J. Williams, G. Bornet, F. Wallner, D. Barredo, T. Lahaye, A. Browaeys, L. Henriet, A. Signoles, C. Hainaut, T. Franz, S. Geier, A. Tebben, A. Salzinger, G. Zürn, and M. Weidemüller (2021), arXiv:2107.14459 [quant-ph].

Schulz, H. J. (1993), Phys. Rev. Lett. **71**, 1864.

Schulz, M., C. A. Hooley, R. Moessner, and F. Pollmann (2019), Phys. Rev. Lett. **122**, 040606.

Schuster, S. C., P. Wolf, S. Ostermann, S. Slama, and C. Zimmermann (2020), Phys. Rev. Lett. **124** (14), 143602.

Schütz, S., and G. Morigi (2014), Phys. Rev. Lett. **113**, 203002.

Schymik, K.-N., S. Pancaldi, F. Nogrette, D. Barredo, J. Paris, A. Browaeys, and T. Lahaye (2021), arXiv:2106.07414 [physics.atom-ph].

Sciolla, B., and G. Biroli (2010), Phys. Rev. Lett. **105**, 220401.

Seetharam, K., A. Lerose, R. Fazio, and J. Marino (2021), "Correlation engineering via non-local dissipation," arXiv:2101.06445 [cond-mat.quant-gas].

Seetharam, K., A. Lerose, R. Fazio, and J. Marino (2022), Phys. Rev. B **105**, 184305.

Sekino, Y., and L. Susskind (2008), Journal of High Energy Physics **2008** (10), 065.

Selke, W. (1988), Phys. Rep. **170** (4), 213.

Semeghini, G., H. Levine, A. Keesling, S. Ebadi, T. T. Wang, D. Bluvstein, R. Verresen, H. Pichler, M. Kalinowski, R. Samajdar, A. Omran, S. Sachdev, A. Vishwanath, M. Greiner, V. Vuletic, and M. D. Lukin (2021), arXiv:2104.04119 [quant-ph].

Seul, M., and D. Andelman (1995), Science **267** (5197), 476.

Shankar, R. (1994), Rev. Mod. Phys. **66**, 129.

Shenoy, S. R., and B. Chattopadhyay (1995), Phys. Rev. B **51**, 9129.

Shimshoni, E., G. Morigi, and S. Fishman (2011), Phys. Rev. A **83** (3), 441.

Shiwa, Y. (2006), J. Stat. Phys. **124** (5), 1207.

Short, A. J. (2011), New J. Phys. **13** (5), 053009.

Sieberer, L. M., S. D. Huber, E. Altman, and S. Diehl (2013), Phys. Rev. Lett. **110** (19), 195301.

Siegman, A. E. (1986), *Lasers* (University Science Books).

Sierant, P., K. Biedroń, G. Morigi, and J. Zakrzewski (2019), SciPost Phys. **7**, 8.

Simon, B., M. Taylor, and T. Wolff (1985), Phys. Rev. Lett. **54**, 1589.

Smith, J., A. Lee, P. Richerme, B. Neyenhuis, P. Hess, P. Hauke, M. Heyl, D. Huse, and C. Monroe (2016), Nature Physics **12** (10), 907.

Sohmen, M., C. Politi, L. Klaus, L. Chomaz, M. J. Mark, M. A. Norcia, and F. Ferlaino (2021), Phys. Rev. Lett. **126**, 233401.

Sondhi, S. L., S. M. Girvin, J. P. Carini, and D. Shahar (1997), Rev. Mod. Phys. **69**, 315.

Sørensen, A., and K. Mølmer (1999), Phys. Rev. Lett. **82**, 1971.

Sørensen, A. S., and K. Mølmer (2001), Phys. Rev. Lett. **86**, 4431.

Sperstad, I. B., E. B. Stiansen, and A. Sudbø (2012), Phys. Rev. B **85** (21), 214302.

Srinivas, R., S. C. Burd, H. M. Knaack, R. T. Sutherland, A. Kwiatkowski, S. Glancy, E. Knill, D. J. Wineland, D. Leibfried, A. C. Wilson, D. T. C. Allcock, and D. H. Slichter (2021), "High-fidelity laser-free universal control of two trapped ion qubits," arXiv:2102.12533 [quant-ph].

Stanley, H. E. (1968), Phys. Rev. **176**, 718.

Storch, D.-M., M. van den Worm, and M. Kastner (2015), New J. Phys. **17**, 063021.

Su, W. P., J. R. Schrieffer, and A. J. Heeger (1979), Phys. Rev. Lett. **42**, 1698.

Surace, F. M., and A. Lerose (2021), arXiv:2011.10583 [cond-mat.quant-gas].

Suzuki, M. (1973), Progress of Theoretical Physics **49** (4), 1106.

Sweke, R., J. Eisert, and M. Kastner (2019), Journal of Physics A: Mathematical and Theoretical **52** (42), 424003.

Swift, J., and P. C. Hohenberg (1977), Phys. Rev. A **15**, 319.

Syed, M., T. Enss, and N. Defenu (2021), Phys. Rev. B **103**, 064306.

Tan, W. L., P. Becker, F. Liu, G. Pagano, K. S. Collins, A. De, L. Feng, H. B. Kaplan, A. Kyprianidis, R. Lundgren, W. Morong, S. Whitsitt, A. V. Gorshkov, and C. Monroe (2021), Nature Physics **17** (6), 742.

Tanzi, L., E. Lucioni, F. Famà, J. Catani, A. Fioretti, C. Gabbanini, R. N. Bisset, L. Santos, and G. Modugno (2019a), Phys. Rev. Lett. **122** (13), 130405.

Tanzi, L., J. G. Maloberti, G. Biagioni, A. Fioretti, C. Gabbanini, and G. Modugno (2021), Science **371** (6534), 1162.

Tanzi, L., S. M. Roccuzzo, E. Lucioni, F. Famà, A. Fioretti, C. Gabbanini, G. Modugno, A. Recati, and S. Stringari (2019b), Nature **574** (7778), 382.

Thirring, W. (1970), Zeit. Phys. **235**, 339.

Thouless, D. (1972), Journal of Non-Crystalline Solids **8-10**, 461, amorphous and Liquid Semiconductors.

Thouless, D. J. (1969), Phys. Rev. **187** (2), 732.

Titum, P., J. T. Iosue, J. R. Garrison, A. V. Gorshkov, and Z.-X. Gong (2019), Phys. Rev. Lett. **123**, 115701.

Titum, P., and M. F. Maghrebi (2020), Phys. Rev. Lett. **125**, 040602.

Torlai, G., B. Timar, E. P. L. van Nieuwenburg, H. Levine, A. Omran, A. Keesling, H. Bernien, M. Greiner, V. Vuletić, M. D. Lukin, R. G. Melko, and M. Endres (2019), Phys. Rev. Lett. **123**, 230504.

Tóth, G., C. Knapp, O. Gühne, and H. J. Briegel (2007), Phys. Rev. Lett. **99**, 250405.

Tran, M. C., C.-F. Chen, A. Ehrenberg, A. Y. Guo, A. Deshpande, Y. Hong, Z.-X. Gong, A. V. Gorshkov, and A. Lucas (2020), Phys. Rev. X **10**, 031009.

Tran, M. C., A. Ehrenberg, A. Y. Guo, P. Titum, D. A. Abanin, and A. V. Gorshkov (2019a), Phys. Rev. A **100**, 052103.

Tran, M. C., A. Y. Guo, Y. Su, J. R. Garrison, Z. Eldredge, M. Foss-Feig, A. M. Childs, and A. V. Gorshkov (2019b), Phys. Rev. X **9**, 031006.

Tranquada, J. M., J. D. Axe, N. Ichikawa, A. R. Moodenbaugh, Y. Nakamura, and S. Uchida (1997), Phys. Rev. Lett. **78**, 338.

Trefzger, C., C. Menotti, B. Capogrosso-Sansone, and M. Lewenstein (2011), Journal of Physics B: Atomic, Molecular and Optical Physics **44** (19), 193001.

Ueda, M. (2017), "Spinor-dipolar aspects of bose-einstein condensation," in *Universal Themes of Bose-Einstein Condensation*, edited by N. P. Proukakis, D. W. Snoke, and P. B. Littlewood (Cambridge University Press) p. 371–386.

Uhrich, P., N. Defenu, R. Jafari, and J. C. Halimeh (2020), Phys. Rev. B **101**, 245148.

Ulm, S., J. Roßnagel, G. Jacob, C. Degünther, S. T. Dawkins, U. G. Poschinger, R. Nigmatullin, A. Retzker, M. B. Plenio, F. Schmidt-Kaler, and K. Singer (2013), Nat. Comm. **4** (1), 1387.

Urban, E., T. A. Johnson, T. Henage, L. Isenhower, D. D. Yavuz, T. G. Walker, and M. Saffman (2009), Nature Physics **5** (2), 110.

Vaidya, V. D., Y. Guo, R. M. Kroeze, K. E. Ballantine, A. J. Kollár, J. Keeling, and B. L. Lev (2018), Phys. Rev. X **8** (1), 011002.

Vajna, S., and B. Dóra (2014), Phys. Rev. B **89**, 161105.

Vajna, S., and B. Dóra (2015), Phys. Rev. B **91**, 155127.

Valtolina, G., K. Matsuda, W. G. Tobias, J.-R. Li, L. De Marco, and J. Ye (2020), Nature **588** (7837), 239.

Van Regemortel, M., D. Sels, and M. Wouters (2016), Phys. Rev. A **93** (3), 032311.

Vanderstraeten, L., M. Van Damme, H. P. Büchler, and F. Verstraete (2018), Phys. Rev. Lett. **121** (9), 090603.

Vasiliev, A. Y., A. E. Tarkhov, L. I. Menshikov, P. O. Fedichev, and U. R. Fischer (2014), New J. Phys. **16** (5), 053011.

Vaterlaus, A., C. Stamm, U. Maier, M. G. Pini, P. Politi, and D. Pescia (2000), Phys. Rev. Lett. **84**, 2247.

Verdel, R., F. Liu, S. Whitsitt, A. V. Gorshkov, and M. Heyl (2020), Phys. Rev. B **102**, 014308.

Verresen, R., M. D. Lukin, and A. Vishwanath (2021), Phys. Rev. X **11**, 031005.

Vidal, G. (2003), Phys. Rev. Lett. **91**, 147902.

Vidal, J., R. Mosseri, and J. Dukelsky (2004), Phys. Rev. A **69**, 054101.

Vilas, N. B., C. Hallas, L. Anderegg, P. Robichaud, A. Winnicki, D. Mitra, and J. M. Doyle (2022), Nature **606** (7912), 70.
Viyuela, O., D. Vodola, G. Pupillo, and M. A. Martin-Delgado (2016), Phys. Rev. B **94**, 125121.
Vodola, D., L. Lepori, E. Ercolessi, A. V. Gorshkov, and G. Pupillo (2014), Phys. Rev. Lett. **113** (15), 156402.
Vodola, D., L. Lepori, E. Ercolessi, and G. Pupillo (2016), New J. Phys. **18** (1), 015001.
Vojta, T. (1996), Phys. Rev. B **53** (2), 710.
Wang, D. W., A. J. Millis, and S. Das Sarma (2001), Phys. Rev. B **64**, 193307.
Wang, W., R. Díaz-Méndez, M. Wallin, J. Lidmar, and E. Babaev (2020), arXiv e-prints , arXiv:2011.01664arXiv:2011.01664 [cond-mat.soft].
Wang, Y., S. Shevate, T. M. Wintermantel, M. Morgado, G. Lochead, and S. Whitlock (2020), npj Quantum Information **6** (1), 54.
Wang, Y. K., and F. T. Hioe (1973), Phys. Rev. A **7** (3), 831, arXiv:arXiv:0801.0020v2.
Watanabe, H., and H. Murayama (2012), Phys. Rev. Lett. **108**, 251602.
Watanabe, H., and H. Murayama (2013), Phys. Rev. Lett. **110**, 181601.
Weber, S., S. de Léséleuc, V. Lienhard, D. Barredo, T. Lahaye, A. Browaeys, and H. P. Büchler (2018), Quantum Science and Technology **3** (4), 044001.
Weber, S., C. Tresp, H. Menke, A. Urvoy, O. Firstenberg, H. P. Büchler, and S. Hofferberth (2017), J. Phys. B **50** (13), 133001.
Weeks, J. D. (1981), Phys. Rev. B **24** (3), 1530.
Wegner, F. J., and A. Houghton (1973), Phys. Rev. A **8** (1), 401.
Weidinger, S. A., M. Heyl, A. Silva, and M. Knap (2017), Phys. Rev. B **96**, 134313.
Weimer, H., M. Müller, H. P. Büchler, and I. Lesanovsky (2011), Quantum Information Processing **10** (6), 885.
Weimer, H., M. Müller, I. Lesanovsky, P. Zoller, and H. P. Büchler (2010), Nature Physics **6** (5), 382.
Wetterich, C. (1993), Phys. Lett. B **301** (1), 90.
Wichterich, H., J. Vidal, and S. Bose (2010), Phys. Rev. A **81**, 032311.
Wilk, T., A. Gaëtan, C. Evellin, J. Wolters, Y. Miroshnychenko, P. Grangier, and A. Browaeys (2010), Phys. Rev. Lett. **104**, 010502.
Wilson, K. G., and J. Kogut (1974), Physics Reports **12** (2), 75.
Wintermantel, T. M., Y. Wang, G. Lochead, S. Shevate, G. K. Brennen, and S. Whitlock (2020), Phys. Rev. Lett. **124**, 070503.
Wright, K., K. M. Beck, S. Debnath, J. M. Amini, Y. Nam, N. Grzesiak, J. S. Chen, N. C. Pisenti, M. Chmielewski, C. Collins, K. M. Hudek, J. Mizrahi, J. D. Wong-Campos, S. Allen, J. Apisdorf, P. Solomon, M. Williams, A. M. Ducore, A. Blinov, S. M. Kreikemeier, V. Chaplin, M. Keesan, C. Monroe, and J. Kim (2019), Nat. Comm. **10** (1), 5464.
Wu, X., X. Liang, Y. Tian, F. Yang, C. Chen, Y.-C. Liu, M. K. Tey, and L. You (2021), Chinese Physics B **30** (2), 020305.
Wu, Y.-L., and S. Das Sarma (2016), Phys. Rev. A **93**, 022332.
Xu, S. (2022), Physics Online Journal **15**, 2.
Xue, M., S. Yin, and L. You (2018), Phys. Rev. A **98**, 013619.
Yamazaki, Y. (1977), Physics Letters A **61** (4), 207.
Yan, B., S. A. Moses, B. Gadway, J. P. Covey, K. R. A. Hazzard, A. M. Rey, D. S. Jin, and J. Ye (2013), Nature **501** (7468), 521.
Yang, H., J. Cao, Z. Su, J. Rui, B. Zhao, and J.-W. Pan (2022), Science **378** (6623), 1009, https://www.science.org/doi/pdf/10.1126/science.ade6307.
Yang, K., L. Zhou, W. Ma, X. Kong, P. Wang, X. Qin, X. Rong, Y. Wang, F. Shi, J. Gong, and J. Du (2019), Phys. Rev. B **100**, 085308.
Yao, N. Y., C. R. Laumann, S. Gopalakrishnan, M. Knap, M. Müller, E. A. Demler, and M. D. Lukin (2014), Phys. Rev. Lett. **113**, 243002.
Yao, N. Y., and C. Nayak (2018), Physics Today **71** (9), 40.
Yong, J., T. R. Lemberger, L. Benfatto, K. Ilin, and M. Siegel (2013), Phys. Rev. B **87** (18), 184505.
Zeiher, J., R. van Bijnen, P. Schauß, S. Hild, J.-y. Choi, T. Pohl, I. Bloch, and C. Gross (2016), Nature Physics **12** (12), 1095.
Zeiher, J., J.-y. Choi, A. Rubio-Abadal, T. Pohl, R. van Bijnen, I. Bloch, and C. Gross (2017), Phys. Rev. X **7**, 041063.
Zeiher, J., P. Schauß, S. Hild, T. Macrì, I. Bloch, and C. Gross (2015), Phys. Rev. X **5**, 031015.
Zener, C. (1932), Proceedings of the Royal Society of London Series A **137** (833), 696.
Zhang, J., P. Hess, A. Kyprianidis, P. Becker, A. Lee, J. Smith, G. Pagano, I.-D. Potirniche, A. C. Potter, A. Vishwanath, *et al.* (2017a), Nature **543** (7644), 217.
Zhang, J., G. Pagano, P. W. Hess, A. Kyprianidis, P. Becker, H. Kaplan, A. V. Gorshkov, Z.-X. Gong, and C. Monroe (2017b), Nature **551** (7682), 601.
Zhu, S.-L., C. Monroe, and L.-M. Duan (2006), Phys. Rev. Lett. **97**, 050505.
Žunkovič, B., M. Heyl, M. Knap, and A. Silva (2018), Phys. Rev. Lett. **120** (13), 6.
Žunkovič, B., A. Silva, and M. Fabrizio (2016), Phil. Trans. Royal Soc. A: Math., Phys. and Eng. Sci. **374** (2069), 20150160.
Zurek, W. H. (1985), Nature **317** (6037), 505.
Zurek, W. H. (1996), Phys. Rep. **276** (4), 177.
Zurek, W. H. (2009), Phys. Rev. Lett. **102**, 105702.
Zurek, W. H., and U. Dorner (2008), Philosophical Transactions of the Royal Society of London Series A **366** (1877), 2953.
Zurek, W. H., U. Dorner, and P. Zoller (2005), Phys. Rev. Lett. **95** (10), 1301.
Zvyagin, A. A. (2016), Low Temperature Physics **42** (11), 971.
Zwerger, W. (2008), Nat. Phys. **4** (6), 444.